Pharmacological aspects of the inhibition of mammalian respiratory complex I

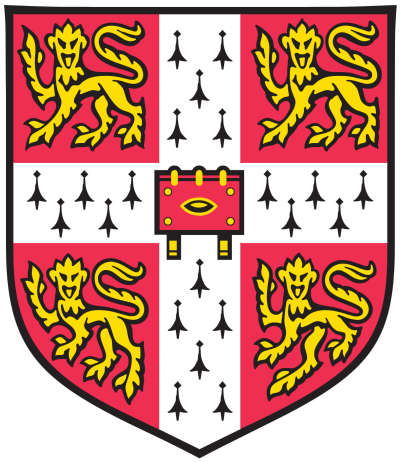

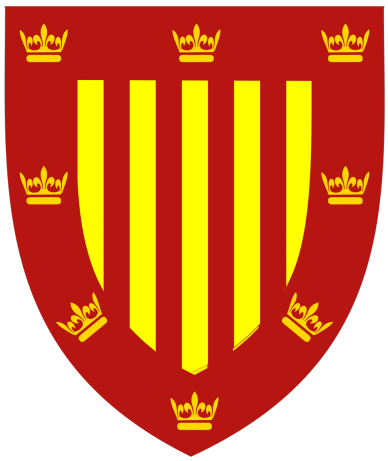

MRC Mitochondrial Biology Unit

Peterhouse College
University of Cambridge

Riccardo Serreli

Dissertation submitted for the degree of *Doctor of Philosophy*
September 2017

Son, in the Church they say to forgive…

Forgiveness is about them and God.

It's my job to arrange the meeting.

(Man on Fire, 2004)

Declaration

This dissertation, entitled "Pharmacological aspects of the inhibition of mammalian respiratory complex I", is the result of my own work and includes nothing which is the outcome of work done in collaboration except as declared in the Preface and specified in the text.

It is not substantially the same as any that I have submitted, or, is being concurrently submitted for a degree or diploma or other qualification at the University of Cambridge or any other University or similar institution except as declared in the Preface and specified in the text. I further state that no substantial part of my dissertation has already been submitted, or, is being concurrently submitted for any such degree, diploma or other qualification at the University of Cambridge or any other University or similar institution except as declared in the Preface and specified in the text.

It does not exceed the prescribed word limit for the relevant Degree Committee.

This work was carried out between October 2013 and September 2017, under the supervision of Dr Judy Hirst. Information and data derived from other sources has been referenced and attributed accordingly.

Riccardo Serreli

September 2017

Acknowledgements

I would like to thank all the people that are responsible, in so many different ways, to the person I am today and that are (at least partially) responsible for my being able to obtain a PhD at the University of Cambridge. In chronological order…

Edi Spiazzi. You have faced enormous challenges and emerged stronger than before, always. You could have achieved anything in life and sacrificed your dreams for your family. You are the example I will always follow. I am honoured to have spent a part of my life with you. Thank you mum.

Piercarlo Serreli. You taught me how to play baseball, poker, chess, basketball, and another million things. Most importantly, you taught me the power of reason and logic above all else, something that I will cherish forever. If fitness is a paramount part of my life (thanks to which I will live much longer and better), I owe that exclusively to you. Thank you dad.

Stefano Serreli. My childhood would not have been the same without you. I am so glad that, no matter what, we can always laugh together. Thank you brother.

All the people who beat me up on a regular basis from 3 until 13 years of age (and their parents that were evidently not aware of the damage they would have inflicted to society with their rotten produce). I wish I could make you aware of which kind of despicable human beings you are but, given your extremely limited intelligence, you would not be able to understand. After all, you have given me the drive to be as different from you as I possibly can. Hopefully, life has given you what you deserve. If not, when I meet you in hell, I will.

Alessandro "*Alexubinik***" Obinu, Paolo "***Cane Pazzo Tannen***" Ticcò** and **Alberto "***Generale Cadorna***" Camerotto**, the best neighbours the world has ever seen. You cannot begin to comprehend how happy I am every time I see you and spend time with you. I am so proud to be able to call you my friends.

Matteo "*Scott Henderson***" Gasparin** and **Sebastiano "***Billy Sheehan***" Pozzobon**, the best musicians I have had the honour to play with. We literally rocked the world, even though most of it did not know it. Most importantly, you rocked my world, and

that's what matters here. Who would have thought that drumming would have made me discover what true friendship is?

Alessandro "*Keystone***" Bertoni**. You've been in hell for the first part of your life but managed, against all odds, to end up in heaven. You are my brother.

Davide "*Daniel Heiman***" Artusato** and **Francesco "***John Petrucci***" Artusato (a.k.a. the Artusato Brothers)**. Your musical prowess expanded my drumming horizons in ways I would have never been able to accomplish on my own. It was an honour to play with you.

Dario "*Sinnerevolution***" Bizzotto**. A world-class artist I am so proud to call my friend. The lab coats you painted for me are a true reflection of astonishing grandeur.

Francesco Novara. Thanks for introducing me to 50 girls in 2 months back in 2001…you probably snogged them all anyway, but it was always great to spend time with you, something I have always looked forward to.

Prof. Guido Mantovani. Did you enjoy laughing at me every time I would bring you the drafts of my economics BSc thesis? Of course you did! I bet the condescending smirks you gave me (and surely many other students) were (and still are) the highlight of your day. Why was I even surprised, after all that agreed very well with what many of your colleagues used to say about you behind your back. I should have just listened to them and get a decent supervisor instead.

Prof. Giuseppe Tattara. You didn't even bother reading the drafts of my economics MSc thesis, and as a result I've lost a summa cum laude because of you. Now I know why everyone at the department dreaded to have you as a supervisor, no wonder. The only reason why I won't be telling you these things in your face is just because the way you talk makes most people plunge into a deep coma from which no one, in recorded history, has ever come back from.

Prof. Dave Adams. You are the best supervisor an undergraduate student could wish for. Master of organic chemistry, master of biotechnology and master of the universe, without your guidance I would have been lost in the recondite maze of 2,4-dichloropyrimidines. It was an honour to work with you.

Dr. Judy Hirst. You accepted a person like me in your brilliant group, something I will always be grateful for. You brought so much value to my thesis and elevated it to a standard I would have never reached on my own, ever. Your invaluable scientific guidance taught me the priceless value of intellectual rigour.

Dr. Hannah "*Maynard James Keenan***" Bridges**. Your help with cellular assays and with the sublime Seahorse XF 96 analyser was unbeatable.

Dr. Andy "*almost the Almighty***" Jones**. Wonderful colleague, scientist extraordinaire, exceptional team member, humble and exemplar human being. Your succinate:O_2 assay deserved at least a Nature paper.

Dr. Justin "*Jordan -The wizard- Rudess***" Fedor**. While the AOX nightmare was upon me, a hand appeared to save me. Thanks to you, those dark reflections mutated into a glowing rainbow and never will I fear again to venture into blackness. Let the spirit of Jordan Rudess (who is still alive at the time of writing this thesis, by the way) guide you, and allow the majestic Korg Kronos to enter your life forever: a future as a world-leading progressive metal keyboard player is waiting for you, even though you may not know it yet.

The guy who does the cleaning at night during weekdays (I don't know what his name is). Seeing you on a daily basis mopping the floor and replacing the bins at 4am during my AOX dark ages was a much needed grip on reality.

Noor "*Dwayne -The Equalizer- Johnson***" Agip**. Simply the best. Thank you so much for our very interesting conversations about anything under the sun and for keeping me in the loop with the "internal affairs" in the group. You really need to write a book about your friends and people you hang out with, the things that happened to you with them would definitely make a whole TV series worth watching. And, above all, thank you for letting me in on your human experience: many would have lost their moral compass, you never did.

Dr. Febin "*DA MAN***" Varghese**, for always being there even when you weren't.

Dr. Roger "*2.5L of coffee a day***" Springett**, for never being there even when you were.

No thanks to **AOX**, the most annoying enzyme on the planet.

Erica "*the Speech-Ninja***" Falconbury**. I would have never imagined to meet someone like you, let alone this person becoming the most important relationship I've ever had. You didn't just dismiss me as an unattractive bald stammering weirdo. You give me pure joy. I will always LAVA YOU.

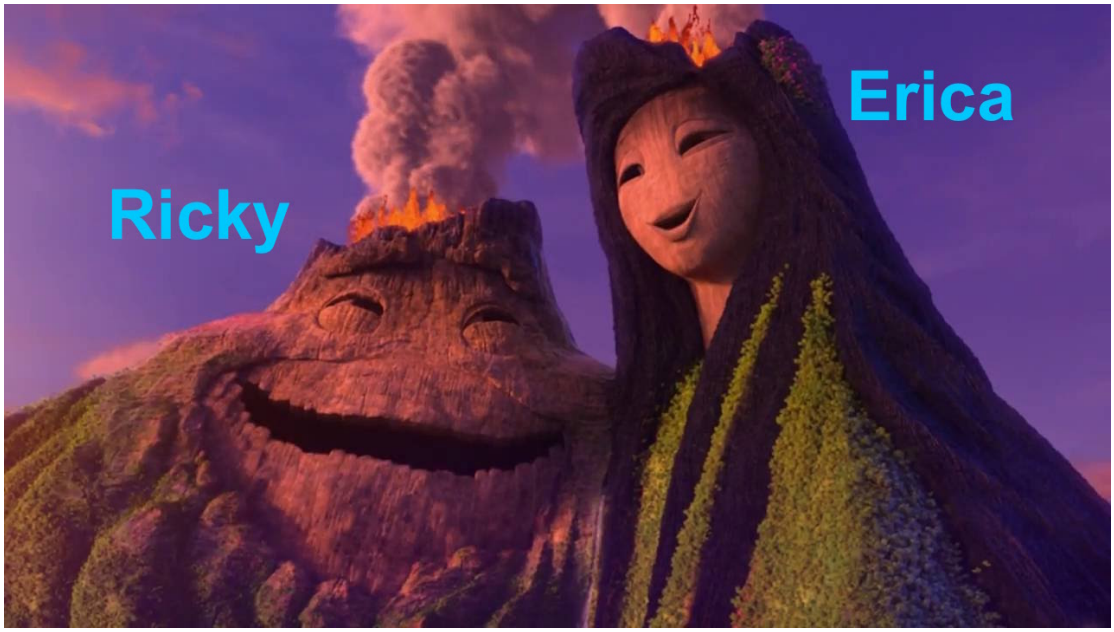

To my family

To Erica

Abstract

Mitochondrial complex I, a large respiratory enzyme located in the inner mitochondrial membrane, catalyses electron transfer from NADH to ubiquinone while concomitantly translocating protons across the membrane to sustain ATP synthesis. A crucial aspect of the pharmacology of complex I is drug-induced mitochondrial dysfunction, particularly its role in liver toxicity. Complex I inhibition causes an energy deficit and can lead to adverse changes in the status of the mitochondrial [NADH]/[NAD^+] pool and increased reactive oxygen species production, causing widespread damage.

A library of molecules that are known candidates for causing complex I-driven drug-induced mitochondrial dysfunction was compiled using database and literature searches and then tested with assays on isolated mammalian complex I, mitochondrial membranes and cultured mammalian cells. The results extend the knowledge of complex I-linked drug toxicity and define a proof-of-principle methodology for the investigation of further unknown candidate molecules. Using this methodology, the Screen-Well V2 library from Enzo Life Sciences, containing 786 FDA-approved drugs, was used to investigate the role of complex I-linked drug toxicity on a wider scale. The results show that complex I is targeted by many structurally unrelated pharmacological compounds, but whether catalysis is inhibited *in vivo* requires drug transport into the mitochondrion, limiting the adverse physiological consequences in most cases tested.

Furthermore, three structure-activity relationship studies were carried out on specific classes of complex I inhibitors: rotenoid natural product compounds, a family of pyrazole-based compounds under investigation as anticancer drugs, and variants on the drug Mubritinib. These studies identified structural determinants of binding to complex I and improve our understanding of complex I inhibition.

Abbreviations

In addition to the abbreviations reported below, standard chemical symbols and SI units are used throughout this thesis

[2Fe-2S]	2-iron-2-sulphur
[3Fe-4S]	3-iron-4-sulphur
[4Fe-4S]	4-iron-4-sulphur
α-KG	*α-Ketoglutarate*
$\Delta\mu H^+$	Proton electrochemical potential
$\Delta\psi$	Membrane potential
Δp	Proton motive force
ΔpH	pH difference across the membrane
A/D	Active/deactive state
AAT	Aspartate amino-transferase
Acetyl-CoA	Acyl-coenzyme A
ACS	Acetyl-CoA synthetase
ADP	Adenosine diphosphate
ALA	Aminolevulinic acid
AML	Acute myeloid leukaemia
AMP	Adenosine monophosphate
ANT	Adenine nucleotide translocator
AOX	Alternative oxidase
ATP	Adenosine triphosphate
$APAD^+$	3-acetylpyridine adenine dinucleotide
APADH	Reduced 3-acetylpyridine adenine dinucleotide
B. taurus	*Bos taurus*
BCA	Bicinchronic acid
BSA	Bovine serum albumin
CPT-1	Carnitine palmitoyltransferase I
Cat	Catalase
CHAPS	3-[(3-cholamidopropyl)-dimethylammonio]-1-propane sulphonate
CL	Cardiolipin

Complex I	NADH:ubiquinone oxidoreductase
Complex II	Succinate:ubiquinone oxidoreductase
Complex III	Ubiquinol:cytochrome *c* oxidoreductase
Complex IV	Cytochrome *c* oxidase
Complex V	ATP synthase
CPT	Carnitine palmitoyltransferase
CYP	Cytochrome P450
Cyt *c*	Cytochrome *c*
DCPIP	2,6-dichlorophenolindophenol
DDM	n-dodecyl-ß-D-maltopyranoside
DMSO	Dimethyl sulfoxide
dQ	Decylubiquinone
dQH_2	Decylubiquinol
DTT	Dithiothreitol
ECAR	Extracellular acidification rate
E. coli	*Escherichia coli*
EDTA	Ethylenediaminetetraacetic acid
EGTA	Ethyleneglycoltetraacetic acid
ETC	Electron transport chain
ETF	Electron transferring flavoprotein
FAD	Flavin adenine dinucleotide
FeCN	Potassium hexacyanoferrate
FeS	Iron-sulphur
FMN	Flavin mononucleotide
FumC	Fumarate hydratase
GPDH	Glycerol 3-phosphate dehydrogenase
GPx	Glutathione peroxidase
GR	Glutathione reductase
H_2O_2	Hydrogen peroxide
HAR	Hexaammineruthenium(III) chloride
HEPES	4-(2-hydroxyethyl)-1-piperazineethanesulfonic acid
HiPIP	High potential iron-sulphur protein
HRP	Horseradish peroxidase

HPLC	High pressure liquid chromatography
IMM	Inner mitochondrial membrane
IMS	Inter-membrane space
INT	2-(4-iodo-phenyl)-3-(4-nitrophenyl)-5-phenyl tetrazolium chloride
IPTG	Isopropyl ß-D-1-thiogalactopyranoside
KCN	Potassium cyanide
LCFA	Long chain fatty acid
MaeB	Oxaloacetate decarboxylating malic dehydrogenase
MAO	Monoamine oxidase
MDH	Malate dehydrogenase
MRC	Mitochondrial respiratory chain
MPT	Mitochondrial permeability transition
mtDNA	Mitochondrial DNA
NaCN	Sodium cyanide
NAD^+	Oxidised nicotinamide adenine dinucleotide
NADH	Reduced nicotinamide adenine dinucleotide
$NADP^+$	Oxidised nicotinamide adenine dinucleotide phosphate
NADPH	Reduced nicotinamide adenine dinucleotide phosphate
NAPQI	N-acetyl-p-benzoquinone imine
NDH	Alternative NADH-ubiquinone oxidoreductase
NOX	NADPH oxidase
NRTI	Nucleoside reverse transcriptase inhibitors
OCR	Oxygen consumption rate
OD_{600}	Optical density at 600 nm
OG	Octyl-glucoside
OMM	Outer mitochondrial membrane
OXPHOS	Oxidative phosphorylation
PC	Phosphatidylcholine
P. denitrificans	*Paracoccus denitrificans*
PE	Phosphatidylethanolamine
P_i	Inorganic phosphate
PMF	Proton motive force
Pxr	Peroxyredoxin

Q_{10}	Coenzyme Q_{10}
$Q_{10}H_2$	Reduced coenzyme Q_{10}
R	Gas constant
RET	Reverse electron transport
ROS	Reactive oxygen species
SAR	Structure-activity relationship
SOD	Superoxide dismutase
SMP	Sub-mitochondrial particle
T. thermophilus	*Thermus thermophilus*
Tris	Tris(hydroxymethyl)aminomethane
Trx	Thioredoxin
VDAC	Voltage-dependent anion channel
Y. lipolytica	*Yarrowia lipolytica*

1 Introduction

1.1 Chemiosmotic Theory

Living organisms are capable of incorporating energy into chemically usable forms so that they can power energetically unfavourable reactions necessary to sustain life. A prominent example of such a molecule is ATP. In eukaryotic cells, mitochondria channel the energy derived from nutrients into the endergonic synthesis of ATP from ADP and inorganic phosphate via the process of oxidative phosphorylation (OXPHOS). An electron transport chain delivers electrons through a series of membrane-bound redox enzymes and electron carriers from redox centres with more negative midpoint potential to redox centres with more positive midpoint potential (from NADH/$FADH_2$ to O_2). The energy from cellular respiration is stored across the inner mitochondrial membrane (IMM) in the form of an electrochemical proton gradient ($\Delta\mu H^+$) which is then used by ATP synthase (complex V) to synthesise ATP[1]. $\Delta\mu H^+$ is expressed in units of voltage of the protonmotive force (PMF or Δp, the energy required to transfer protons across the IMM against the gradient) according to the equation below (F is the Faraday constant, R is the gas constant and T is the temperature in Kelvin).

$$\Delta p = -\frac{\Delta\mu H^+}{F} = \Delta\Psi - \frac{2.3RT}{F}\Delta pH$$

The PMF comprises an electrical term or charge gradient, $\Delta\Psi$, and a chemical gradient of protons, ΔpH, both expressed in terms of difference between the P-phase compartment (intermembrane space or IMS) and N-phase compartment (matrix): in respiring mitochondria, Δp is about 180-220 mV, with the major contributor being $\Delta\Psi$ with about 150-180 mV[2]. At the heart of the chemiosmotic theory, originally proposed by Peter Mitchell, lies the proton translocation capabilities of respiratory complexes in mitochondria: this allows energy from substrate oxidation to be converted and stored in a proton gradient. The four postulates of Mitchell's theory can be summarised as follows[3]

1) The PMF is the result of enzymes in the respiratory chain that couple the sequential electron fluxes to proton movement across the IMM. Reducing equivalents NADH,

$FADH_2$, $Q_{10}H_2$ and reduced cytochrome *c* transfer electrons across the respiratory chain while complexes I, III and IV eject protons into the IMS (see section 1.3).

2) Complex V (a proton-translocating ATPase) couples the redox-generated PMF to ATP synthesis. It can also work in reverse by ejecting protons from the matrix into the IMS with the energy generated by ATP hydrolysis.

3) The potential across the IMM promotes accumulation of cations in the matrix and hinders anions from entering it. Exchange carriers in the IMM satisfy the physiological need to prevent membrane potential-driven cation accumulation in the matrix (which would lead to osmotic swelling) and to ensure transport of substrates and metabolites across the IMM whilst maintaining the membrane potential (*e.g.* transporters that transfer Ca^{2+} in and out of the IMM are the mitochondrial calcium uniporter and mitochondrial H^+/Ca^{2+} and Na^+/Ca^{2+} exchangers, respectively)[4].

4) The IMM is very impermeable to ions, especially protons (ion leaks would otherwise dissipate Δp by short-circuiting the IMM). However, proton leak does happen and is physiologically relevant. Unregulated or basal proton leak through the IMM only accounts for about 5% of the overall proton leak, the rest is catalysed by uncoupling proteins (UCPs), mainly for thermogenesis and regulation of ROS[5].

Figure 1.1 illustrates the concept of an energy transducing membrane in mitochondria.

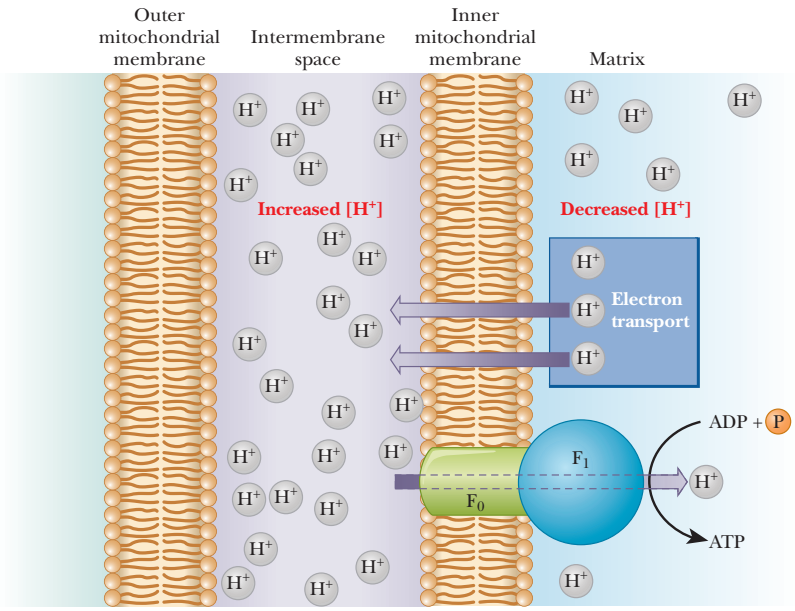

Figure 1.1. Generation of ATP by the proton gradient across the IMM. Protons are pumped in the IMS from the matrix, generating a proton gradient. Complex V generates ATP by transferring protons back to the matrix. Picture taken from Campbell and Farrell[6].

1.2 Mitochondria

Mitochondria are thought to have originated from aerobic bacteria that were engulfed by an ancestral anaerobic (proto)eukaryote. The acquisition of an aerobic symbiont meant that a more efficient metabolism was available for the host: the resulting symbiotic system (along with the transfer of bacterial genes to the nucleus at a later stage) eventually became the eukaryotic cell[7]. It is still debated whether mitochondria were acquired early during eukaryotic evolution or when much of the development of eukaryotic cells was already accomplished[8].

Mitochondria possess a double membrane structure, the outer mitochondrial membrane (OMM) and IMM with the IMS in between. The OMM is recognised as a platform for apoptosis execution and its predominant protein component is the voltage-dependent anion channel (VDAC), a weakly selective channel for anions that transports all water-soluble mitochondrial substrates and metabolites[9]. The IMM is much more extended than the OMM and it can be further divided into the inner boundary membrane, closer to the OMM, and cristae membranes, invaginations of the IMM that begin with narrow openings (crista junctions) and are very rich in OXPHOS enzymes[10]. Figure 1.2 shows how mitochondria are internally structured.

Mitochondria are a highly dynamic organelle and form an integrated network in the cell: depending on the metabolic inputs their morphology can alter from a more hyperfused state (*e.g.* during nutrient withdrawal) to a more fragmented state (*e.g.* during severe stress, nutrient excess or impaired OXPHOS system)[11]. The remodelling of mitochondria within the network is performed by different families of proteins that control the processes of fusion, primarily mitofusin 1, 2 (Mfn) and optic atrophy 1 (OPA1), and fission, primarily dynamin-related protein 1 (Drp1): these events are also vital for mitochondrial quality control, so that fission can segregate damaged mitochondria and fusion can allow exchange of material between viable mitochondria[12].

An important aspect of mitochondrial morphology is mitochondria-associated membranes (MAMs), contact sites between mitochondria and a specialised subdomain of the endoplasmic reticulum that allow faster and direct signalling between these two organelles: key functions of MAMs include regulation of lipid metabolism and calcium homeostasis[13].

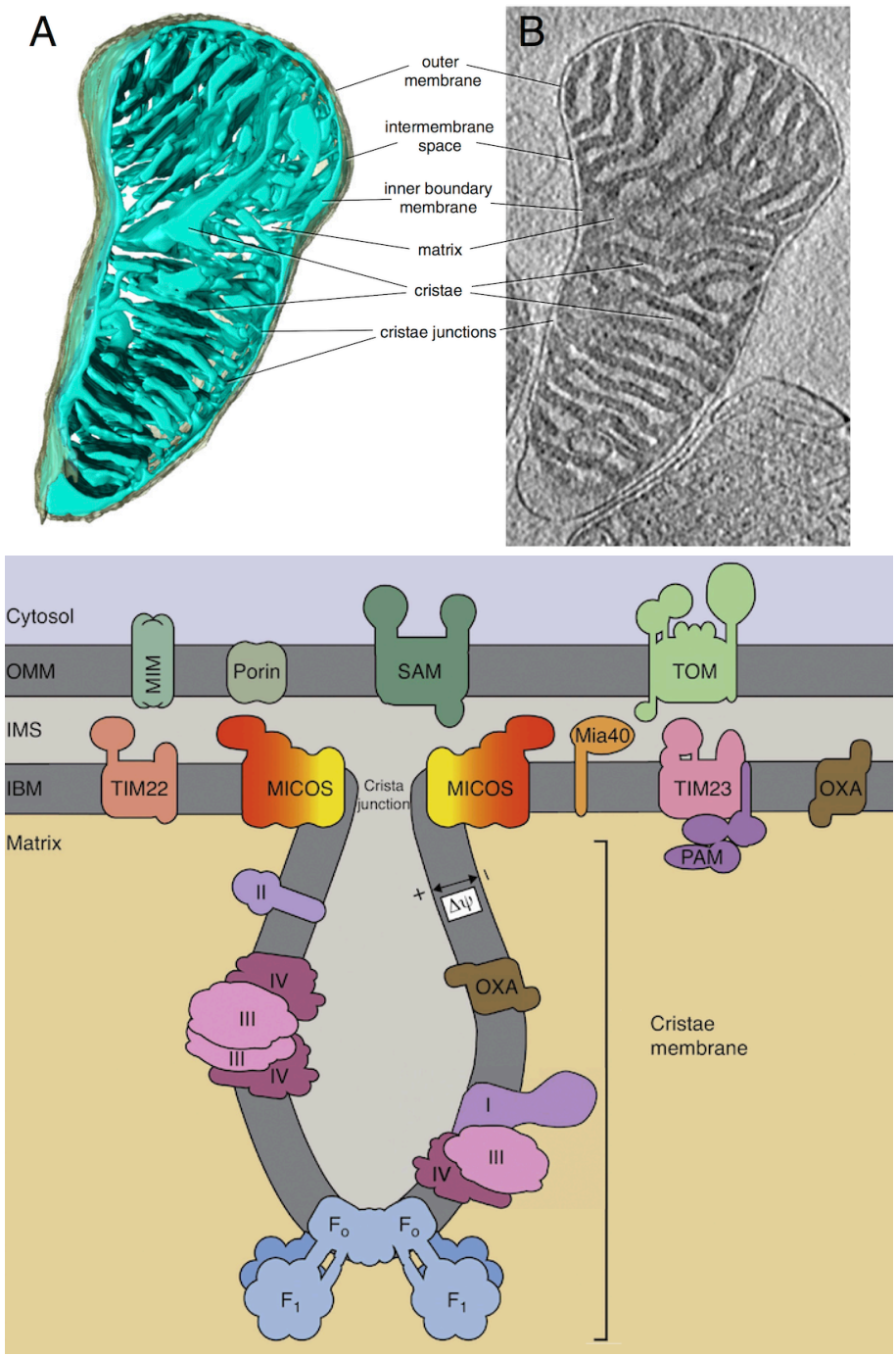

Figure 1.2. Membrane compartments in mitochondria. Top. Three-dimensional volume (**A**) and tomographic slice (**B**) of mouse heart mitochondrion determined by cryo-ET. Picture from Kühlbrandt[14]. **Bottom.** The OMM, IMS and IMM are shown along with typical mitochondrial membrane proteins. The respiratory chain complexes (I, II, III, IV and dimers of V) will be explained in more detail later. MICOS, mitochondrial contact site and cristae organizing system; TIM, translocase of the inner membrane; TOM, translocase of the outer membrane; OXA, oxidase assembly; PAM, presequence translocase-associated motor; MIM, mitochondrial import complex of the outer membrane; MIA, mitochondrial intermembrane space assembly. Picture adapted from van der Laan, Horvath and Pfanner[10].

Mitochondria serve or contribute to a plethora of functions in cells: amino acid metabolism and urea cycle[15], regulation of apoptosis[16], heat generation via UCP-proteins[5], regulation of immune defense, epigenetics and stem cell development[17], β-oxidation of fatty acids[18], Krebs cycle[19], ketone body generation[20], heme biosynthesis[21], calcium storage and signalling[22]. Other functions of mitochondria such as ATP generation, oxidative phosphorylation, ROS formation and signalling, mitochondrial permeability transition and Fe-S cluster biogenesis will be explained in more detail later.

1.3 Structure and functions of enzymes in the respiratory chain

The respiratory chain in mitochondria is classically arranged as shown in Figure 1.3: plant mitochondria possess additional enzymes in their respiratory chain and the canonical enzymes generally have extra subunits than their animal counterparts[23]. Most of the subunits are encoded by the nuclear genome, while mitochondrial DNA encodes 7 subunits of complex I, 1 subunit of complex III, 3 subunits of complex IV and 2 subunits of complex V[24]. Complexes I, III and IV are also known to form multi-enzyme assemblies of different stoichiometries known as supercomplexes[25].

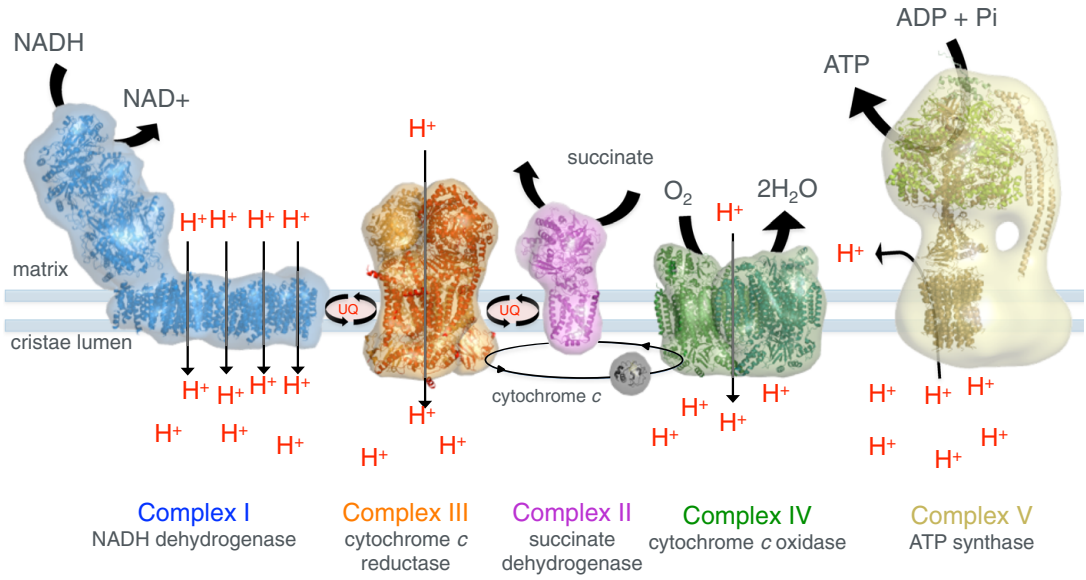

Figure 1.3. Organisation of the respiratory chain. The inner mitochondrial membrane hosts complexes I to V of the respiratory chain and the protonmotive force is generated by the proton gradient via transport of protons across the membrane by complexes I, III, and IV. Endergonic synthesis of free ATP is, then, fuelled by the protonmotive force through complex V. Picture adapted from Kühlbrandt[14].

1.3.1 Complex I

Mitochondrial complex I is located in the IMM, it is made up of 45 subunits (14 conserved core subunits and 31 supernumerary subunits) and it catalyses the oxidation of NADH to NAD^+ and the reduction of ubiquinone to ubiquinol while concomitantly pumping 4 protons from the matrix to the IMS[26].

Figure 1.4 shows the structure of complex I (including the 14 core subunits from the tip of the peripheral arm 51 kDa subunit to the end of the membrane arm ND5 subunit) on the left and a schematic overview highlighting the main functional elements on the right.

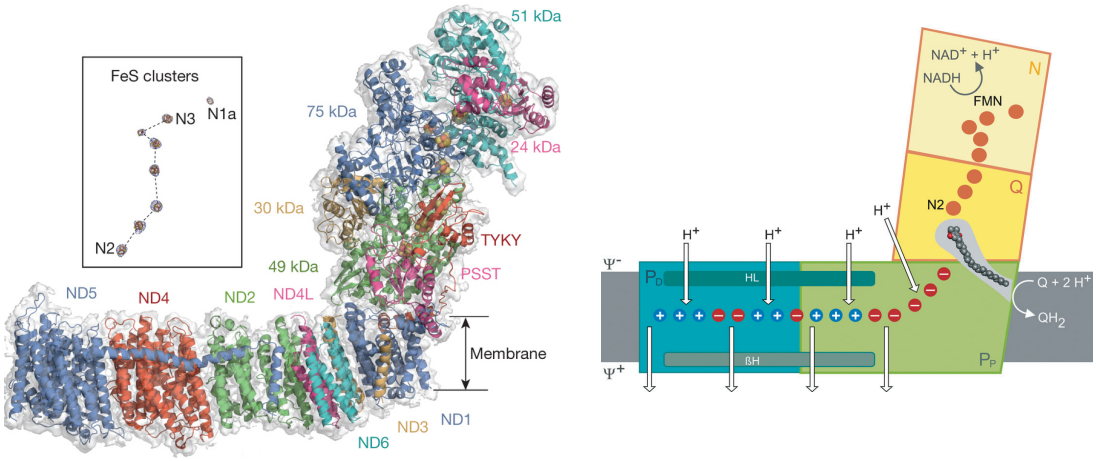

Figure 1.4. The structure of complex I. On the left, intact complex I from *Bos taurus* is shown, with the Fe-S clusters depicted outside the hydrophilic arm for clarity. Picture adapted from Vinothkumar, Zhu and Hirst[27]. On the right, the scheme shows the quinone binding site at the interface between the hydrophilic and membrane domains and the trail of charged residues possibly involved in the proton pumping mechanism, see text for details (picture from Brandt[28]).

The 14 central subunits, common to both prokaryotic and eukaryotic complex I, fulfil the core bioenergetic function of the enzyme (discussed below); the supernumerary subunits in the mitochondrial enzyme are thought to play important roles in biogenesis and assisting the organisation of mitochondrially-encoded hydrophobic subunits[29].

The reaction catalysed by the enzyme is shown below[30]

$$NADH + H^+ + Q + 4H^+_{matrix} \rightarrow NAD^+ + QH_2 + 4H^+_{IMS}$$

In summary, the enzymatic process starts with the binding of the electron donor NADH to the 51 kDa subunit (at the top of the hydrophilic arm), in a juxtaposed configuration over the isoalloxazine system of the flavin mononucleotide (FMN) cofactor to facilitate hydride transfer from the former to the latter cofactor. Then, electrons are transferred through a chain of 7 iron-sulphur (Fe-S) clusters (the role of the additional [2Fe-2S] cluster next to the flavin is unclear) down the hydrophilic arm of the enzyme to the quinone chamber where formation of quinol ensues[31].

1.3.1.1 Substrates and cofactors: NADH and metabolic consequences of complex I inhibition

NAD^+ is obtained in humans by *de novo* synthesis from tryptophan and, more importantly, from salvage pathways from the niacins (nicotinic acid, nicotinamide and nicotinamide riboside)[32]. Figure 1.5 shows the structure of NADH, its standard reduction potential and the chemical change it undergoes upon reduction. While intracellular NAD^+ levels are kept between 0.2 and 0.5 mM, in mitochondria they can be up to four times higher[33].

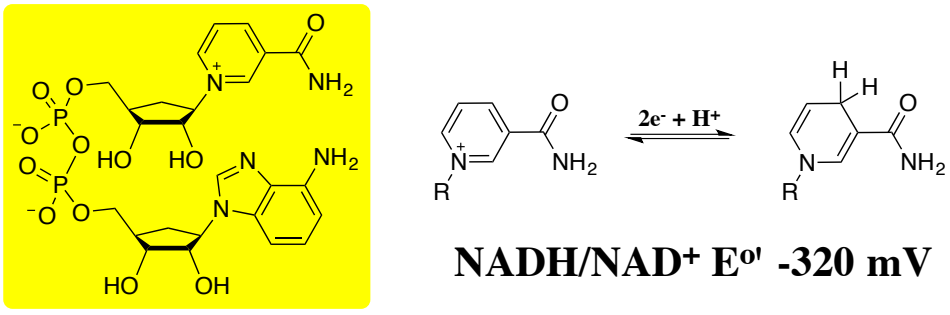

Figure 1.5. NADH structure and its redox states. NADH donates two electrons to complex I via hydride transfer from the nicotinamide ring. Reduction potential taken from Poian and Castanho[34].

Even though in mammals there are a mitochondrial and a nucleocytosolic [NADH/NAD^+] pool (connected with each other by redox shuttles and compartmental NAD^+ biosynthetic pathways)[35], both are kept very oxidised in cells since many cellular processes use NAD^+ as an oxidizing agent to function[36]: obvious examples are the TCA cycle and β-fatty acid oxidation in the mitochondrial matrix, glycolysis and ethanol metabolism in the cytoplasm. In mammals the reducing power of NADH

produced in the cytosol is then transferred into the mitochondrial matrix via either the glycerol 3-phosphate shuttle (which bypasses complex I) or the malate aspartate shuttle (the predominant shuttle in most oxidative tissues[37]), unless it remains in the cytosol where it can be reoxidised by lactate dehydrogenase to form lactate from pyruvate[38].

Figure 1.6 displays major classes of metabolic pathways where NAD^+ and NADH are involved in mammals. Even though NADH can still be oxidized by the nicotinamide nucleotide transhydrogenase in mitochondria (which keeps the NADPH pool reduced at the expense of NADH and proton motive force[39]), an inhibition of complex I causes the NADH/NAD^+ ratio to rise, progressively hampering the above-mentioned processes as well as proton pumping that ultimately leads to decreased ATP production. Furthermore, Santidrian *et al.*[40] reported that a higher NADH/NAD^+ ratio elicited by complex I inhibition (obtained by knockdown of NDUFV1 which encodes the 51 kDa subunit) enhanced the metastatic potential of breast cancer cells (while improving complex I activity reduced tumour growth and metastasis in mice).

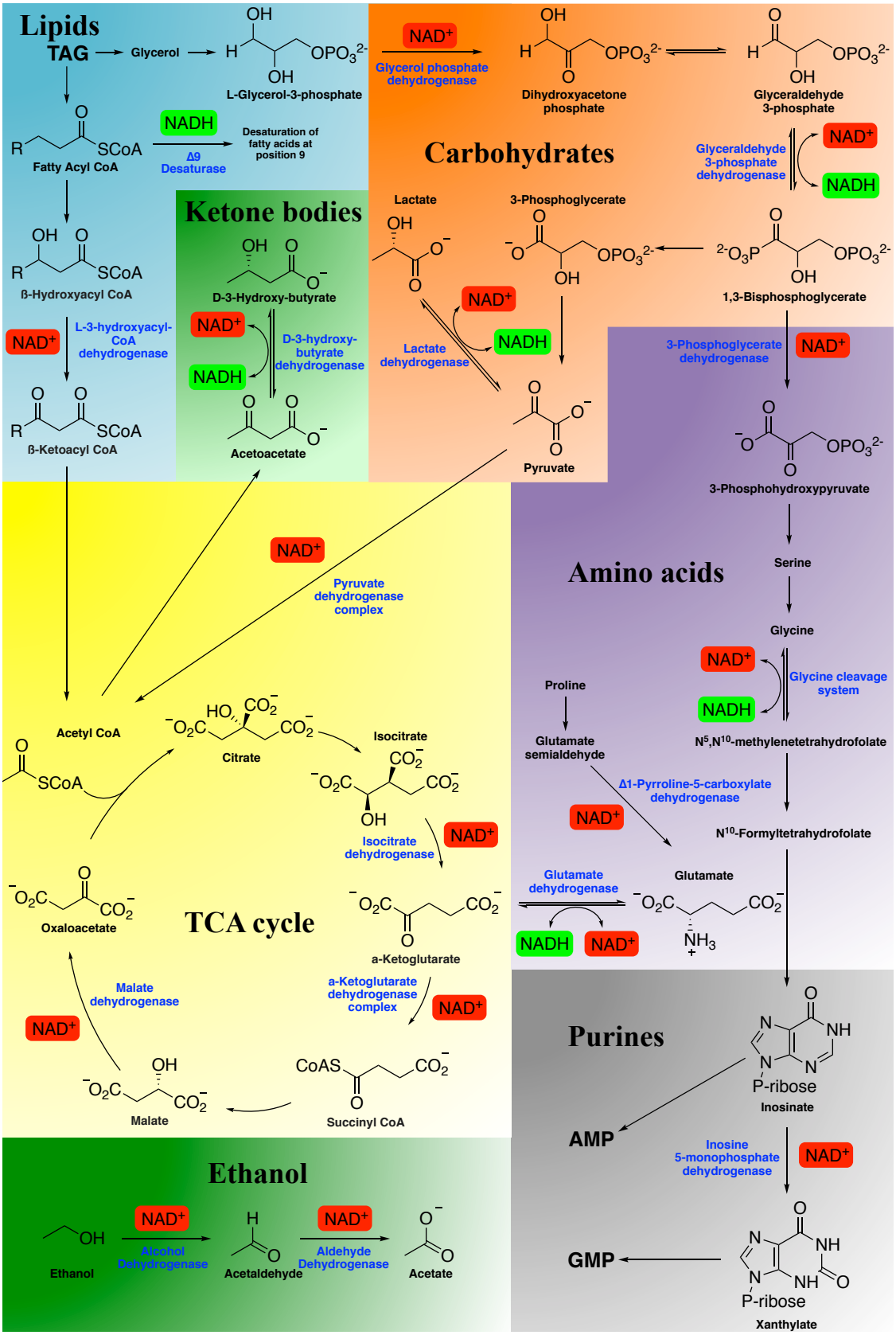

Figure 1.6. Major metabolic pathways using NAD$^+$ or NADH in mammals. Triacylglycerols (TAG, bue area) are split into fatty acids and glycerol: the former will be oxidised and ultimately converted to acetyl CoA towards the TCA cycle (yellow area) which can be redirected towards ketone body formation (light green area), the latter will enter the glycolytic/gluconeogenetic pathway (orange area). The end product of glycolysis, pyruvate, can either be reduced to lactate or converted to acetyl CoA. A side path leads to amino acids and purine biosynthesis (purple and grey areas respectively). Finally, ethanol metabolism requires two equivalent of NAD$^+$ (dark green area). References: Lipids, TCA cycle and glycolysis/gluconeogenesis, McMurry[41]; Desaturase, Nakamura and Nara[42]; Citrate export in TCA cycle, Gnoni *et al.*[43]; Ketone bodies, Newman and Verdin[44]; Ethanol, Louvet and Mathurin[45]; Amino acids, Grant[46], Kikuchi *et al.*[47], Pemberton and Tanner[48]; Purines, Hedstrom[49].

1.3.1.2 Substrates and cofactors: FMN

Figure 1.7 shows the structure of FMN, its standard reduction potential and the different redox states it can assume.

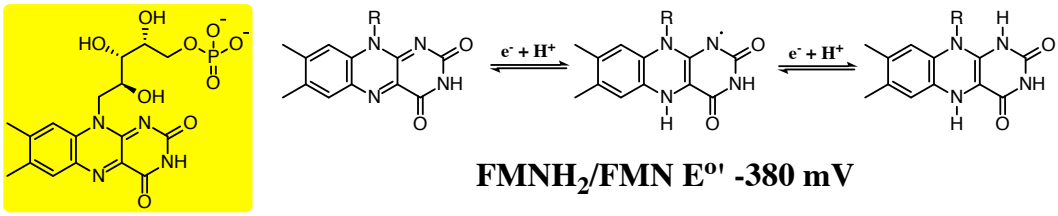

Figure 1.7. FMN structure and its redox states. FMN is capable of assuming different redox states to switch from a two-electrons donor (NADH) to one-electron acceptors (Fe-S clusters). Reduction potential taken from Kussmaul and Hirst[50].

FMN can undergo (just like ubiquinone) one- and two- electron transfer and therefore can serve as a redox switch between obligate two- and one- electron redox partners[51]. The precursor from FMN and FAD is riboflavin (or vitamin B2), which cannot be synthesised by animals and, therefore, it must be acquired from the diet[52]. In humans, riboflavin is converted first to FMN by riboflavin kinase and then FAD synthase adenylates FMN to obtain FAD and also delivers it to the client apo-flavoproteins as a molecular chaperone[53]. It is also noteworthy that transporters for FAD and riboflavin exist in mitochondria[54] and that riboflavin supplementation can be an effective treatment in mitochondrial diseases due to NDUFV1 mutations[55].

1.3.1.3 Substrates and cofactors: Fe-S clusters and electron tunnelling

Figure 1.8 shows the types of Fe-S clusters that can be found in the enzymes of the respiratory chain and the chain of clusters in complex I. Fe-S clusters are inorganic cofactors made up of iron centres and sulphide ions and typically bind to thiolate side chains of protein cysteine residues: they can efficiently shuttle single electrons since the overlap of transition metal orbitals of the iron centres with the orbitals of sulphur allows effective delocalisation across the clusters[56]. The biosynthesis of Fe-S clusters mainly depends on the activity of the cysteine desulfurase NSF1 that provides sulphur atoms by binding to its substrate cysteine and converting it to persulfide (with assistance by accessory protein ISD11 and frataxin): sulphur is then transferred to the scaffold protein ISCU where it will combine with iron[57]. Isoforms of the core components have also been identified in extramitochondrial millieux in humans: they constitute the cytosolic iron-sulphur assembly machinery or CIA[58].

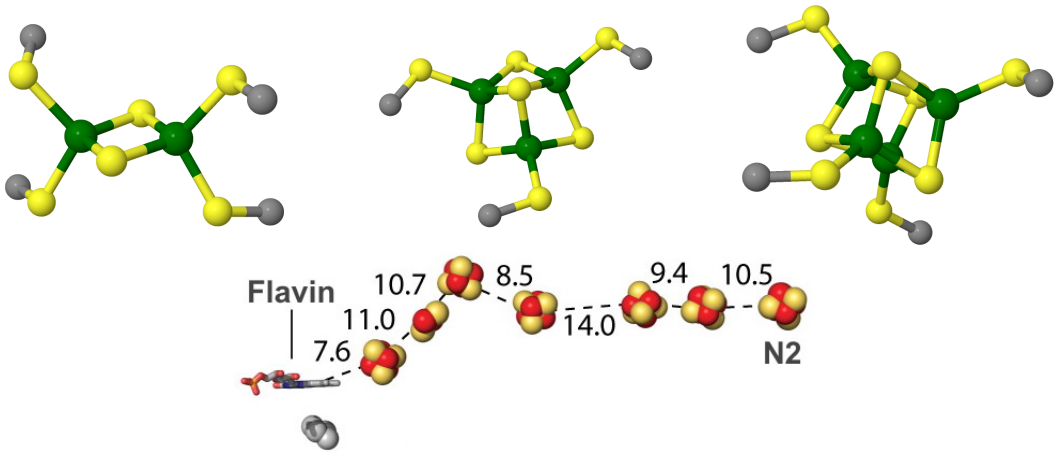

Figure 1.8. Fe-S clusters in the respiratory chain and in complex I. Top. From left to right, exemplifying structures of [2Fe-2S], [3Fe-4S] and [4Fe-4S] Fe-S clusters: the first and the last can be found in complex I, the first in complex III and complex II includes all three types. Colour code: S yellow, Fe green, C grey. Picture from Sharpe and Housecroft[59]. Bottom. FeS clusters in complex I from *Bos taurus*, edge-to-edge distances in Å. Adapted from Hirst[31].

Their role in facilitating electron transfer in proteins is already well-established, and other functions carried out by FeS proteins are molecular oxygen and nitric oxide biological sensing[60] and, more recently discovered, their substantial role in DNA replication and repair[61]. The oxidation state of the iron centres is either (II) or (III), with a high-spin configuration and a tetrahedral geometry: protein bound clusters generally adopt only a pair of overall charge states (for [4Fe-4S] and [2Fe-2S] ferredoxins usually +2/+1, or +3/+2 if they are high potential iron clusters)[62]. Typical reduction potentials range from -700 to -100 mV for clusters that possess cysteine residues, and higher potentials (-100 to 400 mV) for clusters that also possess other ligands, especially histidine[63] (see section 1.3.3 for Rieske protein in complex III). Electron transfer in complex I from the FMN through the Fe-S clusters (and, in general, electron transfers between redox centres in enzymes) occurs via electron tunnelling[64], whereby, under certain conditions, an energetic barrier can be crossed without the energy needed to surmount it[65]. The rate of electronic tunnelling between donor and acceptor depends on four parameters: frequency at which both attain the transition state, difference in their standard potentials, reorganisation energy, both inner sphere (changes in metal-ligand bond lengths and metal centre geometry[a]), and

[a] Electron transfer between Fe-S clusters is generally fast because of a very low inner-sphere reorganisation energy: upon reduction, the strong Fe-S bonds change very little and in both iron oxidation states (II) and (III) tetrahedral geometry is strongly favoured, as opposed to, for instance, four-coordinate Cu(II) and Cu(I) complexes, that favour square planar and tetrahedral geometry, respectively[66].

outer-sphere (changes in solvent molecules orientation) and extent of overlap of their orbitals[67]. Within the protein matrix the latter term is the dominant factor and distance between redox centres is paramount: if this distance happens to be bigger than the threshold value of 14 Å the electron transfer is likely a physiologically unproductive and adverse reaction[68].

The transfer of electrons along the 7 Fe-S clusters in complex I is generally considered to be fast and not rate liming and the longest known distance between clusters (4th and 5th in the sequence, 14 Å in the bovine enzyme) is conserved in *Bos taurus*, *Yarrowia lipolytica* and *Thermus thermophilus*[69]. The potential energy profile for electron transfer in bovine complex I alternates high and low potential FeS clusters[31]. Biological redox chains can often exhibit such an alternating or "roller-coaster" landscape in the energetics of electron transfer (*e.g.* the C-subunit in the photosynthetic reaction centre of purple photosynthetic bacteria *Blastochloris viridis* that facilitates electron transfer to the special pair[70]). Even though the reasons behind the selection pressure to conserve this pattern are not entirely clear, uphill tunnelling steps might play a regulatory role (electron transfer to the chain would accelerate only after a threshold supply of electrons has been accumulated[71]) or even to spatially separate high potential hemes with low potential ones in order to prevent electrostatic interaction from increasing the variability of the chain energy profile[72].

1.3.1.4 Substrate and cofactors: ubiquinone

Figure 1.9 shows the general structure of ubiquinone, its standard reduction potential and the different redox states it can assume. Ubiquinone (or coenzyme Q) is a membrane-bound compound contained in the endomembranes of all animal cells. It consists of a hydrophobic isoprenoid tail that anchor the molecule in membrane lipid bilayers, and a hydrophilic head group that can interact with hydrophilic domains of proteins: it acts as a mobile electron and proton carrier in the respiratory chain (from complexes I and II to complex III, see later) but it has also a role in pro- and anti-oxidant processes[73]. Other enzymes that feed the Q-pool (*i.e.* ubiquinone is their electron acceptor) are electron-transferring flavoprotein ubiquinone oxidoreductase, glycerol 3-phosphate dehydrogenase, dihydroorotate dehydrogenase, choline dehydrogenase, proline dehydrogenase and sulfide:quinone oxidoreductase[74].

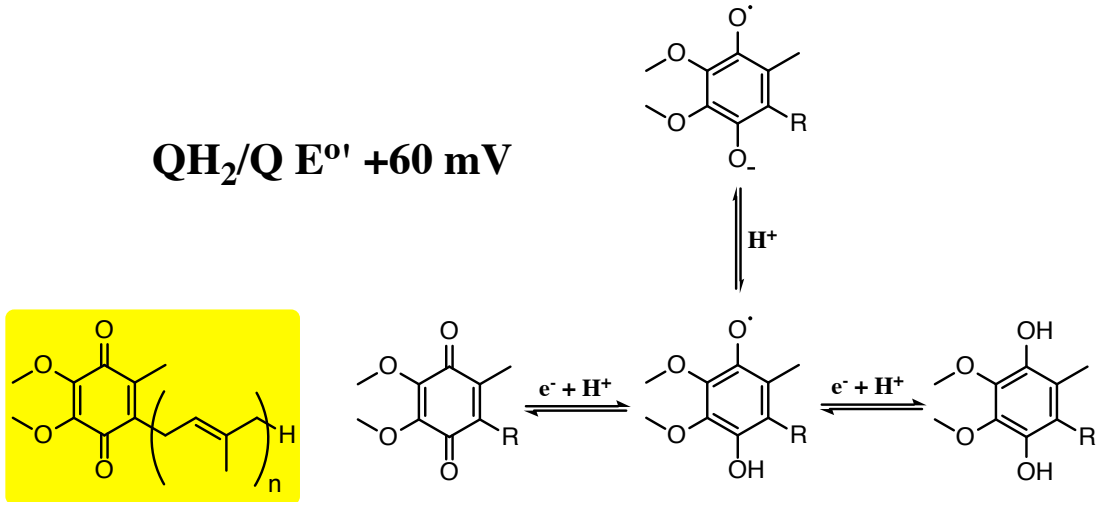

Figure 1.9. Ubiquinone structure and redox states. Ubiquinone, just like FMN, can assume different redox states in order to switch from a two-electron acceptor (complex III) to a one-electron donor (cytochrome *c*, see paragraph on complex III). Reduction potential taken from Vinogradov and Grivennikova[75].

The number of isoprenoid units in the tail varies among species: the predominant forms are Q_{10} in human and dog, Q_9 in rodent and fly, Q_8 in bacteria and Q_6 in yeast[76]. The biosynthesis of ubiquinone has been studied extensively for yeast *Saccharomyces cerevisiae* and the enzymes involved seem to be well conserved in animals, apart from the enzyme that catalyses the committed step of the process (COQ1), the assembly and elongation of the isoprenoid tail. The next steps (attachment of the tail to either one of the 2 precursors, 4-hydroxybenzoic acid or 4-aminobenzoic acid, and ring modifications) are well characterised but the order of reactions in the mammalian system is still not clearly established[77]. In humans, Q_{10} is found at the highest concentrations in heart, kidney, liver and muscle, whereas lung and colon possess the lowest amounts[78]. Finally, the efficacy of Q_{10} supplementation for therapeutic purposes (*e.g.* metabolic control in diabetes[79] and prevention of cardiovascular diseases[80]) is still unclear.

1.3.1.5 Coupling between proton translocation and electron transfer

The exact mechanism of coupling between electron transfer and proton pumping is still unresolved, but it entails two possible major redox energy release points, quinone reduction and, less importantly, reduction of the last cluster N2. The midpoint redox potentials in complex I for FMN and most of the Fe-S clusters are within -370 to -240 mV, hence very similar to the NADH/NAD^+ couple. Only at the last Fe-S cluster of the chain N2 does the potential become more positive (from -20 to -150 mV

depending on the species), and this large energy span (along with the one associated with electron transfter from N2 to ubiquinone) are often assumed to be the major driving force for proton translocation[81]. However, Zwicker *et al.* reported that when the residue responsible for the pH dependency of the redox potential of N2 was mutated (H226M in the 49-kDa subunit in *Yarrowia lipolytica*), the pH dependency was lost and the N2 potential shifted by -80 mV, leaving the proton pumping capacity of complex I unaltered[82]. This suggests that such redox centre is not involved with proton translocation and that the energy to drive this process is linked to redox chemistry of ubiquinone. N2 sequentially transfers two electrons from the FeS wire to ubiquinone (which assumes a semiubiquinone intermediate redox state in the process): notably, the ubiquinone binding site (a long and narrow cavity mostly provided by the PSST, 49- and 30-kDa subunits) is about 20 Å away from the hydrophobic membrane core, where most of the Q pool is located[83]. Once electron transfer from cluster N2 is complete, it is thought that electrostatic interactions would drive conformational changes in the E-channel (ND1 subunit in the corner of the enzyme). At this point, these changes would propagate throughout the membrane arm of the complex via a central axis of charged and polar residues, from ND1 all the way to the end of the membrane domain, ND5, causing proton ejections to the IMS at four sites (three antiporters and the E-channel) from Lys/Glu groups[84]. Whether complex I operates by translocating all four protons at once (one-stroke model) or in two stages (two-stroke model) is still unknown[30].

1.3.1.6 Active and inactive complex I

An interesting feature of mitochondrial complex I is that it can exist in a catalytically active state (A-form) but also in an inactive or dormant state (D-form, sometimes referred to in the literature as “deactive” state). Experimentally, the D-form can be induced by exposing the enzyme to elevated physiological temperatures in the absence of substrate and it is characterised by a so-called temporary lag-phase, wherein NADH oxidation activity is much slower than in the active state: addition of substrate reverts the D-form population into the A-form[85]. Structurally, it has been proposed by Zhu *et al.* that the deactive state is characterised by a disordered loop between transmembrane helices 1 and 2 in ND3, which contributes to the ubiquinone-binding site and, as such, could explain lack of catalytic activity[86]. Some areas of complex I are more exposed in the D-form, such as ND1, ND3 and the NDUFA9

accessory subunit, suggesting an important role for the junction between the hydrophilic and membrane domain of complex I in the conformational rearrangements from A- to D- form[87]. Physiologically, the D-state is manifest when respiration rate is severely decreased and, therefore, the respiratory chain tends to be in a highly reduced state and its activity very limited, especially in highly metabolising tissues such as brain and heart. Subsequent reperfusion (hence reintroduction of oxygen) would eventually restore the A-form status[88]. Crucially, the reactivation of complex I during reperfusion of ischemic tissue brings about oxidative damage and tissue necrosis. It was found that selective S-nitrosation of a key residue in the ND3 region (Cys39) that becomes exposed in the D-form protects from the damage following ischemia-reperfusion injury: the S-nitrosothiol cap is slowly removed by glutathione and thioredoxin, preventing an (unwanted) sudden reactivation of complex I which would cause excessive and damaging formation of ROS[89]. Finally, the D-form in the bovine enzyme has also been shown to possess Na^+/H^+ activity which is abolished when substrate is added and complex I is reactivated[90].

1.3.2 Complex II

Mitochondrial complex II is different in many important aspects from the other enzymes in the respiratory chain: it does not pump protons, it also belongs to the TCA cycle and all of its subunits are encoded by nuclear DNA[91]. Complex II is also known as succinate dehydrogenase (SDH, oxidation of succinate to fumarate) or succinate:ubiquinone oxidoreductase (SQR, reduction of ubiquinone to ubiquinol): additionally, bacterial fumarate reductase (structurally and functionally similar to complex II) catalyses the reverse reaction[92].

The total reaction catalysed by mitochondrial complex II is, therefore, the following[93]

$$Succinate + Q \rightarrow Fumarate + QH_2$$

Complex II is actually a superfamily of enzymes, divided into subfamilies A to E (according to the number of membrane-spanning polypeptides and whether a *b* heme is present or not), but they all share a main structural scaffold, a large soluble domain (where oxidoreduction of succinate and fumarate occurs) with two polypeptide chains (SdhA, a flavoprotein, and SdhB, an iron-sulfur protein containing three Fe-S

clusters) and a smaller membrane domain (where oxidoreduction of ubiquinol and ubiquinone occurs), with other two chains (SdhC and SdhD)[94]. The electron transfer of the enzyme is similar to complex I, since electron transfer proceeds from FAD through a chain of three FeS clusters to ubiquinone. Figure 1.10 shows the structure of complex II on the left and the same structure with the cofactors highlighted on the right.

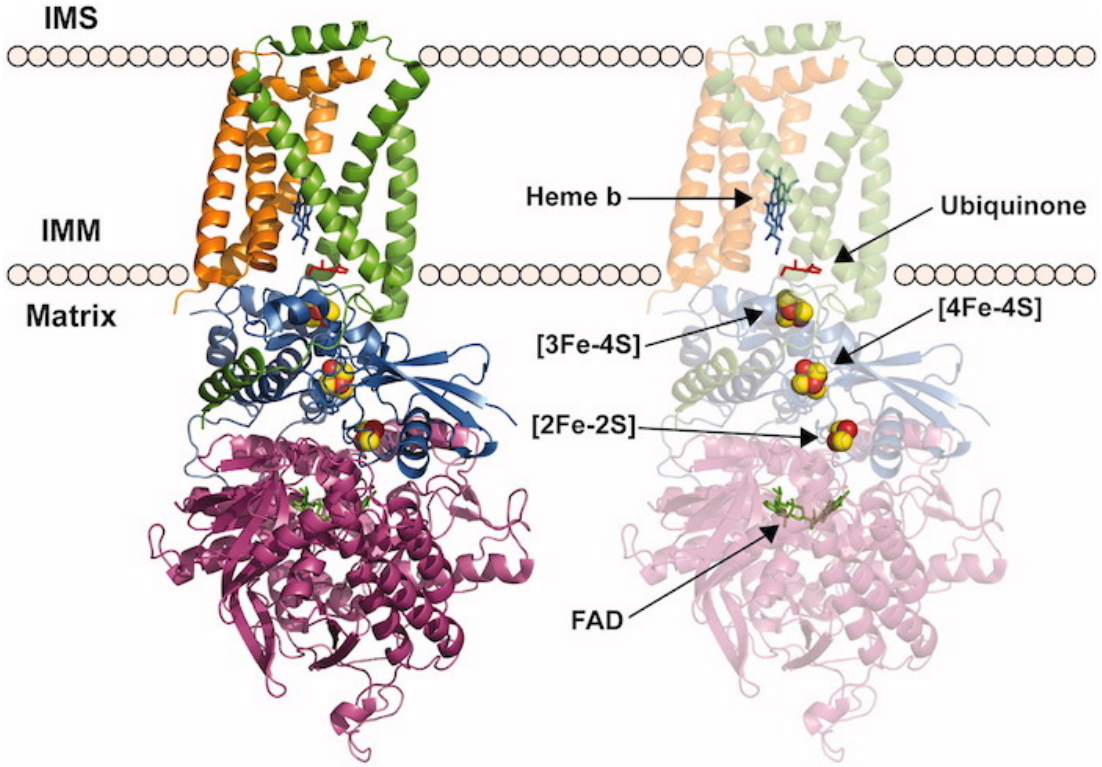

Figure 1.10. The structure of complex II. Porcine succinate dehydrogenase exhibits features typical of the complex II superfamily, namely the four different subunits with FAD and Fe-S clusters in the soluble domain and a *b* heme in the membrane domain. Picture taken from Van Vranken *et al.*[95].

1.3.3 Complex III

Cytochrome *bc*1 (or complex III) catalyses the oxidation of ubiquinol from the IMM Q-pool to ubiquinone and the reduction of two molecules of cytochrome *c*: the energy transfer is coupled to the release of four protons to the IMS, two of which originate from the matrix. The total reaction catalysed by complex III is, therefore, the following[96].

$$QH_2 + 2\ cyt\ c_{ox} + 2H^+_{matrix} \rightarrow Q + 2cyt\ c_{red}\ + 4H^+_{IMS}$$

The homodimeric cytochrome *bc*1 complexes share the same catalytic core, a cytochrome transmembrane subunit containing two *b*-type heme groups (b_L and b_H on account of their low and high potential, respectively) and two soluble domains, a Rieske Fe-S protein[b] called ISP and another cytochrome subunit with a *c*-type heme called cytochrome c_1[97]. Owing to the nature of electron acceptor and donor in this enzyme (ubiquinone carries two electrons whereas cytochrome *c* only carries one), a switch from a two-electron to a one-electron carrier is needed in the catalytic mechanism, the so-called Q cycle. The current level of understanding of the Q cycle involves, critically, a bifurcated electron transfer whereby one molecule of ubiquinol binds to the Q_o site and is sequentially oxidised with one electron taking a high potential path (through the Rieske protein and cytochrome c_1) that will ultimately reduce cytochrome *c*, and the other electron taking a low potential path (through the hemes b_L and b_H) that will ultimately reduce a second ubiquinone molecule (bound to another site, Q_i) to semiubiquinone radical. Another repetition of the cycle will generate another reduced cytochrome *c* and will reduce semiubiquinone to ubiquinol in the Q_i site[98]. Interestingly, movement of the ISP protein was shown to be required for electron transfer from the Q_0 site to c_1[99]. Figure 1.11 shows the structure of complex III on the left and a cartoon illustrating the Q-cycle on the right.

[b] While most FeS centres have negative reduction potentials, Rieske proteins are an exception: their reduction potentials are higher and usually positive because their [2Fe-2S] cluster has one Fe coordinated by two imidazole ligands rather than cysteine, and this stabilises the metal centre as Fe(II)[59].

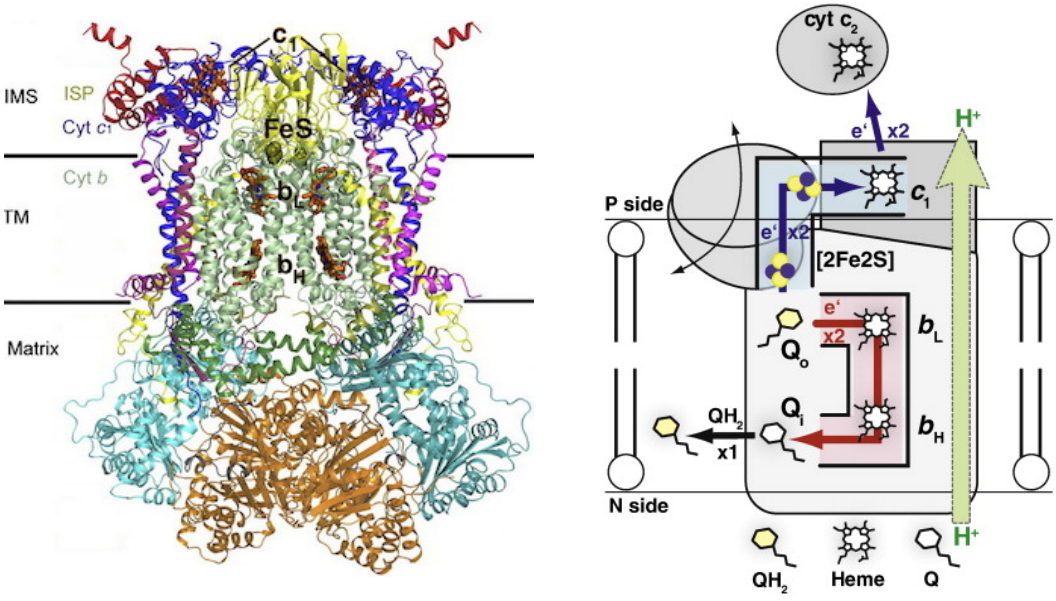

Figure 1.11. Structure of complex III and Q cycle. On the left, *bc*1 homodimer complex from bovine mitochondria is shown. The heme groups and FeS cluster are highlighted in black. Picture taken from Xia et al[98]. On the right, a schematic representation of the Q-cycle is depicted, with the high potential path (blue arrow), low potential path (red arrow) and movement of the Rieske protein (black double-headed arrow) highlighted. Picture taken from Cooley[97].

1.3.4 Complex IV

The terminal enzyme of the respiratory chain in mitochondria is cytochrome *c* oxidase or complex IV. It catalyses the reduction of molecular oxygen to water by delivering 4 "chemical" protons to the former and, at the same time, pumps 4 protons per electron in the IMS to contribute towards Δp. The total reaction catalysed by complex IV is, therefore, the following[100]

$$4cyt\ c_{red} + O_2 + 8H^+_{matrix} \rightarrow 4cyt\ c_{ox} + 2H_2O + 4H^+_{IMS}$$

The eukaryotic enzyme contains an overall of 13 subunits but the three largest subunits include the catalytic core of the enzyme and are very similar to their bacterial counterparts. The prosthetic groups embedded in the main catalytic subunits are, in order of electron transfer sequence, a copper site (Cu_a, with two copper centres), a heme group (heme *a*) and a heme/copper centre (heme a_3/Cu_b)[101]. The mechanism is not unanimously accepted but there is widespread agreement on the major key points: molecular oxygen binds the iron in heme a_3/Cu_b when both metal centres are reduced and then one oxygen atom is transferred as OH^- to Cu_b; further reduction and proton

transfer converts the other oxygen into OH^- and then both hydroxyl ligands become protonated and exit the metal centre as H_2O. Three possible proton-transfer pathways have been identified: K- and D- transfer protons for water formation at the O_2 reduction site, whereas H- is for pumping protons towards the transmembrane proton gradient[102]. Figure 1.12 shows the structure of complex IV on the left and a scheme illustrating the cofactors and the possible proton pathways on the right.

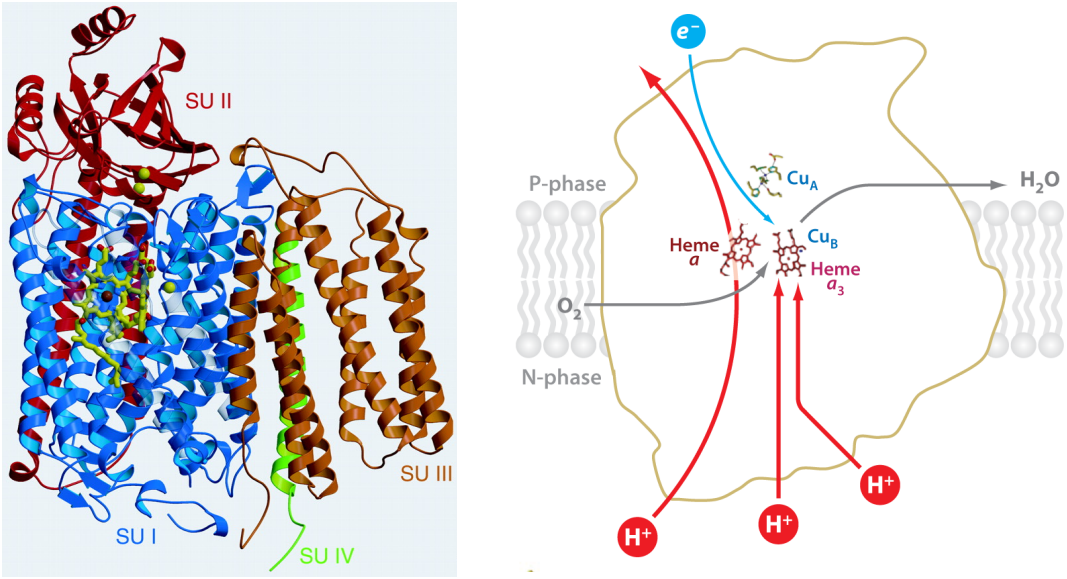

Figure 1.12. Structure of complex IV. On the left. Complex IV from *Rhodobacter sphaeroides* highlighting the major subunits and cofactors. Picture taken from Nyquist *et al.*[103]. On the right, cartoon representing the three putative proton channels and the prosthetic groups in complex IV. Picture taken from Yoshikawa and Shimada[102].

1.3.5 Complex V

The protons pumped from the matrix to the IMS by complexes I, III and IV generate a PMF that is used by ATP synthase (or complex V) to catalyse the conversion of ADP to ATP. The enzyme exists as a dimer in mitochondria, forming V-shaped rows along the cristae that contribute to the curvature of the IMM[104]. The core subunits of bacterial complex V are located in the F_0 membrane sector (a_1, b_2 and $c_{10\text{-}15}$) and in the F_1 hydrophilic sector (α_3, β_3, γ, δ and ε), and the mitochondrial enzyme contains more peripheral subunits to the core ones[105]. The rotational catalytic activity starts with the transport of protons at the interface between the a and c subunits where they are loaded into the membrane part of the rotor: this drives rotation of the rotor and the movement of its hydrophilic part (γ and ε subunits) induces conformational changes

in each β subunit (which can assume ADP-bound, ATP-bound and empty forms) leading to ATP release (complex V can also work in reverse leading to ATP hydrolysis)[106]. Figure 1.13 shows a model of the *c*-ring and the way proton motion drives its rotation.

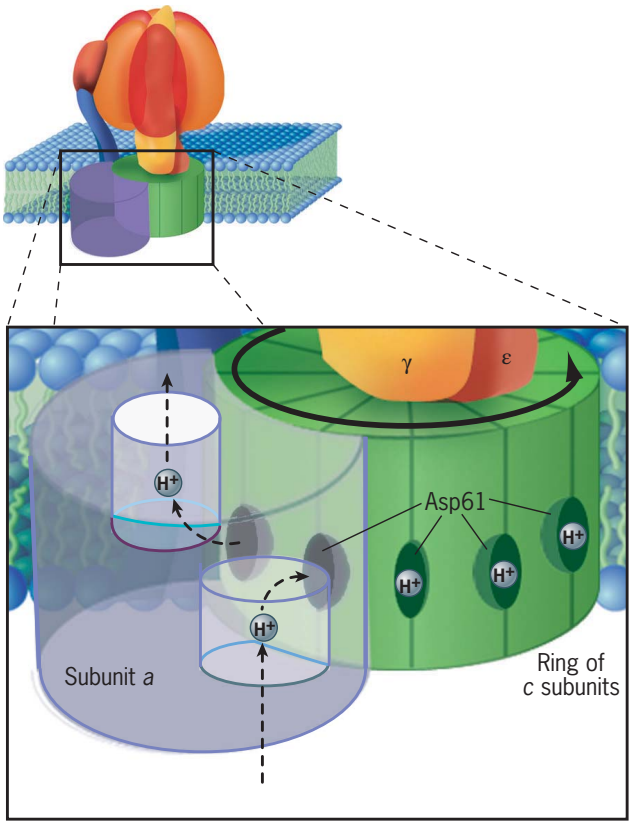

Figure 1.13. Rotation of the *c*-ring fuelled by protons. Each proton from the IMS binds to an acidic residue (Asp61 in *E. coli*) through a half-channel in the *a* subunit. Proton binding elicits successive rotations of the *c*-ring whereby a bound proton undergoes a full circle before entering the matrix via a second half-channel. Picture from Iwasa and Marshall[107].

It is actually the release of ATP from the β subunit that requires the PMF, not formation of the (enzyme-bound) ATP itself, and magnesium ion plays a key role in ATP synthesis, since it acts as a separate substrate with ADP and Pi and it is bound to ATP upon product release: the chemical reaction catalysed by complex V is, therefore, the following[108]

$$ADP^{3-} + P_i^{2-} + Mg^{2+} + H^+ \rightarrow MgATP^{2-} + H_2O$$

Each 360° rotation of the rotor produces 3 ATP molecules and requires a number of protons equal to the number of the c subunits: the bovine enzyme (and most likely all vertebrates) possesses a c_8 ring, thus the bioenergetic cost to complex V is 2.7 protons

per ATP plus one proton that accounts for electrogenic exchange of ATP for ADP combined with non-electrogenic symport of Pi and a proton, totalling to 3.7[109]. The stoichiometry of the *c*-ring is constant within a species but the number of unit varies, from eukaryotic smaller *c*-rings (*e.g. Saccharomyces cerevisiae*, 10 units) to larger prokaryotic and chloroplast larger *c*-rings up to 15 subunits (*e.g. Ilyobacter tartaricus*, 11 units, *Spinacia oleracea*, 14 units)[110]. Figure 1.14 shows a scheme of complex V on the left and its structure from bovine mitochondria on the right.

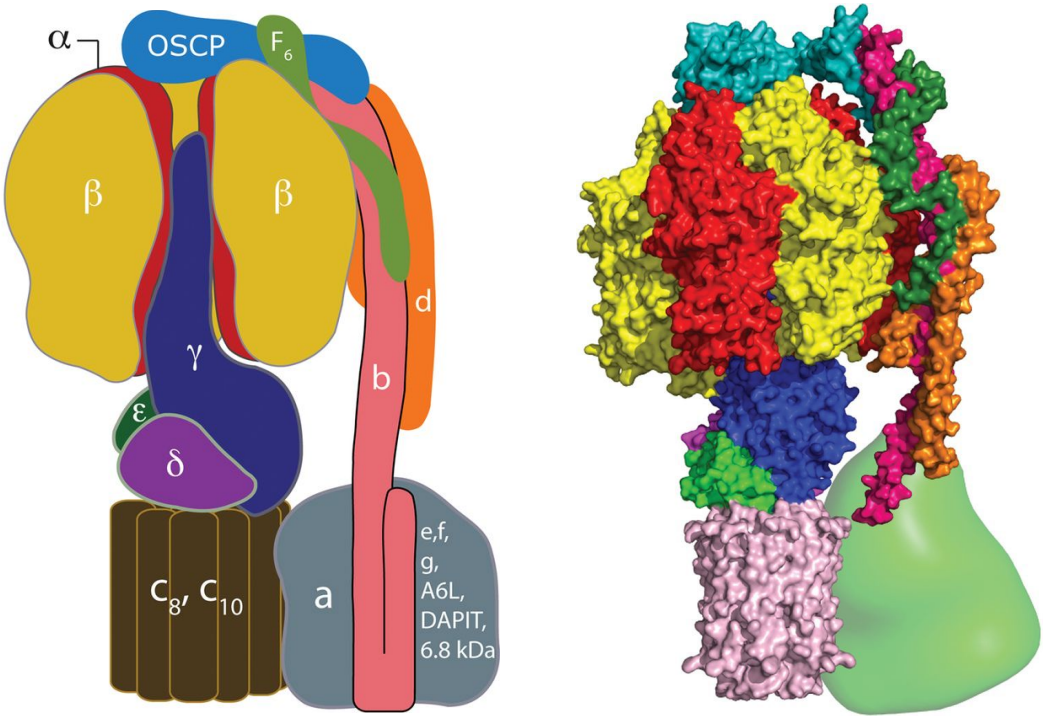

Figure 1.14. Structure of complex V. On the left, cartoon of the mitochondrial enzyme representing the major subunits. On the right, molecular structure from bovine mitochondria. Pictures taken from Walker[109].

1.4 The mitochondrial permeability transition pore

An important topic of mitochondrial physiology, especially linked to drug-induced mitochondrial dysfunction, is the mitochondrial permeability transition (MPT). It is defined as the permeabilisation of the IMM to solutes up to 1.5 kDa (due to the formation of a protein pore) and facilitated by events such as Ca^{2+} overload and oxidative stress[111]. The consequences of MPT are very severe and commonly linked to mitochondrial dysfunction: as for long-lasting openings, these includes mitochondrial depolarisation, arrest of ATP synthesis, depletion of matrix substrates

and ultimately matrix swelling and release of proapoptotic proteins (in contrast to short-term openings that could be involved in physiological Ca^{2+} regulation and ROS homeostasis)[112]. The molecular identity of the protein pore has been (and still is) a matter of intense debate, with many different suggested formulations: genetic inactivation of putative components have disproved the need for once considered indispensable elements of the pore such as the adenine nucleotide translocator (ANT), voltage-dependent anion channel (VDAC), phosphate carrier (PiC) and translocator protein (TSPO). The role of the prolyl isomerase Cyclophilin D (and its inhibitor Cyclosporin A) in modulating the MPT by lowering the Ca^{2+} load required for pore opening is nowadays fully accepted [113]. Crucially, progress in the determination of the molecular identity of the pore has led to the discovery of the possible role of Complex V in MPT: the two leading ideas about the mechanisms on how such enzyme may be involved (through the interface of its dimers or via the *c*-ring) have recently been proposed to act in a unified way[114]. The MPTP is pharmacologically important, inasmuch as it is a viable drug target (for instance, a very recent work highlighted how its pharmacological deactivation via a CypD inhibitor, JW47, can offer neuroprotection in multiple sclerosis in mice[115]; on the other hand, several drugs can trigger MPTP, such as Methapyrilene (via liver glutathione depletion[116]), Minocycline (mitochondrial swelling and *cyt c* release[117]), Betulin (CsA dependent and cholesterol-enhanced *cyt c* and caspase activation[118]) and Tetrandrine (CsA dependent *cyt c* and caspase activation[119]).

1.5 ROS

Reactive oxygen species (or ROS) are reactive byproducts of aerobic metabolism formed within the cell: depending on their chemical nature, they can be divided into radicals (*e.g.* superoxide ion $O_2^{\bullet-}$, hydroxyl $OH^{\bullet}$) and nonradicals (*e.g.* hydrogen peroxide H_2O_2)[120]. The main endogenous ROS-generating cellular systems are depicted in Figure 1.15. Even though O_2 can be irreversibly reduced all the way to water (from a thermodynamic perspective), it is kinetically relatively inert because of spin restriction (it cannot accept two electrons with antiparallel spin at the same time): enzymes that use O_2 as substrate, therefore, employ one-electron cofactors to prevent such electron transfer restriction[121]. The one-electron reduction of O_2 to $O_2^{\bullet-}$ in mitochondria occurs by protein-bound electron carriers and depends not only on

substrate concentration but also on how much enzyme is capable of interacting with O_2 to actually generate superoxide: the reduction is thermodynamically favourable, but it is kinetic factors that mostly control the reaction[122]. Superoxide can then be further reduced to H_2O_2 via a disproportionation reaction, which can occur spontaneously at physiological pH but, more importantly, via superoxide dismutase (SOD): while the CuZn isoform is found in the mitochondrial IMS, the Mn isoform is found in the mitochondrial matrix[123]. Hydrogen peroxide can generate the more reactive and toxic hydroxyl radical in a chemical fashion with an appropriate electron donor: depending on the identity of the latter, the Fenton reaction (reduced iron center such as Fe^{2+} or Cu^{+}) or the Haber-Weiss reaction (superoxide ion) can take place[124].

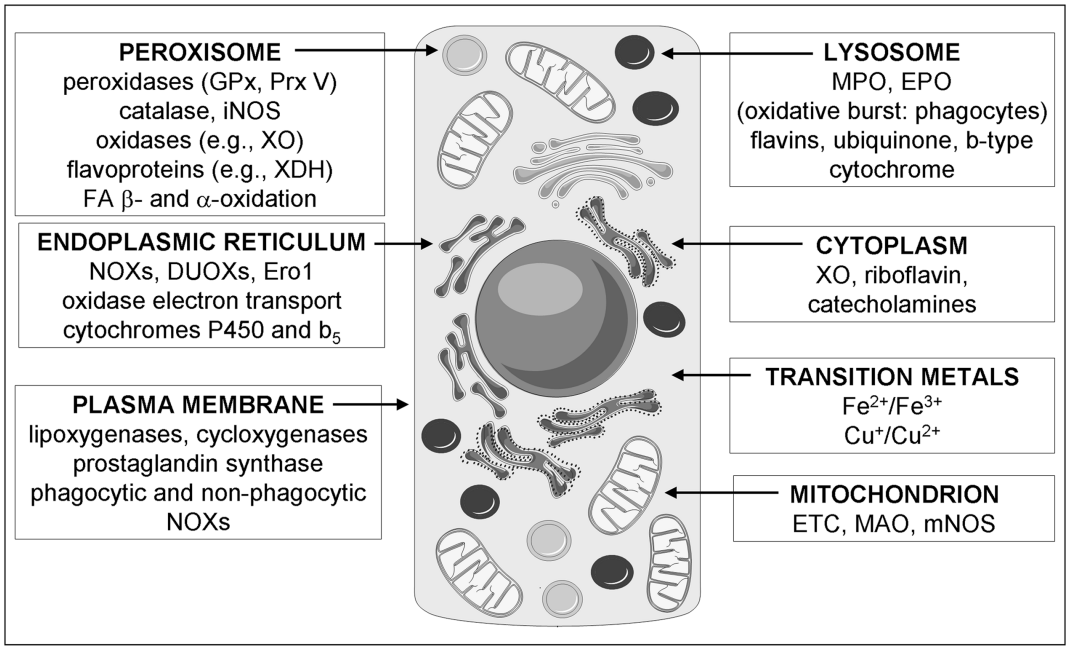

Figure 1.15. The major cellular sources of ROS. Enzymes and chemical electron donors located in the cytoplasm and in several organelles contribute to ROS generation in cells. Particularly relevant to mitochondria are the electron transfer chain (ETC) in the inner mitochondrial membranes and monoamine oxidases (MAO) in the outer mitochondrial membrane. Picture taken from Bachi, Dalle-Donne and Scaloni[120]. NOX, NADPH oxidase; DUOX, dual oxidase; XO, xanthine oxidase; MPO, myeloperoxidase; EPO, eosinophil peroxidase; GPx, glutathione peroxidase; Prx, peroxyredoxin; mNOS, mitochondrial nitric oxide synthase; iNOS, inducible nitric oxide synthase; XDH, xanthine dehydrogenase; Ero1, ER oxidoreductin 1.

Mitochondria are both important sources and sinks of ROS, but whether this organelle is the major cellular source or not is still debated[125]. ROS are key players in signalling pathways regulating immune response, autophagy, cell proliferation, angiogenesis and differentiation, but concentrations large enough to surpass local antioxidant

capabilities can trigger oxidative stress, aging and cell death[126,127]. ROS signalling primary targets are cysteine residues, owing to their intrinsic rich chemistry: ROS-mediated redox modifications include sulfenylation (-SOH), sulfinylation ($-SO_2H$) and sulfonylation ($-SO_3H$) and these modifications play a role in regulation of different protein functions such as ligand binding activity, protein-protein interactions and protein stability[128]. The ROS entity involved in cysteine signalling is H_2O_2 on account of its biochemical features: its steady-state intracellular concentration levels, nM to low μM range, are much higher than $O_2^{\bullet-}$ (due to the very large rate constants for both chemical and SOD-driven dismutation to H_2O_2 and water), it is a mild oxidant and it can easily cross membranes, directly or via aquaporin-mediated transfer[129]. H_2O_2 is primarily metabolised in cells by two enzyme families, peroxiredoxins (Prx) and glutathione peroxidase (GPx), and the enzymes responsible for recycling the enzymes back to their active state with NADPH are thioredoxin (Trx) and glutathione reductase (GR), respectively: the isoform Prx3 is more efficient at scavenging H_2O_2 than Prx5, while Gpx1 (matrix soluble) is more H_2O_2-specific than Gpx4 (which eliminates lipid hydroperoxides)[130]. Catalase, usually considered a peroxisomal H_2O_2 scavenger protein, is also present in mitochondria[131]. Figure 1.16 shows the main ROS degradation pathways in mitochondria.

Mitochondrial complex I can generate ROS while working in reverse (reverse electron transport or RET), where ubiquinol transfers electrons back to complex I while generating NADH via NAD^+ reduction: this happens when $FADH_2$-related substrates (*e.g.* succinate or fatty acids) are preferentially used leading to reduction of the ubiquinone pool and generating a membrane potential and favourable thermodynamic conditions for such an electron transfer to happen[132]. RET at complex I was shown to be the culprit of ROS-linked damage during ischemia/reperfusion injury[133].

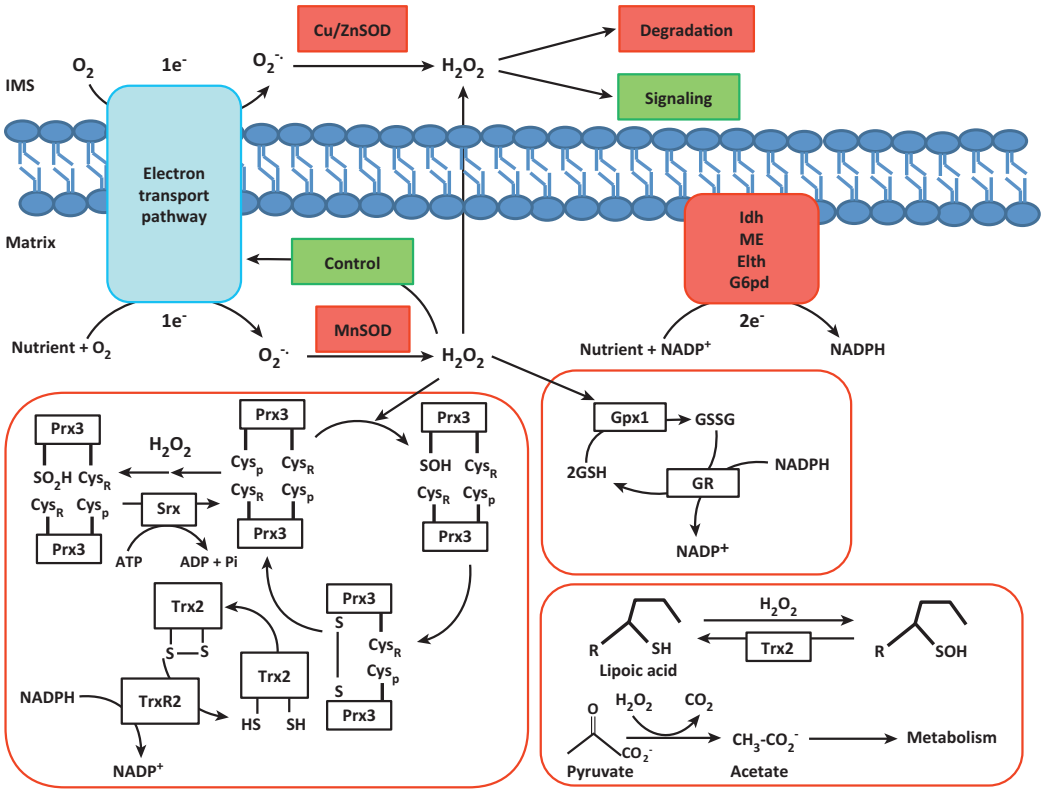

Figure 1.16. $O_2^{\bullet-}$ and H_2O_2 metabolism in mitochondria. The ETC generates $O_2^{\bullet-}$ on both sides of the inner mitochondrial membrane and that is rapidly converted to H_2O_2: its metabolism can involve either Prx or Gpx pathways, and those are regenerated by Trx and GR, respectively, ultimately requiring NAPDH. Other ways of H_2O_2 sequestration involve lipoic acid and pyruvate. Picture taken from Mailloux, McBride and Harper[130]. Idh, isocitrate dehydrogenase; ME, malic enzyme; Elth, energy liberating transhydrogenase; G6pd, glucose-6-phosphate dehydrogenase; GSH, glutathione; GSSG, glutathione disulphide.

1.6 The cellular response to hypoxia and O_2-sensing capabilities of mitochondria

1.6.1 Mitochondrial ROS and hypoxia

One of the roles of mitochondria is to trigger a response upon detection of hypoxia in cells: while the detailed mechanisms are not yet completely understood, the role of ROS production by complex III in hypoxia signalling seems to be critical[134]. ROS (particularly superoxide) are also produced by complexes I and II but they are directed towards the matrix and easily sequestered by MnSOD, as opposed to complex III-generated ROS that can be released to both sides of the inner membrane (especially superoxide that is formed within the inner membrane but ejected in the intermembrane space on account of the huge electrical field inside it) and, as such, exert a potentially more extended signalling power[135]. In order to indirectly modulate

ROS generation at complex III, then, electron flow through this enzyme could be blocked upstream at complex I: this strategy would firstly lead to increased generation of ROS at complex I and, more importantly, to an overall decrease in ATP production due to lower proton pumping by these two enzymes.

A more selective strategy for the same target is to employ compounds that can inhibit ROS formation while keeping other aspects of mitochondrial physiology (proton pumping in particular) unaltered. One such molucule is Terpestacin, an anti-angiogenic drug: its molecular target is Ubiquinol-cytochrome c reductase binding protein (UQCRB), a subunit of complex III which is involved in complex III-mediated ROS generation during the hypoxia response[136,137]. Even more recently, a series of selective suppressors of superoxide generated at complex III that leave energy metabolism and membrane potential unimpaired (called "S3QELs") was introduced[138].

1.6.2 The hypoxia-inducible transcription factor

The reason why targeting mitochondrial ROS (especially originating from the ETC) could be an attractive strategy for cancer therapy is the hypoxia-inducible transcription factor (HIF-1). HIF-1 is a transcription factor that, during hypoxia, targets genes primarily responsible for either increasing O_2 delivery such as erythropoietin (EPO, synthesis of red blood cells) and vascular endothelial growth factor (VEGF, angiogenesis)[139] or decreasing O_2 consumption: these are mainly proteins involved in glucose metabolism such as glucose transporters, glycolytic enzymes, lactate dehydrodenase A (LDHA) and pyruvate dehydrogenase kinase-1 (PDK1)[140]. Figure 1.17 summarises the key points that will be described in this section.

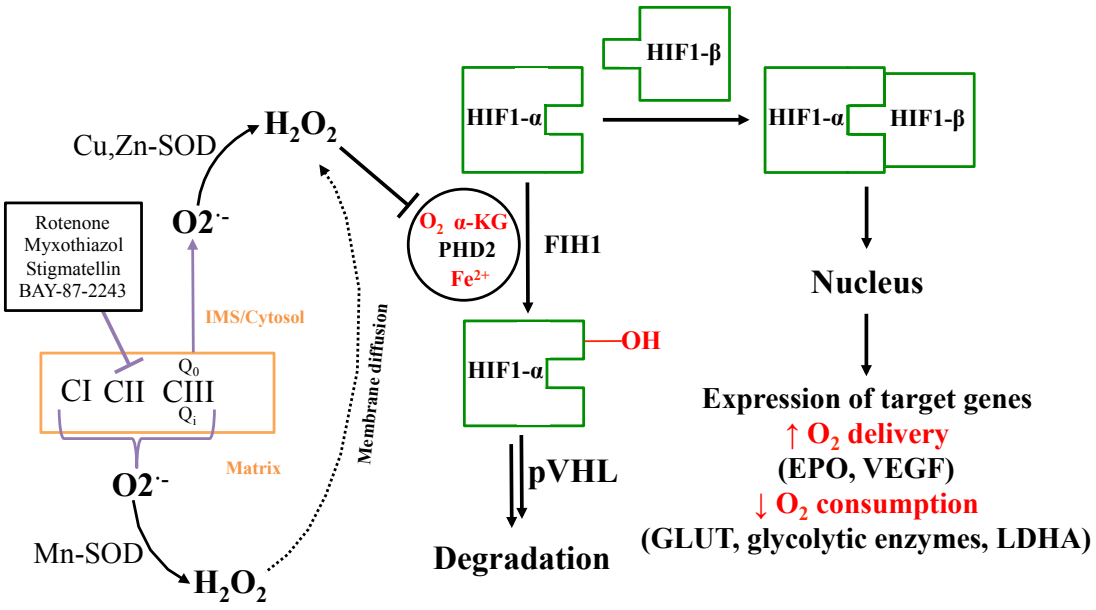

Figure 1.17. Cellular response to hypoxic stress and mitochondria as O_2 sensors. Superoxide ion is produced at higher rates during hypoxia and quickly converted to hydrogen peroxide. In the cytosol, hydrogen peroxide inhibits the enzyme PHD2 which, in normoxic conditions, would otherwise direct HIF1-α towards degradation. Instead, the now active HIF1-α dimerises with HIF1-β and initiates the hypoxic response in the nucleus. EPO, erythropoietin; VEGF, vascular endothelial growth factor; GLUT, glucose transporters; LDHA, lactate dehydrogenase A. References are listed in this paragraph.

1.6.2.1 Structure and activity of HIF-1

HIF-1 is a heterodimer of an unstable, oxygen-sensitive α-unit and a stable, oxygen insensitive β-unit: these two are part of the HIF family of proteins that includes 5 major isoforms[141]. Under normal oxygen cellular concentrations (normoxia), the hydroxylation of HIF1α by prolyl hydroxylase domain protein 2 (PHD2) and factor inhibiting HIF-1 (FIH-1) precede ubiquination by the von Hippel-Lindau protein (VHL) and the eventual proteasomal degradation. During hypoxia, though, the inhibition of hydroxylating enzymes causes stabilisation of HIF1α: dimerization with HIF1β follows, thus allowing the newly formed transcription factor dimer (along with the coactivator p300) to migrate to the nucleus and bind to target genes[142]. Molecular oxygen is a substrate for both PHD2 and FIH but the K_m is much higher for FIH, rendering PHD2 (and, ultimately, HIF1α) very sensitive to O_2 level variations[143].

1.6.2.2 The Warburg effect

The HIF response fits with two major features of cancer cells: hypoxia and greater glucose uptake and metabolism. The growth of cancer cells tends to outpace the blood supply ability to provide them with nutrients and oxygen: the resulting hypoxic

environment is managed by invoking HIFs[144]. Most cancer cells exhibit a peculiar metabolic phenotype called the "Warburg effect" in which glucose uptake is much higher than in normal cells. Most of the glycolytic pathway of cancer cells is devoted to feeding biosynthetic pathways (particularly important is the pentose phosphate pathway for NADPH and nucleotide precursors synthesis) and what is left in the form of pyruvate is preferentially reduced to lactate rather than being oxidised to acetyl CoA and fed into the TCA cycle in mitochondria. Within this phenotype, mitochondrial ATP production still operates, but the TCA cycle is replenished by other fuels such as glutamine, effectively uncoupling glycolysis from OXPHOS[145,146]; in addition, the [NADH]/[NAD^+] balance is kept low by lactate dehydrogenase (which contributes to acidification of the tumor microenvironment) and also by the plasma membrane electron transport (PMET)[147].

1.6.2.3 Mitochondria and ROS in cancer

The hypoxia-response pathway is crucially dependent on mitochondrial ROS, since hypoxia increases mitochondrial ROS generation, especially superoxide from complex III, and this stabilises HIF-1α via inhibition of PHD2, even though the mechanism is still elusive: remarkably, tumour cells are capable of recruiting mitochondria to enhance ROS-derived HIF activation[148]. However, H_2O_2 can actually cross the IMM (either by diffusion of via aquaporins) [149], thus the precise identification of its enzymatic source is not clear-cut (see chapter 6 for a discussion about the mode of action of the drug BAY-87-2243). A recent study by Lee *et al.* showed how PHD2 can be rendered inactive by disulphide bond-mediated dimerization caused by increased ROS levels in oncogenic signalling pathways[150]. More generally, it is now possible to appreciate why cancer cells exhibit very high rates of glycolysis combined with a fully (but different to normal cells) operating TCA cycle: rapidly proliferating cells need ATP to sustain growth, oxidative metabolism in cancer cells produces substantial amounts of ROS that are conveyed towards signalling pathways promoting tumorigenesis and, in order to prevent ROS damage, high levels of antioxidant activity in the form of NADPH are generated[151]. HIF-1α stabilization under hypoxia mediated by ROS from complex III is not a unanimously accepted model: some evidence, for instance, suggests that the increased cytosolic O_2 levels due to reduced electron transport chain activity could be enough to fully stabilise PHDs, thus leading to normal HIF-1α degradation[152].

1.6.2.4 Strategies for cancer therapy targeting the hypoxia response

Given the prominent role of HIF-1 in tumour survival and growth, new possibilities for cancer therapy have emerged in the past 20 years. Inhibitors of HIF-1α can be distinguished according to their mechanism of action: chemical inhibitors include inhibitors of transcription or DNA binding (YC-1, PX-12, Pleurotin, Echinomycin, polyamides, Flavopiridol, Chetomin, Brotezomib), inhibitors of protein translation (Silibinin, 2-Methoxyestradiol, Phenethyl isothiocyanate) and promoters of protein degradation (Geldanamycin, Radicicol, Trichostatin A, Wondonin, Resveratrol). Given their common lack of specificity, more promising fields are monoclonal antibodies (Cetuximab, Herceptin), nucleic adic inhibitors (RX-0047) and heavy-chain antibodies[153].

1.6.3 Mitochondria as drug targets

Mitochondria are promising targets for cancer therapy for a number of reasons: firstly, given the marked difference in the level of expression of genes and mutations across the landascape of tumours, it makes sense to target entities that are omnipresent within neoplastic pathologies; secondly, mitochondria are both energy generators and contain numerous apoptosis-promoting proteins. Anti-cancer agents that act via mitochondrial destabilization are called Mitocans and they are classified according to their site of action: specifically, drugs targeting complex I belong to the class of electron redox chain targeting drugs, examples of which are Tamoxifen, Adaphostin, 3-bromopyruvic acid, α-TOS and MitoVES[154].

Very important in this context is the role of specific and potent ETC inhibitors on ROS production and the subsequent (de)stabilisation of HIF-1 in cells: rotenone, myxothiazol and stigmatellin (the last 2 are complex III Q_0 site inhibitors) lower mitochondrial ROS and destabilise HIF1, whereas antimycin A (a complex III Q_i inhibitor) increases mitochondrial ROS and stabilises HIF1[155]. Another set of alkyliminophenylacetate compounds identified through a small library screening and structurally similar to strobilurins, known complex III inhibitors, was found to inhibit HIF-1 activity[156]. Finally (as it will be explained in detail in chapter 6), the selective complex I inhibitors **BAY-87-2243** and **10759** possess antitumor activity that was found to be linked to complex I-driven HIF deactivation.

1.7 Aims of this thesis

Mitochondrial complex I is a major metabolic hub whose dysfunction can potentially affect a myriad of cellular pathways. Since this enzyme could be the off-target of many drugs it is crucial to extensively characterise it from a pharmacological perspective in order to define, as much as possible, its role within drug-induced mitochondrial dysfunction. In addition, SAR studies are useful tools to elucidate molecular binding and pinpoint mechanisms of toxicity, hence they constitute a major part of this work.

The goal of chapter 3 was to assemble a library of complex I specific inhibitors that are known to cause side effects linked to drug-induced mitochondrial dysfunction with a novel and simple methodology. The compounds were tested with several assays on different systems with the aim of elucidating their role in complex I-based mitochondrial toxicity.

Chapter 4 extends the scope of chapter 3 by analysing a commercial library of FDA-approved drugs and categorising them according to target specificity within OXPHOS and binding site on complex I. An assay with isolated mitochondria on specific complex I inhibitors added physiological relevance and the novel methodology presented to address target categorisation and binding site could be applied to similar enzymes within metabolic pathways similar to complex I.

The work presented in chapter 5 is a SAR study on rotenoids to improve the understanding of rotenone binding to complex I. Hydroxylated species are particularly interesting for their potential therapeutic use as less toxic than lipophilic compounds.

Finally, the work illustrated in chapter 6 consists of two SAR studies based on anticancer agents developed by The Anderson Cancer Centre and Takeda, respectively. Assessing target specificity to complex I and improving the understanding of drug binding to complex I are the key aims.

2 Experimental Methods

2.1 Sources of chemicals and reagents

Estradiol and Doxorubicin were purchased from Cayman Chemical Co. (Ann Arbor, MI); Nefazodone HCl, Clozapine, Tamoxifen citrate, Amlodipine, Aripiprazole, Rosiglitazone maleate, Propafenone HCl, Duloxetine HCl, Iloperidone and Salmeterol were purchased from LKT Laboratories (St. Paul, MN, USA); Fenofibrate, Nisoldipine and decylubiquinone (dQ) were purchased from Santa Cruz Biotechnology, Inc (Santa Cruz, CA); all other chemicals were purchased from Sigma Aldrich (Sigma-Aldrich Company Ltd., Gillingham, Dorset, UK), and were all of purity always higher than 97%. The Screen-Well FDA-approved drug library V2, consisting of 786 compounds, was provided as 10 mM stock solutions in DMSO (BML-2843-0100, Enzo Life Sciences, Farmingdale, NY). Ultra-pure water was obtained from a Milli-Q purification system (Millipore, Watford, UK). Non-aqueous solvents were of HPLC grade.

2.2 Preparation of bovine mitochondrial membranes, isolated complex I and SMPs

2.2.1 Isolation of bovine heart mitochondria

This preparation method was adapted from a protocol by Walker *et al.*[157]. The whole procedure was carried out at 4˚C. Muscle tissue from hearts of freshly slaughtered cows (*Bos taurus*) was separated from fat and connective tissue and mechanically minced. 1 kg portions of the resulting mince were mixed with 1.4 L of mitochondrial buffer (250 mM sucrose and 10 mM tris-SO_4, pH 7.8 at room temperature or RT) and the solid matter filtered out with a single layer of muslin. Filtered batches were mixed with 1.6 L of mitochondrial buffer (+ 200 μM EDTA) and homogenised in a Waring blender for 30 seconds ("high" setting). The resulting homogenate was centrifuged at 2,600 g for 15 minutes in a RC12-BP centrifuge and the supernatant filtered through a single layer of muslin and centrifuged again at 20,400 g for 27 minutes in a SLA 3000 rotor. Finally, the supernatant was discarded and the pellets containing isolated mitochondria stored at -20 ˚C: usually two bovine hearts constitute a ~50 g pellet (wet weight).

2.2.2 Preparation of bovine mitochondrial membranes from isolated bovine heart mitochondria

This preparation method was adapted from a protocol by Walker *et al.*[157]. The whole procedure was carried out at 4˚C. Isolated mitochondrial pellets from the equivalent of two bovine hearts were thawed overnight, resuspended in 2 L of Milli-Q water and homogenised with a Waring blender (2 minutes on "medium" setting). 150 mM (solid) KCl was added and homogenised with the Waring blender further (3 minutes on "medium" setting). The homogenate was centrifuged at 13,700 g for 40 minutes in a SLA-3000 rotor, the supernatant was discarded and the pellet resuspended in 250 mL of buffer (10% glycerol, 20 mM tris-HCl, 1 mM EDTA, pH 7.55 at 4 ˚C). The resulting mitochondrial membrane suspension was stored at -80 ˚C (typical concentration of 10 mg mL^{-1}).

2.2.3 Complex I isolation from mitochondrial membranes

This preparation method was adapted from a method by Sharpley *et al.*[158]. All the steps were carried out at 4 ˚C. 30 mL of mitochondrial membranes were thawed and PMSF (0.005%) was added. Solubilisation with 1% DDM (added dropwise from a 10% stock) was followed by constant stirring for 30 minutes, then the suspension was centrifuged at 47,800 g for 30 minutes. The supernatant was filtered through a 0.22 μm filter (Millipore) and loaded at 2 mL min^{-1} onto a Q-sepharose HP column (GE Healthcare), pre-equilibrated with buffer A (20 mM Tris-HCl, 10% ethylene glycol, 0.2% DDM, 2 mM EDTA, 25 μg mL^{-1} cardiolipin, 25 μg mL^{-1} phosphatidylcholine, 25 μg mL^{-1} phosphatidylethanolamine, pH 7.55 at RT). Lipids were purchased from Avanti. The column was transferred to an Äkta explorer FPLC system (GE Healthcare) and washed with buffer A at 3 mL min^{-1} until the absorbance at 280 nm baselined. At this point the components of the respiratory chain were eluted with a NaCl gradient with buffer B (buffer A + 1M NaCl): 25% buffer B eluted complex V and IV and 35% buffer B eluted complex I. The relevant fractions were pooled and concentrated to ~1 mL (100 kDa cut off filter). In order to separate complex I from any remaining complex IV the concentrated sample was split into two batches and both were run on a 24 mL Superose-6 Increase gel filtration column (GE Healthcare) pre-equilibrated in phospholipid-free buffer A. Complex I fractions were pooled and concentrated as before to ~300 μL, glycerol was added to 20 % and aliquots were

snap frozen to be stored at -80 ˚C. The final concentration was approximately 15 mg mL^{-1} of pure complex I.

2.2.4 Preparation of submitochondrial particles from bovine heart mitochondria

The preparation of submitochondrial particles (SMPs) was adapted from a method described in the literature[159]. All the steps were carried out at 4 ˚C. A pellet of bovine heart mitochondria (~10 g) was resuspended in 40 mL of SMP buffer and the resulting suspension was centrifuged for 12 minutes at 11,300 x g (Ti 45 tubes Beckman Coulter). The supernatants were discarded, the pellets homogenised in 30 mL of buffer and the pH of the suspension was brought to 9 with 2 M Tris for 10 minutes to dissociate endogenous ATPase inhibitor IF1 from ATPase. The suspension was further centrifuged once for 14 minutes at 37900 x g and then twice for 12 minutes at 11300 x g (the supernatant was discarded each time). The resulting pellet was resuspended in 40 mL of SMP buffer, 15 mM of $MgSO_4$ was added and the resulting mixture was sonicated 10 times in 15 seconds bursts each at 150 W, 1 minute intervals. The mixture was centrifuged for 20 minutes at 24700 x g (MLA80 tubes Beckman Coulter): the top 1.5 mL of the supernatant in each tube was collected and the pooled top fractions were centrifuged for 30 minutes at 74700 x g, rinsed with buffer and resuspended to ~10 mg mL^{-1}.

2.3 Microsomal incubations

Human liver microsomes from 50 different individual donors were purchased from Gibco. Drugs were incubated in amber glass vials and the caps were pierced with a small needle to let oxygen through. Drug incubations were carried out in 800 µL of K-P_i buffer (20 mM, pH 7.5 at 37 ˚C) with 0.4 mg mL^{-1} microsomes, 1 U mL^{-1} of glucose-6-phosphate dehydrogenase from *Leuconostoc mesenteroides* (Sigma), 3 mM $MgCl_2$, 1 mM EDTA, 70 U mL^{-1} superoxide dismutase from bovine erythrocytes (Sigma), 70 U mL^{-1} catalase from *Corynebacterium glutamicum* (Sigma). Microsomes were activated with 1 mM $NADP^+$ and 10 mM of glucose-6-phosphate, incubations lasted 6 hours with constant shaking at 37 ˚C. Microsomal mixtures were then quenched with addition of 800 µL of dry ice-cooled Et_2O and mixed up and down several times, placed at -20 ˚C for 3 hours and subsequently at 4 ˚C for 12 hours. Et_2O was then removed by placing the vials in a vacuum desiccator for 1 hour,

the microsomal proteins were pelleted out with centrifugation at 5000 x g for 10 minutes and the supernatants were transferred in clean vials. 50 µL of each supernatant constituted a quarter of the 200 µL total well volume for a regular NADH:O_2 oxidoreduction assay.

2.4 Preparation of enzymes for the succinate:O_2 coupled assay

The method described by Jones and Hirst[160] was followed.

2.4.1 Overexpression of FumC and MaeB

The plasmids carrying the fumarase C (FumC) and decarboxylating malic enzyme (MaeB) genes were generously provided by Todd Weaver at University of Wisconsin-La Crosse and María Drincovich at National University of Rosario, respectively.

The procedure followed for FumC and MaeB over-expression was the same unless otherwise stated. Starter cultures of 50 mL LB supplemented with 50 µg mL^{-1} ampicillin were inoculated and incubated at 37 ˚C whilst shaking overnight. The cultures were scaled up to 4x1 L flasks of LB supplemented with 50 µg mL^{-1} ampicillin and incubated at 32 ˚C with shaking: expression of the protein was induced with 1 mM or 0.1 mM IPTG (FumC or MaeB respectively) when the optical density (OD) at A_{600} was 0.6. Cultures were incubated with shaking overnight at 20 ˚C.

2.4.2 Harvesting and purification of FumC and MaeB

All the steps were carried out at 4 ˚C. Cells were collected by centrifugation at 7000 x g for 15 minutes and resuspended in 120 mL of buffer A for FumC (50 mM potassium phosphate and 300 mM of NaCl, pH 7.8 at 4 ˚C) and buffer B for MaeB (100 mM NaCl, 25 mM imidazole, 20 mM Tris-SO_4 and 10% glycerol, pH 7.4 at 4 ˚C), with three protease inhibitor tablets (Roche) added to each. A pre-cooled Constant cell disruption system was used to lyse cells with two passes at 30 psi. The lysates were then centrifuged at 150000 x g for 45 minutes, the pellets discarded and the supernatants filtered through a 0.2 µm pore filter.

The lysates were loaded on to a 25 mL Ni-sepharose 6 Fast Flow column (GE Healthcare) with a peristaltic pump at 2 mL min^{-1}, transferred to a Äkta Prime plus

FPLC and washed at 2 mL min^{-1} with buffer A (+ 60 mM imidazole) for FumC and buffer B for MaeB until the absorbance at 280 nm returned to baseline. Gradients spread over 40 mL with buffer A (+ 400 mM imidazole) for FumC or buffer B (+ 300 mM imidazole) for MaeB were set up: the proteins were monitored at 280 nm and usually began to elute at 75-80% of the gradient. Pooled fractions were concentrated with 50-kDa centrifugal filters (Amicon) by about 10 (FumC) or 20 (MaeB) fold. Dialysis followed for FumC in buffer C (1 mM DTT, 5 mM EDTA and 10 mM Tris-SO_4, pH 7.0 at 4 ˚C) and for MaeB in buffer D (10% glycerol, 20 mM β-mercaptoethanol and 60 mM Tris-SO_4, pH 7.4 at 4 ˚C). Finally, the proteins were stored at -80 ˚C in 50% glycerol with typical yields of about 36 and 60 mg mL^{-1} for FumC and MaeB, respectively.

2.5 Preparation of recombinant trypanosomal alternative oxidase (AOX)

2.5.1 Expression of AOX in *E. coli* FN102

This protocol was adapted from Jones, Blaza *et al.*, 2016[161]. The *E. coli* strain FN102/pTbAO was used to over-express the alternative oxidase from *Trypanosoma brucei brucei*. The FN102 strain does not possess glutamyl-tRNA reductase (gene *hemA*), which produces 5-aminolevulinic acid (ALA, *i.e.* the strain is auxotrophic for it) in the first step of heme biosynthesis in *E. coli*, a pathway required for the synthesis of cytochrome *bd* quinol oxidase: addition of ALA in the media is therefore essential. FN102/pTbAO cells were added on LB plates supplemented with 100 mg mL^{-1} ampicillin, 100 mg mL^{-1} ALA (both from Sigma-Aldrich) and 50 mg mL^{-1} kanamycin (Merck) and incubated for 18 hours at 37 ˚C. Large colonies were selected to inoculate 300 mL starter cultures in K-broth (0.74 g L^{-1} Na-citrate.$2H_2O$, 2.5 g L^{-1} $(NH_4)_2SO_4$, 10.4 g L^{-1} K_2HPO_4, 3 g L^{-1} KH_2PO_4, 10 g L^{-1} tryptone, 5 g L^{-1} yeast extract, 5 g L^{-1} casamino acids and 0.2 % glucose) supplemented with 100 µg mL^{-1} carbenicillin, 50 µg mL^{-1} kanamycin, 100 µg mL^{-1} ALA and 0.2 % glucose and incubated at 37 ˚C with shaking for ~3 hours until the OD at A_{600} was about 0.6. The cells were collected by centrifugation for 10 minutes at 3000 x g and the media exchanged (to remove ALA and introduce the iron needed for AOX over-expression) with 50 µg mL^{-1} $MgSO_4$, 25 µg mL^{-1} $FeSO_4$, 25 µg mL^{-1} $FeCl_3$, 100 µg mL^{-1} carbenicillin and 0.2 % glucose. The exchange of media was repeated and the second

resuspension amounted to 10 mL of metal-supplemented K-broth concentrated inoculum. Then, 16 L of K-broth supplemented with 50 µg mL^{-1} kanamycin, 100 µg mL^{-1} carbenicillin, 50 µg mL^{-1} $MgSO_4$, 25 µg mL^{-1} $FeSO_4$, 25 µg mL^{-1} $FeCl_3$ and 0.2 % glucose were inoculated to ~0.01 OD with the concentrated inoculum and the resulting cultures were incubated with shaking at 30 ˚C (190 rpm) until the OD at A_{600} reached ~0.6, at which point 25 µM of isopropyl ß-D-1-thiogalactopyranoside (IPTG) was added to induce AOX expression. Cultures were incubated overnight at 30 ˚C with shaking (190 rpm).

2.5.2 Cell disruption and membrane harvesting

Cells were harvested by centrifugation at 7000 x g for 15 minutes, the supernatant discarded and the pellet resuspended to 10 mL g^{-1} of cells in buffer at 4 ˚C (50 mM Tris-HCl, pH 7.5 at RT). 1 mM $MgSO_4$, protease inhibitor tablets (Roche, 1 per 50 mL) and ~5000 U of benzonase were added to the resuspension before being disrupted with a pre-cooled Constant cell disruption system (one pass at 15 kpsi and two passes at 30 kpsi). The lysate was centrifuged for 15 minutes at 8300 x g and the pellet discarded. The supernatant was then centrifuged for 80 minutes at 160,000 x g to reveal a two-layered pellet, a grey-bottom one and a yellowish-upper one. The upper layer of membranes was collected (making sure to leave the bottom layer undisturbed), resuspended to ~20 mL in buffer (50 mM Tris-HCl, pH 7.5 at RT), snap frozen in liquid nitrogen and stored at -80 ˚C.

2.5.3 Purification of AOX

The following steps were carried out at 4 ˚C. A ~20 mL membrane aliquot was thawed for one hour on ice and solubilised at 6 mg of protein mL^{-1} in solubilisation buffer (200 mM $MgSO_4$, 20 % glycerol, 1.4 % octyl-glucoside and 25 mM tris-HCl, pH 7.5 at RT) for another hour (buffer was added dropwise with constant stirring. The sample was centrifuged for 30 minutes at 165,000 x g, the supernatant was filtered through a 0.2 µM filter (Sartorius Stedim) and mixed with TALON cobalt metal affinity resin (Clontech). The resin had been previously washed with 20 times its volume in binding buffer (100 mM $MgSO_4$, 20 % glycerol, 1.4 % octyl-glucoside and 50 mM tris-HCl, pH 7.3 at RT) and it was applied to the solubilised protein solution at a volume 5 times lower. The protein was left to bind to the resin for 45 minutes, the

mixture was centrifuged for 5 minutes at 1000 x g and the supernatant removed. The resin was washed three times in a row with washing buffer (20 % glycerol, 20 mM imidazole, 50 mM $MgSO_4$, 0.042 % dodecyl-maltoside and 20 mM tris-HCl, pH 7.3 at RT) and poured into a XK50 column casing (GE Healthcare) and allowed to settle. The column was then transferred to a Äkta Prime plus FPLC (GE Healthcare) at 3.5 mL min^{-1} with washing buffer, when the absorbance at 280 nm reached baseline it was switched to 50% elution buffer (20 % glycerol, 250 mM imidazole, 50 mM $MgSO_4$, 160 mM NaCl, 0.042 % dodecyl-maltoside and 20 mM tris-HCl, pH 7.3 at RT) and when it reached baseline again it was switched to 100% elution buffer. The fractions containing protein were collected, pooled and concentrated ten times with 30 kDa molecular weight cut off filter (Amicon). The purified protein was dialysed against 2 L of dialysis buffer (50 mM $MgSO_4$, 20 % glycerol, 160 mM NaCl, 0.042 % dodecyl-maltoside and 20 mM Tris-HCl, pH 7.3 at RT) for 5 hours to remove imidazole. The purified protein (with a concentration of ~1.3 mg mL^{-1}, typically ~8 mg overall) was snap frozen with liquid nitrogen and stored at -80 ˚C.

2.6 Preparation of co-reconstituted complex I:AOX:Q_{10} liposomes

This preparation was adapted from Jones, Blaza *et al.*, 2016[161]. In general, 10 mg of phospholipids are required for every 1 mL of preparation. Bovine PC, CL and PE were homogenised together at a ratio of 8:1:1 respectively (lipids were added from a 25 mg mL^{-1} chloroform stock by Avanti). Then, the required amount of Q_{10} dissolved in chloroform was added and the sample thoroughly mixed before evaporating the chloroform with a gentle stream of N_2 followed by vacuum desiccation for 30 minutes. Lipids were resuspended in 650 µL of PL buffer (10 mM Tris-SO_4 and 50 mM KCl, pH 7.5 at 4˚C). The exact amount of buffer was dictated by the volumes of protein (AOX and complex I) and detergent (OG) stocks needed in a later stage in order to maintain a 1 mL final volume. The suspended lipids were extruded nine times thorugh a 0.1 µM pore-tracked edge membrane (Watman) and homogenised again with 160 µL of octyl-glucoside (OG, 10% stock in MQ water) with a final OG concentration of 1.6%. The mixture was sonicated for 10 minutes, placed in a 2 mL Eppendorf and cooled on ice for 10 minutes.

The next steps were carried out at 4 ˚C. After cooling, 0.2 mg of AOX and 0.2 mg of complex I were added to the solubilised lipids and the mixture incubated for 10 minutes. Then, 100 µL of prewashed (1 volume of methanol and at least 20 volumes of MQ water) damp SM-2 Biobeads (from Biorad) were added to remove the detergent. The mixture thus obtained was gently agitated for 4 hours, adding further 100 µL of Biobeads every hour: absence of bubbles indicated the removal of detergent. The Biobeads were removed with spinning through a 1.5 mL coarse centrifugal filter (Bio-Rad). The liposome suspension was centrifuged at 57,500 x g for 45 minutes, the supernatant discarded, the surface of the pellet carefully washed with 300 µL of PL buffer and finally resuspended in 100 µL of PL buffer. A typical preparation yielded ~200 µL of material at ~1.5 mg mL^{-1} of total protein. The concentration of complex I was quantified using the NADH:APAD oxidoreduction reaction[162], and the AOX concentration was assumed to be the difference between the total protein and complex I concentration.

2.7 Reduction of dQ to dQH_2

This protocol was adapted from Kirby *et al.*[163] and it does not require anaerobic conditions (the same procedure was applied for Q_1 reduction to Q_1H_2). 200 µL of a ~50 µM stock of dQ (in EtOH), 100 µL of MQ water and 10 µL of 1 M HCL were combined in a 10 mL glass bottle and ~5 mg of $NaBH_4$ was added. Gentle stirring turned the solution from orange to colourless within seconds with concomitant formation of H_2 gas. The excess $NaBH_4$ was neutralised with successive additions of 10 µL 1 M HCl until gas formation stopped. Then 500 µL of hexane and 500 µL of diethyl ether were added and the resulting 2-phase mixture well shaken. The upper organic phase was transferred to another small glass bottle and organic washing with hexane/diethyl ether repeated another two times. The collected organic layers were pooled, the same volume of 2 M NaCl added and the 2-phase mixture shaken well. The upper organic layer was then removed and evaporated with a gentle stream of N_2. Finally, 300 µL of EtOH and 30 µL of 1 M HCl were added to re-dissolve the crystallised dQH_2. The final concentration of dQH_2 was obtained spectrophotometrically by measuring the absorbance at 289 nm assuming 4140 M^{-1} cm^{-1} as extinction coefficient[164].

2.8 Reduction of cytochrome *c*

Cytochrome *c* was reduced according to a protocol by Spinazzi *et al.*[165]. 130 mg of Na-ascorbate were dissolved in 1 mL of 10 mM K-P_i buffer (pH 7.0 at 4 ˚C) and 100 µL of it were added to 500 µL of 1.5 mM stock of cytochrome *c* and 800 µL of K-P_i buffer. A sudden change in colour from brown to pink-orange signalled the complete reduction of cytochrome *c*. This solution was left incubating with shaking at 4 ˚C for 2 hours and 50 µL of the Na-ascorbate solution were finally added. The resulting mixture was dialysed against 0.5 L of K-P_i buffer for 24 hours at 4 ˚C, during which time the buffer was replaced 4 times. The A_{550}/A_{565} ratio was over 10, indicating complete reduction of cytochrome *c*. The absorbance at 550 nm was always constant when monitored after addition of 100 mM FeCN (which immediately oxidises cytochrome *c*) indicating the absence of residual ascorbic acid (that would slowly reduce cytochrome *c*).

2.9 Analytical methods

2.9.1 Protein quantification by the bicinchonic acid (BCA) assay

All protein concentrations were determined using the Pierce BCA protein assay kit by Life Technologies. The assay measures the increase in absorbance at 562 nm associated with Cu^+ ion following chelation of Cu^{2+} to (and its reduction by) peptide bonds: this reaction took place via a 30 minutes incubation at 37 ˚C. Bovine serum albumin standards (ranging from 0 to 2 mg mL^{-1}) were used to obtain a standard curve against which the protein samples (appropriately diluted) were compared. This method is hampered by chelators (*e.g.* EDTA), reducing agents (*e.g.* DTT) and some detergents (*e.g.* OG).

2.9.2 Phospholipid quantification

This method[166] is based on the formation of phosphomolybdate at 820 nm with multiple sample dilutions compared with standards ranging from 0 to 500 µM KH_2PO_4. Samples or standards (100 µL in boiling tubes) were mixed with 50 µL of MeOH and 30 µL of ethanolic stock of 390 mM $Mg(NO_3)_2$. Tubes were heated with a blue flame making sure to avoid boiling/popping of the samples. When the residue in the tubes turned white heating was stopped and the samples left to cool for 5 minutes.

0.3 mL of 500 mM HCl were added and the tubes heated in a heat block at 99 ˚C for 15 minutes (marbles were placed on top of them to prevent excessive evaporation). Once the tubes cooled down, 0.7 mL of 114 mM ascorbic acid, 2.72 mM $((NH_4)_6Mo_7)_{24}$ and 400 mM H_2SO_4 were added. New marbles were placed on top of the tubes and incubation at 37 ˚C for 1 hour followed. Finally, 200 µL from each tube was transferred into a quartz 96-well plate and absorbance at 820 nm measured.

2.9.3 Q_{10} quantification

The absorbance spectrum of the sample (225-475 nm) was recorded before and after addition of 2 mM KBH_4 to completely reduce the sample. The change in absorbance at 275 nm using 14,020 M^{-1} cm^{-1} as extinction coefficient[167] quantified Q_{10} in the sample. In order to make sure no scattering issues from the high lipid content of the samples were encountered, 1% SDS was first used to fully solubilise the lipids.

2.10 Kinetic measurements

Spectrophotometric absorbance measurements were carried out at 32 ˚C using a Spectra max 348 plus 96-well plate reader (Molecular Devices) with disposable 96-well polystyrene Corning plates (or a Molecular Devices 96 well quartz plate when the absorbance to be monitored was in the UV region). As a standard practice, each well to be monitored was filled up with 160 µL of buffer containing the protein of interest and every reagent but the electron donor. Drugs/inhibitors were added at this stage too and left incubating for 5 minutes before initiating the reaction. Every reaction was started with addition of 40 µL of electron donor that made up 200 µL of well overall volume. Rates were calculated by linear regression of the maximal rate (at least 60 seconds were considered for the linear fit). Well pathlengths were also measured immediately after the end of the reaction measurements to calculate specific activities (expressed as moles per minute per mg of protein) via the water constant method: this is based on the difference in absorbance at 1000 and 900 nm of water whose value is stored in the plate reader factory settings. All the IC_{50} determination experiments (and most of the other assays unless otherwise stated) were performed in triplicates. Inhibitors/drugs were dissolved in either water, MeOH, EtOH or DMSO and the same amount of delivery solvent (5 µL of water or 1 µL of MeOH, EtOH or

DMSO) was added to the control (0 compound concentration) well. Monitored wavelengths and extinction coefficients are given in the table below.

Reaction	System	λ (nm)	ε M^{-1} cm^{-1}	Chromophore
NADH:O_2	Membranes	340-380	4810[168]	NADH
Succinate:O_2		340-380	4810[160]	NADPH
Succinate:dQ		276	18000[169]	dQ
Succinate:ox. Cyt *c*		550-541	18000[169]	Cyt *c*
NADH:ox. Cyt *c*		550-541	18000[169]	Cyt *c*
Red. Cyt *c*:O_2		550-541	18000[169]	Cyt *c*
NADH:Q_{10}	Proteoliposomes	340-380	4810[161]	NADH
NADH:dQ	Isolated complex I	340-380	4810[161]	
NADH:FeCN		420-500	1020[170]	Fe^{3+}
NADH:HAR		340-380	4810[170]	NADH
NADH:APAD		400-450	3160[170]	APAD
ROS		557-620	51600[170]	Resorufin
NADH:Q_1		340-380	4810[171]	NADH

Control assays in the absence of protein, with the highest concentration of inhibitor, were carried out to test for non-enzymatic reactions and for drug interference with assay enzymes (succinate:O_2 and NADH:Q_{10} oxidoreductions and ROS assay).

2.10.1 Kinetic measurements on membranes

Assays were performed in 10 mM Tris SO_4, pH 7.5, 250 mM sucrose (buffer K). The pH of this buffer remains the same upon addition of 100 µM HCl (checked using a pH meter). Concentrations for the assays were as follows:

NADH:O_2 oxidoreduction

30 µg mL^{-1} membranes, 0.9 µM cytochrome *c*, 120 µM NADH (IC_{50} determinations were carried out with 50 µg mL^{-1} membranes and 1.5 µM cytochrome *c*).

Succinate:O_2 oxidoreduction

The coupled enzyme assay by Jones and Hirst[160] was chosen to measure complex II activity. The concentrations of reagents are the same as the ones indicated in the original paper: $NADP^+$ (2 mM), succinate (5 mM), oxaloacetate decarboxylating malic enzyme (MaeB, 300 µg mL^{-1}), fumarase C (Fum C, 60 µg mL^{-1}), $MgSO_4$ (2 mM) and K_2SO_4 (1 mM). 500 nM of rotenone was also added to prevent the

involvement of complex I. 50 µM fumarate were used instead of membranes to test whether drugs inhibit the coupled enzyme system or not. The scheme below illustrates the reactions involved with the coupled assay.

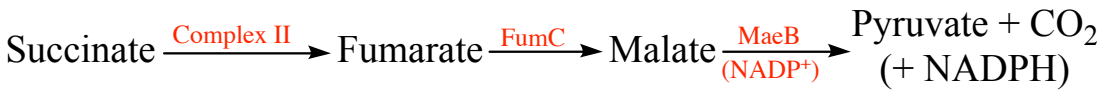

Reduced cytochrome *c*:O_2 oxidoreduction

6 µg mL^{-1} membranes, 1 µM antimycin, 60 µM reduced cytochrome *c*.

dQH_2:cytochrome *c*

30 µg mL^{-1} membranes, 1 µM piericidin, 500 µM NaCN, 60 µM dQH_2, 50 µM cytochrome *c*.

Succinate:cytochrome *c*

10 µg mL^{-1} membranes, 500 µM NaCN, 120 µM cytochrome *c*, 700 nM rotenone, 1 mM succinate.

NADH:cytochrome *c*

10 µg mL^{-1} membranes, 500 µM NaCN, 120 µM cytochrome *c*, 500 nM atpenin, 150 µM NADH.

Succinate:dQ

30 µg mL^{-1} membranes (incubated with 1% DDM for 30 minutes before use), 100 µM dQ, 1 mM NaCN, 2 mM succinate.

2.10.2 Kinetic measurements on isolated complex I

All assays were performed at 32 ˚C in 20 mM Tris-Cl, pH 7.5.

NADH:dQ oxidoreduction

0.5 µg mL^{-1} complex I, 100 µM NADH, 0.075% soy bean asolectin (Avanti Polar Lipids), 0.075% 3-[(3-Cholamidopropyl)dimethylammonio]-1-propanesulfonate (CHAPS, Merck Chemicals Ltd), 100 µM dQ. dQ and ASO/CHAPS were added first,

followed by buffer and enzyme. IC_{50} determinations were carried out with 2 μg mL^{-1} complex I.

NADH:FeCN oxidoreduction

0.3 μg mL^{-1} complex I, 1 mM $Fe(CN)_6^{3-}$ (FeCN), 100 μM NADH.

NADH:HAR oxidoreduction

0.6 μg mL^{-1} complex I, 3.5 mM $Ru(NH3)_6^{3+}$ (HAR), 100 μM NADH. HAR stocks were freshly prepared in MQ water and used the day of preparation.

NADH:APAD oxidoreduction

0.8 μg mL^{-1} complex I, 1 mM APAD, 100 μM NADH.

NADH:Q_{10} oxidoreduction

The buffer was 100 mM Tris-Cl (pH 7.5 at 32 ˚C) and 50 mM KCl, with 0.5 μg mL^{-1} complex I in AOX proteoliposomes (which commonly include 1.5 μg mL^{-1} AOX), 200 μM NADH. When Q_{10} was not present, dQ was added instead (20 μM). Complex I-free runs (Q_1H_2:O_2 assay) were performed to test whether a drug inhibits AOX or not: the buffer was 100 mM Tris-Cl (pH 7.5 at 32 ˚C), proteoliposomes were replaced by AOX enzyme (0.27 μg mL^{-1}) and NADH was replaced by 100 μM Q_1H_2 (the extinction coefficient for Q1 was 13,700 M^{-1} cm^{-1} according to the literature[172] but, rather than at 275 nm as reported, it was decided to follow the oxidation of Q_1H_2 at 272 nm instead after the UV spectrum of Q_1 was obtained).

ROS assay

H_2O_2 formation was followed in 30 μM NADH as the catalase-sensitive horseradish peroxidase-dependent oxidation of 10 μM Amplex Red to resorufin in 8 μg mL^{-1} complex I, 10 U mL^{-1} peroxidase from horseradish (HRP, Sigma), 10 μM Amplex Red, 10 U mL^{-1} superoxide dismutase from bovine erythrocytes (SOD, Sigma), 5000 U mL^{-1} catalase from *Corynebacterium glutamicum* (Sigma)[50]. Complex I-free runs were performed to test whether a drug inhibits horseradish peroxidase or not: complex I was replaced with 0.1% H_2O_2 and 0.023 U mL^{-1} HRP for this purpose.

NADH:Q_1 oxidoreduction

4 μg mL^{-1} complex I, 100 μM Q_1, 0.4 μg mL^{-1} asolectin, 2 μM rotenone, 100 μM NADH.

2.11 OCR and ECAR measurements on cultured human cells

Oxygen consumption rates (OCRs) and extracellular acidification rates (ECARs) on cultured human cells were measured using a Seahorse extracellular flux analyser XF96 at 32 °C.

HeLa (cervical cancer) cells were grown on DMEM supplemented with 10% FBS and 100 units mL^{-1} penicillin, 100 □g mL^{-1} streptomycin at 37 °C in 5% CO_2. 3 x 10^4 cells per well were plated into Seahorse XF96 plates and incubated overnight at 37 °C in 5% CO_2. The medium was exchanged for assay buffer containing DMEM, 4.5 g L^{-1} glucose, 1 mM pyruvate, 32 mM NaCl, 2 mM GlutaMAX, 15 mg L^{-1} phenol red, and 20 mM HEPES (pH 7.4) and the cells placed in a CO_2-free incubator at 37 °C for 60 min. 1 μM rotenone was used to inhibit complex I. To calculate the normalised, rotenone-sensitive OCR rates, the rotenone-insensitive rates (determined at the end of the experiment) were subtracted, and the traces normalised to 100% before drug addition. ECAR data were normalised to 100% before drug addition. The drugs were added 55 minutes after the start of the run and rotenone was added after 300 minutes. When a port injection failed the data from the corresponding well were excluded from the analyses[169].

2.12 OCR and ECAR measurements on isolated mitochondria

Wistar rat liver mitochondria were plated at 18 μg per well in 70 mM sucrose, 220 mM mannitol, 5 mM $MgCl_2$, 10 mM KH_2PO_4, 1 mM EGTA, 0.2 % fatty acid-free BSA, and 2 mM HEPES (pH 7.4 at 37 °C) with 10 mM malate and 10 mM glutamate. They were subsequently adhered by centrifugation at 2000 g for 20 min at 4 °C. The medium was supplemented with a further 5 mM glutamate and 5 mM malate and the mitochondria incubated for 14 min. Three baseline readings were taken before the drugs were added after the beginning of the run. Drugs were left accumulating with

mitochondria for 30 minutes (6 readings) before 4 mM ADP was added. Finally, 2 μM rotenone was added 3 minutes after ADP addition. Data from wells with failed port injections were excluded from the analyses[173].

2.13 Statistical methods

IC_{50} values were determined by, first, measuring the enzymatic specific activity against selected compound concentrations and then translating these data into a plot of specific activity against logarithm 10 of compound concentration (the control well was the 100% activity point). The IC_{50} value was then estimated according to the following four-parameters dose-response curve (where Top is the uninhibited activity, Bottom is the compound insensitive rate, Hill slope is the steepness of the activity percentage plot): calculations for the fitting were performed with GraphPad Prism 6.0 and reported with 95% confidence intervals.

$$\text{Activity \%} = \text{Bottom} + \frac{\text{Top - Bottom}}{1 + 10^{((\log(IC_{50}) - \log([\text{compound}])) \times \text{Hill Slope})}}$$

The concentration range for IC_{50} determination was chosen to obtain data points as evenly spread across the activity percentage plot as possible, with one data point between 100% and 90% residual activity and one data point for the lowest attainable residual activity. Other experimental values are reported as mean averages ± standard error of the mean (SEM). Statistics for OCR and ECAR comparisons were performed using an unpaired 2-tailed Student's t test and the p-values symbols stand for $P > 0.05$ (ns), $0.01<P<0.05$ (*), $0.01<P<0.001$ (**), $0.001<P<0.0001$ (***) and $P<0.0001$ (****). Linear fits were obtained with Microsoft Excel.

3 First drug selection process and assessment of drug-induced mitochondrial dysfunction: a proof of principle study

3.1 Introduction and aims

The most relevant topic regarding the pharmacology of complex I (on account of its economic importance and clinical impact) is drug-induced liver injury (DILI), an adverse hepatic reaction to medication[174]. DILI is the most common reason for drug failure after approval and it is estimated that roughly 11% of acute liver failure cases are caused by it (this percentage does not include acetaminophen associated injury)[175]. Hepatotoxicity is known to be caused by over 1,000 drugs and even if the incidence of this condition is one in 10,000 to 100,000 cases, drug cessation in some patients does not result in improvement and there is no specific medical treatment available: the condition can subsequently lead to liver failure. The importance of DILI is well recognised by the scientific community, and this is demonstrated by the establishment in 2004 of the Drug-Induced Liver Injury Network (DILIN), a research network to collect and analyse cases of liver injury[176]**.** A more recent effort in fostering scientific research on DILI is LIVERTOX, a freely accessible website that includes records on the hepatotoxicity of over 1000 drugs[177].

3.1.1 Overview of DILI

It makes sense that the liver is a major target of drug toxicity because it has a high capacity for xenobiotic metabolism (especially Phase I and II drug metabolism), it is the organ where orally administered drugs are transported before they reach the rest of the body (first-pass effect), it has an unique immune system and it has a significant blood supply from the portal vein[178]. DILI is very difficult to diagnose because there is no unique symptom to distinguish it from any other acute and chronic hepatic condition, it can in fact mimic all forms of liver diseases. Nonetheless, some critical factors have been identified as key determinants of DILI, such as exposure to toxic parent drugs or metabolites (as little as 50 mg), covalent binding of metabolites on cells or formation of glutathione adducts, and inhibition of mitochondrial function or bile salt export pump[179].

Many drug classes can cause DILI, for example anti-tubercular drugs (*e.g.* Isoniazid), non-steroidal anti-inflammatory drugs (*e.g.* Acetaminophen and Ibuprofen), protease inhibitors (*e.g.* Indinavir), nucleoside analogues reverse transcriptase inhibitors (*e.g.* Stavudine), statins (*e.g.* Atorvastatin) and anesthetic agents (*e.g.* Halothane)[180]. Acetaminophen toxicity deserves a special mention: it is the most frequent cause of DILI in the Western World (accounting for 46% cases of acute liver failure in the US from 1998 to 2007) but it is also reproducible in animal models (as opposed to idiosyncratic DILI) and therefore can be considered a paradigm of hepatotoxicity[181]. Briefly, acetaminophen is normally sulfated or glucuronidated during Phase II of drug metabolism but Phase I of drug metabolism predominates at dosage higher than 4 g: acetaminophen is oxidized to N-acetyl-p-benzoquinone imine (NAPQI) which then leads to depletion of glutathione supply and NAPQI binding to cellular proteins, ultimately resulting in cell injury[182].

3.1.2 Mechanisms underlying drug hepatotoxicity: mitochondrial involvement in DILI

Drugs damage the liver mainly because of mitochondrial dysfunction or formation of reactive metabolites: the latter can then lead to either direct toxicity or immune reactions[183]. Mitochondria are always involved in DILI, either directly or indirectly, because hepatic damage ultimately leads to the mitochondrial permeability transition[184]. Figure 3.1 illustrates the six main off-target drug toxicity locations in mitochondria along with their most common associated drugs[185].

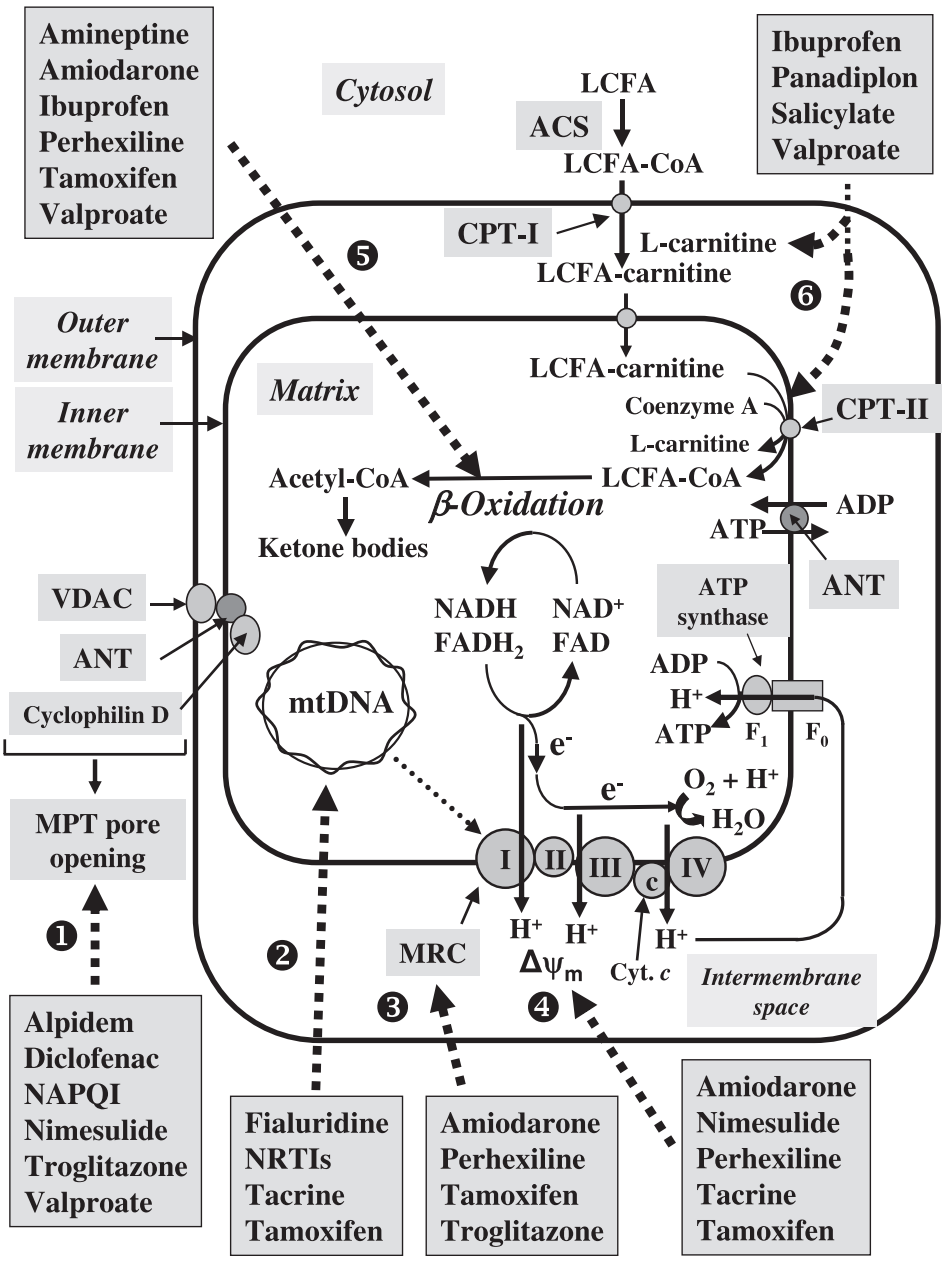

Figure 3.1. Main drug targets in mitochondria. Drugs can hit several molecular targets in mitochondria (1-6, explained in the text below), hence this organelle can be responsible for a wide range of drug-induced conditions: the focus of this work is on complex I in the respiratory chain (number 3). The picture was taken from Labbe, Pessayre and Fromenty[186]. LCFA, long chain fatty acid; CPT, carnitine palmitoyltransferase; ANT, adenine nucleotide translocator; ACS, acyl-CoA synthetase; VDAC, voltage-dependent anion channel; MRC, mitochondrial respiratory chain; MPT, mitochondrial permeability transition; NAPQI, N-acetyl-p-benzoquinone imine; NRTI, nucleoside reverse transcriptase inhibitors.

1) Some drugs may induce opening of the mitochondrial permeability transition pore, resulting in depolarization of the inner mitochondrial membrane, water influx into the matrix and, ultimately, cell death.
2) mtDNA depletion leads to severe consequences, because the synthesis of

OXPHOS polypetides that are encoded by mtDNA can be impaired.

3) Inhibition of respiratory chain enzymes decreases ATP formation and increases ROS formation but can also contribute to lactic acidosis and steatosis (abnormal accumulation of fat), on account of the higher [NADH]/[NAD^+] ratio brought about by insufficient NADH reoxidation: less NAD^+ means impaired ß-oxidation of fatty acids and lowered oxidation of pyruvate, more NADH means higher pyruvate conversion to lactate. This is the main focus of this work since complex I belongs to the respiratory chain.

4) Some drugs are cationic amphiphiles: their lipophilic moiety combined with an amine functional group that tends to be protonated in the inner mitochondrial membrane allows them to be "electrophoretically pushed" into the mitochondrial matrix, dissipating $\Delta\Psi$; depolarization can also be triggered by anionic uncouplers (*e.g.* many NSAIDs) that shuttle back and forth from the intermembrane space (as uncharged species that easily cross the inner membrane) to the matrix (as negatively charged species that are driven back by anion transporters).

5) Inhibition of ß-fatty acid oxidation enzymes mainly causes steatosis, initially as small lipid vesicles in the liver that coalesce into bigger fat vacuoles; steatosis can also progress into steatohepatitis.

6) Lastly, drugs can sequester fatty acid oxidation cofactors such as CoA, therefore limiting catabolism of fatty acids.

The aims of the work in this chapter are to

- test a methodology that combines a side effects-based drug database search with known inhibitors of complex I to obtain a library of compounds that are expected to cause complex I-driven drug-induced mitochondrial dysfunction
- test the drugs that make up the library with an array of routine assays that focus on isolated complex I, on the whole respiratory chain and on cells: consequently, the drugs will be fully characterized according to their effect on complex I and classified accordingly in terms of potency and specificity
- based on the experimental findings from the two points above, a proof of principle will be established and applied to a bigger library of approved drugs (see chapter 4).

3.2 Drug selection process for first drug library

The initial library of drugs to conduct experiments on for this proof of principle study was prepared by identifying elements in common to the following two lists:

1) Drugs with side effects (hepatic and extrahepatic) that might be associated with mitochondrial damage.
2) Complex I inhibitors described in the literature.

3.2.1 Side effects list

The FDA provides a freely accessible database of about 95,000 drugs that can be queried according to side effects that the drug causes, the FDALabel. Other databases were initially interrogated, such as Drug Bank and Toxnet, but with FDALabel it is possible to directly and easily query side effects. Two lists of drugs were created according to the two different classes of side effects included in the database search as follows[ç].

Liver side effects

Hepatitis, steatosis, hepatic steatosis, microvesicular steatosis, macrovesicular steatosis, steatohepatitis[185]; acute liver failure[187,188]; autoimmune hepatitis[189]; liver necrosis, hepatocellular necrosis, hepatic necrosis, toxic hepatitis, liver steatosis, liver jaundice, hepatocellular jaundice, cholestatic jaundice, cholestasis, acute hepatitis, obstructive jaundice, chronic hepatitis, hepatomegaly, phospholipidosis, hepatic (liver) fibrosis, biliary sclerosis, hepatic vein thrombosis, peliosis hepatis, hepatoportal sclerosis, granulomatous hepatitis[190]; cirrhosis, nodular regenerative hyperplasia, hepatic adenoma[191].

Extraliver side effects

Optic neuropathy, pancreatitis[192]; cardiomyopathy[193]; peripheral neuropathy[194]; hyperlactatemia, lactic acidosis[195]; rhabdomyolysis[196]; myopathy[197]; lipoatrophy[198].

The information comprised in the database includes the name of the drug, National Drug Code (NDC) and Unique Ingredient Identifier code (UNII). While the former identifies the drug itself, the latter identifies the active ingredient(s) that make up the

[ç] The FDALabel database was accessed on 24th January 2014.

drug: since the active ingredient of the drug is most important for this study, both drug and inhibitor lists were based on UNII codes.

There were many redundancies in the database results and those were removed: drugs with the same name and drugs with different names but with the same active ingredients were deleted from the list. Also, very often drugs are sold in different versions (*e.g.* slow, fast and extended release), in different amounts of active ingredient or in different forms (*e.g.* chewable, injection, drops, crystals). At the end of the process no two active ingredients (UNII codes) were repeated in either list: the liver list comprises 806 hits (shown in appendix 3.7.3) and the extra-liver list 663 hits (shown in appendix 3.7.4), with 1016 drugs that belong uniquely to either one set or another.

3.2.2 Complex I inhibitors list

The main source for the complex I inhibitors list (*i.e.* compounds that have been reported to inhibit complex I) was the Scripps Institute Webpage on complex I[d]: all of the articles from 1997 onwards were screened and the ones about inhibition of complex I were added to the inhibitors list. In addition, other articles in the literature were used to expand on the original Scripps list. Particularly important was a review by Degli Esposti, where the author also proposed a classification of complex I inhibitors based on both an extensive literature search and original research: type A (antagonists of ubiquinone), type B (they displace ubisemiquinone) and type C (antagonists of ubiquinol)[199]. A UNII code was assigned, where possible, for all of the possible variants (*e.g.* normal, HCl, hydrate, Na^+ salt…), most drugs, however, are available in "normal" and HCl forms. 22 inhibitors that did not have a UNII code were found to have a CAS code instead. 42 inhibitors were species synthesized in medicinal chemistry papers that are not commercially available (they mostly belonged to the family of annonaceous acetogenins)[e]. The final inhibitor list contains 151 complex I inhibitors and their associated UNII codes (shown in appendix 3.7.2).

[d] http://www.scripps.edu/yagi/ci/publications.html, last checked 10th April 2014.
[e] The UNII list that was used to check against the inhibitors and the drugs dates back to 18th November 2013. A more recent list was uploaded (19th April 2014), and even though it contained 30,000 more UNII codes, no further hits were identified.

3.2.3 Intersection of the two lists and generation of the first compound library

When the two lists were compared to find common active ingredients (complex I inhibitors against liver side effects and complex I inhibitors against extraliver side effects), 44 liver and 40 extraliver matches were obtained: 12 drugs exclusive to liver side effects and 8 exclusive to extraliver side effects, the remaining 32 were in common between the two lists (these drugs are reported in appendix 3.7.1).

From the overall 52 hits, the list was then narrowed down to 29 by discarding some drugs for the following reasons:

1) They were structurally similar to each other (*e.g.* imipramine is similar to desipramine and only the latter was purchased)
2) Their IC_{50} in the literature was deemed too high (higher than 1 mM, *e.g.* valproate exhibited an IC_{50} higher than 5 mM with respect to complex I activity)[200]
3) They were very expensive (*e.g.* mirtazapine)
4) They required governmental authorisations (meperidine HCl)
5) They were already the subject of ongoing research in the lab (*e.g.* metformin HCl)

Preliminary NADH:O_2 IC_{50} measurements (see section 3.3.2 for details about this assay) ruled out some of the selected compounds from the proof of principle list because their IC_{50} values are too high to be relevant. It was decided to set the threshold for IC_{50} to 500 μM and not to proceed to further analysis with Acetaminophen (~8 mM), Aspirin (>5 mM), Tetracycline (>2 mM), Na-Ibuprofen (~2.6 mM), Indomethacin (~1.2 mM), Piroxicam (~1 mM) or Ciprofloxacin (~500 μM). Lastly, Simvastatin was ruled out because it did not dissolve to any appreciable degree in several solvents (water, DMSO, EtOH, MeOH, DCM). In the literature the inactive lactone form is usually hydrolysed with aqueous NaOH to the pharmacologically active acidic form to improve solubility[201], but no substantial improvement in solubility could be achieved by this method.

The final list of compounds is presented in Figure 3.2.

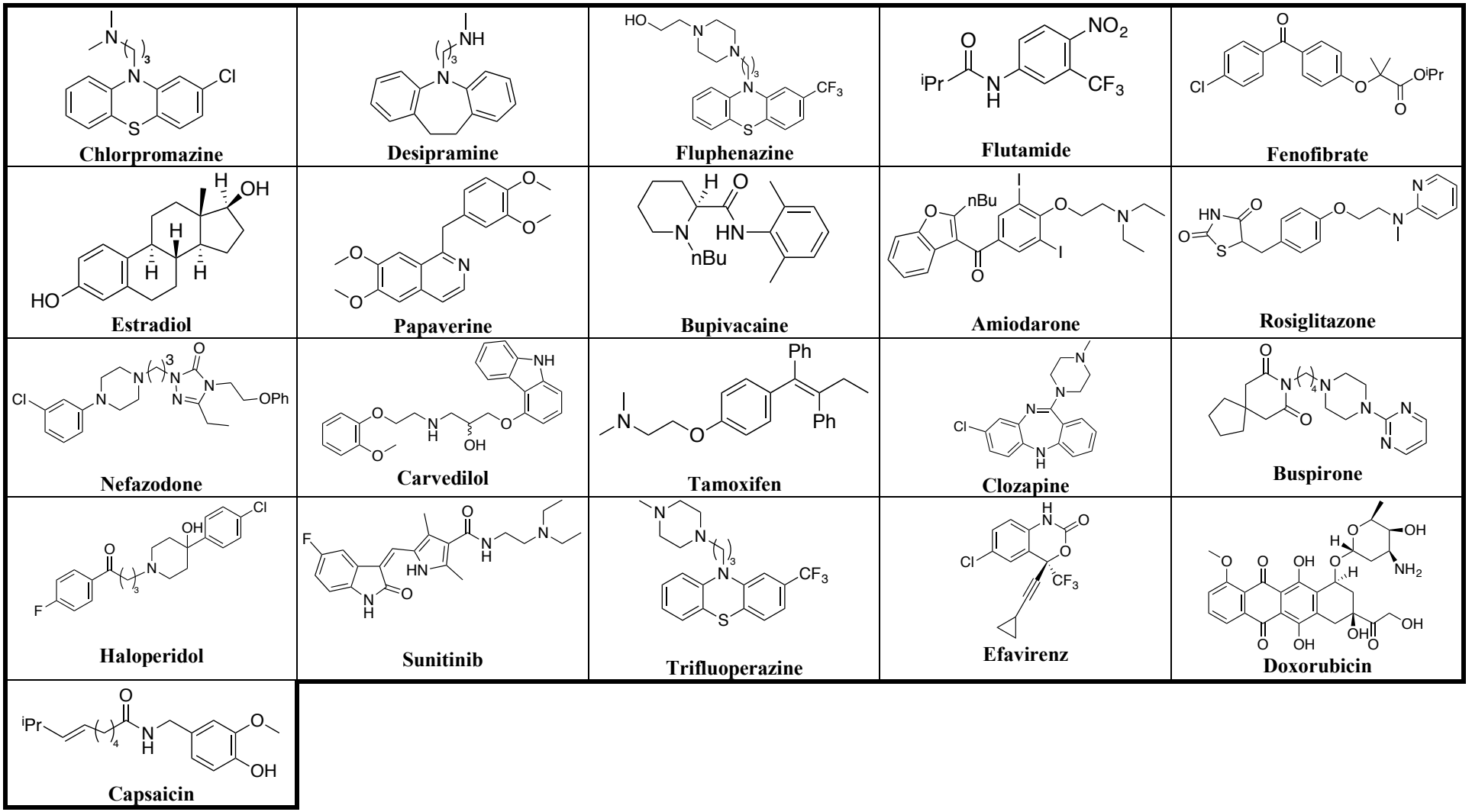

Figure 3.2. Structures of the compounds tested in this chapter. 21 FDA-approved drugs were identified by combining the results from the side effect database search and complex I inhibitors described in the literature.

3.3 Overview of assays and systems

3.3.1 Features of mitochondrial membranes

Mitochondrial membranes from *Bos taurus* (bovine) heart mitochondria (membranes for short) are the main experimental system adopted in this thesis to assess ETC-based drug-induced mitochondrial dysfunction: they are an intermediate step in the isolation of complex I prepared according to Walker *et al.*[157]. In these almost completely unsealed inner mitochondrial membrane fragments (they do retain a small amount of coupling) the active sites of the relevant complexes are accessible to exogenous substrates[202].

Cytochrome *c* was added to assays of membranes (since it is lost during the preparation) and the optimum amount was found to be 1.5 µM for every 50 µg mL^{-1} of protein (the fact that exogenous cytochrome *c* stimulates NADH oxidase activity in mitochondrial preparations treated with KCl has been known for a long time[203]). Figure 3.3 shows how membrane activity responds to cytochrome *c* concentration, both for the NADH:O_2 and succinate:O_2 oxidoreduction assays (see section 3.3.2 for details about these assays).

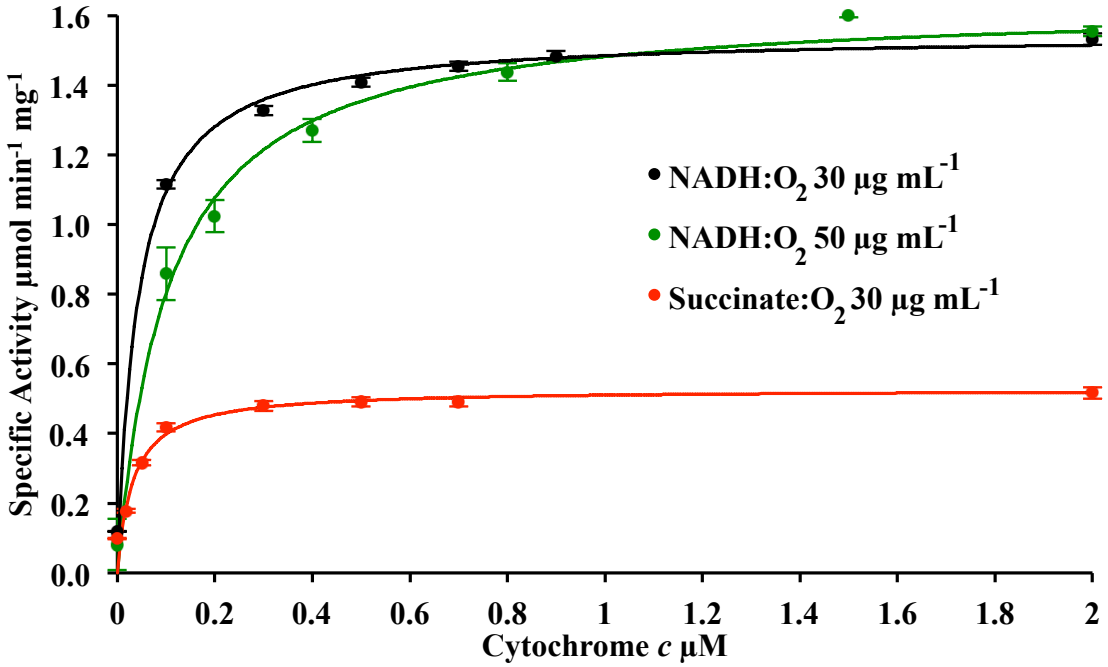

Figure 3.3. Substrate saturation curves for cytochrome *c* in different membrane concentrations. NADH:O_2 and succinate:O_2 sensitivities towards cytochrome *c* were performed at membrane concentrations used in this thesis to determine its optimal concentration. Lines are linear fits according to Michaelis-Menten kinetics.

The biochemical properties of the membrane system, combined with ease of preparation, make it a convenient platform to test drugs on OXPHOS enzymes for inhibition before expanding to more focused experiments with isolated enzymes. The main advantage of membranes over submitochondrial particles (SMPs, inside-out vesicles of the IMM obtained by sonication) is that they are naturally and almost completely uncoupled, so assays do not require addition of an uncoupler that could partially disrupt the lipid membrane and a further injection vehicle.

3.3.2 Assays in membranes and isolated enzymes

The first assay conducted on the selected drugs was NADH:O_2 oxidoreduction in membranes: the data from inhibitor titrations were arranged to display the catalytic activity against the amount of inhibitor used and, as such, they express the sensitivity of the system towards the inhibitor. This assay is the simplest and most general way of testing the potency of a compound against the complex I-IV pathway. It does not indicate which (and in what measure) specific enzymes are inhibited but it lays the foundations of a more thorough investigation into the inhibitory power of selected drugs. The second assay was the NADH:dQ oxidoreduction on isolated complex I: this was performed in order to obtain a more clear-cut assessment of the inhibitory potency of the drugs with respect to the enzyme and therefore to remove any interference by the other enzymes of the respiratory chain. Comparing the results of these two assays with one another enabled a first assessment of how selective these drugs are in targeting complex I. Specificity was also, and more accurately, addressed with the coupled succinate:O_2 assay that measures the activity of complexes II-IV[160]: it has many advantages over conventional assays for complex II that employ artificial electron acceptors such as DCPIP and INT, particularly because it includes the complete catalytic cycle of complex II and is stoichiometric. This experiment was performed to assess the effect of the drugs on the complex II-IV pathway. In order to detect artefacts that could lead to false positives in these assays, it was also confirmed that drug addition did not change the pH significantly and that the drugs did not react directly with NADH, cytochrome *c* or components of the succinate:O_2 assay. Finally, other assays on isolated complex I (FeCN, HAR, APAD, Q_1 and ROS assays) were conducted to assess the role of the flavin site in drug inhibition and whether ROS production was significantly altered by the compounds.

3.3.3 Cellular assays and microsomes

The effects of the drugs on the liver were assessed with the aid of the XF96 Seahorse Extracellular Flux Analyzer on HeLa cells. This platform is instrumental to understand if and in which measure drugs are absorbed by cells and transported into mitochondria. It must be noted that, in HeLa cells, expression of cytochrome P450 (CYP) drug-metabolising enzymes is low[204], therefore the use of these cells in this work mainly addresses (parent) drug transport inside cells and their interaction with mitochondria, not necessarily the effect of drug metabolism. The role of drug metabolites will finally be addressed with drug incubations in human liver microsomes: they are microvesicles derived from fragments of the endoplasmic reticulum upon ultracentrifugation that are commonly used to study drug biotransformation *in vitro*[205].

3.4 Results

3.4.1 Inhibition of complex I

3.4.1.1 NADH:O_2 and NADH:dQ oxidoreduction assays

Table 3.1 reports the IC_{50} values (with confidence interval at 95%) measured for the drugs in the NADH:O_2 assay. All the drugs exhibit either a single- or double-digit μM IC_{50} towards the complex I-IV pathway: the only two exceptions are Bupivacaine (the least potent, with 433 μM) and Nefazodone (the most potent, with 0.83 μM). Nadanaciva *et al.*[206] reported an IC_{50} of 4 μM for Nefazodone and greater than 50 μM for Tamoxifen and Chlorpromazine (two of the most potent drugs in the library) but they used an immunocapture-based assay with solubilised bovine heart mitochondria. The discrepancies could be explained by differences in the total concentration of complex I in the two systems or Q_1 used as electron acceptor (the latter could also be the main reason why Hroudová and Fišar[200] detected an IC_{50} of 96 μM for Desipramine in brain crude mitochondrial fraction, almost 4x the NADH:O_2 IC_{50} measured in membranes using native Q_{10}).

Table 3.1 also reports the IC_{50} values (with confidence interval at 95%) measured for the drugs in the NADH:dQ assay. Similarly to the NADH:O_2 assay, all the drugs exhibit either a single- or double-digit μM IC_{50} towards the isolated enzyme, but this time the average IC_{50} (66.2 μM) is almost twice as high as the average NADH:O_2 IC_{50}

value (38.6 μM). Also, Papaverine and Nefazodone are the most potent drugs (2.04 and 2.28 μM IC_{50} respectively) and Bupivacaine the least potent (254 μM).

3.4.1.2 Comparison between the NADH:O_2 and NADH:dQ assays

The comparison between IC_{50} values from these two assays can be useful to assess the response of the drugs to different Q acceptor species (endogenous Q_{10} in NADH:O_2 and dQ in NADH:dQ), to different aqueous environments (NADH:dQ is performed in the presence of 0.075% asolectin and CHAPS) and, more importantly, to several enzymes as opposed to isolated complex I. Chapter 4 includes a dedicated section on the differences between the NADH:O_2, NADH:dQ and NADH:Q_{10} assays based on data from 150 drugs (not just the 21 in this section). Table 3.1 also reports Hill coefficients for both assays (with associated SEM). Hill coefficients measure the steepness of dose-response curves and an high coefficient can be diagnostic of important features of the inhibitor/drug, such as presence of multiple binding sites (*i.e.* cooperativity), physical phase transitions (*e.g.* colloid formation) or enzyme concentration greater than K_d[207] (see chapter 5 for more information on the subject): comparison between NADH:O_2 and NADH:dQ Hill coefficients can, thus, be informative as far as potential cooperativity is concerned (see section 3.4.2).

Figure 3.4 shows an example of the dose-response curves for Fluphenazine (both the NADH:O_2 and NADH:dQ assays), with IC_{50} values and Hill coefficients graphically highlighted. These plots display two common features of the drugs that emerged in the assays: when complex I is isolated, the drug IC_{50} rises (curve shifts towards right) and the Hill coefficient drops (the red slope is steeper than the blue slope). An interesting discovery is that the IC_{50} values in isolated complex I are almost always greater (several times more, on average) than the corresponding IC_{50} values in the NADH:O_2 oxidoreduction assay: exceptions are Flutamide, Estradiol, Bupivacaine and Capsaicin, where the IC_{50} values for the isolated enzyme are lower (see Table 3.1 and Figure 3.5).

	NADH:O_2					NADH:dQ				
	IC_{50} µM	Confidence interval 95%		**Hill coefficient**	SEM	**IC_{50} µM**	Confidence interval 95%		**Hill coefficient**	SEM
Chlorpromazine	**11.1**	10.0	12.3	**2.08**	0.15	**52.7**	48.3	57.5	**1.46**	0.08
Desipramine	**25.7**	21.6	30.5	**1.47**	0.11	**86.9**	74.1	102	**1.50**	0.14
Fluphenazine	**17.6**	15.6	19.9	**2.24**	0.20	**102**	86.9	119	**1.74**	0.2
Flutamide	**28**	24.9	31.5	**1.63**	0.09	**13.0**	10.6	16.0	**0.97**	0.08
Fenofibrate	**3.6**	3.17	4.17	**1.60**	0.10	**17.1**	15.5	18.8	**1.2**	0.06
Estradiol	**14.2**	12.7	15.9	**1.4**	0.07	**13.9**	11.7	16.5	**1.27**	0.12
Papaverine	**1.7**	1.57	1.88	**1.07**	0.03	**2.04**	1.88	2.22	**1.04**	0.04
Bupivacaine	**433**	402	466	**1.21**	0.03	**254**	222	291	**1.27**	0.08
Amiodarone	**8.55**	8.24	8.88	**2.91**	0.10	**65.7**	54.2	79.7	**1.26**	0.11
Rosiglitazone	**38.1**	31.6	45.8	**1.19**	0.08	**47.6**	41.1	55.0	**1.06**	0.07
Nefazodone	**0.83**	0.78	0.87	**1.13**	0.02	**2.28**	2.17	2.39	**0.92**	0.02
Carvedilol	**6.69**	5.39	8.30	**1.35**	0.09	**10.8**	9.61	12.1	**1.23**	0.07
Tamoxifen	**5.3**	4.67	6	**2.52**	0.26	**168**	90.5	310	**1.05**	0.11
Clozapine	**50.8**	37.8	68.2	**0.93**	0.06	**140**	117	168	**1.27**	0.08
Buspirone	**18.3**	16.4	20.4	**1.07**	0.04	**40.4**	36.3	45.0	**0.77**	0.02
Haloperidol	**2.37**	2.24	2.52	**1.42**	0.04	**8.27**	7.50	9.12	**1.07**	0.05
Sunitinib	**9**	8.28	9.77	**1.48**	0.06	**29.4**	25.7	33.6	**1.03**	0.04
Trifluoperazine	**13**	12.0	14.2	**2.29**	0.15	**213**	131	346	**1.39**	0.17
Capsaicin	**25.8**	22.7	29.2	**1.56**	0.09	**24.7**	22.6	27.1	**1.3**	0.06
Doxorubicin	**85.9**	73.8	100	**1.65**	0.15	/	/	/	/	/
Efavirenz	**11.7**	9.78	14.1	**1.66**	0.17	**32.9**	26.7	40.6	**1.2**	0.10

Table 3.1. Assays with complex I in membranes (NADH:O_2) or isolated (NADH:dQ). Data for the two assays are presented with confidence intervals at 95% for IC_{50} values and Hill Coefficients with corresponding SEM of triplicates. It was not possible to assay Doxorubicin on NADH:dQ (the wells at midrange to high concentrations were too turbid for a reliable spectrophotometric reading). In general, IC_{50} values are lower and Hill coefficients are higher in the NADH:O_2 than in the corresponding NADH:dQ assays.

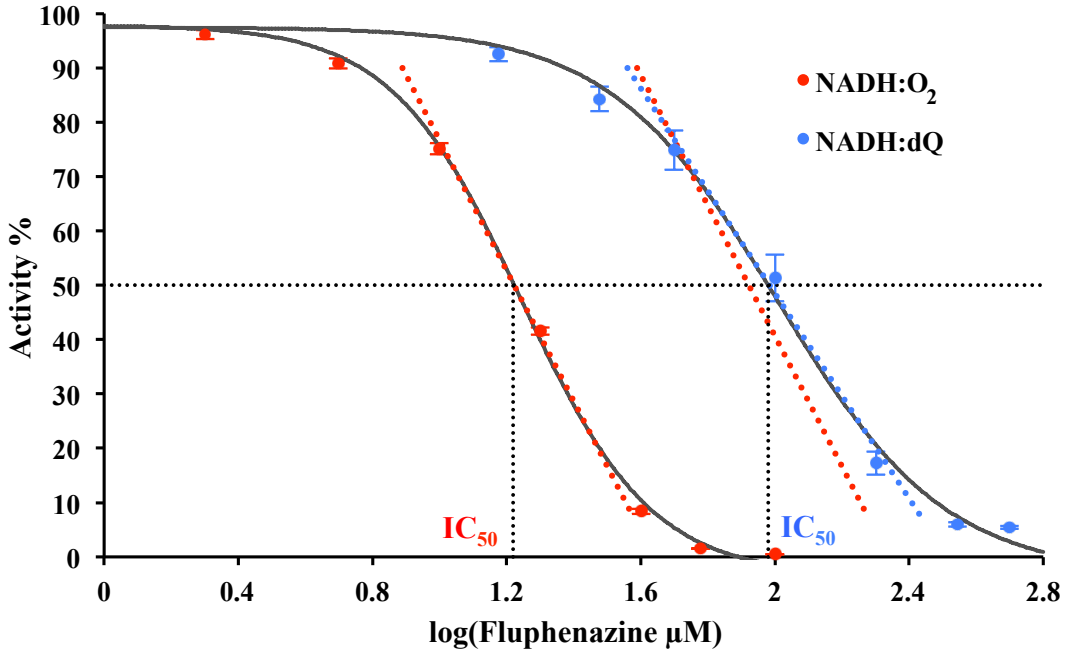

Figure 3.4. Dose-response curves for fluphenazine. The main differences between NADH:O_2 and NADH:dQ assays are highlighted: NADH:dQ exhibits a higher IC_{50} (the curve is shifted to the right) and a lower Hill coefficient (as indicated by the steepness of the curves, NADH:O_2 indicated twice for comparison) than NADH:O_2. Error bars are SEM of triplicates.

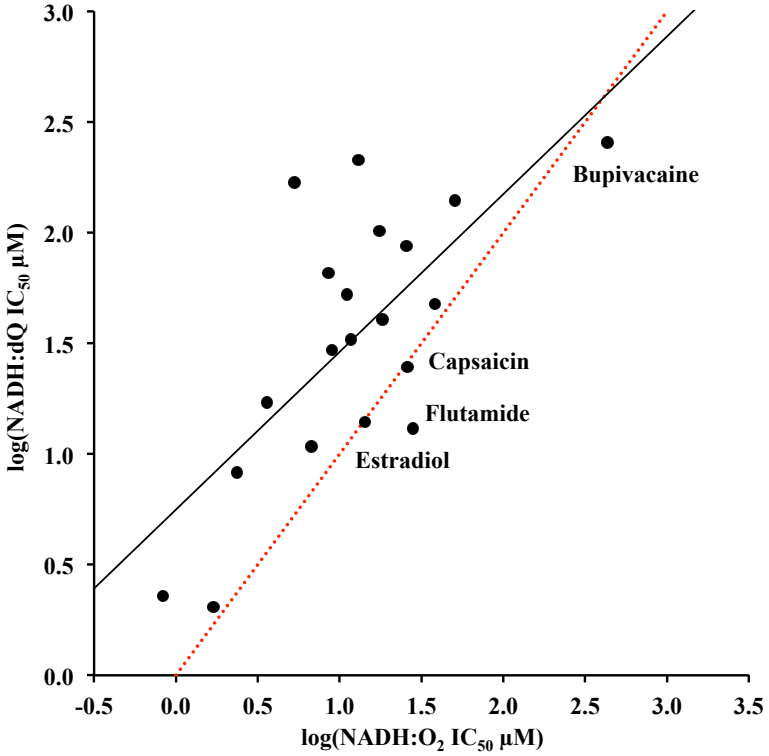

Figure 3.5. Relationship between IC_{50} values for NADH:O_2 and NADH:dQ. The majority of the drugs falls on the left of the 1:1 (red) line, indicating that their potency towards the I-IV pathway is higher than their corresponding potency towards the isolated enzyme (drugs for which the opposite is true are highlighted). Data shown in logarithmic form for better visualisation. The black line is the linear fit of the data.

3.4.2 Succinate:O_2 oxidoreduction assays and OXPHOS specificity

Table 3.2 reports the inhibition in the succinate:O_2 assay, which indicates how specific to complex I a compound is: it was decided to only perform a one point inhibition for each drug at three times the IC_{50} value in their NADH:O_2 assay. 11 drugs inhibit the oxidoreduction to less than 5%, 6 of which cause no inhibition whatsoever. In order to classify drugs as specific complex I inhibitors, a threshold of 15% on the succinate:O_2 percentage inhibition was deemed enough: 7 drugs out of 21 exhibit a value higher than this threshold. In order to investigate this aspect further, the ratio of the NADH:dQ and NADH:O_2 IC_{50} values was calculated for each drug (see Table 3.2): the higher the ratio is, the more the drug inhibits the complex I-IV pathway than it inhibits isolated complex I, and this could be diagnostic of specific complex III and/or IV inhibition (in chapter 4 this indicator will be expanded upon in terms of number of drugs, strengths and limitations). All of the drugs that are above the threshold also exhibit high NADH:dQ to NADH:O_2 ratios. Tamoxifen and Trifluoperazine, the drugs with the highest ratio, have been shown to be mitochondrial complex III inhibitors[208,209] (but see also the role of Tamoxifen-based mitochondrial insult in drug-induced liver injury, section 3.5.1). Furthermore, of the three species with the highest inhibition towards the complex II-IV pathway, namely Amiodarone, Tamoxifen and Sunitinib (44, 36 and 49% inhibition respectively), the latter has the lowest IC_{50} ratio of the three: this could mean that this drug exerts mixed (or non-specific) OXPHOS inhibition, *i.e.* inhibition of complex I could be more important than in the other two species (in chapter 4 Sunitinib is indeed classified as a non-specific inhibitor of OXPHOS). Amiodarone, Trifluoperazine and Tamoxifen also exhibit a remarkable reduction (absolute value) in Hill coefficient from NADH:O_2 oxidoreduction to NADH:dQ oxidoreduction (Table 3.1), and this can be indicative of multiple binding sites along the overall NADH:O_2 chain (*i.e.* complexes III and IV). Indeed, almost all drugs experience this decrease, as a consequence of the removal of enzymes in the assay. Only three drugs show an increase in Hill coefficient (Desipramine, Bupivacaine and Clozapine), but this is not significant and it does not likely reflect a genuine underlying biochemical phenomenon.

Based on these results, the 14 drugs that generate less than 15% inhibition in the II-IV pathway are complex I specific inhibitors (Rosiglitazone and Clozapine may still

deliver some degree of unspecific OXPHOS inhibition since they are the compounds with the highest values in this group). The other 7 drugs are specific inhibitors of other OXPHOS enzyme(s), even though this cannot be said about Doxorubicin because of lack of data for the NADH:dQ assay. Since its NADH:O_2 IC_{50} value is the second highest (see Table 3.1) and its succinate:O_2 percentage inhibition is the fifth highest in the whole library, Doxorubicin seems to inhibit less complex I than other OXPHOS enzymes. Indeed, Doxorubicin is known to inhibit several components of the respiratory chain, including complex IV and creatine kinase, as well as to undergo superoxide ion-based redox cycling on complex I[210] (see also section 3.4.3.1 for ROS assay on Doxorubicin).

Drugs	Succinate:O_2 Inhibition %	SEM	> 15%	(NADH:dQ/NADH:O_2) IC_{50}
Chlorpromazine	1.5	0.7		4.7
Desipramine	2.8	1.9		3.4
Fluphenazine	21.3	0.4	✓	5.8
Flutamide	-3.1	1.3		0.5
Fenofibrate	28.2	1.4	✓	4.8
Estradiol	-2.3	2.9		1.0
Papaverine	0.0	1.3		1.2
Bupivacaine	-0.2	2.7		0.6
Amiodarone	44.3	0.1	✓	7.7
Rosiglitazone	8.5	0.7		1.2
Nefazodone	0.2	0.1		2.7
Carvedilol	4.6	3.4		1.6
Tamoxifen	36.1	0.4	✓	31.7
Clozapine	14.6	0.5		2.8
Buspirone	0.0	1.4		2.2
Haloperidol	1.5	2.8		3.5
Sunitinib	48.5	1.8	✓	3.3
Trifluoperazine	18.4	2.5	✓	16.4
Capsaicin	5.0	1.6		1.0
Doxorubicin	25.3	1.6	✓	/
Efavirenz	3.6	4.2		2.8

Table 3.2. Succinate:O_2 percentage inhibition at three times IC_{50} for NADH:O_2. Negative values indicate total lack of inhibition (*i.e.* higher than control within experimental error). SEM from triplicates. IC_{50} values from Table 3.1.

3.4.3 Flavin-site of complex I

3.4.3.1 Initial assays

The activity of complex I at the flavin site can be assessed by several assays depending on the electron acceptor: NADH:HAR (the electron acceptor is $Ru(NH3)_6^{3+}$), NADH:FeCN (the electron acceptor is $Fe(CN)_6^{3-}$), and ROS (catalase-sensitive horseradish peroxidase-dependent oxidation of Amplex Red to resorufin via H_2O_2). Single point flavin-site experiments were carried out at three times the NADH:dQ IC_{50} for each of the above-mentioned assays, which are presented in Figure 3.6 (Trifluoperazine, Tamoxifen and Amiodarone were tested at 1.5x their NADH:dQ IC_{50} concentration because at higher concentrations they precipitated out of solution in the FeCN assay).

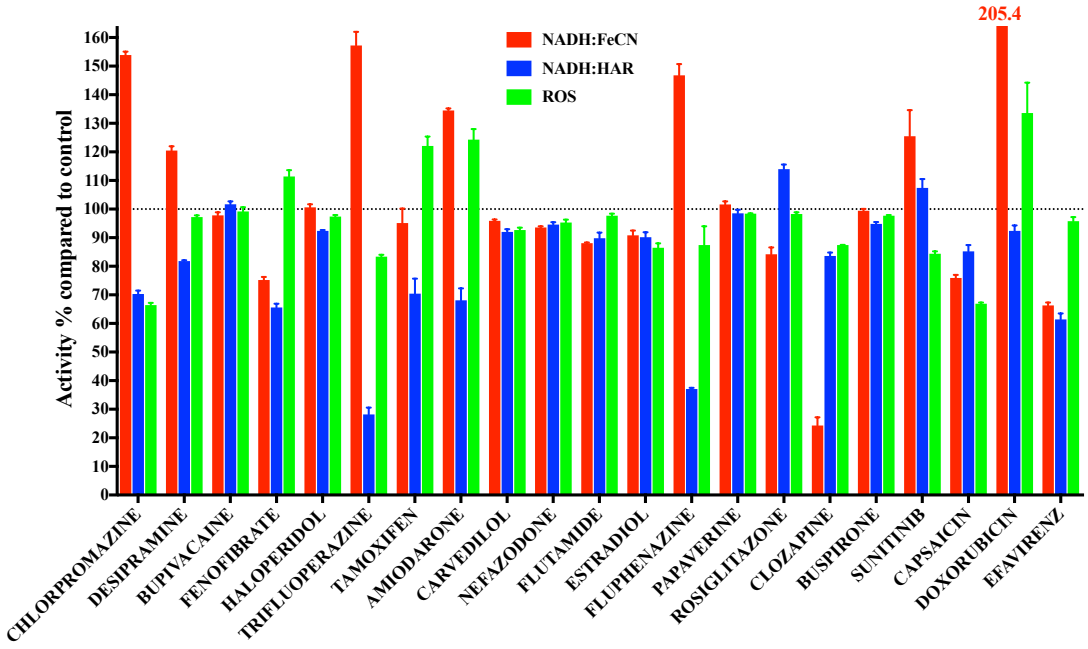

Figure 3.6. Isolated complex I assays for the drugs in the library. All drugs were tested at three times their IC_{50} in the NADH:dQ assay except for the ones that precipitated out of solution at such a high concentration in the FeCN assay, Trifluoperazine, Tamoxifen and Amiodarone. Error bars are SEM.

Often the measured rates did not reflect actual enzymatic inhibition or overactivation. This was particularly true for the FeCN assay (many issues in this assay were also experienced with the Enzo Library drugs, see chapter 4): Amiodarone, Fluphenazine and Trifluoperazine had solubility issues (the pathlengths exhibited were significantly lower than the control); Chlorpromazine, Trifluoperazine, Fluphenazine and

Doxorubicin exhibited a background rate over four times higher than the control rate; finally, the absorbance traces of Clozapine lasted for less than 20 seconds and then levelled off (the inhibition percentage shown in Figure 3.6 refers to such a short-timed rate). Of the drugs left, only a few exhibited either significant (± 20%) inhibition (Fenofibrate, Capsaicin, Efavirenz) or overactivation (Desipramine, Sunitibib) of the NADH:FeCN reaction. Interestingly, Wright and Kuhn[211] reported that Capsaicin inhibited FeCN reductase activity of trans-plasma membrane electron transport in chick forebrain neurons.

Similar issues were found in the NADH:HAR assay. Fenofibrate, Tamoxifen, Amiodarone, Fluphenazine and Efavirenz elicited a background rate over four times higher than the control; Trifluoperazine, Tamoxifen and Amiodarone had solubility issues (the pathlengths exhibited were significantly lower than the control). Of the drugs left, only Chlorpromazine exhibits a significant HAR inhibition (76% residual activity).

As for the ROS assay, the pathlengths exhibited by Tamoxifen and Amiodarone were abnormally low (and this explains the measured overactivation) while Capsaicin inhibited horseradish peroxidase (HRP) enough to compromise the results. Every drug tested with the ROS assay was also tested with the same conditions in the presence of catalase (to remove H_2O_2 from the assay medium): the only compound that returned a significant H_2O_2-free rate was Doxorubicin (3.6x the control catalase rate and 70% the ROS, catalase-free, rate, where normal values for the other drugs were about ± 1.2x and 20%, respectively). Doxorubicin ROS formation was also performed in a glovebox (O_2-free environment) and Amplex red activity not generated by oxygen (*i.e.* artefactual production of ROS) was ruled out. The redox cycling capacity of Doxorubicin (mentioned in section 3.4.2), could explain why this drug was found to generate high amounts of ROS even in the presence of catalase.

3.4.3.2 Structure-activity relationship on dibenzoheterocyclics

In general, the drugs investigated were unreactive towards FeCN, HAR and ROS assays, implying a lack of reactivity at the flavin: for most of them the observed activity was within ± 20% of the control value. Furthermore, the majority of the drugs that induced greater changes appeared to be chemically incompatible with the reagents present in the assays, thus rendering these results dubious. Despite these limitations, a structural pattern emerged from the flavin-site assays data that was thought to reflect an underlying enzymatic phenomenon: four out of six compounds with a dibenzoheterocyclic core (Chlorpromazine, Desipramine, Trifluoperazine and Fluphenazine) exhibited significant overactivation of the NADH:FeCN activity and inhibition of the NADH:HAR activity. This trend, combined with the cheap commercial availability of structurally similar species, made it possible to develop a flavin-site structure-activity relationship (SAR) study to shed light on its underlying causes. Compound titrations over appropriate concentration ranges were conducted for 8 different species with 5 different assays according to the different electron acceptor interacting with the NADH-reduced flavin (FeCN, HAR, APAD, Q_1 and O_2 in the ROS assay). Table 3.3 illustrates the overall findings, which are presented in a relatively descriptive way since the chemical characteristics of the compounds such as turbidity (as an indicator of poor solubility which can lead to artefactual light scattering) and background (*i.e.* complex I-free) rates varied and a proper IC_{50} determination was, thus, unfeasible. The aim was to obtain a set of criteria as objective as possible. The general ascending (or descending) trends as compound concentration increases were described with 5 different labels, illustrated in Figure 3.7 (top). Two representative traces are also shown in Figure 3.7 (bottom). The results are illustrated in Table 3.3 with different colour codes explained in the header row. The highest drug concentration in the titrations was set at 500 μM (or lower when the determination of a titration trend required lower drug concentrations according to preliminary experiments).

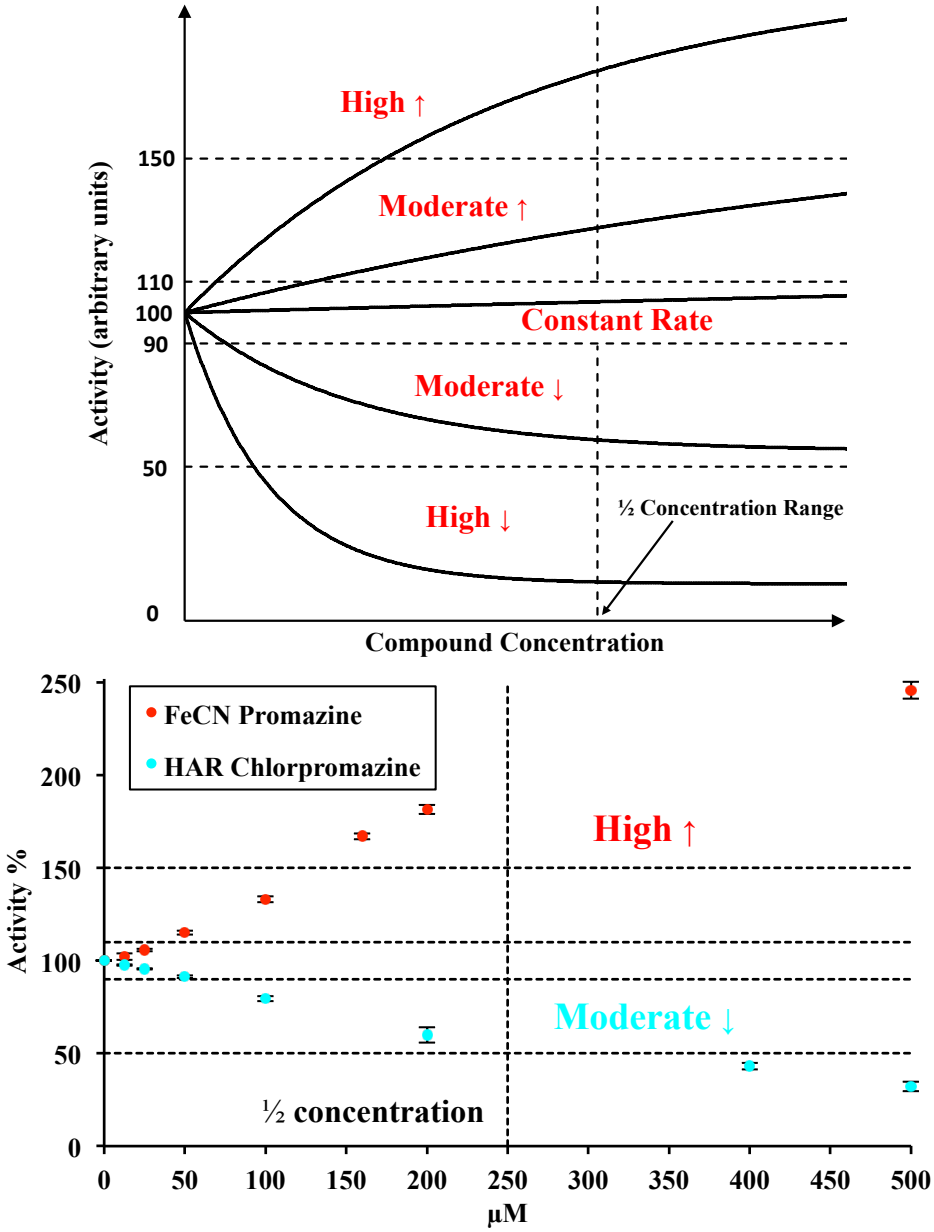

Figure 3.7. Criteria for trend labelling of flavin-site SAR study presented in Table 3.3 and representative traces. Top. In order to present the data as objectively as possible, rates are classified according to which portion of the activity plot data points are within, at ½ the concentration range used in the titration. Colour codes will be illustrated in the header row of Table 3.3. Bottom. Data points related to NADH:FeCN assay with Promazine and NADH:HAR assay with Chlorpromazine are shown. Hashed lines are the same as in the plot on top. Bars are SEM of triplicates.

Colour codes for data presentation

Turbidity issues, either visible by eye or how smaller the pathlengths at the highest compound concentration is compared to control pathlength (if greater than 10%)

Substantial complex I-free rates over complex I-driven rates along the titration (>10%)

Trend labels: High ↑ | Moderate ↑ | Constant | Moderate ↓ | High ↓ (see Figure 3.7)

	FeCN	HAR	APAD	ROS	Q_1
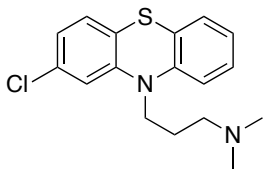 Chlorpromazine	Turbidity Background				Turbidity Background
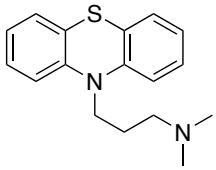 Promazine	Background				Turbidity Background
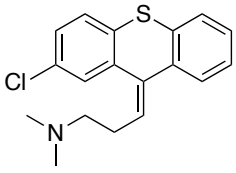 Chlorprothixene					Turbidity Background
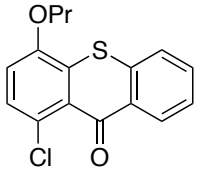 1-Cl-4-^{i}Proxy-9H-thioxanthone		Turbidity			
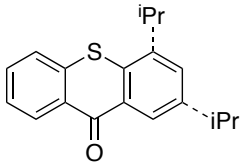 ^{i}Pr-9H-thioxanthone (mixture of isomers)		Turbidity	Essentially 0, negative rate over 50 µM		Background
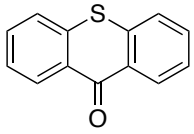 Thioxanthone	Turbidity		Turbidity		
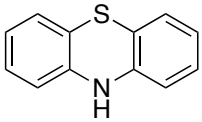 Phenothiazine	Background		Essentially 0, negative rate over 50 µM		Background
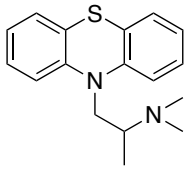 Promethazine	Background				

Table 3.3. Flavin site SAR on compounds sharing a TCA core. Five different complex I flavin-site assays were carried out on 8 structurally similar compounds. Data are presented in terms of turbidity (as a proxy for poor solubility), relative complex I-free rate (background) and trend according to Figure 3.7 as explained in the header row.

The first three and last compounds in Table 3.3 are antipsychotic drugs, phenothiazine is used as a stabiliser and the second three are type II photoinitiators used in polymer generation processes, thioxanthone and two thioxanthone derivatives.

There are some caveats to be aware of when analysing thioxanthone derivatives in a spectrophotometric assay. One of the major drawbacks related to the use of thioxanthone-based molecules can be the generation of radicals with reagents present in the assay mixture (primarily Tris buffer which is used in the isolated complex I assays) by absorption of light at the wavelengths involved in the assays (340, 380, 400, 450, 577, 620 nm). Photoinitiators become excited in a triplet state upon absorption of light and then, when an appropriate coinitiator is present (tertiary amine, alcohol, thiol, ether,…) radicals are generated in a bimolecular process (the typical reaction scheme is depicted in Figure 3.8)[212].

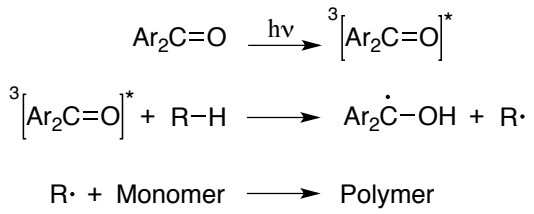

Figure 3.8. General mechanism for type II photoinitiators in polymer formation. Light of appropriate frequency generates an excited triplet species (upon internal system crossing) which interacts with a coinitiator R-H (amines, alcohols, ethers, …) to generate two radicals: the polymerisation will be initiated by the radical coinitiator.

If such radicals are generated (and this happens when the absorption bands and the light emission wavelength overlap) it means that the molecule being assayed is being degraded. Absorption maxima for thioxanthone derivatives are in the range between 230-310 nm and 330-420 nm[213] and tertiary amines are more reactive towards these species as coinitiators than alcohols or ethers[214]. The complex I-free rate should be enough to detect any radical-based mechanism: that is what might happen in the NADH:APAD assay with isopropyl thioxanthone (mixture of isomers) and Phenothiazine, where a significant negative background rate was found at compound concentrations higher than 50 μM (220 and 20% of the corresponding complex I-driven rate at 80 μM in absolute value, respectively, where normally a 1% background rate across the whole titration is seen, see Table 3.3). Thioxanthone has also been tested as a monoamine oxidase (MAO) inhibitor (showing remarkable activity towards the isozyme MAO-A) by following absorbance at 315 and 360 nm[215].

Lastly, isopropyl thioxanthone is a mixture of two isomers (2- and 4-), so the response obtained with the assays is the combined effect of two species.

The FeCN assay exhibits the most significant variations and also many chemical issues (turbidity and elevated background rates). Similarly, the NADH:Q_1 reaction exhibited the most artefacts: the presence of asolectin in the assay could account for the formation of insoluble agglomerates at high drug concentration. The only molecule that interferes with the APAD reaction (without chemical interference) is chloro-propoxy thioxanthone, while the HAR reaction did not always follow the opposite trend of FeCN. The pattern exhibited by the ROS assay across the library suggests that ROS generation at the flavin site of complex I is affected by the central N atom in the dibenzoheterocyclic core; however, it was found that Phenothiazine inhibits HRP directly. The ROS assay performed with high NADH concentration (200 μM as opposed to the regular 30 μM) on the compounds did not show a different pattern than the one seen with low concentration. Thioxanthone (the barest of the molecules when it comes to side chains and substituents, along with Phenothiazine) exhibited a constant rate for all of the flavin reactions: it appears that, in order to possess any complex I flavin activity, a dibenzoheterocycle-based molecule should have either a central N atom, a side Cl atom or an alkyl chain.

In spite of the efforts undertaken to shed light on the relationship between the dibenzoheterocyclic core and flavin site activity at complex I, the conclusions are minor (a possible role for the central N atom of the core in flavin reactivity) and not entirely reliable at best (given the many chemical issues some assays are plagued with). In general, the flavin site of complex I seems relatively unreactive towards the drugs in the library (the same conclusion was drawn in chapter 4 and featured a much larger set of drugs).

3.4.4 Seahorse XF 96 cellular assays

While the OCR is primarily a measure of mitochondrial respiration, ECAR is primarily a measure of lactic acid release, so a Seahorse experiment can be used to screen compounds for mitochondrial impairment and also to determine how well whole cells can invoke glycolysis to compensate for drug-induced mitochondrial dysfunction [216]. Figure 3.9 shows OCR and ECAR traces for five Seahorse experiments: the plots shown are indicative of common patterns of the tested drugs, which are explained in detail in Table 3.4. Table 3.5 reports OCR inhibition and residual ECAR rates from the Seahorse experiments, carried out at three times the IC_{50} value in the NADH:O_2 assay (5-6 drugs were tested in different replicates within a single Seahorse 96 well plate at a time). The data point immediately before rotenone addition was considered, with associated p-values for the unpaired 2-tailed Student's t-tests (t-tests and inhibition/residual percentages refer to the comparison with the control experiments). Furthermore, Table 3.5 includes a labelling system (presented in Table 3.4) to summarise the overall effects of the drugs on cells: the system was designed in order to be as objective as possible in assigning such labels and to include all of the data points in the trace rather than a single one. If the difference between every single control value and the corresponding OCR (or ECAR) value is greater than 20% in absolute value (and statistically significant with $p \leq 0.05$) in the majority of data points between drug and rotenone injections it means that the (upward or downward) trend is significant, otherwise it is assumed to be constant.

OCR	ECAR	LABEL	Explanation
↓	↑	OXPHOS	Inhibition of oxidative phosphorylation by the drug means that OCR is inhibited, the cell relies more on glycolysis and the ECAR trace subsequently rises (this trend is also common with TCA cycle[217,218] or BCL-2[219] inhibitors)
↓	↓	CELL DIES	The drug exerts such a toxic effect on cells that ATP production from both glycolytic and mitochondrial sources is halted, leading to cell death
↓	Constant	FAO	This is the signature of compounds like etomoxir, inhibitors of fatty acid oxidation through CPT-1, a carnitine transporter[220]
Constant	↑	?	This behaviour is unusual and cannot be explained
Constant	Constant	NONE	The drug does not have any detectable effect

Table 3.4. Labels for Seahorse trends in Table 3.5. Trends were defined as whether the majority of the differences between every single control point with their corresponding OCR (or ECAR) points is over 20% (trend) or less (constant rate): five different patterns emerged from the data.

NONE

OXPHOS

CELL DIES

FAO

?

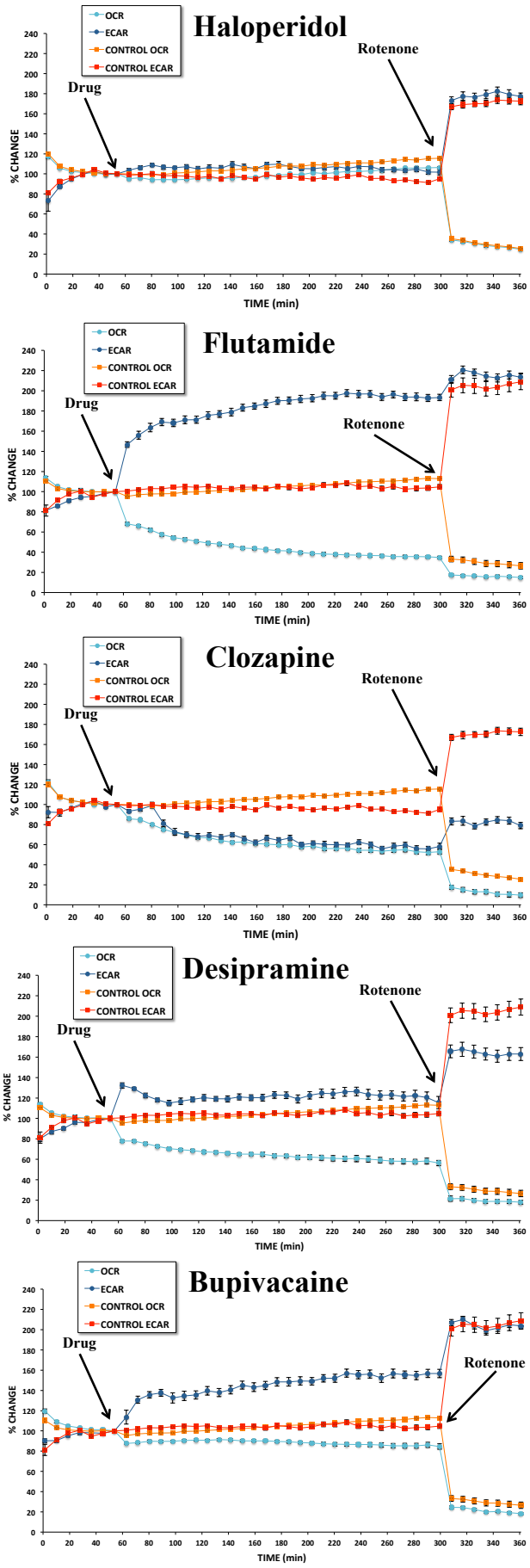

Figure 3.9. Typical patterns of Seahorse experiments. Representative OCR and ECAR traces for the five Seahorse drug patterns illustrated in Table 3.4. Drug and rotenone addition steps are highlighted. Error bars are SEM (n=24 for control, n=8 for drugs).

	SEAHORSE EXPERIMENT							
	MAJOR EFFECT	OCR INHIBITION %			RESIDUAL ECAR %			µM
			SEM	p-VALUE		SEM	p-VALUE	
Chlorpromazine	FAO	52.3	3.8	****	98.3	6.4	ns	33.3
Desipramine	FAO	58.9	3.1	****	116.1	5.9	**	77.1
Fluphenazine	CELL DIES	60.4	2.2	****	53.3	2.2	****	52.8
Flutamide	OXPHOS	80.7	1.6	****	185.9	5.7	****	84.0
Fenofibrate	FAO	26.5	5.1	***	105.5	4.9	ns	10.8
Estradiol	NONE	27.3	3.2	***	106.4	3.6	ns	42.6
Papaverine	OXPHOS	74.8	3.2	****	188.4	11.7	****	5.10
Bupivacaine	?	30.3	3.1	****	151.1	5.4	****	1299
Amiodarone	?	32.1	2.5	****	131.1	3.2	****	25.7
Rosiglitazone	OXPHOS	97.4	2.5	****	219.0	16.9	****	114
Nefazodone	OXPHOS	31.0	1.7	****	123.5	3.3	****	2.49
Carvedilol	?	29.7	2.5	****	111.8	3.0	****	20.1
Tamoxifen	OXPHOS	48.4	2.1	****	127.7	4.1	****	15.9
Clozapine	CELL DIES	61.5	2.8	****	61.3	2.8	****	152
Buspirone	OXPHOS	40.9	2.5	****	121.7	3.2	****	54.9
Haloperidol	NONE	10.7	1.9	***	111.6	2.8	****	7.11
Sunitinib	/	/	/	/	/	/	/	27.0
Trifluoperazine	CELL DIES	41.7	1.8	****	66.5	14.5	**	39.0
Capsaicin	OXPHOS	54.1	2.4	****	145.7	11.2	****	77.4
Doxorubicin	/	/	/	/	/	/	/	258
Efavirenz	OXPHOS	42.5	1.2	****	111.0	5.5	ns	35.1

Table 3.5. Results for the Seahorse experiments (both at three times IC_{50} for NADH:O_2). OCR inhibition and residual ECAR values from the Seahorse experiment are presented with SEM (n≥23 for control, n≥6 for drugs) and p-values and they refer to the last data point prior to rotenone addition. Doxorubicin and Sunitinib Seahorse experiments were not successful due to their colouring of the assay buffer that, very likely, interfered with the fluorescence signals. Drug concentrations were three times their NADH:O_2 IC_{50} values. The labels used to describe the major effects of the Seahorse experiment are explained in detail in Table 3.4. Statistical significance expressed as ****, $p \leq 0.0001$; ***, $p \leq 0.001$; **, $p \leq 0.01$; *, $p \leq 0.05$; ns, $p \geq 0.05$.

Indeed, considering the last data point prior to rotenone addition, all of the drugs in the library inhibit OCR to some extent, whereas the residual ECAR exhibits more varied trends (see Table 3.5). Considering the overall traces, recognisable patterns are inhibition of OXPHOS (substantial in Flutamide, Papaverine, Rosiglitazone and Capsaicin), inhibition of fatty acid oxidation (substantial for Chlorpromazine and Desipramine, borderline for Fenofibrate), cell death (substantial in Fluphenazine, Clozapine and Trifluoperazine) and lack of effects in cells (Estradiol and Haloperidol). The pattern followed by Bupivacaine, Amiodarone and (borderline) Carvedilol (constant OCR in tandem with increase of ECAR) does not have a clear explanation. As for the inhibition of fatty acid oxidation pattern, Pike *et al.*[220] reported that inhibition of fatty acid transporter carnitine palmitoyltransferase I (CPT-1) only

generated a modest increase in glycolysis rate in SF188 (human glioblastoma) cells but a significant decrease in OCR. They ascribed the effect to endogenous fatty acid oxidation in cells playing further roles than just ATP synthesis and linked the former to NADPH generation and, therefore, to the antioxidant system of the cell. Since fatty acid oxidation generates one equivalent of NADH for each two-carbon unit oxidised, its inhibition would keep the NADH pool more oxidised, thus lightening the burden for complex I. This would be measured as a lower OCR, while the lack of compensatory glycolysis (constant ECAR) could reflect a negligible effect if fatty acid oxidation on the net cellular ATP demand. Furthermore, the ECAR trace does not reach the control levels after rotenone addition in the Seahorse fatty acid oxidation pattern (see Desipramine trace in Figure 3.9 and later in this section) and this could be indicative of cellular ROS damage due to the above-mentioned link between fatty acid oxidation inhibition and hampered the cellular antioxidant machinery.

The only instances where the ECAR decreased significantly just before rotenone addition (Fluphenazine, Clozapine and Trifluoperazine, Table 3.5) experienced a decrease in OCR too: this means that the drugs have a detrimental effect on cells, disrupting both OXPHOS and glycolytic systems. It must be pointed out, however, that an inhibitor of hexokinase (the first enzyme of the glycolytic pathway), 2-deoxyglucose, brought about the same response in HeLa cells than the compounds assumed to cause cell death in this work, namely lowering of both OCR and ECAR traces (even though the OCR decrease was minor compared to the ECAR one)[221]. The metabolic response of cancer cells to glycolysis inhibitors has been shown to be uniform in terms of ECAR (it diminishes), while in terms of OCR the response varies: in theory it should climb to reflect the higher mitochondrial respiration invoked to compensate for ATP depletion but inhibitors of different glycolytic enzymes exhibited various OCR trends[222]. Cell death is also reflected by the difference in ECAR (after rotenone addition) between control and drug traces: if they are roughly at the same level it means that glycolysis was not affected, whereas if the ECAR of the drug is significantly less than control it means that over the time course of the experiment glycolysis was severed (see final portion of the ECAR trace of Clozapine, Figure 3.9, lower panel, compared to the other ECAR traces). This last feature of the drugs, combined with a significant OCR decrease parallel to ECAR over time, were

the reasons why compounds that exhibited such metabolic signature were deemed toxic for cells, even though it is possible that their effect is glycolysis inhibition.

In a study by Dyckens *et al.* [223], Nefazodone and Buspirone were tested at concentrations similar to this work (6.25 and 25 μM respectively) in HepG2 cells, leading to the same pattern in oxygen consumption and ECAR. In another study, Funes *et al.*[224] reported a significant (and concentration-dependent) decrease in basal respiration in human cell lines glioma U-251MG and neuroblastoma SH-SY5Y at 25 μM. Different results were found by Nadanaciva *et al.*[216], for Chlorpromazine, Clozapine and Rosiglitazone (tested at 300, 300 and 100 μM respectively): while Chlorpromazine increased both OCR and ECAR, Clozapine and Rosiglitazone had no effect on either. Flutamide, on the other hand (at 84 μM) generated an increase in ECAR and decrease in OCR in line with this work. It could be that the results obtained by Nadanaciva are due to the different expression of drug metabolising enzymes in the cell line they used, HepG2 (less than 1% of those found in normal human hepatocytes[225]) compared with the cell line used in this work, HeLa (whose expression of drug-metabolising enzymes is low as mentioned in section 3.3.3 but possibly not as low as in HepG2). Similarly, the results obtained by Dyckens and Funes could indicate that the toxicity observed by the drugs is not linked to formation of reactive metabolites (hence the similar findings to this work). One interesting feature of HepG2 cells that could be relevant in this context is that the expression of drug-transporting proteins is generally higher than in HeLa cells[226].

3.4.5 Drugs pK_a and intracellular accumulation

Literature therapeutic plasma concentration and pK_a values are reported in Table 3.6 in order to present physiologically relevant information on the drugs, along with the corresponding IC_{50} values for the NADH:O_2 assay. It must be borne in mind that pK_a values, as reported in the literature, often do not differentiate between protons from an acid and from the conjugate acid of a base, thus cannot specify whether a neutral molecule is an acid or a base (especially when the drug contains both acidic and basic groups)[227]: Table 3.6, therefore, includes the charge of the drugs at physiological pH. Also, calculated logP (clogP) values were obtained to find out whether a relationship between hydrophobicity of the drugs and their potency exists: as illustrated in Figure 3.10, the correlation coefficient between NADH:O_2 IC_{50} values and clogP is -0.025,

indicating lack of substantial correlation (when the IC_{50} is expressed in logarithmic terms, the correlation becomes -0.27). Interestingly, removing the drug with the highest NADH:O_2 IC_{50} values (Bupivacaine, 433 nM) raises both correlation coefficients between clogP and IC_{50} in normal and logarithmic form (-0.53 and -0.40, respectively). As for the relationship between drug potency towards NADH:dQ and hydrophobicity, the correlation coefficients between IC_{50} values and clogP are 0.30 and 0.28 (IC_{50} values in normal and logarithmic form, respectively); when Bupivacaine is removed from the set they become 0.32 and 0.27, respectively. However (and as it will be explained more thoroughly in chapter 4), the NADH:dQ assay is afflicted by experimental limitations, so the apparent positive correlation coefficient between potency and hydrophobicity may, in fact, be the result of artefacts.

	Therapeutic Concentration µM	pK_a	Charge at physiological pH	NADH:O_2 IC_{50} µM	clogP	MW
Chlorpromazine	0.5[228]	9.2[229]	P[230]	11.1	4.54	319
Desipramine	1.9[228]	9.9[231]	P[231]	25.7	3.90	266
Fluphenazine	0.01[228]	10.0[229]	P[232]	17.6	3.97	438
Flutamide	0.4[233]	4.8[234]	N[234]	28	3.27	276
Fenofibrate	13.9[235]	/	**Neutral**	3.6	5.28	361
Estradiol	< 1nM[236]	10.7[237]	**Neutral**[237]	14.2	3.75	272
Papaverine	3.00[228]	8.1[238]	P[238]	1.7	3.08	339
Bupivacaine	5.2[228]	8.1[239]	P[240]	433	4.52	288
Amiodarone	5.3[228]	9.4[241]	P[242]	8.55	7.64	645
Rosiglitazone	0.8[228]	6.1[243]	**Neutral**[243]	38.1	3.08	357
Nefazodone	4.0[228]	6.5[244]	**Neutral**[244]	0.83	4.65	470
Carvedilol	0.4[228]	7.8[245]	P/**Neutral**[246]	6.69	3.51	405
Tamoxifen	0.2[247]	10.8[248]	P[248]	5.3	6.35	372
Clozapine	2.5[228]	7.6[232]	P/**Neutral**[232]	50.8	3.40	327
Buspirone	0.01[228]	7.6[249]	P[250]	18.3	1.78	386
Haloperidol	0.1[228]	8.65[251]	P[252]	2.37	3.66	376
Sunitinib	0.1[253]	8.95[253]	P[254]	9	2.93	398
Trifluoperazine	0.02[255]	8.97[229]	P[256]	13	4.66	408
Capsaicin	8.1 nM[257]	10.1[258]	**Neutral**[258]	25.8	3.75	305
Doxorubicin	0.2[228]	8.6[259]	P[259]	85.9	1.50	544
Efavirenz	12.7[260]	10.2[261]	**Neutral**[262]	11.7	4.46	316

Table 3.6. Literature values for therapeutic concentration and pK_a. Literature values for therapeutic concentration and pK_a are presented for the drugs tested in this chapter. IC_{50} values for NADH:O_2 are taken from Table 3.1. Green cells indicate which drug therapeutic concentration is higher than its corresponding NADH:O_2 IC_{50} level. P, positive charge; N, negative charge. clogP values calculated using MarvinSketch Version 16.5.2.0 Consensus Model by ChemAxon. MW, molecular weight.

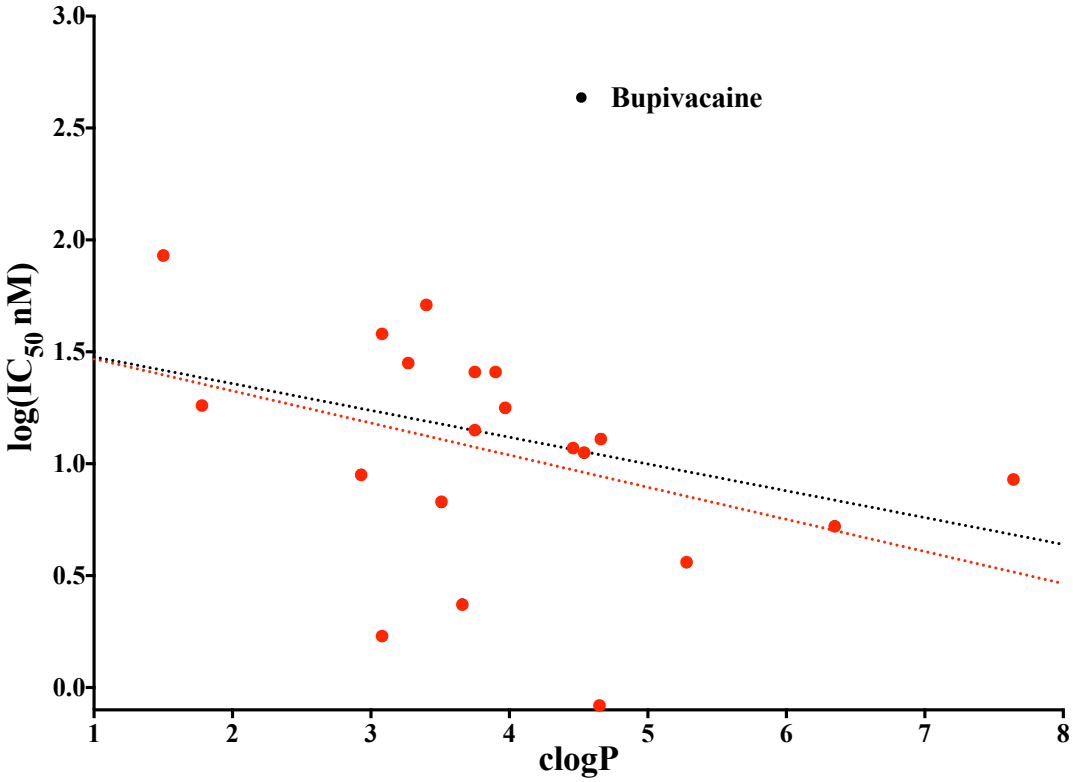

Figure 3.10. Relationship between hydrophobicity and inhibitory potency for the drugs featured in this chapter. Even though the correlation between the two variables is negative (as illustrated by the linear fit between them, black dashed line), it is not substantial. When the drug with the highest NADH:O_2 IC_{50} value, Bupivacaine, is not considered, the correlation between potency and hydrophobicity becomes more significant.

As for pK_a values, if the charge of the drug at physiological pH is positive (*i.e.* the pK_a of its conjugate acid is higher than 7.3-7.4), transport inside mitochondria could be enhanced (the matrix is more negatively charged than the intermembrane space), resulting in intramitochondrial accumulation of the drug: however, this would more likely occur with phenols than with amines because, once in the matrix, deprotonation could cause the (deprotonated) amine to cross the IMM back. It must be further pointed out that such transport depends on other factors as well (*e.g.* the structure of the drug) hence the pK_a can be considered a necessary but not sufficient condition for electrophoretically-driven membrane crossing. Even though the pK_a alone does not necessarily mean that the drug will be able to cross the inner mitochondrial membrane, several drugs with high pK_a lower the OCR to a considerable degree (*e.g.* Chlorpromazine, Desipramine and Capsaicin, Table 3.5, only the latter being neutral at physiological pH, Table 3.6). Remarkably, some drugs with a pK_a similar or lower than physiological pH decrease the OCR to an even lower level while promoting glycolysis (Flutamide, Papaverine and Rosiglitazone, Table 3.5), irrespective of

charge. Hence, it appears that the pK_a values are not predictive of OCR inhibition, in fact some drugs possess the same pK_a values and charge (Fluphenazine and Bupivacaine 8.1, Clozapine and Buspirone 7.6), and yet their penetration into mitochondria (as approximated by the OCR percentage inhibition) is different (in the former couple of drugs 60.4 and 30.3%, in the latter 61.5 and 40.9%, respectively): this means that pK_a and charge are not enough to predict intramitochondrial accumulation of a drug.

Only three drugs exhibit an IC_{50} for the NADH:O_2 assay that is therapeutically relevant (green cells in Table 3.6), Fenofibrate, Nefazodone and Efavirenz (in chapter 4 a dedicated section to this issue will be presented, in particular for the phenomenon of drug overdose that transcends the therapeutic boundary). These drugs are also neutral at physiological pH.

3.4.6 Incorporation of drug metabolism in mitochondrial membrane assays

3.4.6.1 Metabolism of xenobiotics: an introduction

Drugs, and more in general xenobiotics, are substrates of a wide range of drug-metabolising enzymes in our body: the actions of these enzymes are traditionally classified into a first transformation to a more polar metabolite (Phase I oxidations and reductions) commonly followed by a (Phase II) conjugation reaction where a polar handle is attached to the metabolite to make its excretion easier[263]. This is true in particular for orally ingested drugs: on its way to reaching systemic circulation, an oral dose is metabolised by different enzymes in the gut wall cells and primarily by the liver (through the portal vein), a process named the first-pass effect[264].

Phase I metabolising enzymes include peroxidases (the substrate is oxidised while hydrogen peroxide is reduced)[265], flavin monooxygenase (FMOs, nucleophilic centres containing a lone pair are converted into the corresponding oxides and they act on a more restricted range of compounds than CYP450, see later)[266], molybdenum hydroxylases (aldehyde oxidase and xanthine oxidoreductase, they catalyse oxidative hydroxylations of alkyl bonds), FAD-dependent amine oxidases (they catalyse the deamination of amines and oxidation of polyamines)[267], aldo-keto reductases and the short-chain dehydrogenases/reductases (they catalyse the reduction of aldehydes and ketones to secondary alcohols)[268,269]. Phase II enzymes involve the addition of a polar

handle onto their substrate, commonly after the action of Phase I enzymes: UDP-glycosyltransferases add sugars (especially glucuronic acids in mammals but also N-acetylglucosamine, glucose and galactose)[270], sulfotransferases add sulfonate to a hydroxyl or primary amine group[271], N-acetyltransferases add acetyls onto a nitrogen in arlyamines, arylhydroxylamines and arylhydrazines[272], and glutathione transferases add glutathione (via its sulfur atom)[273].

The dominant category of drug-metabolising enzymes is the cytochromes P450 (CYP450): according to a very recent estimate, about 96% of all metabolic oxidation-reduction of drugs are catalysed by this Phase I class, three-fourths of which are accounted for by only 5 isoforms, 1A2, 2C9, 2C19, 2D6 and 3A4 (27% just by 3A4 on its own)[274]. There are 57 genes in humans encoding for isoforms of CYP450, 16 of which (based on a classification according to their major substrate class) act on xenobiotics, the others act on sterols, fatty acids, eicosanoids and vitamins (the substrates of 8 isoforms are still unknown)[275]. The range of reactions they catalyse and the diversity of substrates are truly astonishing: literally hundreds of different reactions such as hydroxylations, dealkylations, epoxidations are known[276]. The typical catalytic cycle of CYP-mediated metabolic transformation of compounds is depicted in Figure 3.11[277]. A general substrate R-H binds to the protein cavity (step 2), NADPH provides electrons that are needed to reduce the iron metal centre (step 3) and to convert the peroxyl radical ligand to the peroxide (step 5). The electrons are not transferred directly but through P450 reductase, a protein embedded in the endoplasmic reticulum whose cofactors include a FAD and FMN group which are sequentially reduced during electron transfer[278]. After formation of a Fe(IV) oxide metal centre (step 7), the irreversible step of oxygen addition across the R-H bond follows.

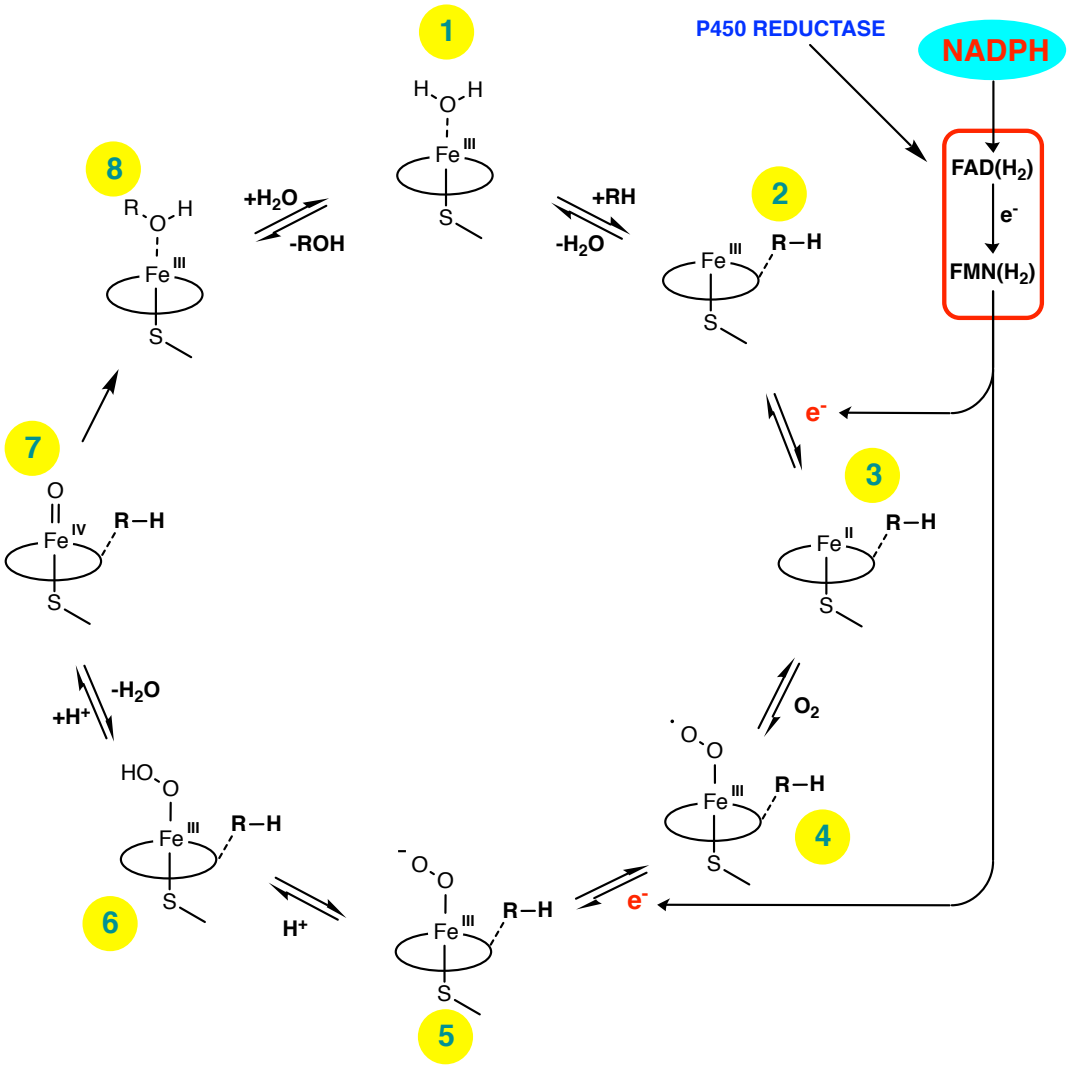

Figure 3.11. General catalytic cycle for CYP450-mediated oxidation of substrate RH. After substrate binding to the protein cavity (2), electrons are transferred from the P450 reductase system to the Fe(III) centre (3) and to the dioxygen radical ligand (5). Water loss at this point (6) leaves an iron(IV)-oxo centre which delivers oxygen across the R-H bond of the substrate (8) to generate the corresponding product ROH. Scheme adapted from Olsen, Oostenbrink and Jørgensen[277].

Most of the CYP450s are localised in the endoplasmic reticulum, even though six isoforms are known to be present in mitochondria[279]: much of the enzymes, as well as P450 reductases, stick out of the ER membrane (to which they are attached by the amino terminus) into the cytosol[280]. Furthermore, several members of the CYP450 class are bimodally targeted proteins, hence they can be present in multiple cellular sites on account of multimodal targeting signals[281].

3.4.6.2 Incorporation of drug metabolism in mitochondrial membrane assay

In vitro drug metabolism assays often employ human liver microsomes, a well established and convenient way to mimic CYP-mediated metabolism, since they contain all CYP450 enzymes (as well as FMOs): homogenised liver samples are first centrifuged at lower force to obtain the S9 fraction, which contains a wide array of both Phase I and II enzymes; then, the S9 fraction is ultracentrifuged (commonly 100,000g for at least one hour) to precipitate microsomes[282].

There are not many examples in the literature of "one-pot" assays that combine microsomal-driven metabolite formation with assessment of metabolism induced toxicity: these mostly take the form of gel-encapsulated microsomes on silica/quartz plates that are physically and directly connected to cytotoxicity assays[283-286]. Figure 3.12 summarises the protocol to incorporate drug microsomal incubations in the NADH:O_2 assay with mitochondrial membranes: drugs were incubated at a concentration that would give at least 50% inhibition in the assay (or the highest available concentration permitted by compound stocks concentration).

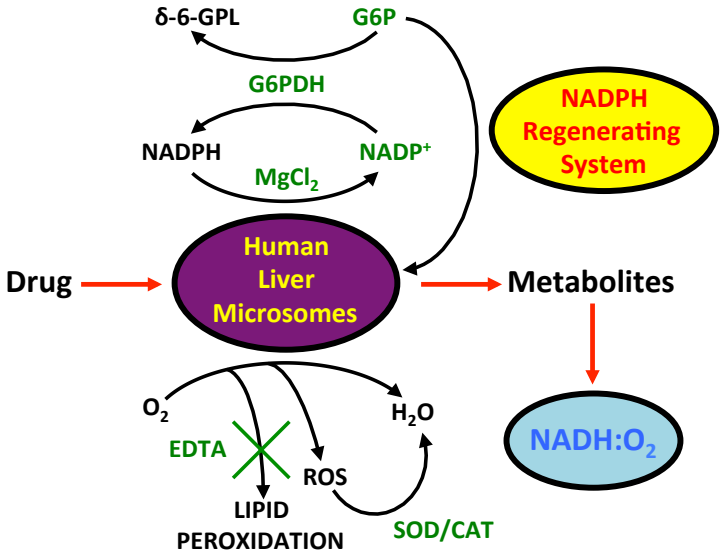

Figure 3.12. Schematic procedure for incorporating microsomal metabolism into the NADH:O_2 assay. The drug is incubated with a NADPH-regenerating system that also feeds a separate intraluminal $NADP^+$ pool coupled to reductase enzymes. $MgCl_2$ is added to support NADPH binding to P450 reductase, EDTA prevents lipid peroxidation and SOD/CAT stop ROS from building-up excessively. G6P, glucose 6-phosphate; δ-6-GPL, 6-phosphoglucono-δ-lactone; G6PDH, glucose 6-phosphate dehydrogenase; SOD, Superoxide dismutase; CAT, Catalase.

Adapting a typical microsomal protocol so that the outcome (*i.e.* microsomal incubation of the drug) could be subsequently employed in a NADH:O_2 assay to test metabolism-induced toxicity was challenging: many variables were taken into consideration in order to optimise the final procedure and whose main points are explained below.

- Even though carbonate **buffer** would more appropriately reflect an *in vivo* environment, the experimental difficulties that would be encountered usually lead one to choose phosphate buffer (other buffers can affect CYP450 activity)[287].
- Since **NADPH** is needed for CYP450 activity, it needs to be introduced in the microsomal incubation, either directly or via a NADPH-generating system with appropriate cofactors: isocitrate dehydrogenase with isocitrate or glucose 6-phosphate dehydrogenase with glucose 6-phosphate (G6P). It was recently found that carbonyl reductase activity in microsomes (especially from the enzyme 11β-hydroxysteroid dehydrogenase type 1) is localised inside the lumen, to where NADPH and $NADP^+$ do not have easy access: G6P can easily enter this milieu by a transporter protein and feed a separate intraluminal $NADP^+$ pool coupled to reductase enzymes[288]. A G6P-driven NADPH-generating system is, therefore, a better choice to feed CYP450 in microsomal incubations than just NADPH. Assays with activated microsomes always exhibited 30 to 50% higher absorbances at 340 nm than the assays with inactivated microsomes, indicating that NADPH (whose UV spectrum is identical to NADH) had been formed during the incubation.
- **EDTA** was added to curtail NADPH- and iron-dependent lipid peroxidation which could degrade CYP450[289].
- A low **microsomal protein concentration** (0.4 mg mL^{-1}, where the common range in the literature is 1-2 mg mL^{-1}) was used to prevent the phenomenon of nonspecific binding, whereby (especially hydrophobic) compounds bind to the lipid-protein milieu of the microsomal membrane and are not metabolised[290].
- **Drugs** dissolved in organic solvents as **stocks** were added to the incubation making sure that the overall concentration of the solvent was less than 0.5%: a concentration higher than 1% can be severely detrimental to CYP450 metabolism and activity[291].

- Several organic solvents were trialled for **quenching** and even though lowering the temperature below water freezing point would be enough, rather than organic solvent addition [292], the latter is preferable because microsomal proteins denature and precipitate out of solution fully: this releases all of the substrates and products and removes a source of artefacts in the NADH:O_2 assay (*i.e.* microsomes that are still active can oxidise NADPH and also, to a lower extent, NADH, leading to overestimation of rates). Diethyl ether was chosen because of its extremely limited chemical reactivity and ease of removal via evaporation.
- Human liver microsomes are known to generate significant amounts of ROS in the presence of NADPH and NADH as reductant[293], and this (combined with consumption of endogenous substrate) could explain the about 10 times higher NADPH-consumption rate than the actual drug-to-metabolite conversion rate[294]: **superoxide dismutase** and **catalase** were therefore added to avoid build-up of species with a potential for metabolite degradation[295,296].
- **$MgCl_2$** is added to support the binding of NADPH to P450 reductase[297].
- The incubations were all carried out in **amber glass vials** to prevent metabolite photodegradation and interaction with plastic[298].
- The literature describes many different **centrifugation speeds** to pellet the microsomal fraction out of the incubation mixture: 5000 x g was deemed enough to remove the vast majority of microsomes and not too much to degrade metabolites in the process[f].
- The **drug incubation time** with microsomes, 6 hours, was much longer than a typical microsomal protocol [299] : this was done to ensure that the biotransformation reactions went to completion and also to exhaust the above-mentioned NADH oxidase activity of any microsomal protein that could survive the later stages of the process and that could, ultimately, affect the results of the NADH:O_2 assay.

The results for a test set of compounds are shown in Figure 3.13: microsomes were activated with G6P and $NADP^+$ and the (drug-inhibited) NADH:O_2 specific activity with inactivated microsomes signifies the amount of drug that has survived the incubation process. Rotenone was added for comparison and, interestingly, exhibited

[f] During preliminary experiments, it was found that some drugs like Efavirenz, Capsaicin and Fenofibrate maintained their potency towards the NADH:O_2 pathway after dilution in aqueous buffer but lost it almost completely after centrifugation at 10,000 x g for 10 minutes.

the highest deactivation (*dihydro*-rotenone and Deguelin were also detoxified to a similar extent). The only drugs in the library that after metabolism caused a significantly weaker inhibition than the corresponding parent compounds are Papaverine, Nefazodone, Capsaicin and Promazine. Chlorpromazine and Desipramine exhibited similar residual activity regardless of whether microsomes were activated or not. All of the other drugs exhibited no inhibition: evidently these compounds are not compatible with the microsome protocol, possibly due to aqueous degradation.

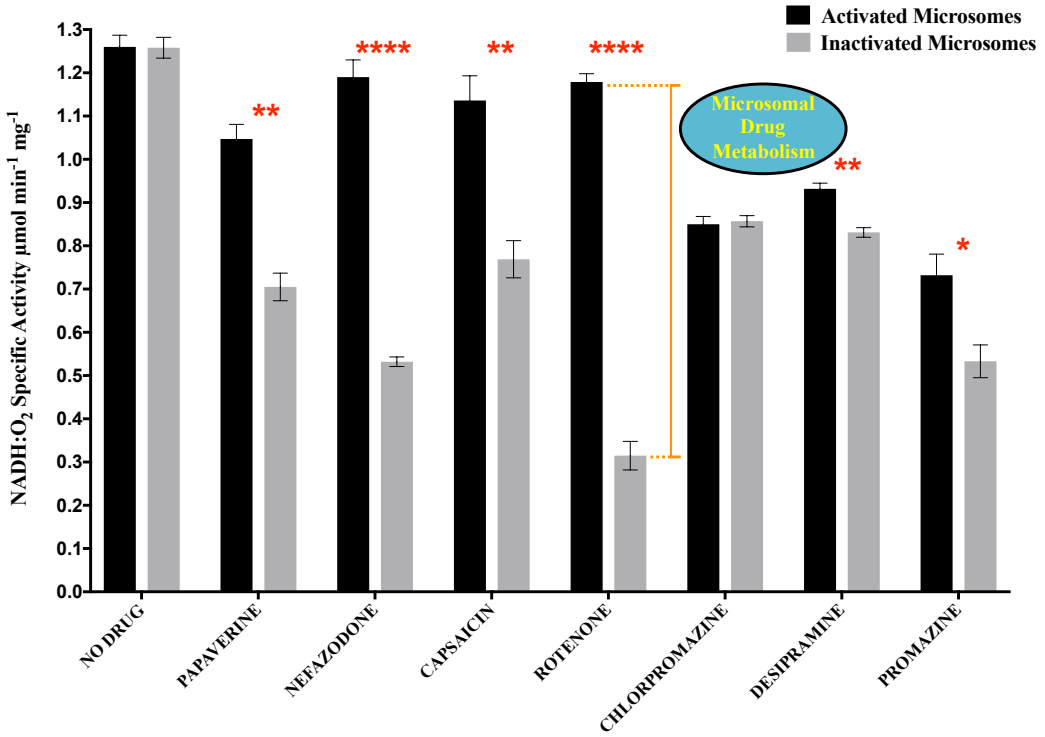

Figure 3.13. Compounds that cause a lower inhibition of the NADH:O_2 assay after microsomal metabolism. When microsomes are activated with NADPH, their catalytic activity transforms papaverine, nefazodone, capsaicin and rotenone to such an extent (greatest in rotenone) to contain their toxicity as captured by the NADH:O_2 assay and as shown by the blue line for nefazodone. Statistical significance expressed as ****, $p \leq 0.0001$; ***, $p \leq 0.001$; **, $p \leq 0.01$; *, $p \leq 0.05$. Error bars are SEM of triplicates.

These results indicate that those compounds become less toxic (at least from an OXPHOS perspective) once CYP450 are involved. However, for some drugs, CYP450-mediated activity via the proposed protocol could be so slow that metabolites do not form in appreciable amounts during the incubation period and, therefore, what is mostly left is the parent drug; an alternative explanation is that metabolites are as damaging to the complex I-IV pathway as their corresponding parent compound. Due to time and budget constraints it was decided to conclude

investigations at this point, but mass spectrometry could be used in order to discern how extensive the metabolism of compounds in these incubations is, and hence to be able to draw some conclusions on metabolite toxicity. The intensity of the parent drug peak in the incubation with inactivated microsomes would be compared to the intensity of the same peak in the incubation with activated microsomes and this should be enough to tell the extent of CYP450 mediated metabolism; additionally, the presence of peaks at +16 and +32 compared to the parent drug peak in the activated microsome product would be diagnostic of typical CYP450 metabolism (*i.e.* addition of one or two oxygens).

3.5 Discussion

3.5.1 Types of inhibition

The data collected permit an evaluation of the type of inhibition the drugs elicit on the respiratory chain. Criteria were defined for potency (NADH:O_2 IC_{50} less than 15 μM, see Table 3.1) and (lack of) specificity towards complex I (succinate:O_2 inhibition greater than 15% and ratio of NADH:dQ over NADH:O_2 IC_{50} values greater than 5, see Table 3.2). Potent and specific complex I inhibitors (7 drugs) tick off only the former indicator, whereas potent and specific inhibitors of the II-IV pathway (3 drugs) tick off all three of them. Furthermore, if a drug exhibits just potency and significant inhibition of succinate:O_2 it is classified as an OXPHOS inhibitor (Fenofibrate and Sunitinib, the low NADH:dQ/NADH:O_2 ratio indicates that complex I is involved too). Finally, lack of potency but presence of both specificity indicators defines a specific inhibitor of the II-IV pathway (Fluphenazine). This drug classification is presented in Table 3.7, along with data from Seahorse and molecular charge at physiological pH.

Balijepalli et al.[300] found that Haloperidol is indeed a specific and potent inhibitor of complex I in mouse brain mitochondria: also in line with this work, Chlorpromazine was found to be a specific inhibitor and Clozapine did not inhibit appreciably complex I (see Table 3.7). Fluphenazine, on the other hand, was found to be as potent an inhibitor of complex I as Chlorpromazine, perhaps an effect of Fluphenazine being more capable of inflicting oxidative damage to the enzyme in mouse brain, according to their proposed mechanism of inhibition.

Tamoxifen is the only drug that is classified as a potent and specific complex II-IV inhibitor and, at the same time, elicits its cellular effects via an OXPHOS type of inhibition (see Table 3.7). Indeed, Tamoxifen is a major contributor to drug-induced liver injury through several mechanisms of mitochondrial toxicity[301] and was found to electrophoretically accumulate in mitochondria[302,303]. Theodossiou *et al.*[304] recently reported that its mechanism of toxicity involves redox cycling of its oxidative metabolites around complex III: Fe centres may participate in such coupling, generating Fe^{2+} and, ultimately, hydroxyl radical OH· à la Fenton. This could mean that, given the cellular effects detected by Tamoxifen in this work, HeLa cells possess enough drug-metabolising enzymes to physiologically mimic some pharmacological events (see section 3.4.4).

From the experimental findings presented here it can be concluded that the selected drugs indeed inhibit complex I to different extent and degree of specificity: the method applied for their selection was successful and the FDLabel is a reliable database for identifying culprits in OXPHOS-related drug-induced mitochondrial dysfunction.

3.5.2 Chemical structures

The drugs exhibit some common structural features that might play a role in their inhibitory potency. For instance, dibenzoheterocycles (a ring with at least an heteroatom flanked by two benzene rings) are included in Chlorpromazine, Fluphenazine, Trifluoperazine (first generation antipsychotics with phenothiazine moiety), Clozapine and Desipramine (second generation antipsychotic and a major metabolite of tricyclic antidepressant or TCA, respectively, both with a dibenzazepine moiety)[305] and Carvedilol (a beta blocker), see Figure 3.14.

	POTENCY	(LACK OF) SPECIFICITY		Type of inhibition	Cellular effect Seahorse	Charge
	NADH:O_2 IC_{50} < 15 µM	Succinate:O_2 % inhibition > 15%	(NADH:dQ/NADH:O_2) IC_{50} >5			
Chlorpromazine	✓			Potent and specific CI	FAO	P
Desipramine					FAO	P
Fluphenazine		✓	✓	Specific towards II-IV	CELL DIES	P
Flutamide					OXPHOS	N
Fenofibrate	✓	✓		OXPHOS	FAO	Neutral
Estradiol	✓			Potent and specific CI	NONE	Neutral
Papaverine	✓			Potent and specific CI	OXPHOS	P
Bupivacaine					?	P
Amiodarone	✓	✓	✓	Potent and specific II-IV	?	P
Rosiglitazone					OXPHOS	Neutral
Nefazodone	✓			Potent and specific CI	OXPHOS	Neutral
Carvedilol	✓			Potent and specific CI	?	P/Neutral
Tamoxifen	✓	✓	✓	Potent and specific II-IV	OXPHOS	P
Clozapine					CELL DIES	P/Neutral
Buspirone					OXPHOS	P
Haloperidol	✓			Potent and specific CI	NONE	P
Sunitinib	✓	✓		OXPHOS	/	P
Trifluoperazine	✓	✓	✓	Potent and specific II-IV	CELL DIES	P
Capsaicin					OXPHOS	Neutral
Doxorubicin		✓	/	/	/	P
Efavirenz	✓			Potent and specific CI	OXPHOS	Neutral

Table 3.7. Summary of relevant data for drugs featured in this work. By combining data for potency (Table 3.1) and specificity (Table 3.2), it is possible to determine the type of inhibiton pattern drugs exert in the respiratory chain. Cellular effects (Seahorse, Table 3.5) and charge at physiological pH (Table 3.6) are also presented. Green cells indicate which drug therapeutic concentration is higher than its corresponding NADH:O_2 IC_{50} level.

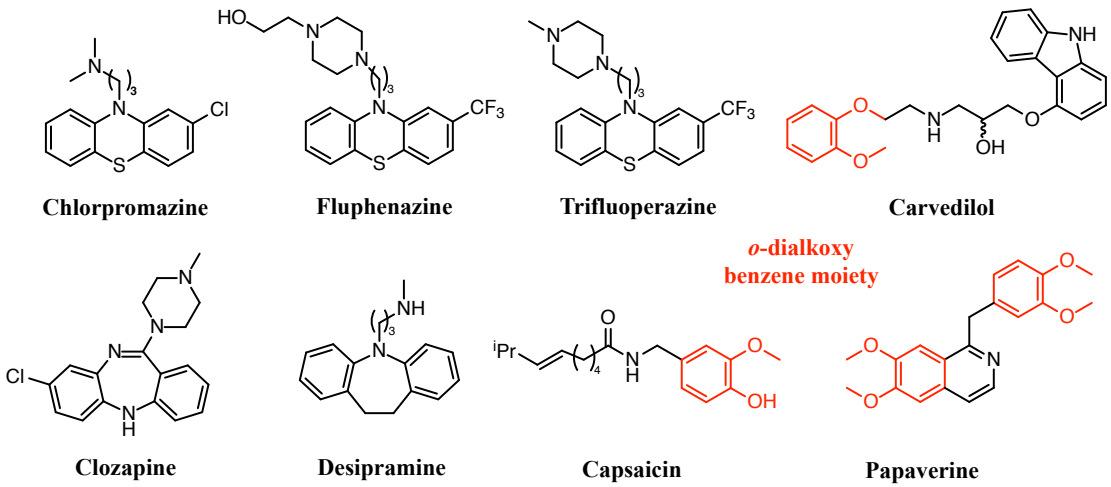

Figure 3.14. Dibenzoheterocycles and *o*-dialkoxy containing molecules in the library. The compounds core is a ring with at least an heteroatom flanked by two benzene rings. Carvedilol, Capsaicin and Papaverine possesses a feature in common with rotenone, the *o*-dialkoxy benzene ring (highlighted in red).

All of these drugs except Carvedilol share some inhibitory trends: they possess fairly low IC_{50} values (both in NADH:O_2 and NADH:dQ assays), inhibited the complex II pathway to different degrees (even though their benzoheterocycle moiety does not seem to correlate with the succinate:O_2 assay) and exhibited a strong OCR inhibition. Carvedilol, instead, has the lowest IC_{50} among the drugs with a tricyclic moiety (but also the lowest OCR inhibition, which might indicate that it does not penetrate cells easily), and this can be ascribed to another common structural feature of some of the drugs, the A-ring rotenone-like *o*-dialkoxy benzene moiety, present in Capsaicin and Papaverine too (a benzene ring with 2 alkyl groups ortho to each other, see Figure 3.14). The fact that only Papaverine possesses such a moiety (actually two) with the same alkyl substitution pattern as in rotenone (*i.e.* two methoxy groups) is reflected in its very low IC_{50} and high OCR inhibition compared to Capsaicin and Carvedilol. This dimethoxy substitution pattern in rotenone seems to be specific for complex I in bovine and not in other species, *e.g.* potato tuber and *Escherichia coli*[306]. See chapter 4 for structural classification of FDA-approved drugs and chapter 5 for a SAR study on rotenone both based on this feature.

3.5.3 Mitochondriotropics

Drug accumulation in subcellular compartments is an important topic in pharmacology and while some organelles may be the intended targets, others may be

the unwanted recipients. This is the case of weakly basic drugs that accumulate in acidic lysosomes on account of their being membrane-permeable when uncharged and membrane-impermeable when ionised: this phenomenon (referred as ion trapping or lysosomotropism) is one of the causes of anticancer multidrug resistance[307]. As for drug mitochondrial accumulation, mitochondriotropics were described as compounds with a delocalised positive charge that accumulate due to the electrochemical gradient across the IMM but their definition was extended to any agent that targets mitochondria irrespective of charge and accumulation[308].

A study by Horobin *et al.*[309] challenged the traditional view of mitochondriotropics as mostly compounds with delocalised positive charge that target mitochondria and accumulate within them. They generated a dataset of 110 known mitochondriotropics from the literature and discovered that only about a third were lipophilic cations, as many compounds were acids. Amphiphilicity was not a molecular property for targeting mitochondria since 2/3 of the dataset was either weakly or not amphiphilic at all. A more recent cheminformatics structure-localisation relationship study was carried out by the Rosania group in order to identify unique physicochemical properties of compounds that would explain their subcellular accumulation patterns[310]. They stratified the compounds with known subcellular localisation into low (less than 500 Da) and high (more than 500 Da) molecular weight with the aim of better identifying such patterns: they concluded that mitochondrial accumulation exhibited opposite patterns in the two categories, increasing with molecular weight below the threshold and decreasing with molecular weight above the threshold. This could hint at an optimum drug molecular weight for mitochondrial accumulation close to 500 Da but also advise caution when fluorophores probes are attached to compounds for detecting their subcellular accumulation: probes (and more generally any chemical modification aimed at increasing mitochondriotropism) can alter physicochemical properties of the compound, hence influencing its organelle targeting paradigm which also depends on the cytoskeletal network, dissolved macromolecules and other dispersed organelles[311]. It is interesting to note that Fluphenazine and Trifluoperazine have both a molecular weight between 400 and 500 Da and they both cause cell death, but this is probably due to their very similar structure (see Figure 3.14). Molecular weight does not seem to be a good predictor of mitochondrial targeting in the low range either, since the drugs with less than 300 Da (Desipramine,

Flutamide, Estradiol and Bupivacaine) all exhibit different cellular effects see (Table 3.5 and Table 3.6).

3.5.4 Known metabolism of drugs

Rotenone and Deguelin are primarily metabolised by CYP3A4 and CYP2C19 in human microsomes and their major metabolites are Rotenolone and Tephrosin, respectively[312]: their IC_{50} in NADH:O_2 membranes is 132 and 84 nM, much higher than their corresponding parent compounds, 8 and 12 nM respectively (see chapter 5) and this is reflected in the loss of inhibitory potency upon activation (see Figure 3.13). Figure 3.15 shows the main human metabolites of Capsaicin[313], Papaverine[314,315] and Nefazodone[316] with parent compounds in black, metabolites in orange. Given their minor structural changes and loss of potency upon microsomal metabolism, it seems that significant binding interactions with complex I are found in the rotenone-like *o*-dialkoxy moiety of Papaverine and in the isopropyl unit of Capsaicin. Nefazodone undergoes a drastic modification and likely the *m*-chloro benzene moiety is key to effective complex I binding. Interestingly, biotransformation of these compounds generates more hydrophilic metabolites, as expressed by their clogP values, see Figure 3.15, (the same happens during the biotransformation of Rotenone and Deguelin into their major metabolites, from 3.3 to 2.7 in terms of clogP for both, see chapter 5). This suggests that the binding sites for these compounds could be located in the membrane domain of complex I.

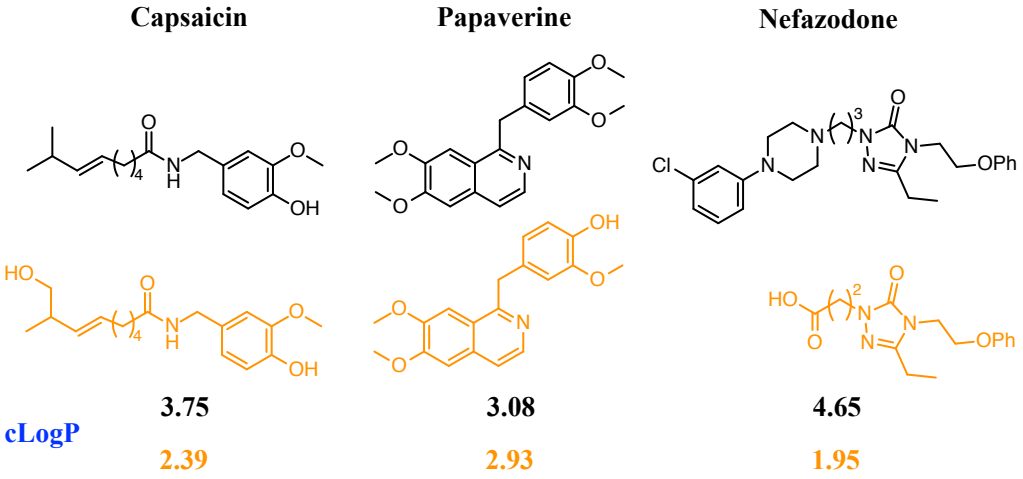

Figure 3.15. Major products of human metabolism for Capsaicin, Papaverine and Nefazodone. Nefazodone undergoes a substantial excision while Capsaicin and Papaverine metabolic changes are minor. Parent compounds are shown in black, metabolites are shown in orange. clogP values calculated using MarvinSketch Version 16.5.2.0 Consensus Model by ChemAxon.

3.6 Summary

The main experimental findings obtained in this work are summarised for each drug in Table 3.7. Most of the compounds chosen with the method proposed in this chapter turned out to be potent OXPHOS inhibitors with different degrees of specificity towards complex I: their characterisation was thorough, both in terms of biological systems and variety of assays performed. Ideally the methodology could be applied to any mitochondrial enzyme suspected to be the culprit of drug-induced mitochondrial dysfunction with the aim of identifying relevant toxicophores. In this regard, complex I inhibition does not seem to be restricted to a specific molecular scaffold (at least outside the flavin site), and this highlights the pharmacological relevance of this enzyme. Furthermore, the overall findings have been extremely useful to lay out a protocol of assays to be subsequently used to characterise a commercial library of approved drugs in chapter 4.

Specificity of inhibition was tested by comparing the effects of the drugs to two different biochemical pathways, complex I-IV (with NADH:O_2 oxidoreduction assay) and complex II-IV (with succinate:O_2 oxidoreduction assay), and it was discovered that very few drugs (Amiodarone, Tamoxifen and Sunitinib) could target, to some extent, the second pathway: this proves that the FDALabel database, in tandem with an extensive literature search, is a reliable method for obtaining an appropriate library of drugs to assess complex I-driven drug-induced mitochondrial dysfunction.

Flavin-site directed assays failed to detect any substantial patterns, indicating that the main target of the drugs lies somewhere else in complex I.

The Seahorse experiment in HeLa cells showed that drugs exhibited diverse effects in cells, demonstrating that transport mechanisms (irrespective of pK_a and charge) are important for drug toxicity.

Finally, the role of drug metabolism was assessed with microsomes: for some drugs, it resulted in considerable decrease in potency towards the NADH:O_2 pathway. Even though the results are encouraging, mass spectrometry is needed to confirm the viability of such a novel methodology.

3.7 Appendixes

3.7.1 Compounds obtained by intersecting complex I inhibitors and FDALabel database search (liver and extraliver side effects)

Drugs in common between the two side effects: Amiodarone, Amitriptyline, Aspirin, Citalopram, Clozapine, Ciprofloxacin, Desipramine, Divalproex, Doxorubicin, Efavirenz, Estradiol, Fenofibrate, Gemfibrozil, Ibuprofen, Ifosfamide, Indomethacin, Ketoconazole, Metformin, Mirtazapine, Nefazodone, Olanzapine, Paroxetine, Pioglitazone, Piroxicam, Propofol, Rosiglitazone, Sevoflurane, Simvastatin, Sorafenib, Tamoxifen, Tretinoin, Valproate.

Drugs exclusive to liver side effects: Bupivacaine, Capsaicin, Carvedilol, Chlorpromazine, Fluphenazine, Flutamide, Halothane, Isoflurane, Meperidine, Papaverine, Probenecid, Ranolazine.

Drugs exclusive to extraliver side effects: Buspirone, Haloperidol, Imipramine, Methamphetamine, Nitroglycerin, Risperidone, Sunitinib, Tetracycline.

3.7.2 Complex I inhibitors obtained from the literature

Alpha-Tocopherol Succinate, 1-Methyl-4-Phenyl-1,2,3,6-Tetrahydropyridine, 2-Methoxyestradiol, 2,4-Dinitrophenol, Acrolein, Alpidem, Amiodarone, Amitriptyline, Amobarbital, Ampicillin, Anandamide, Annonacin, Apigenin, Artemisinin, Aspirin, Aureothin, Bisphenol A Diglycidyl Ether, Basic Red 2, Benzamil, Benzimidazole, Berberine, Bezafibrate, Buformin, Bupivacaine, Buspirone, Laureth-8, Capsaicin, Carvedilol, Celastrol, Chlorpromazine, Ciprofloxacin, Citalopram, Clofibrate, Clofibric Acid, Clozapine, Chromone, Cianidanol, Ciglitazone, Cinnarizine, Ciprofibrate, Cubebin, Cyhalothrin, Deacetylketoconazole, Deguelin, Dequalinium Chloride, Desethylamiodarone, Desipramine, Dichlorvos, Diclofenac, Dicyclohexylcarbodiimide, Diospyrin, Diphenyleneiodonium, Doxorubicin, Ebselen, Efavirenz, Eipa, Epicatechin, Epicatechin Gallate, Epigallocatechin, Epigallocatechin Gallate, Estradiol, Farnesol, Fenazaquin, Fendiline Hydrochloride, Fenofibrate, Fenpyroximate, Flunarizine, Fluphenazine, Flutamide, Gallocatechin, Gemfibrozil, Gossypol, Haloperidol, Halothane, Ibuprofen, Idebenone, Ifosfamide, Imipramine, Indomethacin, Isoflurane, Isoproterenol, Kaempferol, Kanamycin, Ketamine,

Ketoconazole, Lauryl Sulfate, Malvidin Chloride, Mdma, Meperidine, Metformin, Methamphetamine, Methionine, Methoxychlor, Miconazole, Mirtazapine, Mucidin, N-Methyl-4-Phenylpyridinium, N-Methyl-L-Aspartic Acid, Nanafrocin, Naringenin, Nefazodone, Nitroglycerin, O-Phenanthroline, Olanzapine, Oxidopamine, Palmidrol, Papaverine, Paroxetine, Perhexiline, Phenethylamine, Phenformin, Pioglitazone, Piroxicam, Polymyxin B, Potassium Dichromate, Prasterone, Probenecid, Propofol, Pyridaben, Pyrimidifen, Ranolazine, Resveratrol, Rhein, Risperidone, Rosiglitazone, Pyriminil, Pyrocatechol, Pyrvinium Pamoate, Quercetin, Quinazoline, Sevoflurane, Simvastatin, Sodium Chromate, Sodium Palmitate, Sorafenib, Sunitinib, Tacrine, Tamoxifen, Tebufenpyrad, Tetracycline, Thioridazine, Thiothixene , Tolfenpyrad, Tretinoin, Trichloroethylene, Trifluoperazine, Troglitazone, Valproic Acid, Verticipyrone, Zinc Chromate.

3.7.3 Drugs from FDALabel (liver side effects)

Abacavir Sulfate, Abatacept, Acamprosate Calcium, Acarbose, Acetaminophen, Acetazolamide, Acetylcysteine, Acheta Domesticus, Acitretin, Acyclovir, Adalimumab, Adapalene, Adefovir Dipivoxil, Ado-Trastuzumab Emtansine, Agave Sisalana Fiber, Albendazole, Albumin Aggregated, Albumin Human, Aldesleukin, Aliskiren Hemifumarate, Allopurinol, Allopurinol Sodium, Alosetron Hydrochloride, Alpha 1-Proteinase Inhibitor Human, Alprazolam, Alprostadil, Ambrisentan, Ambrosia Artemisiifolia Pollen, Ambrosia Trifida Pollen, American Chestnut, Amiloride Hydrochloride, Aminocaproic Acid, Aminophylline, Aminosalicylic Acid, Amiodarone Hydrochloride, Amitriptyline Hydrochloride, Amlodipine Besylate, Amoxapine, Amoxicillin, Amoxicillin Sodium, Amphotericin B, Anastrozole, Anidulafungin, Antihemophilic Factor Human, Antithrombin Alfa, Antithrombin Iii Human, Aprotinin, Arabica Coffee Bean, Arginine, Aripiprazole, Armodafinil, Artemether, Artemisia Douglasiana Pollen, Ascorbic Acid, Aspirin, Atazanavir Sulfate, Atenolol, Atomoxetine Hydrochloride, Atorvastatin Calcium Trihydrate, Atovaquone, Atropine Sulfate, Auranofin, Azathioprine, Azithromycin Dihydrate, Azithromycin Monohydrate, Azithromycin, Unspecified Form, Aztreonam, Bacillus Calmette-Guerin Substrain Connaught Live Antigen, Bacillus Calmette-Guerin Substrain Tice Live Antigen, Balsalazide Disodium, Bedaquiline Fumarate, Belatacept, Benazepril Hydrochloride, Bendroflumethiazide, Benzalkonium Chloride, Betamethasone, Betamethasone Acetate, Betamethasone Sodium Phosphate,

Bicalutamide, Bisoprolol Fumarate, Bluefish, Boceprevir, Bortezomib, Bosentan, Bosutinib Monohydrate, Brimonidine Tartrate, Brinzolamide, Budesonide, Budesonide (11.Beta.,16.Alpha.(S)), Bumetanide, Bupivacaine Hydrochloride, Buprenorphine, Buprenorphine Hydrochloride, Bupropion Hydrobromide, Bupropion Hydrochloride, Busulfan, Butalbital, Caffeine, Calcitonin Salmon, Canakinumab, Candesartan Cilexetil, Capecitabine, Capreomycin Sulfate, Capsaicin, Captopril, Carbamazepine, Carbidopa, Carvedilol, Carvedilol Phosphate, Casein, Caspofungin Acetate, Cefaclor, Cefazolin Sodium, Cefdinir, Cefixime, Cefoperazone, Cefotaxime Sodium, Cefpodoxime Proxetil, Cefprozil, Ceftaroline Fosamil, Ceftriaxone Sodium, Cefuroxime Axetil, Celecoxib, Cephalexin, Cephalexin Anhydrous, Certolizumab Pegol, Cetirizine Hydrochloride, Cevimeline Hydrochloride, Chenodiol, Chloroquine Phosphate, Chlorothiazide, Chlorothiazide Sodium, Chlorpheniramine Maleate, Chlorpromazine Hydrochloride, Chlorpropamide, Chlorthalidone, Cholestyramine, Choline, Choline Fenofibrate, Choline Magnesium Trisalicylate, Cidofovir, Cilastatin Sodium, Cimetidine, Cimetidine Hydrochloride, Ciprofloxacin, Ciprofloxacin Hydrochloride, Citalopram Hydrobromide, Citric Acid Monohydrate, Clarithromycin, Clavulanate Potassium, Clavulanic Acid, Clindamycin, Clindamycin Hydrochloride, Clindamycin Palmitate Hydrochloride, Clindamycin Phosphate, Clomiphene Citrate, Clomipramine Hydrochloride, Clonazepam, Clonidine, Clonidine Hydrochloride, Clopidogrel Bisulfate, Clozapine, Coagulation Factor Ix Human, Coagulation Factor Vii Human, Coagulation Factor X Human, Cobicistat, Codeine Phosphate, Codeine Sulfate, Colchicine, Corcorus Capsularis Fiber, Corticotropin, Cortisone Acetate, Cotton Seed, Cow Milk, Cupric Chloride, Cupric Oxide, Cyanocobalamin, Cyclobenzaprine Hydrochloride, Cyclophosphamide, Cyclosporine, Cyproheptadine Hydrochloride, Dacarbazine, Dactinomycin, Dalfopristin, Danazol, Dantrolene Sodium, Dapsone, Darbepoetin Alfa, Darunavir Ethanolate, Dasatinib, Daunorubicin Citrate, Deferasirox, Deferiprone, Deferoxamine Mesylate, Delavirdine Mesylate, Demeclocycline Hydrochloride, Deracoxib, Dermatophagoides Farinae, Dermatophagoides Pteronyssinus, Desflurane, Desipramine Hydrochloride, Desirudin, Desloratadine, Desogestrel, Desvenlafaxine, Desvenlafaxine Succinate, Dexamethasone, Dexamethasone Phosphate, Dexamethasone Sodium Phosphate, Dexlansoprazole, Dextromethorphan Hydrobromide, Diatrizoate Sodium, Diazepam, Diclofenac Epolamine, Diclofenac Potassium, Diclofenac Sodium, Dicloxacillin Sodium, Didanosine, Diflunisal, Digoxin, Dihydrocodeine Bitartrate, Diltiazem

Hydrochloride, Dimyristoylphosphatidylcholine, Dimyristoylphosphatidylglycerol, Diphenhydramine Citrate, Diphenhydramine Hydrochloride, Diphenoxylate Hydrochloride, Dipyridamole, Disopyramide Phosphate, Disulfiram, Divalproex Sodium, Docetaxel, Docetaxel Anhydrous, Docusate Sodium, Dolutegravir Sodium, Donepezil Hydrochloride, Dorzolamide Hydrochloride, Doxazosin Mesylate, Doxorubicin Hydrochloride, Doxycycline, Dronedarone, Drospirenone, Duloxetine Hydrochloride, Edetate Calcium Disodium, Efavirenz, Egg Phospholipids, Eletriptan Hydrobromide, Eltrombopag Olamine, Elvitegravir, Emtricitabine, Enalapril Maleate, Enalaprilat, Enflurane, Enfuvirtide, English Sole, Entacapone, Entecavir, Epirubicin Hydrochloride, Eprosartan Mesylate, Equine Thymocyte Immune Globulin, Erythromycin, Erythromycin Ethylsuccinate, Erythromycin Stearate, Erythropoietin, Escitalopram Oxalate, Esomeprazole Magnesium, Esomeprazole Sodium, Esomeprazole Strontium, Estradiol, Estradiol Acetate, Estradiol Cypionate, Estradiol Hemihydrate, Estradiol Valerate, Estrogens, Conjugated, Estrogens, Conjugated Synthetic A, Estrogens, Conjugated Synthetic B, Estrogens, Esterified, Estrone Sodium Sulfate, Estropipate, Eszopiclone, Etanercept, Ethacrynate Sodium, Ethacrynic Acid, Ethambutol Hydrochloride, Ethinyl Estradiol, Ethionamide, Etidronate Disodium, Etodolac, Etomidate, Etonogestrel, Etravirine, Everolimus, Exametazime, Exemestane, Ezetimibe, Factor Ix Complex, Factor Xiii Concentrate (Human), Famciclovir, Famotidine, Febuxostat, Felbamate, Felis Catus Dander, Felis Catus Hair, Felodipine, Fenofibrate, Fenofibric Acid, Fenoprofen Calcium, Fentanyl, Ferrous Gluconate, Ferumoxides Non-Stoichiometric Magnetite, Fibrinogen Human, Filgrastim, Flax Seed, Floxuridine, Fluconazole, Flucytosine, Fludrocortisone Acetate, Fluorometholone, Fluoxetine Hydrochloride, Fluoxymesterone, Fluphenazine Decanoate, Fluphenazine Hydrochloride, Flurbiprofen, Flutamide, Fluvastatin Sodium, Fluvoxamine Maleate, Folic Acid, Fosamprenavir Calcium, Fosfomycin Tromethamine, Fosinopril Sodium, Fosphenytoin Sodium, Fulvestrant, Furosemide, Gabapentin, Gabapentin Enacarbil, Gadoxetate Disodium, Galantamine Hydrobromide, Gamma-Aminobutyric Acid, Ganciclovir Sodium, Gemcitabine Hydrochloride, Gemfibrozil, Gemifloxacin Mesylate, Gemtuzumab Ozogamicin, Gentamicin Sulfate, Glatiramer Acetate, Glimepiride, Glipizide, Glucarpidase, Glyburide, Glycerin, Goat Milk, Gold Sodium Thiomalate, Golimumab, Grain Mill Dust, Griseofulvin, Guanidine Hydrochloride, Haemophilus Influenzae Type B Capsular Polysaccharide Meningococcal Outer Membrane Protein Conjugate Antigen,

Haemophilus Influenzae Type B Strain 20752 Capsular Polysaccharide Tetanus Toxoid Conjugate Antigen, Halothane, Hepatitis A Virus Strain Cr 326F Antigen (Formaldehyde Inactivated), Hepatitis A Virus Strain Hm175 Antigen (Formaldehyde Inactivated), Hepatitis B Virus Subtype Adw Hbsag Surface Protein Antigen, Hepatitis B Virus Subtype Adw2 Hbsag Surface Protein Antigen, Histamine, Histamine Phosphate, Histidine, House Dust, Human Botulinum Neurotoxin A/B Immune Globulin, Human C1-Esterase Inhibitor, Human Clostridium Tetani Toxoid Immune Globulin, Human Cord Blood Hematopoietic Progenitor Cell, Human Cytomegalovirus Immune Globulin, Human Hepatitis B Virus Immune Globulin, Human Immunoglobulin G, Human Papillomavirus Type 11 L1 Capsid Protein Antigen, Human Papillomavirus Type 16 L1 Capsid Protein Antigen, Human Papillomavirus Type 16 L1 Capsid Protein Residues 2-471 Antigen, Human Papillomavirus Type 18 L1 Capsid Protein Antigen, Human Papillomavirus Type 18 L1 Capsid Protein Residues 2-472 Antigen, Human Papillomavirus Type 6 L1 Capsid Protein Antigen, Human Rabies Virus Immune Globulin, Human Rho(D) Immune Globulin, Hydralazine Hydrochloride, Hydrochlorothiazide, Hydrocodone Bitartrate, Hydrocortisone, Hydrocortisone Acetate, Hydrocortisone Cypionate, Hydrocortisone Sodium Succinate, Hydroflumethiazide, Hydromorphone Hydrochloride, Hydroxyprogesterone Caproate, Ibritumomab Tiuxetan, Ibuprofen, Ifosfamide, Iloprost, Imatinib Mesylate, Imiglucerase, Imipenem, Indapamide, Indinavir Sulfate, Indomethacin, Infliximab, Interferon Alfa-2A, Interferon Alfa-2B, Interferon Alfacon-1, Interferon Beta-1A, Interferon Beta-1B, Interferon Gamma-1B, Ipilimumab, Irbesartan, Irinotecan Hydrochloride, Isocarboxazid, Isoflurane, Isometheptene Mucate, Isoniazid, Isosorbide Dinitrate, Isosorbide Mononitrate, Isotretinoin, Itraconazole, Ivermectin, Japanese Encephalitis Virus Strain Nakayama-Nih Antigen (Formaldehyde Inactivated), Ketoconazole, Ketoprofen, Ketorolac Tromethamine, Khuskia Oryzae, Labetalol Hydrochloride, Lacosamide, Lamivudine, Lamotrigine, Lansoprazole, Leflunomide, Lenalidomide, Lepirudin, Letrozole, Leuprolide Acetate, Levetiracetam, Levocetirizine Dihydrochloride, Levodopa, Levofloxacin, Levonorgestrel, Levothyroxine, Levothyroxine Sodium, Lincomycin Hydrochloride, Lindane, Liothyronine, Liothyronine Sodium, Lisdexamfetamine Dimesylate, Lisinopril, Lomefloxacin Hydrochloride, Lomitapide Mesylate, Lopinavir, Losartan Potassium, Lovastatin, Loxapine Succinate, Lumefantrine, Lysine Hydrochloride, Magnesium Salicylate, Maraviroc, Measles Virus Strain Enders'

Attenuated Edmonston Live Antigen, Mebendazole, Mebrofenin, Meclofenamate Sodium, Medroxyprogesterone Acetate, Mefenamic Acid, Megestrol Acetate, Melopsittacus Undulatus Feather, Meloxicam, Melphalan Hydrochloride, Memantine Hydrochloride, Menthol, Meperidine Hydrochloride, Mephenytoin, Meprobamate, Mercaptopurine, Meropenem, Mesalamine, Mesna, Metformin Hydrochloride, Methadone Hydrochloride, Methazolamide, Methenamine, Methimazole, Methocarbamol, Methotrexate Sodium, Methyclothiazide, Methyl Aminolevulinate Hydrochloride, Methyl Salicylate, Methyldopa, Methyldopate Hydrochloride, Methylergonovine Maleate, Methylprednisolone, Methylprednisolone Acetate, Methylprednisolone Sodium Succinate, Methyltestosterone, Metoclopramide Hydrochloride, Metolazone, Metoprolol Succinate, Metoprolol Tartrate, Mexiletine Hydrochloride, Micafungin Sodium, Midazolam Hydrochloride, Mifepristone, Milnacipran Hydrochloride, Minocycline Hydrochloride, Mipomersen Sodium, Mirtazapine, Misoprostol, Mitoxantrone Hydrochloride, Mivacurium Chloride, Modafinil, Moexipril Hydrochloride, Montelukast Sodium, Morella Cerifera Pollen, Moricizine Hydrochloride, Morphine, Morphine Sulfate, Moxifloxacin Hydrochloride, Mumps Virus Strain B Level Jeryl Lynn Live Antigen, Muromonab-Cd3, Mycophenolate Mofetil, Mycophenolate Sodium, Nabumetone, Nadolol, Nafcillin Sodium, Nalmefene Hydrochloride, Naloxone, Naloxone Hydrochloride, Naloxone Hydrochloride Dihydrate, Naltrexone, Naltrexone Hydrochloride, Nandrolone Decanoate, Naproxen, Naproxen Sodium, Nateglinide, Nefazodone Hydrochloride, Neisseria Meningitidis Group A Capsular Polysaccharide Diphtheria Toxoid Conjugate Antigen, Neisseria Meningitidis Group C Capsular Polysaccharide Diphtheria Toxoid Conjugate Antigen, Neisseria Meningitidis Group W-135 Capsular Polysaccharide Diphtheria Toxoid Conjugate Antigen, Neisseria Meningitidis Group Y Capsular Polysaccharide Diphtheria Toxoid Conjugate Antigen, Nelfinavir Mesylate, Nevirapine, Niacin, Niacinamide, Nicardipine Hydrochloride, Nifedipine, Nilotinib, Nilutamide, Nimodipine, Nisoldipine, Nitrofurantoin, Nitrofurantoin Monohydrate, Nizatidine, Norelgestromin, Norethindrone, Norethindrone Acetate, Norfloxacin, Nortriptyline Hydrochloride, Octreotide Acetate, Ofatumumab, Ofloxacin, Olanzapine, Olanzapine Pamoate, Olmesartan Medoxomil, Olsalazine Sodium, Omeprazole, Omeprazole Magnesium, Orlistat, Ormetoprim, Oseltamivir Phosphate, Oxaliplatin, Oxandrolone, Oxaprozin, Oxazepam, Oxcarbazepine, Oxycodone Hydrochloride, Oxycodone Terephthalate, Oxymetholone, Oxymorphone

Hydrochloride, Oxytetracycline Hydrochloride, Oxytocin, Paclitaxel, Palivizumab, Pamabrom, Pancuronium Bromide, Pantoprazole Sodium, Papaverine Hydrochloride, Paroxetine Hydrochloride Anhydrous, Paroxetine Hydrochloride Hemihydrate, Paroxetine Mesylate, Peginterferon Alfa-2A, Peginterferon Alfa-2B, Pegvisomant, Penicillamine, Penicillin G Potassium, Penicillin G Sodium, Pentamidine Isethionate, Pentazocine Hydrochloride, Pentoxifylline, Pergolide, Perindopril Erbumine, Periplaneta Americana, Perphenazine, Phenazopyridine Hydrochloride, Phenol, Phentermine Hydrochloride, Phenylephrine Bitartrate, Phenylephrine Hydrochloride, Phenyltoloxamine Citrate, Phenytoin, Phenytoin Sodium, Phytonadione, Pilocarpine Hydrochloride, Pindolol, Pinus Banksiana Pollen, Pioglitazone Hydrochloride, Piperacillin Sodium, Piroxicam, Pitavastatin Calcium, Poliovirus Type 1 Antigen (Formaldehyde Inactivated), Poliovirus Type 2 Antigen (Formaldehyde Inactivated), Poliovirus Type 3 Antigen (Formaldehyde Inactivated), Polythiazide, Ponatinib Hydrochloride, Posaconazole, Potassium Bicarbonate, Potassium Chloride, Potassium Phosphate, Monobasic, Povidone-Iodine, Pravastatin Sodium, Prazosin Hydrochloride, Prednisolone, Prednisolone Acetate, Prednisolone Sodium Phosphate, Prednisone, Probenecid, Prochlorperazine, Prochlorperazine Edisylate, Prochlorperazine Maleate, Progesterone, Proguanil Hydrochloride, Promethazine Hydrochloride, Propafenone, Propafenone Hydrochloride, Propofol, Propoxyphene Hydrochloride, Propoxyphene Napsylate, Propranolol Hydrochloride, Propylthiouracil, Protein C, Prothrombin, Pseudoephedrine Hydrochloride, Pseudoephedrine Sulfate, Pyrazinamide, Quinapril Hydrochloride, Quinidine Gluconate, Quinidine Sulfate, Quinine Sulfate, Quinupristin, Rabeprazole Sodium, Raltegravir Potassium, Ramelteon, Ramipril, Ranitidine Hydrochloride, Ranolazine, Regorafenib Monohydrate, Repaglinide, Reserpine, Ribavirin, Rifabutin, Rifampin, Rifapentine, Rilonacept, Rilpivirine Hydrochloride, Riluzole, Ritonavir, Rituximab, Rivaroxaban, Rivastigmine, Rivastigmine Tartrate, Ranolazine, Regorafenib Monohydrate, Repaglinide, Reserpine, Ribavirin, Rifabutin, Rifampin, Rifapentine, Rilonacept, Rilpivirine Hydrochloride, Riluzole, Ritonavir, Rituximab, Rivaroxaban, Rivastigmine, Rivastigmine Tartrate, Rizatriptan Benzoate, Rocuronium Bromide, Ropinirole Hydrochloride, Rosiglitazone Maleate, Rosuvastatin Calcium, Rubella Virus Strain Wistar Ra 27/3 Live Antigen, Rufinamide, Safflower Oil, Salicylamide, Salmonella Typhi Ty2 Vi Polysaccharide Antigen, Salsalate, Saquinavir Mesylate, Selegiline Hydrochloride, Sequoia Sempervirens Pollen, Sertraline Hydrochloride,

Sevoflurane, Sildenafil Citrate, Silver Sulfadiazine, Simvastatin, Sirolimus, Sitagliptin Phosphate, Sitotroga Cerealella, Sodium Acetate, Sodium Chloride, Sodium Phosphate, Dibasic, Anhydrous, Sodium Phosphate, Monobasic, Monohydrate, Sodium Salicylate, Sorafenib, Soybean Oil, Spinosad, Spironolactone, Stavudine, Sulfacetamide Sodium, Sulfadiazine, Sulfadimethoxine, Sulfamethizole, Sulfamethoxazole, Sulfasalazine, Sulfisoxazole Acetyl, Sulfur, Sulindac, Sumatriptan Succinate, Tacrolimus, Tacrolimus Anhydrous, Tadalafil, Tamoxifen Citrate, Tapentadol Hydrochloride, Tazobactam Sodium, Telaprevir, Telbivudine, Telithromycin, Telmisartan, Temozolomide, Tenofovir Disoproxil Fumarate, Terbinafine Hydrochloride, Teriflunomide, Testosterone, Testosterone Cypionate, Testosterone Enanthate, Thalidomide, Theophylline, Theophylline Anhydrous, Thioguanine, Thrombin Human, Thyroid, Unspecified, Tiagabine Hydrochloride, Ticarcillin Disodium, Ticlopidine Hydrochloride, Timolol Maleate, Tinzaparin Sodium, Tipranavir, Tizanidine, Tizanidine Hydrochloride, Tocilizumab, Tofacitinib Citrate, Tolazamide, Tolbutamide, Tolcapone, Tolmetin Sodium, Tolvaptan, Topiramate, Toremifene Citrate, Torsemide, Tramadol Hydrochloride, Trandolapril, Tranylcypromine Sulfate, Trazodone Hydrochloride, Tretinoin, Triamcinolone Acetonide, Triamcinolone Diacetate, Triamcinolone Hexacetonide, Triamterene, Trichophyton Mentagrophytes, Trichophyton Rubrum, Trientine Hydrochloride, Trifluoperazine Hydrochloride, Trimethadione, Trimethoprim, Tromethamine, Trovafloxacin Mesylate, Tuberculin Purified Protein Derivative, Tyrosine, Urochloa Mutica Pollen, Urokinase, Ursodiol, Valacyclovir Hydrochloride, Valdecoxib, Valganciclovir Hydrochloride, Valproate Sodium, Valproic Acid, Valsartan, Varicella-Zoster Virus Strain Oka/Merck Live Antigen, Vecuronium Bromide, Venlafaxine Hydrochloride, Verapamil Hydrochloride, Vitamin A Palmitate, Von Willebrand Factor Human, Voriconazole, Warfarin Sodium, Wine Grape, Zafirlukast, Zidovudine, Zileuton, Zinc Acetate, Zinc Oxide, Ziprasidone Hydrochloride, Zonisamide.

3.7.4 Drugs from FDALabel (extraliver side effects)

Abacavir Sulfate, Abiraterone Acetate, Acamprosate Calcium, Acetaminophen, Acitretin, Adalimumab, Adefovir Dipivoxil, Ado-Trastuzumab Emtansine, Agalsidase Beta, Albumin Human, Aldesleukin, Alemtuzumab, Alglucosidase Alfa, Aliskiren Hemifumarate, Allopurinol, Allopurinol Sodium, Almotriptan Malate, Alogliptin

Benzoate, Alteplase, Altretamine, Amiloride Hydrochloride, Aminocaproic Acid, Aminophylline, Amiodarone Hydrochloride, Amitriptyline, Amitriptyline Hydrochloride, Amlodipine Besylate, Amoxapine, Amphetamine Aspartate, Amphetamine Sulfate, Amphotericin B, Anagrelide Hydrochloride, Anhydrous Citric Acid, Antimony Potassium Tartrate, Aprepitant, Aripiprazole, Arsenic Trioxide, Asenapine Maleate, Asparaginase Erwinia Chrysanthemi, Aspirin, Atazanavir Sulfate, Atenolol, Atomoxetine Hydrochloride, Atorvastatin Calcium Trihydrate, Atovaquone, Atropine Sulfate, Auranofin, Azacitidine, Azathioprine, Azathioprine Sodium, Azithromycin Dihydrate, Azithromycin Monohydrate, Azithromycin, Unspecified Form, Bacillus Anthracis Strain V770-Np1-R Antigens, Baclofen, Balsalazide Disodium, Bedaquiline Fumarate, Benazepril Hydrochloride, Bendroflumethiazide, Benzphetamine Hydrochloride, Betamethasone, Betamethasone Acetate, Betamethasone Sodium Phosphate, Bexarotene, Bismuth Subcitrate Potassium, Bismuth Subsalicylate, Bisoprolol Fumarate, Boceprevir, Bortezomib, Bosutinib Monohydrate, Botulinum Toxin Type A, Brentuximab Vedotin, Brompheniramine Maleate, Buprenorphine, Bupropion Hydrobromide, Bupropion Hydrochloride, Buspirone Hydrochloride, Busulfan, Cabazitaxel, Cabozantinib S-Malate, Caffeine, Calcitriol, Calcium Chloride, Canagliflozin, Candesartan Cilexetil, Capecitabine, Captopril, Carbamazepine, Carbidopa, Carfilzomib, Carprofen, Caspofungin Acetate, Cefdinir, Ceftriaxone Sodium, Celecoxib, Certolizumab Pegol, Chenodiol, Chlorambucil, Chloroquine Phosphate, Chlorothiazide, Chlorothiazide Sodium, Chlorpheniramine Maleate, Chlorthalidone, Cholestyramine, Choline Fenofibrate, Chromic Chloride, Cidofovir, Cimetidine, Cimetidine Hydrochloride, Ciprofloxacin, Ciprofloxacin Hydrochloride, Cisatracurium Besylate, Cisplatin, Citalopram Hydrobromide, Clarithromycin, Clevidipine, Clofarabine, Clomiphene Citrate, Clomipramine Hydrochloride, Clonidine Hydrochloride, Clopidogrel Bisulfate, Clozapine, Cobicistat, Codeine Phosphate, Codeine Sulfate, Colchicine, Colesevelam Hydrochloride, Conivaptan Hydrochloride, Corticotropin, Cortisone Acetate, Crizotinib, Crofelemer, Cyclobenzaprine Hydrochloride, Cyclophosphamide, Cyclosporine, Cytarabine, Dabrafenib Mesylate, Dalfopristin, Danazol, Dapsone, Daptomycin, Darunavir Ethanolate, Dasatinib, Daunorubicin, Daunorubicin Citrate, Daunorubicin Hydrochloride, Decitabine, Deferasirox, Deferiprone, Delavirdine Mesylate, Demeclocycline Hydrochloride, Denosumab, Desflurane, Desipramine Hydrochloride, Desogestrel, Desvenlafaxine, Desvenlafaxine Succinate,

Dexamethasone, Dexamethasone Phosphate, Dexamethasone Sodium Phosphate, Dexlansoprazole, Dexmethylphenidate Hydrochloride, Dexrazoxane, Dextroamphetamine Saccharate, Dextroamphetamine Sulfate, Dextrose Monohydrate, Diatrizoate Meglumine, Diatrizoate Sodium, Diazoxide, Diclofenac Potassium, Diclofenac Sodium, Didanosine, Difenoxin Hydrochloride, Digoxin, Dihydrocodeine Bitartrate, Diltiazem Hydrochloride, Dimyristoylphosphatidylcholine, Dl-, Dimyristoylphosphatidylglycerol, Dl-, Diphenhydramine Hydrochloride, Diphenoxylate Hydrochloride, Dipyridamole, Disopyramide Phosphate, Disulfiram, Divalproex Sodium, Docetaxel, Docetaxel Anhydrous, Dolasetron Mesylate, Donepezil Hydrochloride, Doxercalciferol, Doxorubicin Hydrochloride, Doxylamine Succinate, Drospirenone, Duloxetine Hydrochloride, Efavirenz, Egg Phospholipids, Eletriptan Hydrobromide, Elvitegravir, Emtricitabine, Enalapril Maleate, Enalaprilat, Enfuvirtide, Entacapone, Entecavir, Epirubicin Hydrochloride, Eprosartan Mesylate, Eribulin Mesylate, Erlotinib Hydrochloride, Ertapenem Sodium, Erythromycin, Erythromycin Ethylsuccinate, Erythromycin Stearate, Escitalopram Oxalate, Esomeprazole Magnesium, Esomeprazole Sodium, Esomeprazole Strontium, Estradiol, Estradiol Acetate, Estradiol Cypionate, Estradiol Hemihydrate, Estradiol Valerate, Estrogens, Conjugated, Estrogens, Conjugated Synthetic A, Estrogens, Conjugated Synthetic B, Estrogens, Esterified, Estropipate, Eszopiclone, Ethacrynate Sodium, Ethacrynic Acid, Ethambutol Hydrochloride, Ethinyl Estradiol, Ethiodized Oil, Etidronate Disodium, Etodolac, Etonogestrel, Etravirine, Everolimus, Exenatide, Ezetimibe, Febuxostat, Felbamate, Felodipine, Fenofibrate, Fenofibric Acid, Fenoprofen Calcium, Fentanyl, Fentanyl Citrate, Firocoxib, Flecainide Acetate, Fluconazole, Flucytosine, Fludarabine Phosphate, Fludrocortisone Acetate, Fluoxetine Hydrochloride, Flurbiprofen, Fluvastatin Sodium, Fluvoxamine Maleate, Fosamprenavir Calcium, Foscarnet Sodium, Fosinopril Sodium, Fosphenytoin Sodium, Furosemide, Gabapentin, Gadobenate Dimeglumine, Ganciclovir Sodium, Gefitinib, Gemfibrozil, Gemifloxacin Mesylate, Gentamicin Sulfate, Glatiramer Acetate, Glimepiride, Glipizide, Glutamine, Glyburide, Glycerin, Glycerol Phenylbutyrate, Glycopyrrolate, Gold Sodium Thiomalate, Griseofulvin, Guaifenesin, Haloperidol, Haloperidol Decanoate, Haloperidol Lactate, Hepatitis B Virus Subtype Adw Hbsag Surface Protein Antigen, Hetastarch, Human Albumin Microspheres, Human Papillomavirus Type 11 L1 Capsid Protein Antigen, Human Papillomavirus Type 16 L1 Capsid Protein Antigen, Human Papillomavirus Type 18 L1 Capsid

Protein Antigen, Human Papillomavirus Type 6 L1 Capsid Protein Antigen, Hydralazine Hydrochloride, Hydrochlorothiazide, Hydrocodone Bitartrate, Hydrocortisone, Hydrocortisone Acetate, Hydrocortisone Cypionate, Hydrocortisone Sodium Succinate, Hydroflumethiazide, Hydromorphone Hydrochloride, Hydroxychloroquine Sulfate, Hydroxyethyl Starch 130/0.4, Hydroxyurea, Hyoscyamine Sulfate, Ibuprofen, Icosapent Ethyl, Idarubicin Hydrochloride, Ifosfamide, Iloperidone, Imatinib Mesylate, Imipramine Hydrochloride, Imipramine Pamoate, Imiquimod, Indapamide, Indinavir Sulfate, Indomethacin, Insulin Aspart, Insulin Detemir, Insulin Glargine, Insulin Glulisine, Insulin Human, Insulin Lispro, Insulin Pork, Interferon Alfa-2A, Interferon Alfa-2B, Interferon Alfacon-1, Interferon Beta-1A, Interferon Beta-1B, Interferon Gamma-1B, Iodipamide Meglumine, Iodixanol, Iohexol, Iopamidol, Iopromide, Iothalamate Meglumine, Ioversol, Ioxaglate Meglumine, Ioxaglate Sodium, Ioxilan, Ipilimumab, Irbesartan, Irinotecan Hydrochloride, Isoniazid, Isosorbide Dinitrate, Isosorbide Mononitrate, Isotretinoin, Itraconazole, Ixabepilone, Ketoconazole, Ketoprofen, Ketorolac Tromethamine, Labetalol Hydrochloride, Lamivudine, Lamotrigine, Lanreotide Acetate, Lansoprazole, Leflunomide, Lenalidomide, Leuprolide Acetate, Levetiracetam, Levocarnitine, Levodopa, Levofloxacin, Levonorgestrel, Linagliptin, Linezolid, Liothyronine Sodium, Liraglutide, Lisdexamfetamine Dimesylate, Lisinopril, Lomefloxacin Hydrochloride, Lomitapide Mesylate, Lopinavir, Lorazepam, Losartan Potassium, Lovastatin, Loxapine, Lurasidone Hydrochloride, Magnesium Hydroxide, Magnesium Oxide, Magnesium Sulfate, Mannitol, Maprotiline Hydrochloride, Maraviroc, Maropitant Citrate, Mebrofenin, Mecasermin, Medroxyprogesterone Acetate, Mefenamic Acid, Megestrol Acetate, Melarsomine Dihydrochloride, Meloxicam, Memantine Hydrochloride, Meprobamate, Mesalamine, Metformin Hydrochloride, Methadone Hydrochloride, Methamphetamine Hydrochloride, Methotrexate Sodium, Methyclothiazide, Methyldopa, Methyldopate Hydrochloride, Methylphenidate, Methylphenidate Hydrochloride, Methylprednisolone, Methylprednisolone Acetate, Methylprednisolone Sodium Succinate, Methyltestosterone, Metolazone, Metoprolol Succinate, Metoprolol Tartrate, Metronidazole, Mexiletine Hydrochloride, Mifepristone, Miglustat, Milnacipran Hydrochloride, Minocycline Hydrochloride, Mirtazapine, Misoprostol, Mitoxantrone Hydrochloride, Moexipril Hydrochloride, Montelukast Sodium, Morphine Sulfate, Moxifloxacin Hydrochloride, Mycophenolate Mofetil, Mycophenolate Sodium,

Nabumetone, Nadolol, Naloxone Hydrochloride, Naltrexone, Naltrexone Hydrochloride, Naproxen, Naproxen Sodium, Nefazodone Hydrochloride, Nelarabine, Nelfinavir Mesylate, Nesiritide, Nevirapine, Niacin, Nilotinib, Nitrofurantoin, Nitrofurantoin Monohydrate, Nitroglycerin, Norelgestromin, Norepinephrine Bitartrate, Norethindrone Acetate, Norfloxacin, Nortriptyline Hydrochloride, Octreotide Acetate, Ofloxacin, Olanzapine, Olanzapine Pamoate, Olmesartan Medoxomil, Olsalazine Sodium, Omega-3-Acid Ethyl Esters, Omeprazole, Omeprazole Magnesium, Oprelvekin, Orlistat, Oxaliplatin, Oxaprozin, Oxcarbazepine, Oxycodone Hydrochloride, Oxymorphone Hydrochloride, Oxytetracycline Hydrochloride, Paclitaxel, Paliperidone, Paliperidone Palmitate, Pancrelipase, Pancrelipase Amylase, Pancrelipase Lipase, Pancrelipase Protease, Pantoprazole Sodium, Paroxetine Hydrochloride Anhydrous, Paroxetine Hydrochloride Hemihydrate, Paroxetine Mesylate, Pasireotide, Pazopanib Hydrochloride, Pegaspargase, Peginterferon Alfa-2A, Peginterferon Alfa-2B, Pemetrexed Disodium, Penicillamine, Penicillin G Benzathine, Penicillin G Procaine, Pentamidine Isethionate, Pentazocine Hydrochloride, Pergolide, Perindopril Erbumine, Perphenazine, Pertuzumab, Phentermine Hydrochloride, Phenylephrine Hydrochloride, Pilocarpine Hydrochloride, Pimobendan, Pimozide, Pioglitazone Hydrochloride, Piperacillin Sodium, Piroxicam, Pitavastatin Calcium, Podofilox, Polythiazide, Pomalidomide, Ponatinib Hydrochloride, Posaconazole, Potassium Bromide, Potassium Chloride, Potassium Phosphate, Monobasic, Potassium Sulfate, Pramipexole Dihydrochloride, Pravastatin Sodium, Prazosin Hydrochloride, Prednisolone, Prednisolone Acetate, Prednisolone Sodium Phosphate, Prednisone, Pregabalin, Procainamide Hydrochloride, Progesterone, Propafenone, Propafenone Hydrochloride, Propofol, Propoxyphene Hydrochloride, Propoxyphene Napsylate, Propranolol Hydrochloride, Protriptyline Hydrochloride, Pseudoephedrine Hydrochloride, Pyrazinamide, Pyridoxine Hydrochloride, Pyrilamine Maleate, Quetiapine Fumarate, Quinapril Hydrochloride, Quinine Sulfate, Quinupristin, Rabeprazole Sodium, Raltegravir Potassium, Ramipril, Ranitidine Hydrochloride, Regadenoson, Repaglinide, Reserpine, Reteplase, Ribavirin, Rifampin, Rifapentine, Rilpivirine Hydrochloride, Riluzole, Risperidone, Ritonavir, Rivastigmine, Rivastigmine Tartrate, Rocuronium Bromide, Roflumilast, Ropinirole Hydrochloride, Rosiglitazone Maleate, Rosuvastatin Calcium, Rotigotine, Safflower Oil, Saquinavir Mesylate, Saxagliptin Hydrochloride, Secretin Human, Selegiline Hydrochloride,

Sertraline Hydrochloride, Sevoflurane, Sildenafil Citrate, Simvastatin, Sipuleucel-T, Sirolimus, Sitagliptin Phosphate, Sodium Benzoate, Sodium Bicarbonate, Sodium Chloride, Sodium Lactate, Sodium Nitroprusside, Sodium Phenylacetate, Sodium Phenylbutyrate, Sodium Phosphate, Dibasic, Anhydrous, Sodium Phosphate, Monobasic, Monohydrate, Sodium Picosulfate, Sodium Sulfate, Somatropin, Sorafenib, Sorbitol, Sotalol, Sotalol Hydrochloride, Soybean Oil, Spironolactone, Stavudine, Succinylcholine Chloride, Sulfadiazine, Sulfamethizole, Sulfamethoxazole, Sulfasalazine, Sulfisoxazole Acetyl, Sulindac, Sumatriptan, Sumatriptan Succinate, Sunitinib Malate, Tacrolimus, Tacrolimus Anhydrous, Tadalafil, Tamoxifen Citrate, Tapentadol Hydrochloride, Tazobactam Sodium, Teduglutide, Telaprevir, Telbivudine, Telithromycin, Telmisartan, Temsirolimus, Tenecteplase, Tenofovir Disoproxil Fumarate, Terbinafine Hydrochloride, Teriflunomide, Tetrabenazine, Tetracycline Hydrochloride, Thalidomide, Theophylline, Theophylline Anhydrous, Thiotepa, Ticlopidine Hydrochloride, Tigecycline, Tipranavir, Toceranib Phosphate, Tolcapone, Tolmetin Sodium, Tolvaptan, Topiramate, Torsemide, Tramadol Hydrochloride, Trametinib Dimethyl Sulfoxide, Trandolapril, Tretinoin, Triamcinolone Acetonide, Triamcinolone Diacetate, Triamcinolone Hexacetonide, Triamterene, Trientine Hydrochloride, Trilostane, Trimethoprim, Trimipramine Maleate, Trospium Chloride, Trovafloxacin Mesylate, Urokinase, Ursodiol, Valdecoxib, Valganciclovir Hydrochloride, Valproate Sodium, Valproic Acid, Valsartan, Vandetanib, Vardenafil Hydrochloride Trihydrate, Varenicline Tartrate, Venlafaxine Hydrochloride, Verapamil Hydrochloride, Vigabatrin, Vincristine Sulfate, Vinorelbine Tartrate, Voriconazole, Warfarin Sodium, Ziconotide Acetate, Zidovudine, Zinc Acetate, Ziprasidone Hydrochloride, Zolmitriptan, Zonisamide, Ziprasidone Hydrochloride, Zolmitriptan, Zonisamide.

4 Characterisation of complex I within drug-induced mitochondrial dysfunction: the Enzo Library

4.1 Introduction and aims

The knowledge and methods developed in chapter 3 provided a basis for screening a much bigger set of drugs. The "Enzo SCREEN-WELL FDA approved drug library V2" was chosen for drug screening: the library includes 786 drugs that belong to 44 different classes and well represents the universe of (FDA-approved) pharmaceuticals. By combining the ability of an assay to detect inhibition of complexes I-III-IV (NADH:O_2 oxidoreduction) with another assay that detects inhibition of complexes II-III-IV (succinate:O_2 oxidoreduction) it is possible to identify specific inhibitors of complex I (and II). Furthermore, the availability of assays that assess the activity of isolated complex I at the flavin-site and at the Q-site allows identification of the drug binding site within the complex. SMPs and isolated mitochondria may then be used to further characterize the role of drugs in complex I inhibition. Finally, a proposal for the described methods to be applied to other enzymes that are similar to complex I, in terms of mechanism and location in crossing metabolic pathways, has been laid out.

4.1.1 Aims

The aims of this work are to

1) Obtain a pharmacological characterization of the effect of FDA approved drugs on complex I, both within the ETC and in isolation.

2) Present a method that combines results from two assays that measure activity from converging metabolic pathways (I-III-IV and II-III-IV) to pinpoint target specificity within the ETC.

3) Present a method that combines results from assays that measure two different aspects of complex I activity (NADH:dQ or Q_{10} and NADH:APAD or FeCN) to determine the binding location of a drug within the complex (Q-site or flavin-site).

4) Investigate the determinants of complex I inhibition within specific therapeutic classes.

4.1.2 Choice of the appropriate library

Several libraries of approved drugs are commercially available so it was necessary to develop criteria for selecting the most appropriate one: the libraries with a number of drugs close to 1000 (the chosen order of magnitude for the number of drugs to be tested) were the Prestwick, the Pharmakon and the Screen-Well Enzo V2. The most important criterion adopted for the library selection was that it must include the highest number of drugs known to cause drug-induced mitochondrial dysfunction: it was therefore decided to build up a "virtual library" of drugs in exactly the same way as it was obtained in chapter 3, this time including drug-induced side effects related to brain and nervous system (apathy, ataxia, muscular weakness, polymyoneuropathy, facial and peripheral paresthesia, neuromuscular blockade[317], schwannopathy[318]), kidney (Fanconi syndrome, proximal tubular dysfunction, acute tubular necrosis[319], glucosuria, aminoaciduria, phosphaturia, bicarbonaturia [320]) and heart (myopericarditis, sinus tachycardia, reversible arrhythmias, prolonged QT interval, flattening of T wave[321]), not just liver and extraliver[g].

Once the drugs associated with those side effects were collected, redundancies were removed according to generic drug names and, subsequently, according to UNII codes (many drugs include several UNII codes each). The final number of UNII codes unique to each set is presented in Table 4.1, which illustrates the filtering process.

	Database hits according to organ-based side effects				
	Brain	**Extraliver**	**Heart**	**Kidney**	**Liver**
Initial entries	12702	23354	9025	935	24518
Drugs without redundancies	841	1376	734	105	1315
UNII EXPANSION					
Unique UNIIs to each set	798	991	595	92	1454

Table 4.1. Database filtering process during the choice of the library. The FDALabel database search returned many redundancies (both within the initial list of drugs and the subsequent UNII expansion) that were eliminated in order to obtain the final list of UNII codes unique to each set.

[g] The FDALabel database was accessed on 23rd October 2014

At this point the UNII codes were converted to their associated items and narrowed down to only include drugs (differences in covalently attached species such as carboxylic acids and esters were kept): items discarded included roots, pollens, different counterions for the same molecules (*e.g.* HCl, besylate, phosphates,…), insects (*e.g.* acheta domesticus), bacteria, herbs, viruses, proteases inhibitors and proteins. After this filtering process, 1185 unique compounds were left and those formed the "virtual library" to which the three commercial libraries were compared. Other criteria for the selection process included price, number of times the library was used in recent scientific papers (after 2012), number of drugs in common with the DrugBank database[h] (approved drugs and nutraceuticals, bioactive molecules derived from food that provide physiological benefits beyond nutrition[322]) and number of drugs that possess at least one dimethoxybenzene moiety, a feature of interest inasmuch as it is possessed by the canonical inhibitors of complex I rotenone and piericidin (see chapter 3). The overall results are summarized in Table 4.2.

Eventually, the Screen-Well library was chosen, also because the drugs that constitute it are all FDA-approved, differently than the other two (the Prestwick library contains drugs approved by different agencies, not just FDA, and the Pharmakon also includes compounds that have reached clinical trial, not necessarily approved drugs).

	PRESTWICK	**SCREEN-WELL**	**PHARMAKON**
Number of drugs included	1280	786	1600
Drugs in common with "virtual" drug-induced mitochondrial dysfunction library	466	533	540
Literature references after 2012	10	13	5
Price	€ 10,600	£ 5800	$ 9800
Dimethoxybenzene moiety drugs	25	31	27
DrugBank Approved Drugs	643	613	698
DrugBank Nutraceuticals	9	3	14

Table 4.2. Comparison of the three commercially available drug libraries considered for purchase. Several criteria were considered, but the most important one was how many drugs each library has with the "virtual" library generated with the method described in chapter 3.

[h] The DrugBank database was accessed on 26th October 2014

4.1.3 Introduction to the method

The characterization of complex I was based on the assays used in chapter 3 and is summarised in Figure 4.1. The NADH:O_2 oxidoreduction assay in membranes was the first experiment to filter out weak ETC inhibitors and isolate compounds that interact strongly with complex I: the 200 drugs with the highest inhibitory potency were chosen. In addition, the minor degree of coupling present in membranes allowed to identify 19 compounds that caused a limited degree of stimulation of the rate of NADH:O_2 oxidoreduction, and as such they could be potential uncouplers (7 of those belong to the drug class of bisphosphonates, the other 12 exhibited the highest residual activity in the NADH:O_2 initial screening). While the potential uncouplers are tested with SMPs (which possess a higher degree of coupling), the 200 most potent inhibitors are then tested with the succinate:O_2 oxidoreduction assay: by combining the results of the two oxidoreduction assays it is possible to identify specific inhibitors of complex I and II. While the most potent complex I-specific inhibitors are tested against isolated mitochondria, specificity towards the other ETC complexes is assessed with succinate:dQ, succinate:cyt *c* and (red.) cytochrome *c*:O_2 oxidoreduction assays. The same 200 drugs are then tested on isolated complex I and arranged in order to highlight Q-site inhibitors as opposed to flavin-site inhibitors. Since the ROS assay requires a conspicuous amount of isolated enzyme, the drugs tested for their effect on ROS formation are the ones that exhibited the highest inhibition in isolated enzyme assays. Finally, the overall results of the database search to identify the drugs featured in chapter 3 were validated in this chapter thanks to the availability of the library.

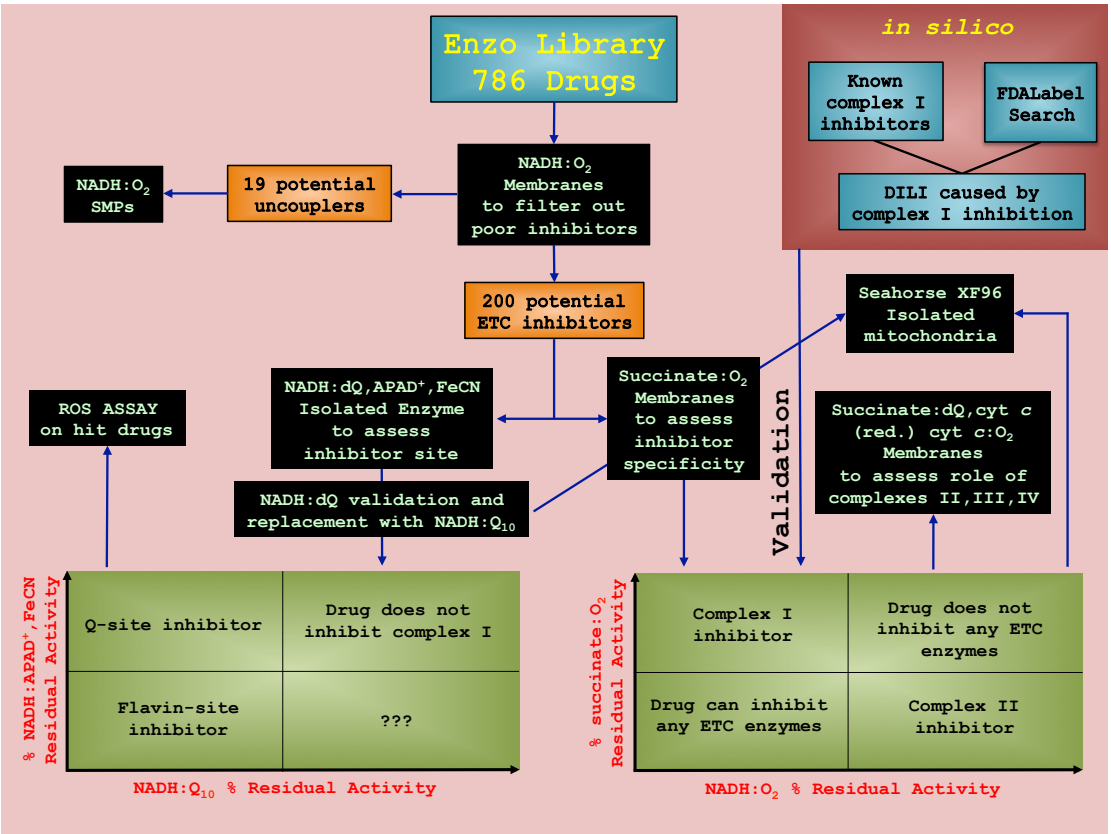

Figure 4.1. Pharmacological characterisation of complex I. The Enzo library drugs were tested in different systems (membranes, isolated complex I, mitochondria and SMPs) to assess target specificity and to validate the FDALabel search featured in chapter 3.

4.2 Mitochondrial membrane-based assays

Membranes for short are the main experimental system adopted in this chapter to assess ETC-based drug-induced mitochondrial dysfunction, since they contain all of the respiratory chain enzymes (see chapter 3 for more information on this system).

4.2.1 NADH:O_2 oxidoreduction in membranes: initial screening

NADH:O_2 oxidoreduction covers the electron flow from complex I to IV and it was the first experiment to be conducted on the whole library in order to filter out drugs whose inhibitory power was not deemed interesting: the results are shown in Figure 4.2. It would have been overly cumbersome to perform IC_{50} determinations on all of the drugs in the library: it was therefore decided to obtain one-point percentage activity determinations instead at 50 µM for each drug. The average specific activity for control (drug-free) experiments was 1.24 ± 0.09 µmol min^{-1} mg^{-1} (standard deviation), so the percentage variability was ± 7.3%.

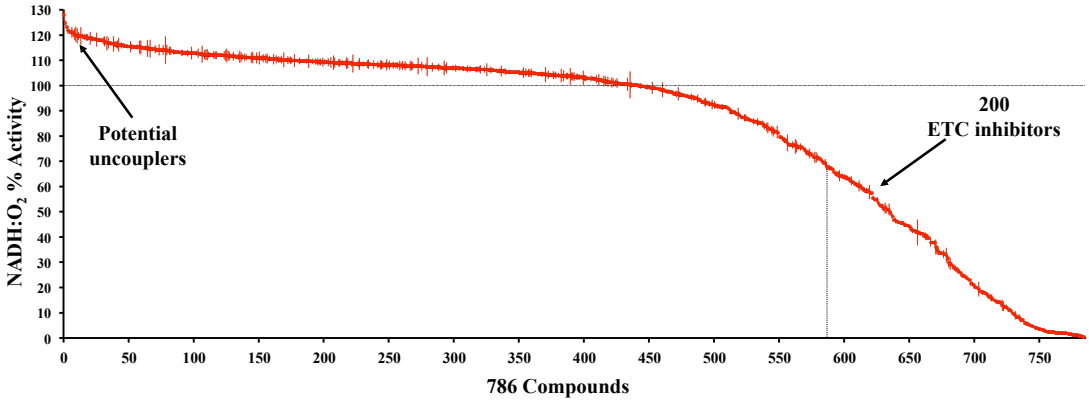

Figure 4.2. Initial classification of drugs according to their inhibitory potency towards the NADH:O_2 pathway. The 200 compounds with the lowest residual activity were selected for follow-up experiments. Also, given the (limited) coupling capability of mitochondrial membranes it was possible to isolate potential uncouplers. Each drug is presented with SEM of duplicates.

The 200 most potent compounds (Daunorubicin and Tamoxifen exhibited the highest and lowest residual activity in this set of drugs, 68% and 0% residual activity respectively) were identified as the most promising complex I-specific inhibitors and chosen for the next stage of characterisation, the succinate:O_2 and isolated complex I assays. On the other hand, potential uncouplers were tested in SMPs because this system is much more coupled than membranes and, as such, should be more sensitive towards uncoupling conditions.

In order to detect artefacts that could lead to false positives, general chemical reactivity of the drugs to experimental conditions was addressed by running the NADH:O_2 assay without the protein and only Nisoldipine was found to exhibit a chemically-driven loss of absorbance at 340-380 nm in NADH:O_2 buffer. Follow-up experiments with Nisoldipine and structurally similar calcium channel blockers Nifedipine and Amlodipine confirmed that the former is the only compound that exhibited significant loss of absorbance over time in aqueous buffer (340-380 nm absorbance dropped by 15% after 2 minutes), as opposed to the other two which were stable in aqueous solution (Nisoldipine is also stable in DMSO). Nisoldipine and, in general, 1,4-dihydropyridines derivatives, are known to undergo considerable hydrolytic[323] and photochemical[324] degradation.

Solubility issues were addressed by quantifying the difference in pathlength between a drug and the corresponding control experiment in the assay: it was decided to set the

threshold for insoluble drugs when their pathlength was more than 10% lower than the control (pathlengths of the control, drug-free, experiments were never 5% lower than their average). The following drugs were identified: Amiodarone in both NADH:O_2 and succinate:O_2, Clofazimine and Nilotinib in NADH:O_2, Tazarotene in succinate:O_2, Nepafenac, Medroxyprogesterone, Mitoxantrone and Danazol in isolated complex I assays.

The data from the drugs featured in chapter 3 (Hill parameters of NADH:O_2 IC_{50} measurements) were used to obtain their expected residual activity at the same drug concentration used in the NADH:O_2 first screening assay (50 µM). Such expected values were then compared with their actual residual activity in the experiments performed on the Enzo library: the correlation coefficient between the two series is 0.97, indicating a high agreement between the two sets of data. Figure 4.3 shows where the drugs featured in chapter 3 can be found along the NADH:O_2 trace displayed in Figure 4.2 and their expected inhibitory power at 50 µM according to data presented in chapter 3.

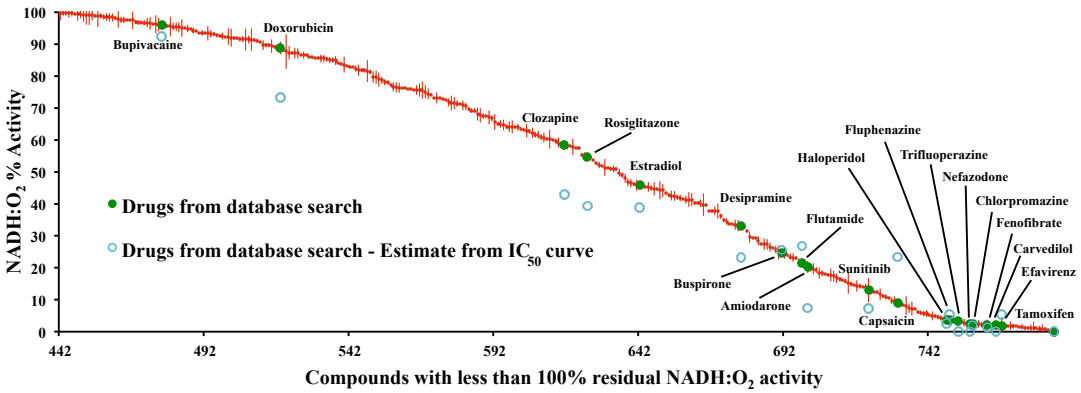

Figure 4.3. Drugs featured in chapter 3 within the initial NADH:O_2 screening. All the drugs featured in chapter 3 were highlighted in the NADH:O_2 trace displayed in Figure 4.2, plus their expected inhibitory potency at 50 µM according to the data presented in chapter 3.

4.2.2 Therapeutic plasma concentration of drugs in the Enzo library

The therapeutic plasma concentrations for 195 out of the 200 drugs were obtained from the literature (references for five drugs were not available, see appendix 4.9) and it was found that the vast majority of them (176) are lower than 5 µM. An IC_{50} value was estimated for each drug (using the Hill equation) in order to compare it with the corresponding therapeutic plasma concentration (see Figure 4.4, the high end of the

literature plasma level range was considered in the plot for each drug, when available). Top and bottom Hill parameters were assumed to be 100 and 0, respectively, and the Hill coefficient was set at -1.2. The latter value was chosen in line with the other experimental IC_{50} values determined in this thesis with membranes; however the estimates do not change significantly when the Hill coefficient is set at -1 or -1.5. By plugging the three parameters into the standard Hill equation it is possible to work backwards and estimate the IC_{50} value.

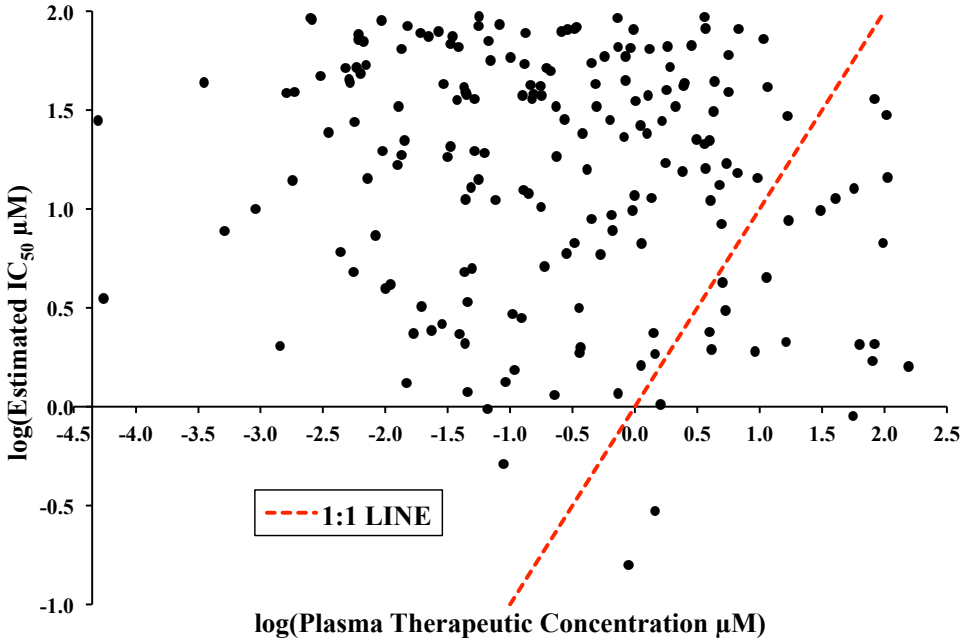

Figure 4.4. Estimated IC_{50} values and plasma therapeutic concentrations for the drugs with the lowest residual activity in the NADH:O_2 plot. Values are in logarithmic form for better visual representation. Four drugs have undetectable plasma concentrations and were not included in the plot. The red dashed line indicates where the two variables assume the same value.

There are 23 drugs (out of 191) whose estimated IC_{50} is lower than their corresponding therapeutic concentrations (data point on the right of the 1:1 red line in Figure 4.4): for these compounds, therapeutic blood levels are likely to cause a significant effect on complex I. Interestingly, 7 of these 23 drugs are antineoplastic agents and 6 are antifungals (Clotrimazole, Sulconazole, Miconazole, Terbinafine, Oxiconazole, and Ketoconazole, see section 4.2.7 for details of antifungal drugs featured in this work).

There are a number of caveats to be aware of when dealing with plasma drug levels:

1) The plasma concentration of the drug can be different from the concentration in target cells (*e.g.* some drugs in the library come in the form of antifungal creams, so the epidermal concentrations would be a more appropriate indicator). The property of kinetic homogeneity (*i.e.* the drug concentration in plasma is directly related to its concentration at the receptor site where it produces its therapeutic effects) is the main assumption in this regard[325].

2) Intracellular accumulation mechanisms (not captured by plasma drug concentration measurements) may be central to the drug mechanism of action[169].

3) Drug metabolites produced by drug-metabolising enzymes are often important in determining the biological response to a pharmaceutical. This is particularly true in the case of drugs that undergo first-pass effect (*i.e.* reaching the liver for metabolism before systemic diffusion in the body)[264]: drug concentration measurements are, in fact, taken after this stage.

4) Therapeutic plasma concentrations are based on the assumption that drugs are administered accurately, according to the prescribed dosage: this does not take into account the important phenomenon of overdose (whether it be accidental or suicidal). Almost 40,000 people died of pharmaceutical overdose in 2010 in the US alone[326], while the DILI-related deaths are estimated to be in the US, by extension, about 100,000[327], so in the same order of magnitude than pharmaceutical overdose-related deaths.

4.2.3 Succinate:O_2 oxidoreduction and determination of drug specificity towards complex I

The succinate:O_2 oxidoreduction assay is based on coupled enzyme reactions: it is, therefore, crucial to check whether a drug inhibits the coupled enzyme system or not to avoid artefacts. Not only was testing the drugs against the coupled enzyme system of this assay (fumarase and malic enzyme) a requirement for its validity, it was also required to rule out potential aggregation-based inhibition (the phenomenon whereby protein targets can be inhibited by drug-like organic molecules through colloid-like aggregation in aqueous media at micromolar or submicromolar concentrations[328,329]). This can be tested by checking the activity of the drug towards different and unrelated enzymes[330], and the coupled enzyme system of the succinate:O_2 assay may serve this

purpose. Only four drugs were found to inhibit the enzyme coupled system enough to compromise the results, Nisoldipine, Raloxifene, Hexachlorophene and Pazopanib, pointing to the possibility of aggregation-based inhibition: therefore, it appears that the succinate:O_2 assay is robust since just 2% of the tested drugs interfere with it[i].

The inhibition of any of the ETC enzymes from complex I or II down the chain will result in a lower specific activity detected (depending on how rate-limiting the inhibited enzyme is within the chain). As NADH:O_2 oxidoreduction relies on complexes I, III and IV and succinate:O_2 oxidoreduction relies on complexes II, III and IV, comparison of the inhibition of the two pathways allows the compounds to be classified into 4 groups conveniently: specific inhibitors of complex I (60 drugs), specific inhibitors of complex II (12 drugs), non-specific inhibitors (the drug could inhibit both complex I and complex II, or complex III and/or complex IV, hence it could be a Q-site-type inhibitor, 46 drugs) and relatively weak inhibitors of both pathways (82 drugs) (Figure 4.5)[i]. Importantly, the boundaries that define the four regions are arbitrary, so, for the purposes of this thesis, it was decided to set both of them to the average level of residual activities for each pathway (78.5% for succinate:O_2 and 29.7% for NADH:O_2). The drugs that are classified as relatively good inhibitors of at least one of the two pathways (as opposed to poor inhibitors) are, therefore, 118 (out of 786 overall in the library) and these fit into one of three categories according to their target(s) within the respiratory chain. The average specific activity for (control) drug-free experiments in the succinate:O_2 assay was 0.59 ± 0.07 μmol min^{-1} mg^{-1} (standard deviation).

[i] The Enzo Life Science tech team stated that there has never been any incidence of aggregation-based inhibition happening or being reported by customers as in February 2016.

[i] The class "non-specific" could be misleading because, for instance, a specific inhibitor of complex IV, beyond a certain concentration, would fall into this category (as it will be seen in section 4.2.5). Even though this terminology will be maintained throughout the thesis, the meaning of "non-specific" inhibition is more akin to "unresolved" inhibition.

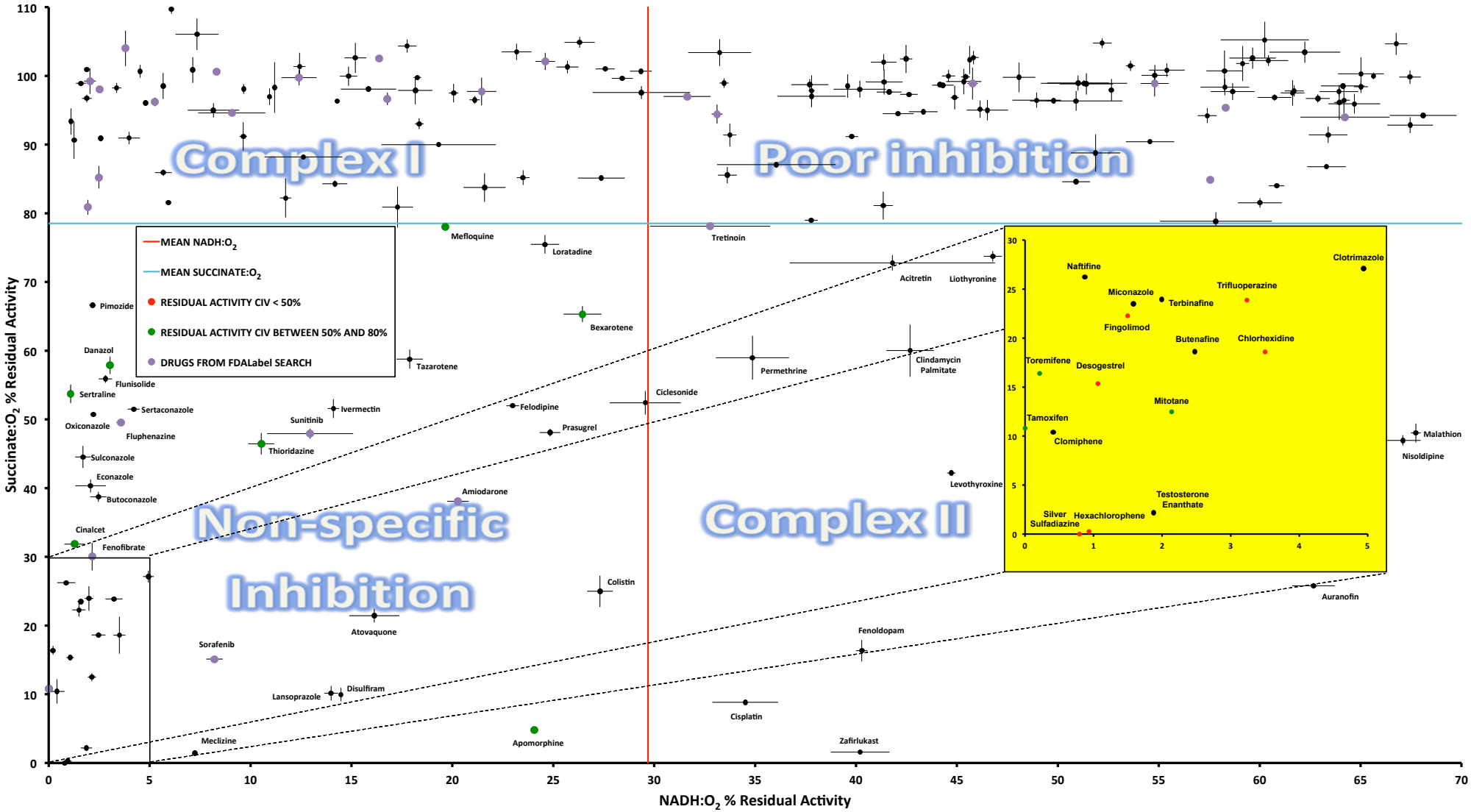

Figure 4.5. Drug specificity towards OXHPOS enzymes. The NADH:O_2 and succinate:O_2 assays results can be conveniently combined to isolate four different regions and identify specific inhibitors of complex I and II. The drugs in the bottom-left corner could inhibit both complex I or II (the only enzymes that the two pathways do not have in common) but also complex III or IV (the enzymes in common between the two pathways): these compounds were also tested for complex IV activity with the reduced cytochrome *c*:O_2 assay but only 6 of them appear to be potent inhibitors of such enzyme. The plot also shows where the hits from the FDALabel search are distributed, with 13 drugs identified as specific inhibitors of complex I. Error bars are SEM of duplicates. Drugs were tested at 50 µM each.

4.2.4 Validation of the results obtained in chapter 3

The drugs tested in chapter 3 were the result of a database search (FDALabel) combined with a set of drugs known to be complex I inhibitors from the literature: of the 52 overall hits (violet points in Figure 4.5), 8 are not included in the Enzo library. The availability of a commercial library of approved drugs allowed to test the validity of the method employed in chapter 3 by analysing the results of the 44 drugs in common between the two libraries. 17 drugs were not tested for succinate:O_2 activity since their NADH:O_2 residual activity is greater than the chosen threshold. Of the remaining 27 drugs, 13 are specific inhibitors of complex I, 6 are non-specific inhibitors, 7 are poor inhibitors and one is a complex II specific inhibitor.

Figure 4.6 shows the drugs analysed (and colour-coded according to the result presented) in chapter 3, mapped in the same position as Figure 4.5 for comparison[k]. Drugs which inhibited the succinate:O_2 pathway more than 15% at 3x NADH:O_2 IC_{50} are highlighted in orange and drugs whose NADH:O_2 IC_{50} was found to be less than 20 µM are highlighted in green (the NADH:O_2 IC_{50} values for the drugs in the first group are lower than 20 µM too).

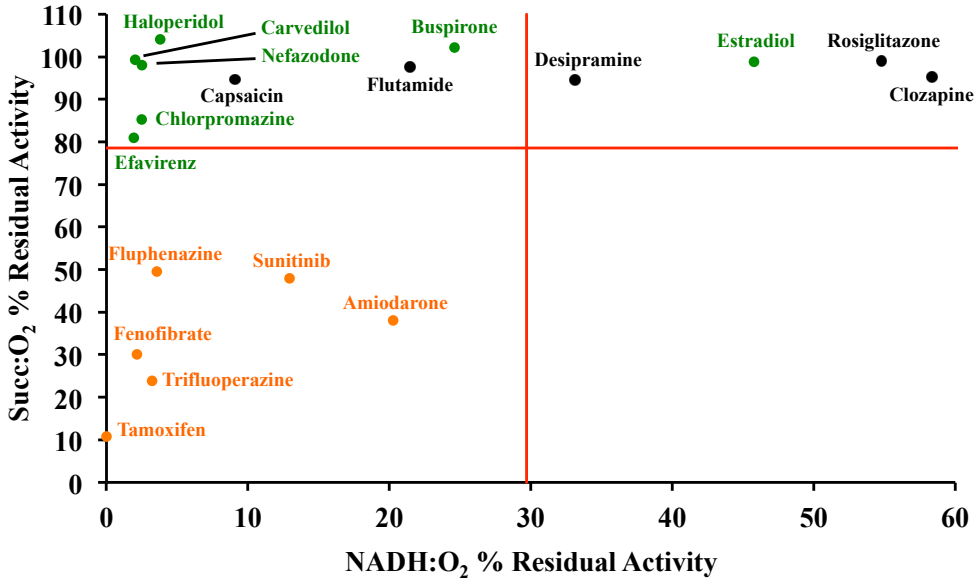

Figure 4.6. Inhibition specificity of the drugs tested in chapter 3. The drugs featured in chapter 3 are mapped in the same positions as Figure 4.5 and coloured according to the results presented in chapter 3. Orange drugs exhibited the highest inhibition in the succinate:O_2 assay, the NADH:O_2 IC_{50} of the green (and orange) drugs is less than 20 µM.

[k] Three drugs are missing from the set of drugs in chapter 3: Papaverine is not included in the Enzo library, Bupivacaine and Doxorubicin exhibited NADH:O_2 residual activity higher than the chosen threshold for the succinate:O_2 assay.

4.2.5 Confirmation using ETC canonical inhibitors and cytochrome *c*

Canonical inhibitors of the ETC (rotenone for complex I, atpenin for complex II, myxothiazol and antimycin for complex III and NaCN for complex IV) and cytochrome *c* were used to validate the succinate:O_2 against NADH:O_2 plot shown in Figure 4.5. The results are shown in Figure 4.7.

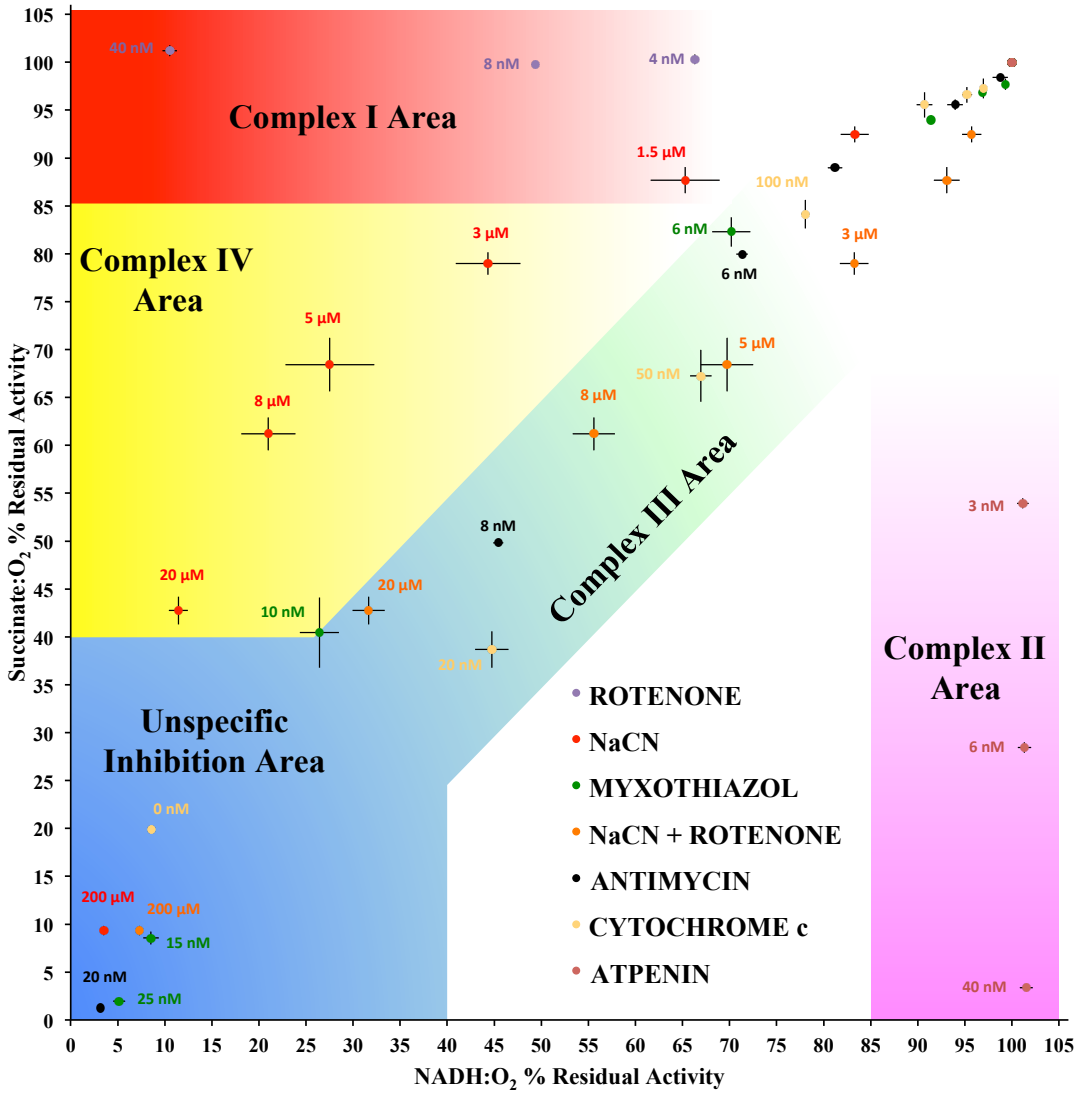

Figure 4.7. Canonical inhibitors ETC map. Specific ETC inhibitors were tested in membranes to obtain their location in the succinate:O_2 vs NADH:O_2 plot. NaCN was also tested with the IC_{50} concentration of rotenone (9 nM) against complex I and cytochrome *c* was included in the analysis. Selected concentrations are shown. Bars are SEM of triplicates.

Complex I and II specific inhibitors should not inhibit the succinate:O_2 and NADH:O_2 pathways, respectively, hence the corresponding areas in the plot should run parallel to each axis (red and pink areas in Figure 4.7 for rotenone and atpenin). Cytochrome

c, the substrate needed for both pathways, was found to fall within the 1:1 line of the plot as its concentration lowers: this is equivalent to following the substrate saturation curves for both NADH:O_2 and succinate:O_2 (see chapter 3) pathways as cytochrome *c* concentration decreases. Specific complex III inhibitors like antimycin and myxothiazol were found to fall in a diagonal area running through the 1:1 line of the plot (turquoise to azure area in Figure 4.7): complex I and II seem to be similarly rate-limiting towards complex III in their corresponding pathways. Complex IV specific inhibitors like NaCN fall in the yellow area of the plot in Figure 4.7: they first exhibit a stronger inhibition in the NADH:O_2 pathway than in the succinate:O_2 one, so it seems that complex I is more rate-limiting for the NADH:O_2 than complex II is for the succinate:O_2 pathway. This can be explained by the different specific activities of the two assays and by the relative capacity of complexes III and IV to catalyse electron transfer (*i.e.* whether it is the former or the latter that is more rate-limiting within the chain). In the NADH:O_2 assay, the rate is about 1.3-1.7 μmol min^{-1} mg^{-1}, compared to a rate of 0.5-0.7 μmol min^{-1} mg^{-1} for succinate:O_2 (see chapter 3 for the corresponding substrates saturation curves). If complex IV is more rate-limiting, at first its inhibition will mostly affect the NADH:O_2 pathway (the one with the highest rate) and by the time the NADH:O_2 rate will equal the succinate:O_2 rate the percentage inhibition of the two pathways will also be equal (*i.e.* the NaCN inhibition line in Figure 4.7 will tend to approach the 1:1 line in the plot). In agreement with this interpretation, lowering the rate of the NADH:O_2 experiment by selective inhibition of complex I with rotenone (9 nM, rate decreased by about 50%) brings the NaCN line in Figure 4.7 inside the complex III corridor (*i.e.* close to the 1:1 line). Additionally, antimycin and myxothiazol exhibit sigmoidal inhibitor titration curves in both NADH:O_2 and succinate:O_2: these are indicative of complex I and II being more rate-limiting within their corresponding pathways with respect to complex III[331]. Briefly, the capacity to oxidise ubiquinol by complex III is in excess compared to the capacity to reduce it by complex I or II, hence significant inhibition of complex III will occur only when the inhibitor concentration will render quinol oxidation more rate-limiting. This can be seen in Figure 4.8 (bottom panel), where sigmoidal titration curves for antimycin are shown for both NADH:O_2 and succinate:O_2: such sigmoidal pattern is also present when complex IV is cut out from the chain (NADH:cytochrome *c* and succinate:cytochrome *c* assays). In contrast, non-saturating concentrations of NaCN generate a hyperbolic inhibition curve for NADH:O_2, but increasing

concentrations of rotenone lower the rate of electron transfer along the chain and, as a result, the titration curves shift from hyperbolic to sigmoidal (see Figure 4.8 top panel). Overall, the data illustrated in Figure 4.8 suggest that a small percentage of inhibition of complex III generates a smaller inhibition of the overall respiratory flux than the same percentage of inhibition on complex IV, therefore complex III possess an higher capacity for transferring electrons than complex IV in mitochondrial membranes.

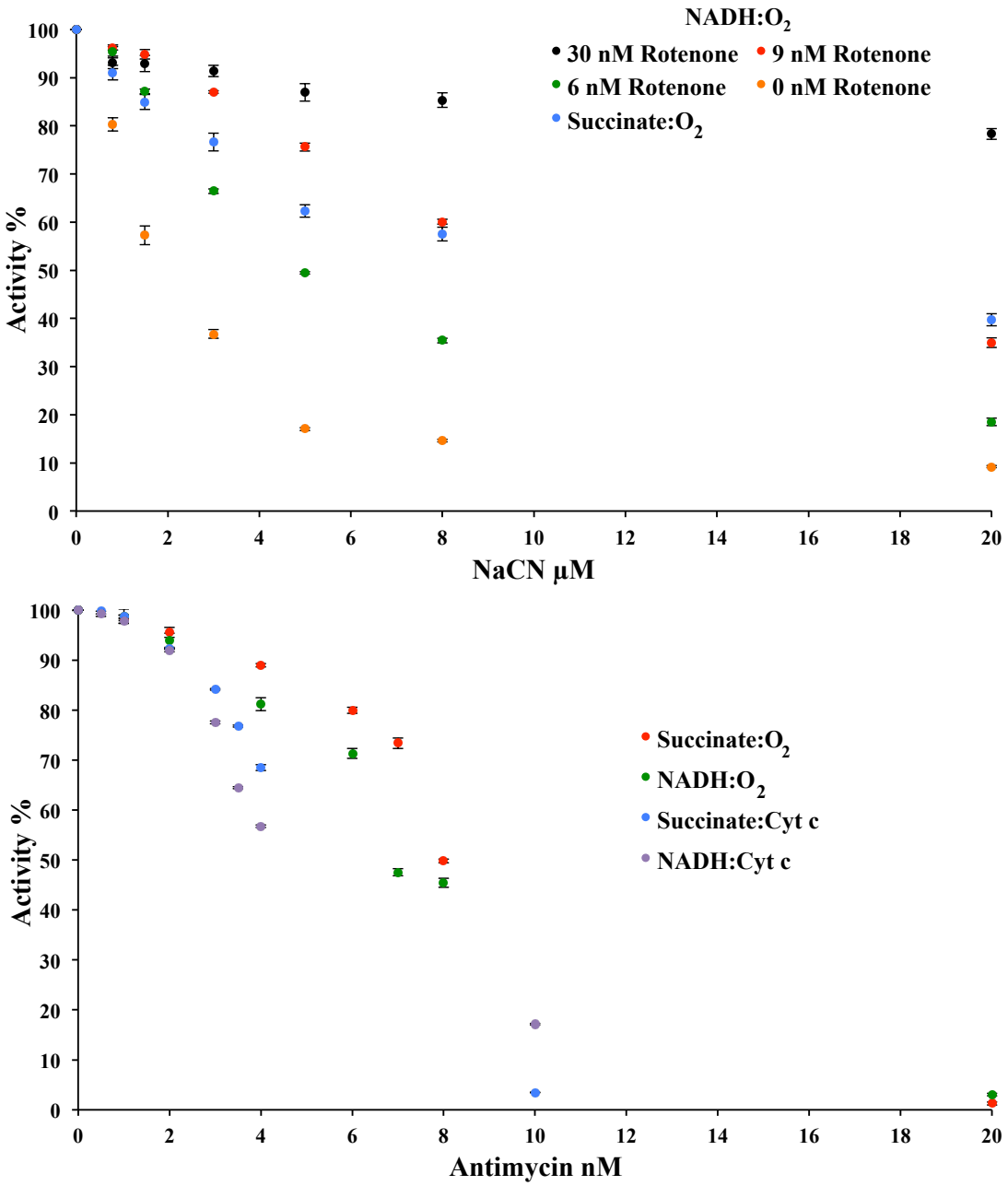

Figure 4.8. Titration curves for different experiments with NaCN and antimycin. Top panel, NaCN titration curves for NADH:O2 with different rotenone concentrations (succinate:O_2 curve shown for comparison). Bottom panel, Antimycin titration curves for four different pathways within the respiratory chain. SEM of triplicates are reported.

Examples of cyanide respiratory inhibition of both hyperbolic and sigmoidal nature have been reported (the former in rat liver SMPs[332], the latter in permeabilised human muscle fibers where the sigmoidal character become less pronounced when succinate was added to glutamate/malate respiration[333]): this indicates that the capacity to transfer electron in the respiratory chain by complex IV can vary significantly between different systems. It must be pointed out that both NADH:O_2 and succinate:O_2 experiments always exhibit perfectly straight (absorbance) traces up until they run out of substrate, and this is diagnostic of steady-state conditions being reached almost immediately after the reaction started. Furthermore, the OXPHOS complexes and substrates are not in a 1:1 stoichiometric ratio in the mitochondrial IMM with respect to one another: in bovine heart, mean molar ratios are about 1 x complex I, 2 x complex II, 4 x complex III, 8 x complex IV, 74 x ubiquinone and 10 x cytochrome c[334]. This means that it is not complex I and II that are rate-limiting towards complex III *per se* but, rather, they are rate-limiting within the mitochondrial membrane system.

4.2.6 Investigating cytochrome *c* (reduced):O_2 oxidoreduction in membranes for non-specific inhibitors: determining the role of complex IV

Given that the full ETC is available for testing in mitochondrial membranes it was possible to perform the (reduced) cytochrome *c*:O_2 oxidoreduction assay: by monitoring the complex IV-catalysed oxidation of (reduced) cytochrome *c* by O_2, drugs for which complex IV is a biological target can be identified. It is important to note that the protein concentration was five times lower than the other membrane-based assays discussed so far (6 as opposed to 30 μg mL^{-1}) because the rate would have been too fast to detect, while the drug concentration was kept at 50 μM. The most potent complex IV inhibitors were found among the 46 non-specific inhibitors in Figure 4.5, since these compounds exhibit a high level of inhibition of both NADH:O_2 and succinate:O_2 pathways (there was no significant inhibition detected among the 12 complex II specific inhibitors). Just six out of 46 drugs inhibited complex IV by more than 50% at 50 μM concentration and two of these results are questionable: Silver Sulfadiazine is provided as a suspension in the library due to its very low solubility and Hexachlorophene inhibits the coupled enzyme system in the succinate:O_2 assay, so both drugs could easily form aggregates. The other four are Fingolimod (14.9%

residual activity), Desogestrel (18.5%), Chlorhexidine (23.1%) and Trifluoperazine (48.4%).

Evidently, complex IV does not appear to be a promising pharmacological target if, of almost 800 candidate inhibitors, only four demonstrably inhibit it, even at such a high drug to protein concentration ratio. The remaining 40 compounds in the non-specific inhibition area of Figure 4.5 (out of the overall 46 tested) are either complex III inhibitors or they inhibit more than one of the complexes I, II and III. Notably, all of these three enzymes use ubiquinone/ol as a substrate, and thus overlapping inhibition could indicate targeting of ubiquinone-binding sites.

4.2.7 Structural filters and the role of antifungal agents

The 200 drugs featured in Figure 4.5 were evaluated for similarities between them based on their molecular structures and their class. Although these drugs are structurally very diverse, three structural scaffolds occur in a substantial proportion of the set (Figure 4.9 upper panel). The three structural motifs are an *ortho*-dialkoxy benzene motif (14 drugs, 44 drugs in the whole library), a tricyclic antidepressant (TCA) moiety (16 drugs, 18 drugs in the whole library not including an anthraquinone core) and a *meta*-Cl benzene moiety (13 drugs, 16 drugs in the whole library). While the first two classes are mainly complex I inhibitors (except for Apomorphine, Fenoldopam, Thioridazine and Trifluoperazine that interact more strongly with the complex II pathway), drugs that belong to the third class cluster together in the non-specific region: this functional group is common to many antifungal drugs, as it can be seen when the 200 drugs are classified according to clinical application (Figure 4.9 lower panel). Several antifungal classes[335-337] are present in the library (22 drugs in total) and 10 of them were found to be non-specific ETC inhibitors, according to Table 4.3.

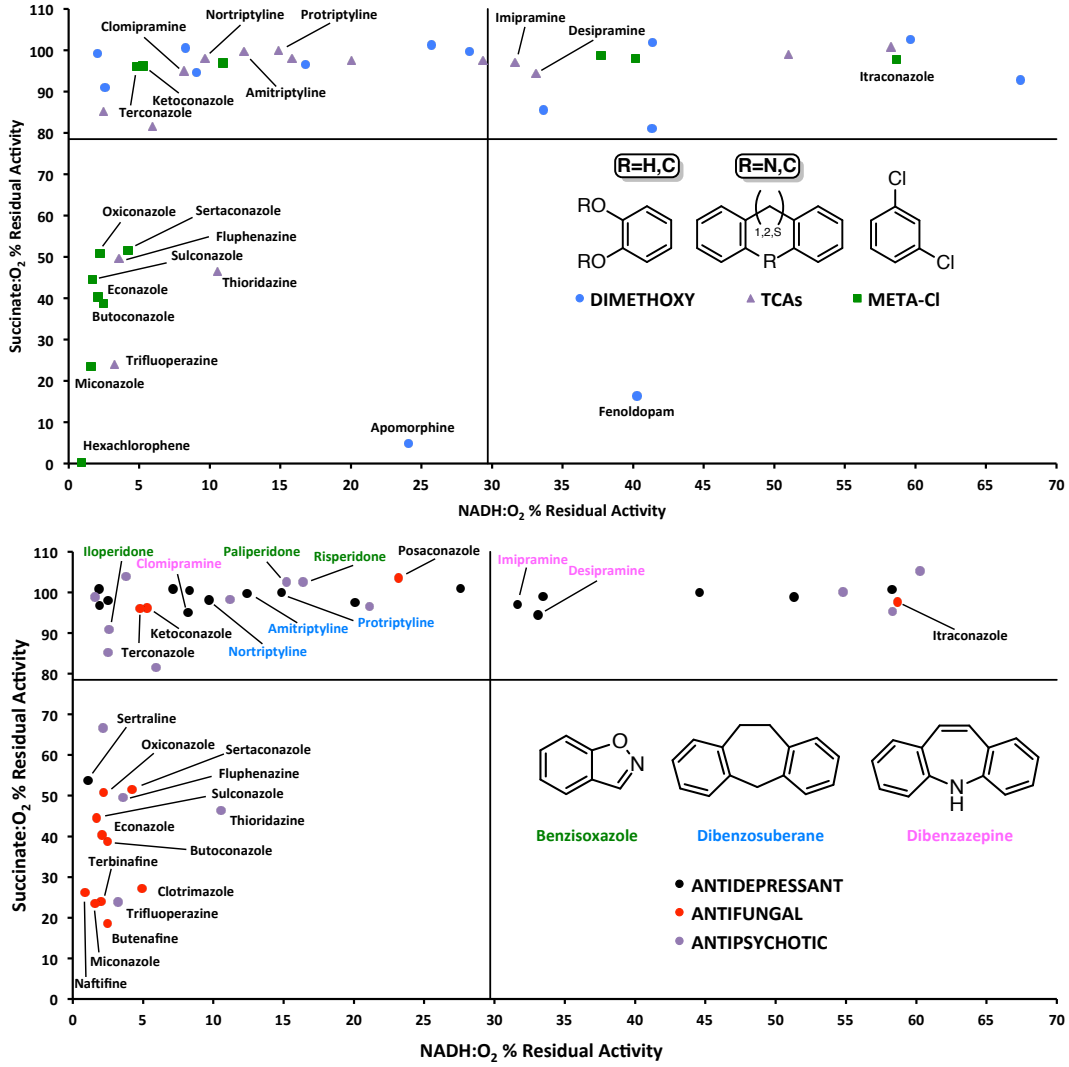

Figure 4.9. Structural filters and types of drugs. In the upper panel, drugs possessing particular moieties cluster together as mostly non-specific inhibitors (*meta*-Cl) or specific complex I inhibitors (*ortho*-dimethoxy and TCA). In the lower panel, many antifungal drugs, especially first generation azoles, are non-specific ETC inhibitors and most of them share a *meta*-Cl benzene ring. Common structural features of antidepressants and antipsychotics are indicated with colour-coded labels.

Imidazoles of 14 α-Sterol demethylase and especially squalene epoxidase inhibitors are the most potent antifungals against the NADH:O_2 pathway and they are all classified as non-specific inhibitors (except for Ketoconazole which is specific to complex I). Three of the 14 α-Sterol demethylase triazoles are complex I specific inhibitors. The other categories of antifungals do not appear to inhibit any of the pathways to a significant degree.

Antifungal type/class		*meta*-Cl	Drug	Residual Activity % at 50 μM	
14 α-Sterol demethylase inhibitors				**NADH:O_2**	**Succ:O_2**
	Imidazole	✓	Oxiconazole	2.2	50.7
		✓	Sertaconazole	4.2	51.5
		✓	Sulconazole	1.7	44.5
		✓	Econazole	2.1	40.3
		✓	Butoconazole	2.5	38.7
		✓	Miconazole	1.6	23.5
		✓	Ketoconazole	5.3	96.2
			Clotrimazole	4.9	27.1
	Triazole	✓	Terconazole	4.8	96.0
			Posaconazole	23.2	103.5
		✓	Itraconazole	58.7	97.7
			Voricozanole	96.8	/
			Fluconazole	123.2	/
Squalene epoxidase inhibitors					
	Allylamines		Terbinafine	2.0	23.9
			Naftifine	0.9	26.2
	Benzylamines		Butenafine	2.5	18.6
Fungal mitosis inhibitors			Griseofulvin	99.1	/
Polyene inhibitors of fungal membrane stability			Amphotericin B	95.8	/
			Nystatin	75.6	/
			Natamycin	95.3	/
Fungal wall synthesis inhibitors (Echinocandins)			Micafungin	70.5	/
Hydroxypyridones (Iron chelators)			Cyclopirox	99.0	/

Table 4.3. Antifungal drugs for human use in the Enzo Library. The antifungal drugs in the library display a wide range of potencies, with 14 α-Sterol demethylase Imidazoles being the most potent category towards complex I and the Squalene Expoxidase being the most potent category towards complex II.

Both antipsychotics and antidepressants tend to concentrate in the complex I region, with some antipsychotics like Thioridazine, Trifluoperazine and Fluphenazine exhibiting higher inhibition of the succinate:O_2 pathway. None of the drugs included in these categories appears in the complex II specific inhibitor region. Benzisoxazoles-based antipsychotics (see lower panel in Figure 4.9) included in the library are Risperidone, Paliperidone and Iloperidone and they are all specific complex I inhibitors: they are very structurally similar to each other (Paliperidone is actually a metabolite of Risperidone and, interestingly, both affect the expression of the complex I accessory subunit NDUFS4 in rats[338]). Intriguingly, the only other benzisoxazole-containing drug in the library, Zonisamide (an anticonvulsant), does not inhibit the NADH:O_2 pathway at all: this compound lacks both the fluorine atom

in the benzisoxasole moiety and the whole piperidine-containing side compared to the other three. Figure 1.10 shows the structural differences among the four species.

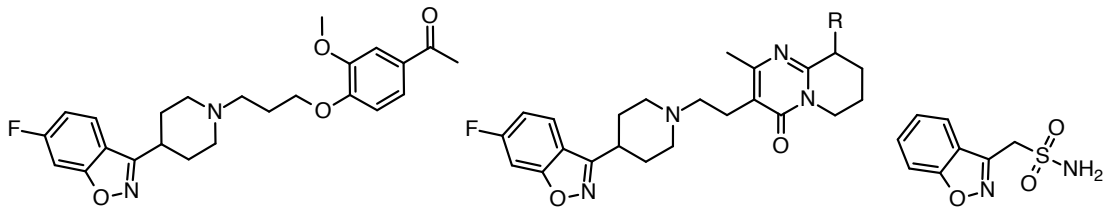

Figure 4.10. Drugs containing a benzisoxazole moiety in the Enzo library. Zonisamide is the only benzisoxazole-containing compound in the library that does not inhibit the NADH:O_2 pathway. Differences with the other compounds are the fluorine atom in the benzisoxasole moiety and the whole piperidine-containing side.

Since the TCA structural core is the main structural feature of TCA drugs, it is no surprise that several drugs appear in both plots in Figure 4.9: of particular importance are antidepressants in the complex I specific region that share either a dibenzosuberane (Amitriptyline, Nortriptyline and Protriptyline) or dibenzazepine (Clomipramine and borderline complex I-specific Desipramine and Imipramine) core (see lower panel in Figure 4.9). While other dibenzosuberanes (antihistamine Cyproheptadine and muscle relaxer Cyclobenzaprine) still retain NADH:O_2 activity (51.0 and 15.8% respectively) but do not interact with the succinate:O_2 pathway, dibenzazepine anticonvulsants Carbamazepine and Oxcarbazepine do not inhibit the NADH:O_2 pathway at all. Intriguingly, the antidepressant Sertraline (the only antidepressant to exhibit non-specific inhibition) has been shown to possess antifungal activity[339,340].

4.3 Assays on isolated complex I and target resolution of non-specific OXPHOS inhibitors

A set of standard assays[158] was applied to the isolated complex to investigate whether the compounds are inhibitors that act at the flavin site or at the ubiquinone binding site, and whether they affect the production of reactive oxygen species. To test the effects on the overall rate of catalysis (including the activity of both active sites) the NADH:dQ oxidoreductase reaction was initially used but given its several drawbacks it was eventually replaced with the NADH:Q_{10} assay (see section 4.3.1). It must be

pointed out, however, that a compound that inhibits the Q-site in complex I would be indistinguishable from a compound binding to (and inhibiting) a proton pump subunit, since ubiquinone reduction and proton pumping are coupled processes. Complex I-specific assays were employed, alongside other assays in membranes, to identify other categories of OXPHOS inhibitors (complex III- and non-specific, see section 4.3.2). Finally, to test the effects on the flavin site within complex I, the FeCN, APAD and ROS reactions were used.

4.3.1 The NADH:dQ and NADH:Q_{10} oxidoreduction assays: testing the Q-site and indirectly determining potential specific complex III inhibitors

The NADH:dQ assay tests Q-site activity for the isolated complex (involving the entire catalytic cycle) but there are some drawbacks when comparing it to the NADH:O_2 in membranes. The frequency distribution of drugs plotted according to residual activity shows that the drugs tested distribute differently within the two experiments: the NADH:dQ distribution is shifted further to the right (black and red bars in Figure 4.11), indicating that this assay is less susceptible to inhibition than the NADH:O_2 assay. In order to overcome the limitations of the NADH:dQ assay unveiled in this work (listed later on in this paragraph) a NADH:Q_{10} assay in proteoliposomes was performed. In this assay the physiologically relevant ubiquinone Q_{10} is constantly recycled upon reduction by complex I via an excess of alternative oxidase (AOX) within a reconstituted proteoliposome environment[341]. AOX is a component of the mitochondrial respiratory chain in many plants and fungi and oxidises ubiquinol by concomitantly reducing oxygen, thus bypassing complexes III and IV, without pumping protons[342]. Collectochlorin (a specific and potent AOX inhibitor) was tested on Q_{10}-free (complex I-containing) proteoliposomes with added dQ, and a sigmoidal titration curve was obtained, suggesting that AOX was not the rate-limiting enzyme (the NADH:dQ rate in proteoliposomes was about 50% lower than the NADH:Q_{10} rate). The 150 drugs that inhibited the NADH:O_2 pathway the most (residual activity of less than 49%) were tested with the NADH:Q_{10} assay and the improvement on detection of complex I inhibition compared to the NADH:dQ assay was remarkable: the overall NADH:Q_{10} distribution is much closer to the NADH:O_2 one than to NADH:dQ (blue bars in Figure 4.11).

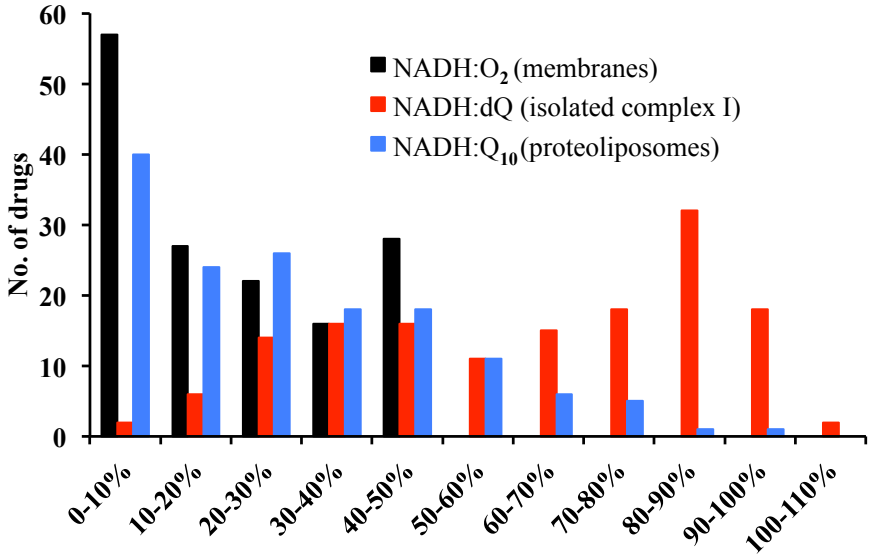

Figure 4.11. Frequency distribution of drugs according to percentage residual activity in NADH:O_2, NADH:dQ and NADH:Q_{10}. The drugs affect the NADH:O_2 and NADH:dQ oxidoreductions differently: while the O_2 pathway distribution is centred on low residual activity, the dQ pathway distribution is shifted to higher residual activity. The NADH:Q_{10} assay brings the overall data closer to the NADH:O_2 distribution.

The limitations of the NADH:dQ are even clearer when analysed in conjunction with other assays: several drugs in the library exhibit contradictory values of NADH:O_2, succinate:O_2 and NADH:dQ assays. Namely the low residual activity of the first and high residual activity of the second should point towards complex I inhibition which is not detected by the third, whose residual activity remains high (50% or more). For example, Paroxetine exhibits residual activities of 8.3, 100.6 and 82.8% for NADH:O_2, succinate:O_2 and NADH:dQ, respectively; similarly, for Nortriptyline the corresponding values are 9.7, 98.1 and 84.2 %. Figure 4.12 (black and grey points) shows how the NADH:dQ assay does not detect complex I inhibition with 41 drugs previously determined as complex I specific inhibitors in membranes (their residual activity is higher than 50%). The area in the plot in Figure 4.12 includes 73 drugs overall (60 specific inhibitors of complex I as illustrated in section 4.2.3 plus other 13 included by lowering the succinate:O_2 threshold from 78.5 to 50%), hence 32 drugs out of 73 leave a residual activity in the NADH:dQ assay less than 50%. The NADH:Q_{10} assay is, again, better at detecting complex I inhibition than NADH:dQ, since only four drugs (highlighted in Figure 4.12, red and green points) within the 73 in the area are not detected as inhibitors (as opposed to 41 with the NADH:dQ assay).

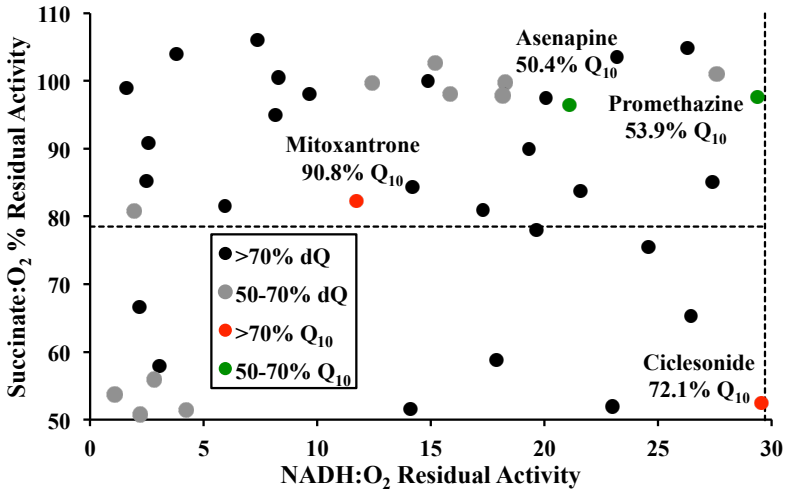

Figure 4.12. Comparison of NADH:dQ and NADH:Q_{10} inability to detect complex I inhibitors. 41 drugs in the complex I specific inhibitor category are not detected as such by the NADH:dQ assay. The NADH:Q_{10} assay, instead, is far more effective, lowering the number of undetected drugs to only four (highlighted in the plot). Dots refer to percentage residual activity as indicated in the legend.

In addition, the correlation coefficient between the NADH:O_2 and NADH:dQ results is 0.13 and the correlation coefficient between the NADH:O_2 and NADH:Q_{10} results is 0.69: such an improvement is likely due to chemical incompatibilities of some drugs with the NADH:dQ assay environment that are mostly resolved by the NADH:Q_{10} assay. Since the NAHD:Q_{10} assay depends on Q_{10} being reoxidised by AOX, drugs needed testing on AOX too in order to rule out drug interference with the Q_{10} regeneration system: only Miconazole, Oxiconazole and Amiodarone were incompatible with the NADH:Q_{10} assay[1]. It is possible, however, that AOX activity may be affected by the (proteo)liposome environment in the NADH:Q_{10} assay and, as such, may react differently to compounds when tested in isolation in aqueous buffer.

[1] All the drugs were tested on isolated AOX enzyme with Q_1H_2 as electron donor (the reaction catalysed is therefore Q_1H_2:O_2) at a concentration of AOX 6x less than the actual NADH:Q_{10} assay (0.27 as opposed to 1.7 µg mL^{-1}): Oxiconazole and Miconazole exhibited the lowest residual activity (less than 5%) and Amiodarone exhibited a descending (not ascending) absorbance trace in the assay. Also, 14 randomly selected drugs out of the overall 150 were tested at 0.34 µg mL^{-1} of isolated AOX in the Q_1H_2:O_2 assay and their residual percentage activity increased by at least 30%.

There are several reasons that can explain the shift in distribution from NADH:O_2 to NADH:dQ

1) The dQ assay contains asolectin and CHAPS, so drug diffusion in the medium is different than in NADH:O_2 conditions. The hydrophobic phase is bigger by mass in the experimental conditions of the NADH:dQ assay (0.075% of asolectin or 750 μg mL^{-1}) than in the NADH:O_2 assay (30 μg mL^{-1} of membranes include about 10 μg mL^{-1} of lipid, assuming a protein-to-lipid ratio of about 3:1 commonly found in the IMM[343]).
2) Q species are different (native Q_{10} vs dQ) and so is their reduction potential.
3) In the NADH:O_2 assay complex I is surrounded by its native membrane whereas in the dQ assay asolectin and CHAPS provide an artificial membranous environment, hence the enzyme activity can be affected by the different environment it resides in.
4) The drugs in membranes may have more than one target, hence the collective response from the chain can be different from the isolated enzyme.
5) The concentration of complex I in the two assays (isolated enzymes and membranes) is different, therefore the enzymatic response to the drugs will be different accordingly.

Specificity towards OXPHOS enzymes can be addressed by plotting the NADH:O_2 against NADH:Q_{10} values for drugs, similarly to the IC_{50} ratio between NADH:O_2 and NADH:dQ described in chapter 3. In this plot (see Figure 4.13, where drug categories are colour-coded to correspond to the succinate:O_2 against NADH:O_2 plot in Figure 4.5), non-specific inhibitors (red dots) are concentrated below the 1-to-10 line (*i.e.* their ratio of residual activity of NADH:Q_{10} over residual activity of NADH:O_2 is higher than 10). A situation where the NADH:Q_{10} residual activity for a drug is much higher than the corresponding residual activity for NADH:O_2 could be diagnostic of complex III specific inhibition. This, of course, implies that (as it was seen in paragraph 4.2.6) complex IV is very rarely a target for drugs in this library; also, the concentration of complex I in the two assays (isolated enzymes and membranes) is different, therefore the enzymatic response to the drugs will be different accordingly. Nonetheless, it is still possible to define areas of the plot in Figure 4.13 where complex III-specific inhibitors are most likely to be found: the three lines 1-to-2, 1-to-4 and 1-to-10 delimit the regions where the ratio of residual

activity of NADH:Q_{10} over NADH:O_2 is greater than 2, 4 and 10 respectively (a complex III-specific inhibitor should be found progressively more likely on the right of these lines). As the area enlarges (going from 10 to 4), more complex I specific inhibitors (green dots) are progressively included. There are 17 drugs in the 1-to-4 region, 15 of which are classified as non-specific inhibitors and two are classified as complex I specific inhibitors. Of the three drugs identified as complex-III specific inhibitors (see later section 4.3.2, underlined in Figure 4.13), two fall below the 1:4 line (Meclizine and Atovaquone) and one is close to the 1:2 line (Fenoldopam). Other hits (highlighted but not underlined in Figure 4.13) include two of the drugs that the NADH:Q_{10} assay failed to identify as complex I-specific inhibitors (Ciclesonide and Mitoxantrone, see Figure 4.12) and Permethrin, which was reported to be a complex I-specific inhibitor and not to inhibit complex III by Gassner *et al.*[344]. It must be pointed out that, in such study, the authors tested complex I activity with duroquinone using freeze-thawed rat liver SMPs with a 70-80% of rotenone-sensitive activity (bovine membranes and SMPs have about 96% rotenone-sensitive activity or higher). In addition, complex III activity was tested with a duroquinol:cytochrome *c* assay that, similarly to the membrane-based complex III activity assay presented in this work (see section 4.6.3) is plagued by a substantial background activity (spontaneous ubiquinol oxidoreduction was reported at 38% of the total activity). Finally, the activity of complex III was monitored at 520 nm instead of 550 nm for cytochrome *c* reduction (the difference in absorbance between oxidised and reduced cytochrome *c* at the former wavelength is much lower than at the latter).

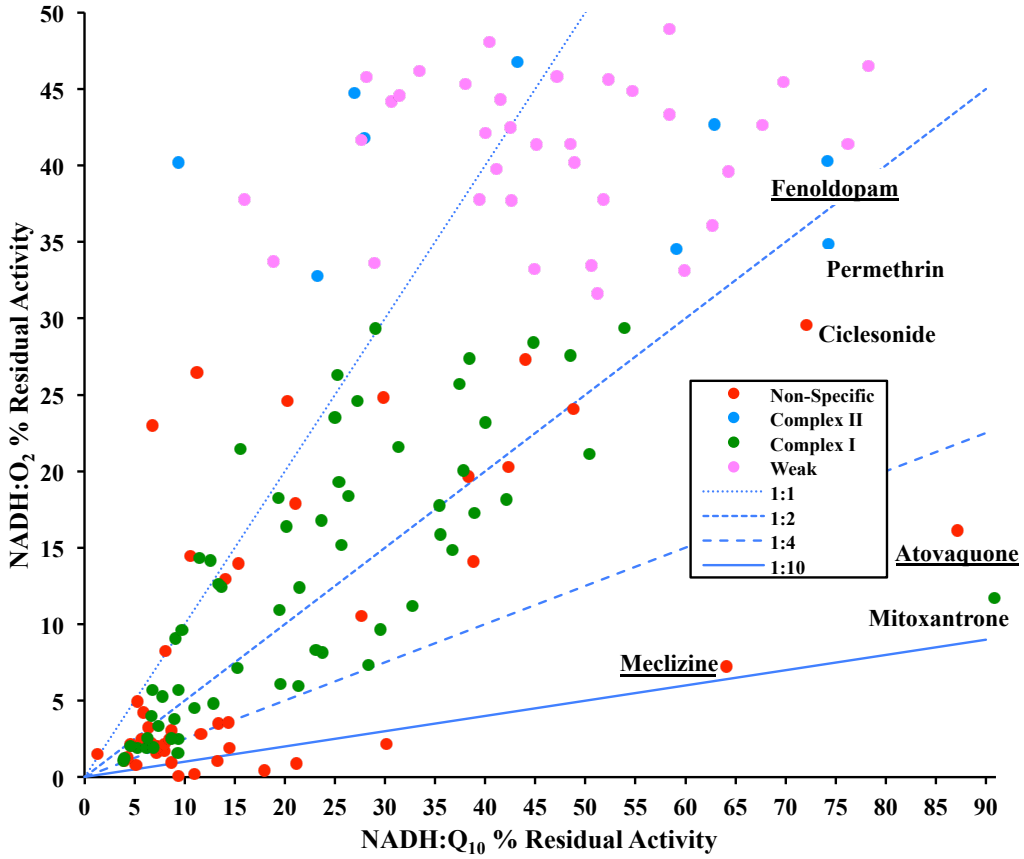

Figure 4.13. NADH:O_2 and NADH:Q_{10} values for the most potent 150 drugs. The plot shows the values for the two assays for each drug in addition to their inhibition specificity according to Figure 4.5. Dots below the 1-to-2, 1-to-4 and 1-to-10 lines are drugs whose ratio of residual activity of NADH:Q_{10} over NADH:O_2 is higher than 2, 4 and 10 respectively. Complex III specific inhibitors identified in section 4.3.2 are highlighted and underlined. Other drugs in the complex III areas close to the three specific inhibitors are highlighted but not underlined.

4.3.2 Focus on a subset of Complex I- and III-specific and non-specific inhibitors

The results illustrated in section 4.3.1 allowed three drug categories to be defined, according to whether their residual activity in NADH:O_2, succinate:O_2 and NADH:Q_{10} assays fall within appropriate ranges: the compounds thus found could now be further characterized. Importantly, these categories reflect two critical aspects of ETC inhibition that this work encompasses, target specificity (complex I- and III-specific inhibitors) and drug ability to interact with more than one ETC enzyme (non-specific inhibitors). Figure 4.14 shows the three drug categories thus created and their activity level thresholds for the three assays. Succinate:dQ (complex II) and succinate:cyt *c* (complex II-III pathway) assays in mitochondrial membranes were performed on the complex III-specific and non-specific inhibitors to determine more

precisely the involvement of complexes II and III. Also, IC_{50} values in NADH:O_2 were obtained for complex I specific inhibitors. The data is illustrated in Table 4.4 and Table 4.5, with table header rows presented in the same colour codes for the three drug categories used in Figure 4.14. Data from other assays, therapeutic blood concentrations, pK_a levels, charge at physiological pH and also whether the drugs caused mitochondrial side effects (based on the FDALabel search featured in chapter 3) are presented for reference. Lastly, significant inhibition of succinate:dQ, succinate:cytochrome *c* and (red.) cytochochrome *c*:O_2 were defined as residual activities less than 50% (pink), 20% (green) and 50% (teal) respectively (Table 4.4).

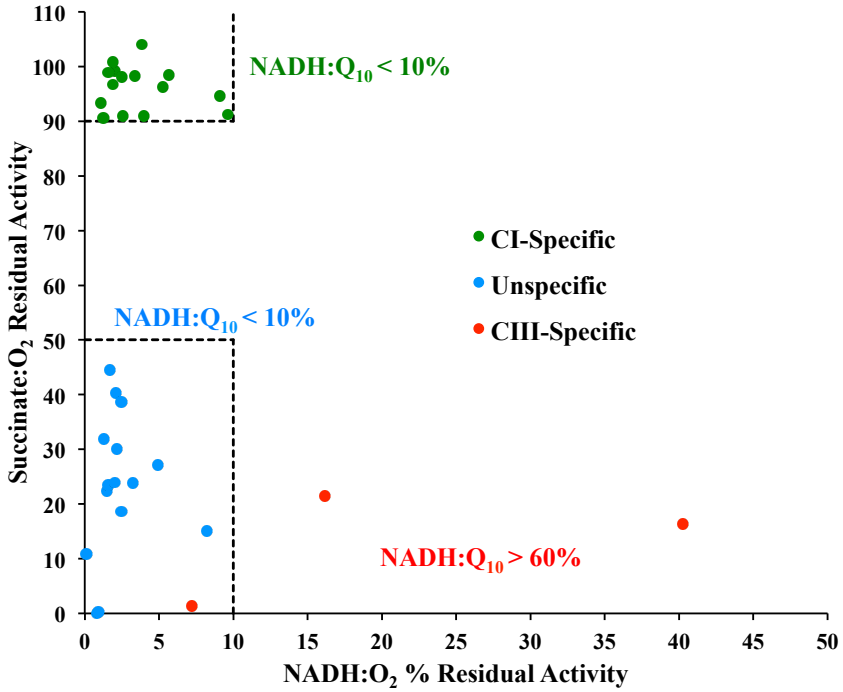

Figure 4.14. Three important categories of drugs according to their ETC targets. Of all the drugs whose NADH:Q_{10} and NADH:O_2 activities were both less than 10%, complex I-specific (green) and non-specific (blue) inhibitors exhibited succinate:O_2 activity higher than 90% and lower than 50%, respectively. Complex III-specific (red) inhibitors exhibited the lowest succinate:O_2 activity among drugs whose NADH:Q_{10} activity was higher than 60%. Header rows in Table 4.4 and Table 4.5 share the same colour code.

Non-specific and complex I-specific inhibitors possess either a positive or neutral charge at physiological pH (Sulfadiazine and Hexachlorophene are the only two compounds with negative charge), and some of them have already been described in chapter 3 (Trifluoperazine, Fenofibrate and Tamoxifen in Table 4.4, Carvedilol, Nefazodone, Haloperidol and Capsaicin in Table 4.5). The three complex III-specific inhibitors exhibit different charges altogether.

As for complex III specific inhibitors, Atovaquone is a known complex III inhibitor in different systems: *Plasmodium falciparum*, *Pneumocystis jirovecii*, FaDu[345] (human hypopharyngeal carcinoma) and MCF-7[346] (breast cancer) cells. Interestingly, Mootha and co-workers found that Meclizine induced an increase in OCR and a decrease in ECAR in STHdh$^{Q7/7}$ (mouse striatal), human HEK293 (embryonic kidney) and HeLa cells, but had no effect on respiration of isolated mitochondria from mouse kidney (indistinguishable for the control experiment)[347]. They later ascribed this effect to Meclizine inhibiting CTP:phosphoethanolamine cytidylyltransferase, a cytosolic enzyme that participates in the Kennedy pathway of phosphatidylethanolamine biosynthesis[348].

Of note among the non-specific inhibitors (Table 4.4) is Fingolimod, a drug used to treat multiple sclerosis. Low residual activity in NADH:O_2, succinate:cytochrome *c* and (red.) cytochrome *c*:O_2 assays and high residual activity in the succinate:dQ assay suggest strong inhibition of complexes I, III and IV. One of the major side effects of Fingolimod is liver injury in the form of elevated blood liver enzymes several times the upper limit levels, which tend to return to normal levels once the dosage is reduced[349]. Some enzymes in hepatocytes (especially aminotransferases and alkaline phosphatases) but also in other tissues (especially muscle[350]) are markers of cellular injury: in normal conditions their serum concentrations is very low but events leading to necrosis or cell membrane injury (often but not exclusively associated with ROS overproduction[351]) cause leakage into the serum, thus increasing their concentrations therein[352]. The mechanism whereby Fingolimod leads to elevated liver enzymes remains unknown[353] but it is possible that its substantial inhibition of OXPHOS enzymes is a contributing factor. In this regard, Fingolimod is extensively metabolised by humans, with only 23% of the parent drug left untouched[354].

Among the complex I specific inhibitors (Table 4.5), exposure of mouse 3T3-L1 adipocytes to Nebivolol (the compound with the highest NADH:O_2 and NADH:Q_{10} inhibition) was interestingly found to increase expression levels of complex I, II and transcription factors involved in mitochondrial biogenesis[355]. These may be the result of Nebivolol interaction with organelles outside mitochondria, since it did not have an effect on respiration of isolated mitochondria (see section 4.5).

Drug	NADH:		Succinate:			(Red.) cyt *c*:O_2 %	Therapeutic concentration µM	pK_a	Charge at physiological pH	Mito side effects	
	Q_{10} %	O_2 %	O_2 %	dQ %	cyt *c* %					Liver	Extraliver
COMPLEX III-SPECIFIC INHIBITORS											
	> 60%										
Meclizine	64.1	7.2	1.4	80.1	1.7	102.7	0.28	6.2	Neutral		
Atovaquone	87.1	16.1	21.4	102.0	10.0	105.7	56.7	5.0	N	✓	✓
Fenoldopam	74.2	40.3	16.3	105.2	7.9	91.4	0.15	8.0	P		
NON-SPECIFIC INHIBITORS											
	< 10%	**< 10%**	**< 50%**	**< 50%**	**< 20%**	**< 50%**					
Fingolimod	1.3	1.5	22.3	68.6	**8.1**	**14.9**	0.1	7.8	P/Neutral		
Cinacalcet	4.4	1.3	31.8	71.7	**5.9**	70.0	0.1	10.3	P		
Econazole	4.8	2.1	40.3	66.4	28.5	97.8	1.4 nM	6.6	Neutral		
Ag·Sulfadiazine	5.1	0.8	0.0	96.0	44.5	**4.7**	56.0	6.5	N	✓	
Clotrimazole	5.3	4.9	27.1	**44.5**	33.3	95.7	5.0	4.7	Neutral		
Butoconazole	5.7	2.5	38.7	64.1	30.2	112.6	0.04	6.8	P/Neutral		
Trifluoperazine	6.4	3.2	23.9	80.8	70.0	**48.4**	0.02	9.0	P	✓	
Miconazole	7.2	1.6	23.5	72.5	**16.9**	107.5	155.6	6.7	P/Neutral		
Terbinafine	7.3	2.0	23.9	80.0	**14.1**	86.7	4.1	7.1	P/Neutral	✓	✓
Sulconazole	7.9	1.7	44.5	69.7	36.0	104.2	80.0	6.7	P/Neutral		
Fenofibrate	7.9	2.2	30.0	83.8	**19.7**	112.8	13.9	/	Neutral	✓	✓
Sorafenib	8.1	8.2	15.1	86.5	**14.3**	91.9	97.6	12.9	Neutral	✓	✓
Butenafine	8.5	2.5	18.6	86.7	**16.1**	85.4	17 nM	7.9	P/Neutral		
Hexachlorophene	8.7	0.9	0.3	**7.2**	**1.3**	**8.2**	1.6	3.9	N		
Tamoxifen	9.4	0.1	10.8	59.0	**3.0**	51.8	0.15	10.8	P	✓	✓

Table 4.4. Characterization of complex III-specific and non-specific inhibitors. Complex III-specific and non-specific inhibitors have the same colour codes of Figure 4.14 (red and blue, respectively), with thresholds for specific assays highlighted in the same colours. Thresholds for succinate:dQ, succinate:cytochrome *c* and (red.) cytochrome *c*:O_2 to identify significant inhibition in pink, green and teal, respectively. Therapeutic concentrations, pK_a values and charge at physiological pH are reported for comparison. FDALabel database search results (from chapter 3) in terms of mitochondrial-associated liver and extraliver side effects are also presented.

Drug	NADH: O_2 %	NADH: Q_{10} %	Succinate:O_2 %	NADH:O_2 IC_{50} µM	Therapeutic concentration µM	pKa	Charge at physiological pH	Mito side effects: Liver	Mito side effects: Extraliver
COMPLEX I-SPECIFIC INHIBITORS									
	< 10%	**< 10%**	**> 90%**						
Nebivolol	1.1	3.9	93.4	1.2	0.05	8.4	**P**		
Salmeterol	1.3	4.0	90.7	2.0	0.02	10.2	**P**		
Carvedilol	2.0	4.6	99.2	6.7	0.40	7.8	**P/Neutral**	✓	
Fluoxetine	1.9	5.3	100.9	6.6	1.45	8.8	**P**	✓	✓
Duloxetine	1.9	6.2	96.7	8.6	0.36	9.3	**P**	✓	✓
Iloperidone	2.6	6.3	90.9	12.0	0.02	7.7	**P/Neutral**		✓
Calcipotriene	4.0	6.7	90.9	12.7	0.1 nM	/	**Neutral**		
Propafenone	3.4	7.4	98.2	9.6	5.3	9.3	**P**	✓	✓
Ketoconazole	5.3	7.8	96.2	11.5	11.3	6.5	**Neutral**	✓	✓
Nefazodone	2.5	8.7	98.0	0.8	4.0	6.5	**Neutral**	✓	✓
Haloperidol	3.8	9.0	104.0	2.4	0.1	8.65	**P**		✓
Capsaicin	9.1	9.1	94.6	25.8	8.1 nM	10.1	**Neutral**	✓	
Aripiprazole	1.6	9.3	98.9	1.7	1.12	7.6	**P/Neutral**	✓	✓
Oxybutynin	5.7	9.4	98.5	17.0	0.04	8.0	**P/Neutral**		
Ethinyl Estradiol	9.6	9.7	91.2	12.2	1 nM	10.0	**Neutral**	✓	✓

Table 4.5. Characterization of complex I-specific inhibitors. Complex I-specific inhibitors have the same colour code of Figure 4.14, green, with thresholds for specific assays highlighted in the same colours. NADH:O_2 IC_{50}s for each drug are presented. Therapeutic concentrations, pK_a values and charge at physiological pH are reported for comparison. FDALabel database search results (from chapter 3) in terms of mitochondrial-associated liver and extraliver side effects are also presented.

4.3.3 Flavin site assays: NADH:FeCN and NADH:APAD

By plotting the results of a flavin-site assay (carried out with isolated enzyme) against the results of a Q-site assay (similarly to what was done for membranes with NADH:O_2 and succinate:O_2 assays, see Figure 4.5), four different areas can be isolated: flavin-site inhibitor and Q-site inhibitor regions are on the left hand-side of the plot (see Figure 4.15 and Figure 4.16). Given the sequential nature of the electron transfer mechanism from NADH (first) to ubiquinone (last) through complex I, no drug should appear in the bottom-right corner: in fact, if a drug inhibits the flavin site the electron transfer should be affected throughout complex I and hence detected by the NADH:dQ assay too. Hence, a drug should appear in this region because it is incompatible with the assay system. It is possible, however, that a compound could selectively bind to the reduced flavin-site and block access to FeCN.

The first attempt at this methodology was made with NADH:FeCN oxidoreduction to assess flavin-site reactivity but it turned out to be very prone to artefacts (Figure 4.15): 18 drugs exhibit substantial protein-free FeCN activity[m]. The NADH:APAD assay was chosen instead: it fails to identify as many hits compared to NADH:FeCN (on account of its much narrower vertical variability) but only 10 drugs exhibited very erratic traces[n] (labelled as "Dubious APAD activity" in Figure 4.16). This assay gives a more conservative response for both drug interaction with complex I and for identification of drugs that belong to the bottom right region: likely this is due to the hydride transfer on which the assay is based that avoids side reactions that single-electron artificial acceptors are prone to.

The horizontal and vertical lines are, again, arbitrary and were set equal to the average inhibition percentages, 28.4% for NADH:Q_{10}, 99.3% for NADH:FeCN and 98.5% for NADH:APAD: the very high mean residual activities for both APAD and FeCN indicate a poor overall reactivity of the flavin site of complex I towards drugs. This can also be gathered by the very few drugs that appear to exhibit significant flavin-site activity: these are compounds that were tested for ROS activity (see section 4.3.4).

[m] Protein-free activity in the FeCN assay is defined substantial if the raw rate is higher than 15% the normal raw rate.

[n] The APAD reaction always gives very straight traces with a R^2 value of at least 0.995. The drugs were considered to have an erratic trace when they exhibited an average R^2 of less than 0.96.

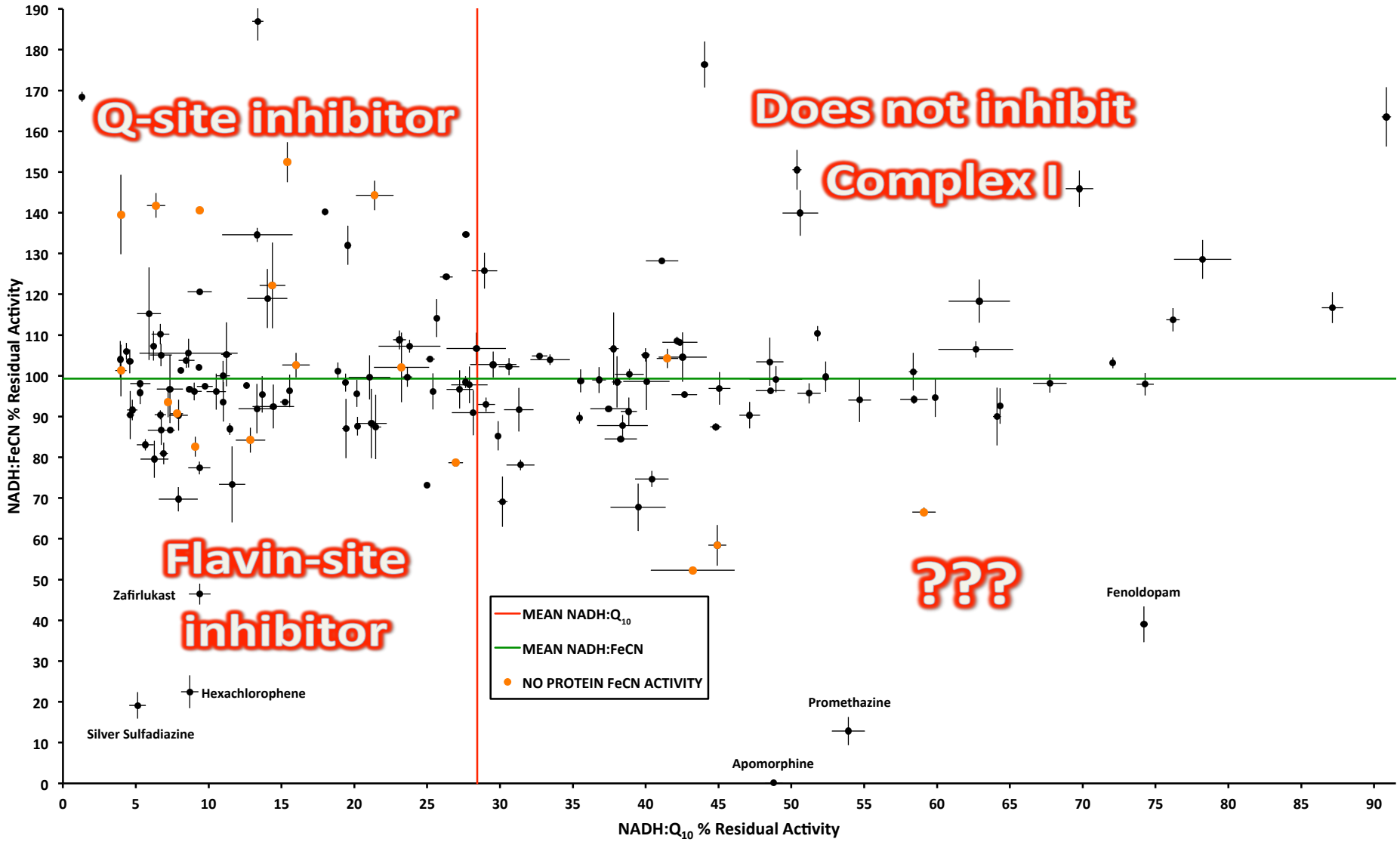

Figure 4.15. Drug binding site determination on complex I with FeCN assay. The NADH:Q_{10} and NADH:FeCN results can be conveniently combined to isolate regions where Q-site and flavin-site inhibitors should fall into. This assay, though, is very prone to artefacts: 18 drugs exhibit a very high complex I-free activity (orange points). The average residual activity in the FeCN assay is 100.2%, hence the FeCN-related flavin site reactivity is generally not affected by these drugs. Error bars are SEM of duplicates. Drugs tested at 50 µM.

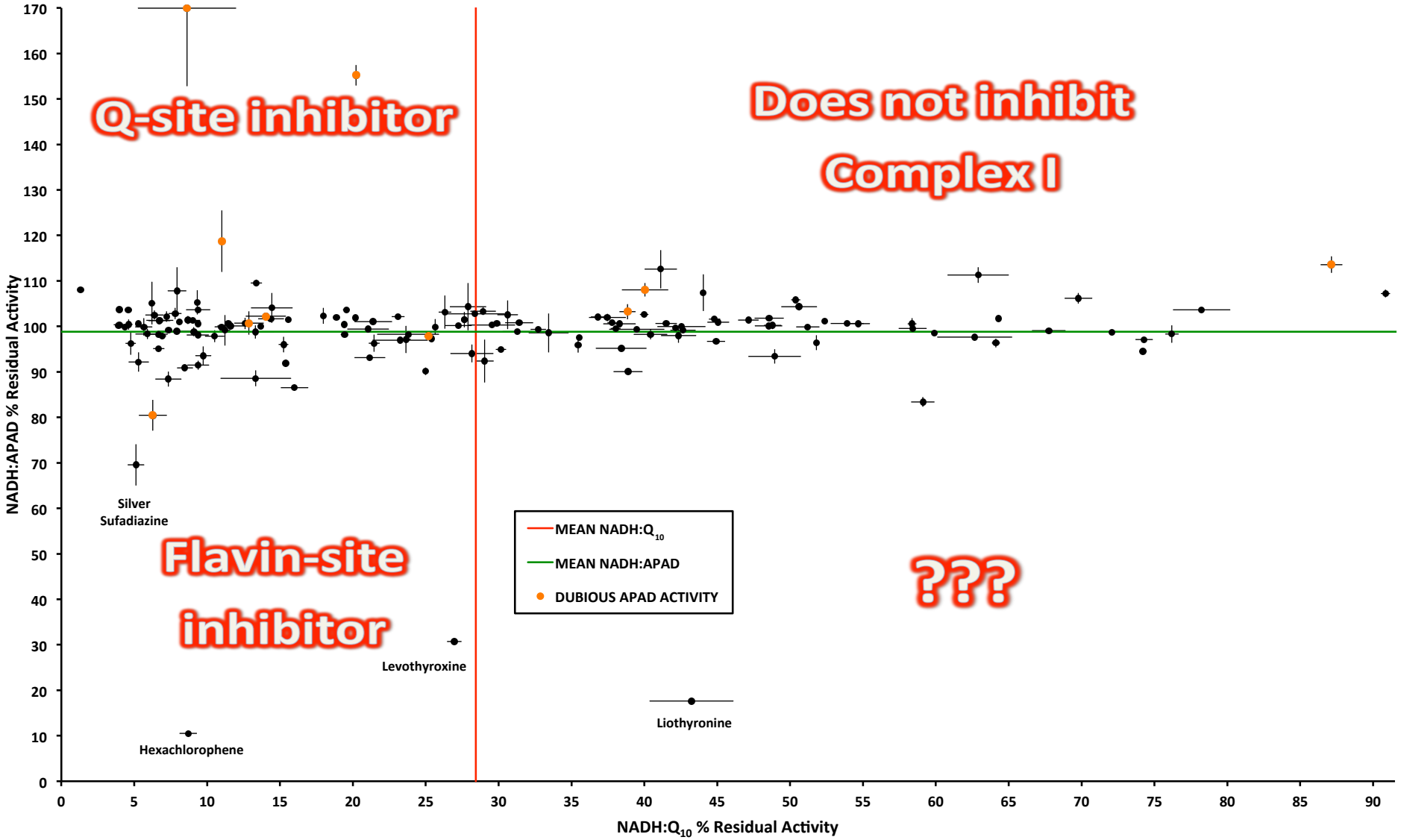

Figure 4.16. Drug binding site determination on complex I with APAD assay. The average residual activity in the NADH:APAD assay is 98.8%, thus confirming the general lack of reactivity of the drugs towards the flavin site. The artefacts detected in this assay are different than the one encountered in the FeCN one: a very erratic trace was found in 10 drugs overall (orange points). Anyway, the drugs exhibit a much lower vertical variability than in the FeCN assay. Error bars are SEM of duplicates. Drugs tested at 50 µM.

4.3.4 ROS assay

The compounds that showed the highest flavin-site inhibition (both in APAD and FeCN assays) were chosen for a ROS assay follow-up (Table 4.6). This experiment detects H_2O_2 production via peroxidase-catalysed conversion of Amplex Red to Resorufin. Any superoxide is quickly converted into H_2O_2, either chemically or enzymatically via superoxide dismutase. All of the drugs were tested for interaction with HRP to rule out artefact detection, similarly to what was done in the succinate:O_2 assay (see paragraph 4.2.3). Fenoldopam and Apomorphine are the most potent HRP inhibitors, followed by Promethazine and Liothyronine. It is assumed that the extent of HRP inhibition of the other drugs is not enough to hamper the H_2O_2 detection system. Hexachlorophene is the strongest hit but its mild HRP inhibition combined with its promiscuous activity in membranes cast serious doubts on its being a genuine inhibitor of complex I flavin-site activity, including ROS. The remaining three drugs tested are Levothyronine, Zafirlukast (both seem to be mild ROS inhibitors) and Sulfadiazine, which does not inhibit ROS production at all. It appears that these drugs prevent complex I-driven ROS formation very poorly.

DRUGS	ROS ACTIVITY	HRP ACTIVITY
	X% ROS/HRP residual activity at **Y** drug concentration (μM)	
Apomorphine	/	2.0 ± 0.1% **2**
Hexachlorophene	9.2 ± 0.1% **150**	67.8 ± 0.9% **50**
Fenoldopam	/	2.0 ± 0.0% **0.5**
Levothyroxine	85.4 ± 0.8% **100**	47.8 ± 3.9% **50**
Liothyronine	76.9 ± 3.0% **100**	62.3 ± 1.2% **0.5**
Promethazine	42.8 ± 0.7% **200**	73.7 ± 1.7% **1**
Sulfadiazine	101.9 ± 0.2% **280**	101.3 ± 0.8% **100**
Zafirlukast	61.6 ± 0.0% **100**	52.1 ± 1.6% **50**

Table 4.6. ROS assay results with the most powerful flavin-site inhibitors in the library. This small set of drugs did not exhibit a strong potency against complex I-driven ROS formation and also some of the compound inhibited HRP which the ROS assay is based on. Data are reported with SEM of triplicates.

4.4 SMPs: accounting for potential uncouplers

The majority of the compounds in the library do not inhibit the NADH:O_2 pathway and the above-mentioned mild coupling of mitochondrial membranes could be used to detect uncouplers: these drugs should therefore stimulate activity in the NADH:O_2 assay to a higher level than that of the control. The NADH:O_2 assay performed with SMPs (also in uncoupled conditions with gramicidin to rule out direct complex I activation) to better capture uncoupling properties of the drugs were unsuccessful: the 12 compounds that exhibited the highest residual activity in the NADH:O_2 initial screening (see Figure 4.2) did not produce the same results with SMPs. Similarly, the compounds that belong to the class of bisphosphonates (discussed in detail in paragraph 4.5) all share a very high NADH:O_2 activity in membranes that is not reflected in a corresponding high activity in SMPs. Figure 4.17 shows the results of the NADH:O_2 assay in SMPs and in membranes for comparison.

It is possible that these results may be explained by experimental error in the NADH:O_2 assay that is measured as overactivation of the complex I-IV pathway. An alternative explanation invokes the strong sonication process needed to make SMPs that does not happen in the preparation of mitochondrial membranes. The resulting structural differences between the two systems (*e.g.* different parts of the membrane phospholipid bilayer may be exposed to the drugs) could bring about more favourable interactions between the drug and mitochondrial membranes than with SMPs, hence explaining the different uncoupling features of the compounds in different systems. Lastly, while membranes are prepared with just one centrifugation step, SMPs require six (see chapter 2): the lack of membrane elements lost during SMP purification could play a role in the different reactivity of these compounds towards the two systems.

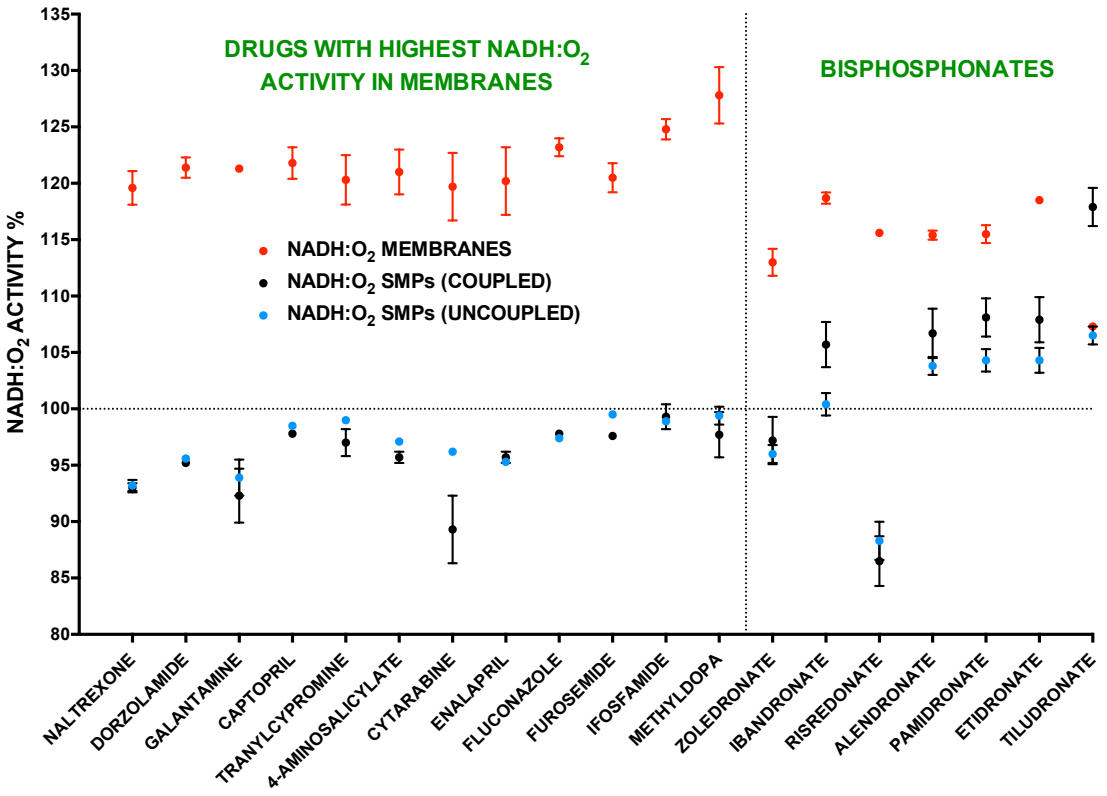

Figure 4.17. Potential uncouplers tested with SMPs. Drugs that exhibited the highest NADH:O_2 residual activity were tested in this system: none of them was capable of raising the residual activity higher than with membranes. Error bars are SEM of duplicates.

4.5 Inhibition of respiration in isolated mitochondria

The effects of complex I-specific inhibitors (see section 4.3.2) on respiration of isolated rat liver mitochondria (measured by Seahorse XF 96) were studied in order to extend the scope and pharmacological relevance of this work. The drugs were tested at 60 µM each (their IC_{50} in membranes is around 10 µM, see Table 4.5): after addition of glutamate/malate and a waiting time of 14 minutes, drugs were injected. 30 minutes later ADP was injected to stimulate respiration, followed 3 minutes later by rotenone. Figure 4.18 shows some representative OCR traces for the experiment. The results are shown in Figure 4.19 and presented as percentage of inhibition compared to control, including statistical significance (Papaverine was included in the experiment because of the data presented in chapter 3, even though it does not belong to the Enzo library, see section 4.2.4).

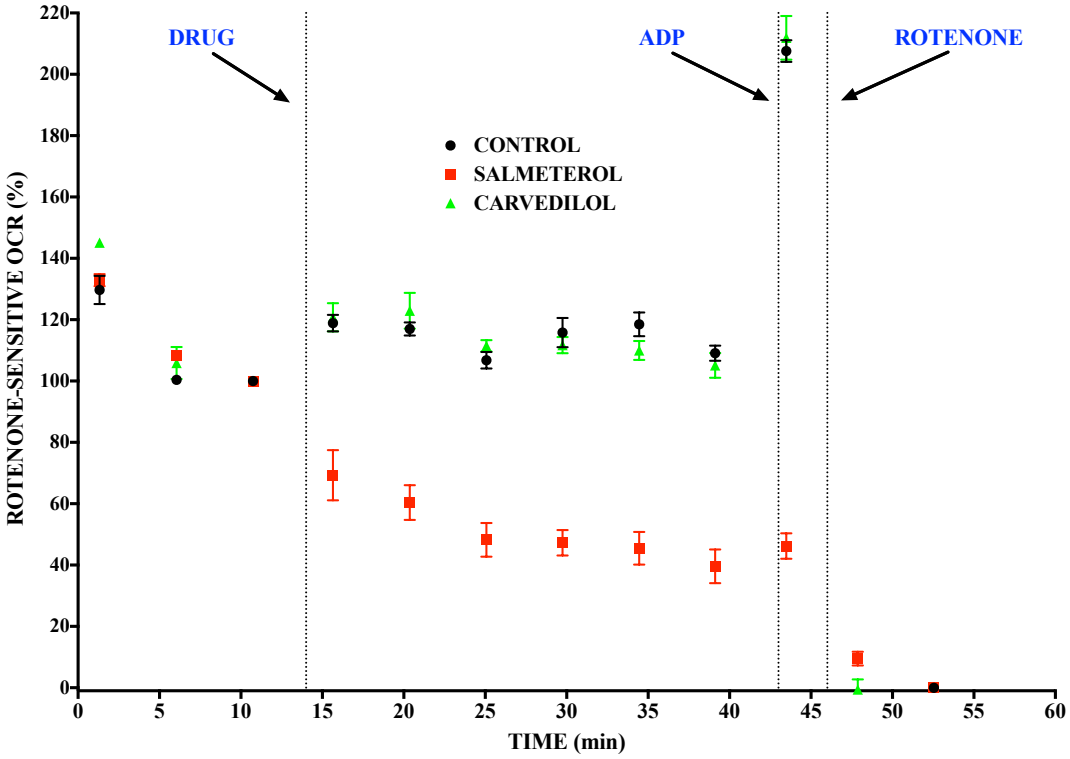

Figure 4.18. Representative OCR traces of Seahorse experiments on isolated mitochondria. The OCR percentages are normalised with respect to the last measured OCR prior to drug addition. Data show means ± SEM (n=6 for control, n=4 for Salmeterol, n=3 for Carvedilol).

Salmeterol and Papaverine are the drugs that inhibit mitochondrial respiration the most, followed by Propafenone, Ketoconazole and Nefazodone. Propafenone and Papaverine also exhibited the highest difference between inhibition of basal state and that of ADP-stimulated respiration. Remarkably, Capsaicin did not inhibit mitochondrial function in this assay but inhibited OCR and increased ECAR in HeLa cells at 75 µM; conversely, Papaverine also inhibited OCR and increased ECAR in HeLa cells at 6 µM, but it did inhibit OCR in rat liver mitochondria (see chapter 3 where both Papaverine and Capsaicin were labelled as OXPHOS inhibitors in cells). The other drugs, however, do not lower, to an appreciable degree, oxygen consumption in isolated mitochondria. It is possible that transport inside mitochondria is paramount to exert their inhibitory power and for some drugs such transport is hindered. Alternatively, accumulation processes inside mitochondria could explain their contradictory pharmacological properties. In this regard, Sgobbo *et al.*[356] found that Carvedilol caused a mild decrease of the respiration rate in H9C2 (embryonic rat heart) cells in addition to a significant complex I inhibition in cell lysates (the same

concentration of 20 μM was used for both experiments and the cells in the former experiment were incubated with Carvedilol for 24 hours before measurements were taken). A slow accumulation in mitochondria could, thus, explain why Carvedilol failed to curtail respiration in isolated liver mitochondria (see Figure 4.19): the incubation time may not have been long enough.

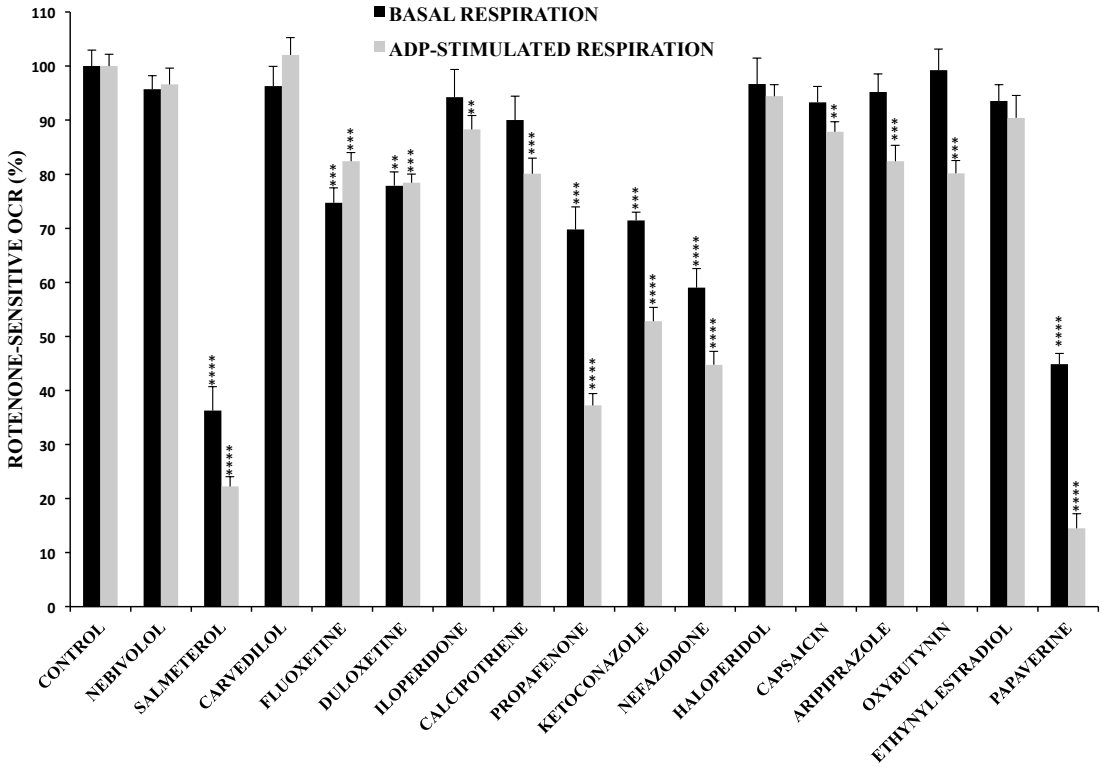

Figure 4.19. Drug inhibition of rotenone-sensitive respiration in isolated mitochondria. Complex I-specific inhibitors at 60 μM were left to interact with rat liver mitochondria (respiring on glutamate and malate) for 30 minutes (basal respiration % inhibition) before ADP was added (ADP-stimulated % inhibition). Rotenone-insensitive rates were subtracted. Statistical significance expressed as ****, $p \leq 0.0001$; ***, $p \leq 0.001$; **, $p \leq 0.01$; *, $p \leq 0.05$. Error bars are SEM (n=6 for control, n=5 for Fluoxetine, Iloperidone, Haloperidol, Aripiprazole, Oxybutynin and Papaverine, n=4 for Salmeterol, Calcipotriene, n=3 for the other drugs).

4.6 Discussion

The 789 drugs that constitute the Enzo library were screened for complex I-mediated toxicity following the methodology applied in chapter 3 and illustrated in Figure 4.1. 118 ETC inhibitors were identified from the first screening (60 specific to complex I, 12 to complex II and 46 non-specific). The former results were used in conjunction with the NADH:Q_{10} results to isolate potent complex I-, III-specific and non-specific

inhibitors (15, 3 and 15 respectively). The site of action within complex I was examined and very few compounds (if any) were found to target the flavin site. While complex I-specific inhibitors were also tested in isolated mitochondria, complex-III specific and non-specific inhibitors were assayed to further characterise their main targets within OXPHOS. Lastly, experiments with SMPs failed to identify uncouplers.

4.6.1 *In-silico* methods

The selection process that led to the choice of the Enzo drug library culminated with the generation of a "virtual" library of 1185 compounds that came from a database search according to an organ-based mitochondrially-linked side effects (see section 4.1.2). There are 25 drugs in common between the five different categories (brain, extraliver, heart, kidney and liver), 18 of which are included in the library: interestingly, only two of those inhibited the NADH:O_2 pathway enough to warrant a follow-up succinate:O_2 assay, Tretinoin (32.8% and 78.1% of residual activity in NADH:O_2 and succinate:O_2, respectively) and Amoxapine (51.3% and 98.9% of residual activity in NADH:O_2 and succinate:O_2, respectively). The other 16 drugs did not affect the NADH:O_2 pathway: this indicates that drug-induced mitochondrial dysfunction is a complex condition that cannot just be detected by assays aimed at the ETC but requires a more extensive and comprehensive treatment. On the other hand, the *in silico* method for specific complex I inhibitors determination featured in chapter 3 was validated and proved to be rather successful, considering its ease and free availability of the database source.

4.6.2 Bisphosphonates as potential uncouplers

The experiments performed with SMPs failed to validate the drugs with the highest NADH:O_2 activation as uncouplers (see section 4.4). Nonetheless, an interesting pattern emerged, concerning drugs that treat osteoporosis and similar skeletal disorders. The drug class of bisphosphonates (replacing a phosphoric acid anhydride moiety with a central P-C-P in lieu of a P-O-P which make the drugs resistant to enzymatic hydrolysis and heat[357]), all accelerate the NADH:O_2 rate to a significant degree (see heading row of Table 4.7). Interestingly, the other two drugs in the whole library that treat similar skeletal disorders (Calcitriol and Raloxifene) contain no phosphorous atoms and are both classified as complex I-specific inhibitors.

The pharmacology of bisphosphonates is based on the cluster of negative charges around the P-C-P core at physiological pH: this causes a remarkable affinity and prolonged binding to the positively charged surface of bone mineral[358]. The intensity of the negative charge depends on whether an amino group is present or not (the pK_a values of nitrogen-containing groups, especially the pyridinyl group in Risedronate, can be very close to physiological pH[359]): five pK_a values or four can be experimentally determined, with an overall negative charge of -2 or -3 respectively[360]. The residual activity in the NADH:O_2 assay, along with substituents and pK_a values associated with the previously mentioned overall charge ($pK_{a,3}$), are presented in Table 4.7 for every bisphosphonate tested.

These drugs are the only ones in the library with a P-C-P core and they all activate the NADH:O_2 pathway to a significant degree: intriguingly, the only compound in the series that does not possess a OH group as central substituent, Tiludronate, is the one that activates the pathway the least. These drugs possess at least a double negative charge at physiological pH and it is interesting that they could actually exhibit uncoupling properties not detected by SMPs: since this system is positively charged on the inside of the lumen the drugs might shuttle protons across the (inverted) IMM.

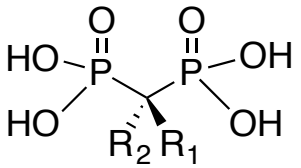

DRUG	R_1	R_2	$pK_{a,3}$	NADH:O_2 %
Alendronate	**OH**	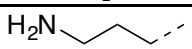	6.77[361]	115.4 ± 0.4
Ibandronate		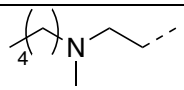	6.37[361]	118.7 ± 0.5
Pamidronate		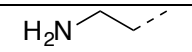	6.01[362]	115.5 ± 0.8
Etidronate		CH_3	7.03[363]	118.5 ± 0.3
Risedronate		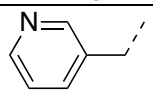	6.10[359]	115.6 ± 0.1
Zolendronate		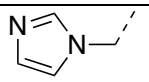	6.63[364]	113.0 ± 1.2
Tiludronate	**H**	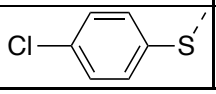	6.90[365]	107.3 ± 0.0

Table 4.7. The bisphosphonate drugs in the Enzo library. All drugs exhibit a significant activation of the NADH:O_2 pathway but their negative charge makes it unlikely to be caused by uncoupling. Error is SEM of duplicates.

4.6.3 Antifungals

Several antifungal drugs significantly inhibit the complex I pathway (with the exception of Echinocandins, Hydroxipiridones and inhibitors of fungal membrane stability and fungal mitosis, see Table 4.3) while exhibiting a heterogeneous response towards complexes II-IV. They are mostly first generation azole compounds[366], classified as imidazoles in Table 4.3. Since fungi are eukaryotic organisms and their mitochondrial respiration is basically identical to their human counterparts, it is possible that complex I inhibition contribute to the antifungal nature of imidazoles along with their primary target, lanosterol 14 α-demethylase (a key enzyme in ergosterol biosynthesis)[367].

On the other hand, the antifungals squalene epoxidase inhibitors Butenafine, Naftifine and Terbinafine, displayed in Table 4.8, share a naphthylmethylamine structural core and the ratio of their residual activity towards the NADH:dQ assay over the NADH:O_2 assay is higher than 3: this is a feature that complex III specific inhibitors should possess (see paragraph 4.3.1). Remarkably, Cinacalcet (a calcimimetic) is the only other drug in the whole Enzo library that is structurally very similar to the three antifungals and exhibits the same response towards relevant assays: high ratio of residual activity towards NADH:dQ over NADH:O_2 assays and no significant inhibition towards either complex I flavin-site or complex IV activities. Furthermore, all of these drugs are categorised as non-specific ETC inhibitors (bottom left area of Figure 4.5) and are all located below the 1:2 line in Figure 4.13: it is, therefore, likely that these compounds be specific inhibitors of complex III. A dQH_2: cytochrome *c* assay was, therefore, carried out in membranes with these 4 drugs to test their inhibitory potency towards complex III: remarkably, no inhibition was detected. Since the electron donor is dQH_2 in this assay (rather than $Q_{10}H_2$), it is possible that these drugs could block Q_{10} access to complex III and dQ, being smaller, is not affected and could gain entrance without interference[ø]. It was recently found that the mechanism of squalene epoxidase inhibition by Terbinafine involves the tert-butyl group being buried in the catalytic pocket: the naphthylmethylamine moiety then blocks one of the two entrances to the catalytic site directly while the other is blocked by conformational change upon inhibitor binding[368]. Since the other three drugs possess a

[ø] It must be pointed out that the dQH_2:cytochrome *c* assay is the least reliable of the membrane-based assays presented in this thesis, mainly because of its very high signal-to-noise ratio (the rate of the chemical reaction between the two substrates is substantial) and artefacts due to reduced dQ.

similar long hydrophobic "handle" the inhibitory mechanism towards complex III could occur in a similar fashion. Additionally, the NADH:Q_{10} assay reveals a stronger inhibition of complex I than the NADH:dQ assay: this means that the compounds should be more correctly classified as non-specific inhibitors.

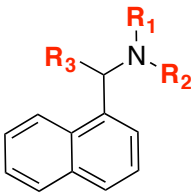

				Electron donor				Electron acceptor		
				Residual % Activity in assay						
				Succinate		Red. Cyt *c*		NADH		
R_1	R_2	R_3	Name	Ox. Cyt *c*		O_2		dQ (Q_{10})	FeCN	APAD
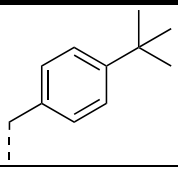	Me	H	Butenafine	17.4	18.6	85.4	2.5	72.2 (8.5)	103.8	90.9
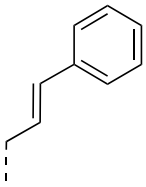	Me	H	Naftifine	15.0	26.2	106.3	0.87	73.3 (21.2)	88.3	93.1
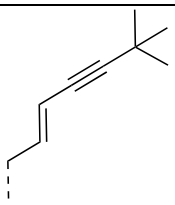	Me	H	Terbinafine	15.0	23.9	86.7	2.0	47.9 (7.3)	96.7	89.6
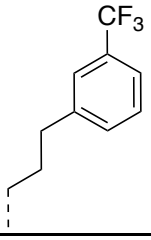	H	Me	Cinacalcet	10.0	31.8	70.1	1.3	61.5 (4.4)	106.0	99.8

Table 4.8. The four naphthylmethylamines in the Enzo library. The results of several assays in membranes and isolated enzyme are presented for Butenafine, Naftifine, Terbinafine (squalene epoxidase antifungals) and Cinacalcet (calcimimetic). Electron donors are in the green row and electron acceptors are in the red row below the green one.

4.6.4 Complex II-specific and non-specific inhibitors

Complex II specific inhibitors do not share many structural similarities at all, apart from a hexose core in Auranofin and Clindamycin, a 8 carbon-long conjugated tail in Acitretin and Tretinoin and the almost indentical compounds Levothyroxine and Liothyronine.

The drugs that deliver the highest degree of non-specific inhibition (yellow inset in Figure 4.5) are the most potent drugs of the library against ETC enzymes and some structural similarities are noteworthy. Three of those are selective estrogen receptor modulator or SERMs (Toremifene, Tamoxifen and Clomiphene) and since they are clustered very close together the minor structural differences between them should not affect their binding interactions. Also, it is possible that these drugs (especially Tamoxifen) exert a general non-specific action towards the OXPHOS enzymes that is not related to their binding sites at all but just linked to their diffusion in membranes. Testosterone Enanthate and Desogestrel share a steroideal core, yet the former (with a longer alkyl chain on the 5-membered ring as ester) exerts a more potent effect on the complex II pathway. Conversely, Desogestrel is the fourth most potent complex IV inhibitor in the library: Danazol shares the same steroideal structure but its potency is much lower (from 18.6 to 54.6% residual activity in the reduced cytochrome *c*:O_2 assay).

Hexachlorophene was used as an antimicrobial agent in soaps, detergents and cosmetics during the 1960s and 1970s and it was then discontinued upon discovering its toxicity in animal models along with severe side effects in humans (*e.g.* dermal rashes, wounds, premature labour)[369,370]. Not surprisingly, Hexachlorophene is the drug that generated significant inhibition in all of the assays and enzymes it was tested on: NADH:O_2, dQ and Q_{10}, succinate:O_2, dQ and cyt *c*, reduced cyt *c*:O_2, fumarase/malic enzyme, HRP and ROS.

4.6.5 Flavin-site and isolated mitochondria assays

Overall, the flavin site of complex I seems a very poor target for inhibition by drugs: given the wide variety of compounds tested in this work with 3 different flavin-site assays it seems reasonable to conclude a structure-based drug design for lead discovery would likely not produce fruitful results when applied to the flavin-site of complex I (or indeed to complex IV, see section 4.2.6). The ROS assay did not reveal any potent complex I-mediated ROS inhibitor but, interestingly, identified at least 4 major inhibitors of HRP (even though it must be pointed out that Apomorphine has been shown to be a potent antioxidant and free radical scavenger[371]): it is worthy of note that the almost identical Liothyronine and Levothyroxine exhibit a potency range that spans over 2 orders of magnitude towards inhibition of this enzyme.

The Seahorse experiment with isolated mitochondria identified Salmeterol (a long-acting β2-adrenoceptor agonist used to treat asthma and chronic obstructive pulmonary disease) as a potent inhibitor of mitochondrial function. Its mechanism of action and long-lasting duration reside in its lipophilicity and a long side chain: the former allows the drug to remain in the lipid cell membrane and to resist tissue washing, the latter anchors at an exosite of the target in the cell membrane permitting its continuos activation[372] (the shorter and structurally similar Salbutamol is cleared from tissues more rapidly because of its higher hydrophilicity[373]). It is, therefore, likely, that hydrophobicity could contribute to the inhibition of mitochondrial respiration by Salmeterol.

4.7 Application of the methodologies to enzymes similar to complex I: pyruvate carboxylase

Finally, it is proposed that the method followed in this work with complex I could be adapted to other enzymes that share both its position in converging metabolic pathways and its sequential mechanism of action: the enzyme pyruvate carboxylase (PC) is a potential candidate. This enzyme catalyses the first step in the gluconeogenetic pathway, is the major anaplerotic enzyme and resides in the mitochondrial matrix. The reactions catalysed by the enzyme are the following

1) $$HCO_3^- + ATP \rightleftarrows (HCO_3^-)(PO_3^{2-}) + ADP$$

$$(HCO_3^-)(PO_3^{2-}) = (CO_2^-)(O)(PO_3^{2-}) = (CO_2^-)(P_i)$$

2) $$(biotin)Enzyme + (CO_2^-)(P_i) \rightleftarrows (CO_2)(biotin)Enzyme + P_i$$

3) $$(CO_2)(biotin)Enzyme + pyruvate \rightleftarrows (biotin)Enzyme + oxaloacetate$$

The first two reactions use up one equivalent of ATP to load the biotin cofactor of PC with CO_2 (one oxygen atom from bicarbonate ends up in the phosphate ion), hence carboxyphosphate formation followed by biotin activation. The last reaction, transcarboxylation, incorporates the biotin-activated CO_2 group to pyruvate to form oxaloacetate[374]. This means that the enzyme activity can be broken down into different steps that could, in theory, be individually assayed. Furthermore, the product of the enzyme, oxaloacetate, is a metabolic crossroads between the major pathways of gluconeogenesis and TCA cycle (Figure 4.20). Such similarities with complex I thus

render PC a promising enzyme to be characterized with the methods proposed in this chapter.

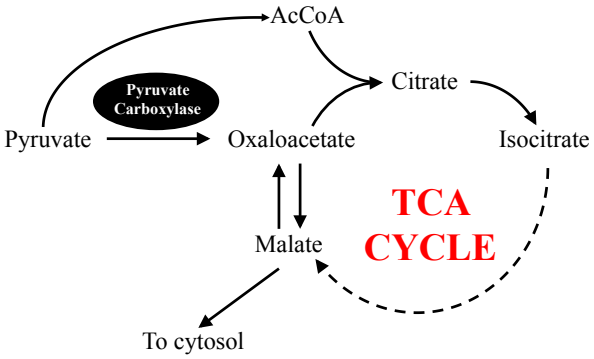

Figure 4.20 The enzyme pyruvate carboxylase in mitochondria. The enzyme location crosses, similarly to complex I, different metabolic pathways (TCA cycle and gluconeogenesis) and, as such, a similar methodology to the one applied in this chapter could be used to assess the specificity of a drug towards an enzyme.

4.8 Conclusions

Thanks to the availability of a library of approved drugs and novel methods to express the data from assays and experimental systems routinely used in our lab, key findings in the role of complex I-mediated drug-induced mitochondrial dysfunction have been revealed in this chapter. One of the main conclusions of this chapter is that many drugs included in the Enzo library affect complex I to different extents. The availability of several assays allowed to address the issue of identifying ETC drug targets and complex I appears to be the enzyme that is affected the most within OXPHOS, either in isolation or concomitantly with other respiratory chain enzymes. The drugs are structurally different between one another and this indicates how sensitive complex I is towards inhibition: this should emphasise the ubiquitous role of complex I in one of the recognised mechanisms of drug-induced mitochondrial dysfunction, impairment of mitochondrial respiration[375]. Out of 786 compounds that well reflect the variety of current approved drugs, experiments with membranes identified 118 ETC inhibitors, of which 60 are specific to complex I, 12 to complex II and 46 are non-specific. One of the major conclusions of this thesis is, therefore, that membranes are a biological system of easy preparation that could be applied to preliminary compound screening in HTS drug discovery protocols: that is why it was decided to adopt this system (and the facile NADH:O_2 assay) to perform the very first

drug screening on the whole library. Additionally, complex IV was not found to be an important target for any of the drugs. Lastly, while Salmeterol and Papaverine were identified as inhibitors of mitochondrial respiration from a broader perspective than the other assays, the results obtained in chapter 3 were validated thanks to the methodologies followed in this chapter.

Finally, results are not as clear-cut with isolated complex I assays as they are with membrane-based ones: it emerged nonetheless that the flavin site of complex I is a poor target for drugs and that the NADH:Q_{10} assay can be used in conjunction with membrane-based assays to identify complex I-, III-specific and non-specific ETC inhibitors.

4.9 Appendix - Literature therapeutic concentration for drugs included in membrane-based assays

References for 5 drugs (Halcinonide, Mestranol, Methylclothiazide, Phenoxybenzamine and Testosterone enanthate) were not available.

Alitretinoin [376], Alosetron [377], Aprepitant [378], Atomoxetine [379], Auranofin [380], Bexarotene [381], Butenafine [382], Butoconazole [383], Calcipotriene [384], Calcitriol [385], Capsaicin[257], Chlorhexidine [386], Ciclesonide [387], Cilostazol [388], Cinacalcet [389], Clindamycin Palmitate [390], Clofazimine [391], Clomiphene [392], Clotrimazole [393], Cyproheptadine [394], Danazol [395], Darifenacin [396], Dasatinib [397], Daunorubicin [398], Desogestrel[399], Desoximetasone[400], Dexchlorpheniramine[401], Dexmedetomidine[402], Dicloxacillin [403], Dicyclomine [404], Dienogest [405], Dobutamine [406], Dofetilide [407], Droperidol [408], Drospirenone [409], Dutasteride [410], Econazole [411], Efavirenz [412], Epinastine [413], Estradiol[405], Estrone[405], Ethinyl Estradiol [414], Etonogestrel [415], Exemestane [416], Ezetimibe [417], Fenofibrate[235], Fingolimod[354], Flavoxate [418], Flunisolide [419], Gefitinib [420], Guanabenz Acetate [421], Guanfacine [422], Ibutilide [423], Idarubicin [424], Imiquimod [425], Ivermectin [426], Lansoprazole [427], Latanoprost [428], Lindane[429], Liothyronine[430], Loperamide[431], Lovastatin[432], Malathion[433], Meclizine[434], Medroxyprogesterone Acetate [435], Megestrol Acetate [436], Miconazole [437], Mifepristone [438], Misoprostol [439], Mitoxantrone [440], Nabumetone [441], Naftifine [442], Nepafenac [443], Nilutamide [444], Norethindrone [445], Orlistat [446], Oxiconazole [447],

Oxybutynin[448], Palonosetron[449], Pazopanib[450], Permethrin[451], Pioglitazone[452], Posaconazole[453], Prasugrel[454], Progesterone[455], Raloxifene[456], Ranolazine[457], Salmeterol[458], Sertaconazole[459], Silver Sulfadiazine[460], Sorafenib Tosylate[461], Sunitinib Malate[462], Tamoxifen[247], Tamsulosin[463], Tazarotene[464], Terbinafine[465], Terconazole[466], Tetrabenazine[467], Tolterodine Tartrate[468], Toremifene Base[469], Travoprost[470], Tretinoin[471], Sulconazole[330], Acitretin, Albendazole, Amiodarone, Amitriptyline, Amoxapine, Apomorphine, Aripiprazole, Asenapine Maleate, Atovaquone, Azelastine, Benztropine Mesylate, Betaxolol, Bicalutamide, Biperiden, Bisoprolol Fumarate, Brompheniramine Maleate, Buspirone, Carvedilol, Celecoxib, Chloroquine Diphosphate, Chlorpromazine, Clemastine Fumarate, Clomipramine, Clopidogrel Hydrogen Sulfate , Clozapine, Colistin Sulfate, Cyclobenzaprine, Desipramine, Desloratadine, Dimenhydrinate, Disulfiram, Donepezil, Doxazosin Mesylate, Doxepin, Duloxetine, Esmolol, Felodipine, Fenoldopam Mesylate, Fluoxetine, Fluphenazine· HCl, Flutamide, Fluvoxamine Maleate, Haloperidol, Hexachlorophene, Iloperidone, Imipramine, Isotretinoin (13-Cis-Retinoic Acid), Ketoconazole, Ketotifen Fumarate, Labetalol, Levothyroxine, Loratadine, Loxapine Succinate, Maprotiline, Mefloquine, Mitotane, Montelukast, Nicardipine, Nisoldipine, Nortriptyline, Orphenadrine Citrate, Paliperidone, Paroxetine, Pentamidine Isethionate, Perphenazine, Pimozide, Promethazine, Propafenone, Propranolol, Protriptyline, Pyrimethamine, Quetiapine Fumarate, Risperidone, Rosiglitazone, Saquinavir Mesylate, Sertraline, Simvastatin, Thioridazine, Ticlopidine, Trazodone, Trifluoperazine, Trimipramine Maleate, Verapamil, Zafirlukast, Ziprasidone[255], Amlodipine, Cisplatin, Granisetron, Itraconazole, Mycophenolate Mofetil, Nebivolol, Nefazodone[472].

4.10 Appendix - Literature pK_a values for drugs included in the membrane-based assays

Aripiprazole[473], Atovaquone[474], Butenafine[475], Butoconazole[476], Calcipotriene[477], Capsaicin[478], Carvedilol[473], Cinacalcet[479], Clotrimazole, Duloxetine[473], Econazole[480], Ethinyl Estradiol[481], Fenofibrate[482], Fenoldopam[483], Fingolimod[484], Fluoxetine[485], Haloperidol[251], Hexachlorophene[481], Iloperidone [486] , Ketoconazole, Meclizine, Miconazole[473], Nebivolol [487] , Nefazodone[244], Oxybutynin [488] , Papaverine [489] ,

Propafenone[481], Salmeterol[490], Silver Sulfadiazine[481], Sorafenib[491], Sulconazole[492], Tamoxifen[248], Terbinafine[481], Trifluoperazine[229].

4.11 Appendix - Literature charge at physiological pH

Aripiprazole[473], Atovaquone [493], Butenafine[475], Butoconazole[476], Calcipotriene[477], Capsaicin[478], Carvedilol[246], Cinacalcet[479], Clotrimazole[473], Duloxetine[473], Ethynyl Estradiol[481], Fenoldopam[483], Fingolimod[484], Fluoxetine[485], Haloperidol[252], Hexachlorophene[481], Iloperidone[486], Ketoconazole[473], Meclizine[473], Miconazole[473], Nebivolol[494], Nefazodone[244], Oxybutynin[488], Propafenone[481], Salmeterol[490], Silver Sulfadiazine[481], Sorafenib[491], Tamoxifen[248], Terbinafine[481], Trifluoperazine[256].

5 SAR studies on derivatives of Rotenone and Deguelin as potential anticancer agents

5.1 Introduction

Rotenone is an isoflavonoid natural compound extracted with organic solvents from plants of the Leguminosae family (*e.g. Lonchocarpus*, *Derris*, *Tephrosia*) in the form of cubé resin[495]. It is a canonical inhibitor of complex I that is routinely used as an experimental tool to selectively block electron transfer within the respiratory chain in cells and isolated systems from numerous different species; it has also been reported to induce cellular metabolic dysfunction, resulting in symptoms that resemble Parkinson's disease (PD), Leber's hereditary optic neuropathy (LHON) and metabolic retinal dysfunction in mice and rats[496]. Rotenone was used as an agricultural insecticide to control acari, trips and aphids for many years, due to its short persistence in the environment and safety towards nontarget organisms[497]; today it is mostly used in fish management strategies to eliminate undesirable populations[498]. Rotenone is classified as moderately hazardous by the WHO, but there are only a few reports on toxicity in humans[499]: its toxicity is associated with augmented ROS production, decline in intracellular ATP levels and (given its high lipophilicity and subsequent ability to cross the blood brain barrier) accumulation in the brain, ultimately inducing neuronal cell death[500]. Recently, rotenone has also been used in pigs towards the development of an *in vivo* large animal model for mimicking complex I-driven metabolic crisis and evaluating pharmaceutical interventions[501]. However, in-depth SAR studies on rotenone and its analogues (rotenoids) are scarce. This chapter describes a collaboration with the Chemistry Department at Cambridge University to bridge this gap: a library of 66 rotenoids was synthesised by Dr. David Russell and the analysis of their potency on mammalian complex I is presented here.

5.1.1 Aims

The aims of this work are to

- improve understanding of how rotenone analogs bind to complex I
- identify structural determinants of binding within the rotenone core

- identify bioactive hydroxylated rotenoids that are less neurotoxic than their lipophilic counterparts due to their inability to cross the blood brain barrier, but that still retain their potency on complex I, for development as anticancer compounds.

5.1.2 The rotenone family

The major ingredients of cubé resin are rotenone, deguelin, rotenolone and tephrosin, the four rotenone natural products[495,502]. Structurally, rotenoids are characterised by a chromano-chromanone unit (a fused four-ring system, rings A-D) in addition to a fifth ring (E-) whose size differentiates rotenone (5-membered) from deguelin (6-membered)[503]. Figure 5.1 shows the above-mentioned four major rotenoids and their usual ring labelling system[504].

A commonly underappreciated aspect of rotenoids is their three-dimensional structure: two-dimensional representations of rotenone fail to effectively convey its wedge-like shape, shown in the X-ray crystal structure[505] in Figure 5.1. In this regard, an important structural aspect of rotenoids is that their B-C rings collectively form a *cis*-decalin system, whereby one 6-membered ring joins another one so that it is axial at one point of attachment and equatorial at the other[506]. Even though *cis*-decalin systems can undergo ring inversion, steric hindrance may prevent it in many rotenoids.

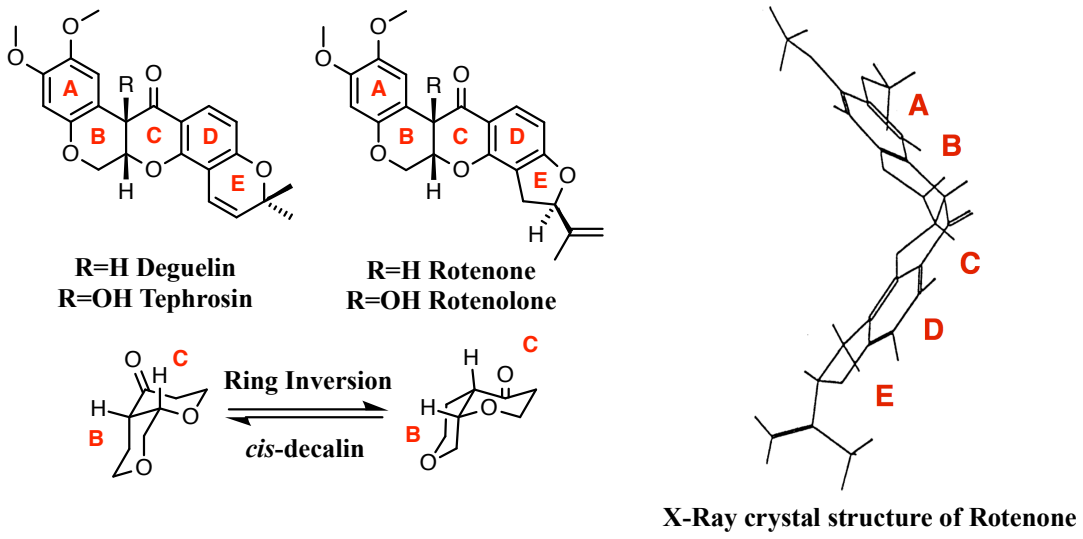

Figure 5.1. 2D and 3D features of the rotenoid skeleton. The conventional 2D representations of rotenone and deguelin (with their ring labelling system) do not effectively convey their three-dimensional shape. Focussing on the B-C ring junction (a *cis*-decalin) illustrates this point. The X-ray crystal structure of rotenone reveals its 3D geometry.

5.1.3 Rotenoids as anticancer agents

Several studies have described the different biochemical mechanisms underlying the *in vitro* anticancer activity of rotenone and deguelin. Casida[507,508] recognised that the *in vitro* activity of rotenoids against complex I correlates with, and is followed by, a decrease in activity of ornithine decarboxylase, an enzyme involved in polyamine biosynthesis that is upregulated in neoplastic transformation[509]. A study by Chiaradonna and co-workers showed that specific complex I inhibitors, such as rotenone, piericidin A and capsaicin (used at low concentrations not harmful to normal cells), induced cell death in hyperglycolytic cancer cells whose respiration was raised via glucose depletion[510]. This study is an example of how mitochondrial reactivation could be a strategy in cancer therapeutics[511].

In addition to the effects of rotenone on complex I, deguelin and two of its analogues, SH-1242 and L80, have been found to bind to the ATP-binding pocket of heat shock protein Hsp90, a molecular chaperone that contributes to the maturation of several oncogenic proteins, thus disrupting its function[512,513]. Deguelin was also shown to be effective at reducing proliferation in two prostate cancer cell lines *in vitro*[514]; it also appeared to be more strongly active against the more malignant cells tested in the study (possibly due to their increased proliferation rates), thus making rotenoids a particularly promising family of compounds towards this type of cancer[515].

5.1.4 Rotenone as a complex I inhibitor and its putative binding site

Rotenone is used experimentally to selectively inhibit complex I in many different systems, but some species are known to possess an affinity for rotenone much lower than that of the mammalian enzyme. For example, complex I from *Trypanosoma brucei*[516], *Solanum tuberosum* (potato tuber) and *Escherichia coli*[517] exhibit IC_{50} values for rotenone of about 10 μM, while the IC_{50} for the bovine enzyme is about 8 nM (see section 5.3.1).

The binding site of rotenone in complex I is yet to be identified, but several lines of evidence point to its approximate location. Experiments by Earley used tritiated radiolabelled rotenoid-based probes to covalently bind rotenone to its binding site in bovine complex I by incubation in the dark followed by photolysis: it was recognised that rotenoids could photolabel their binding site easily on account of their

benzoketone moiety in rings C and D becoming a ketyl radical upon UV irradiation. In the first experiment[518] a tritiated arylazidoamorphigenin probe (an analogue of rotenone in which the azido moiety becomes a reactive nitrene upon UV irradiation, see Figure 5.2, left) was found to react non-specifically to several complex I subunits in the membrane domain. The non-specificity was ascribed to the hydrophobicity of the probes, and so tritiated dihydrorotenone was tested (see Figure 5.2, right): this turned out to be a superior probe because of its greater affinity for complex I[519]. The hydrophobic domain subunit ND1 was identified in both experiments as the major site of labelling.

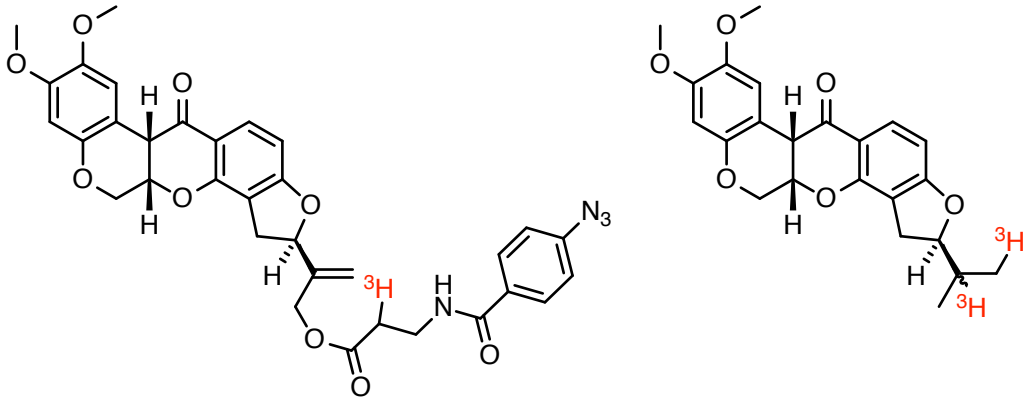

Arylazidoamorphigenin **Dihydrorotenone**

Figure 5.2. The radiolabelled probes used by Early and co-workers. The arylazidoamorphigenin probe (left) was replaced with a dihydrorotenone probe (right) because of its stronger binding to complex I. Tritiated hydrogens are shown in red.

Later, Brandt's group studied the relationships between the binding sites of several canonical inhibitors of complex I: rotenone, piericidin A and capsaicin. Direct competition binding assays suggested the existence of a common binding domain with partially overlapping sites for all the inhibitors, and the idea of a large ubiquinone binding pocket that could include such a domain was put forward[520]. The idea of a large ubiquinone catalytic site spacious enough for rotenoids to bind was also put forward by Miyoshi and co-workers, even though it was also concluded that the binding sites of ubiquinone and rotenone are different within the cavity[521]. Site-directed mutagenesis studies then indicated that the inhibitor binding site is formed by the 49-kDa and PSST subunits, and identified key residues lining the site that, when mutated, may lead to rotenone resistance[522]. Interestingly, the affinity of rotenone to complex I from *Yarrowia lipolytica* is lower than in the mammalian enzyme: the

S192T mutation in the 49-kDa subunit of complex I from the former species (to make the residue the same as the bovine enzyme) led to a dramatic rise in sensitivity to rotenone (the IC_{50} values were about 160, 260 and 540 nM for bovine heart mitochondria, S192T mutation and parental strain, respectively), in addition to a slight reduction (about 20%) in ubiquinone reductase activity[523]. Figure 5.3 shows that this residue is located close to the ubiquinone binding site and proximal to the ND1 subunit in the bovine enzyme.

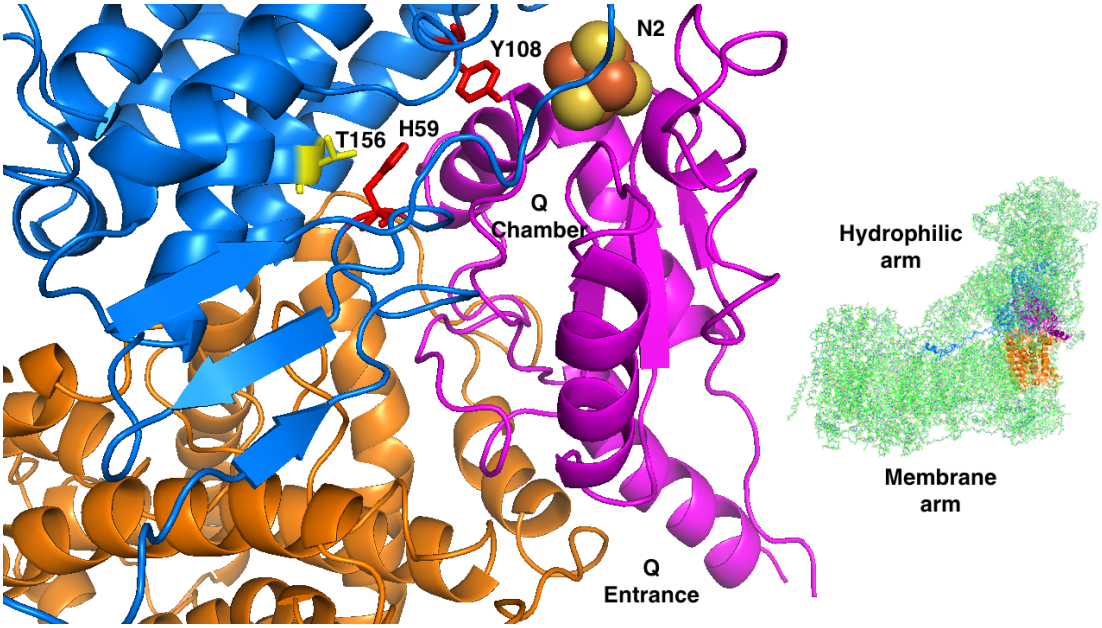

Figure 5.3. Complex I quinone binding sites in the mammalian enzyme. Complex I from *Bos taurus*, colour code 49 kDa (blue), PSST (magenta) and ND1 (orange), T156 residue (corresponding to S192 in *Yarrowia*) highlighted in yellow; Y144 and H59, key residues for ubiquinone binding highlighted in red, are adjacent to the binding site of the ubiquinone head group. Original structure from Hirst[86].

Casida and co-workers also showed that the binding site for a photoaffinity ligand based on pyridaben, a specific complex I inhibitor, involved the PSST subunit in different systems (bovine and bacterial) and that rotenone binds to the same (or to a closely coupled) site[524]. Their work was later used as accessory evidence by Dupuis and co-workers, who localised the rotenone binding site to the interface between the 49 kDa and PSST subunits via mutations on the 49 kDa subunit C-terminus in *Rhodobacter capsulatus*[525].

Since the main contact area of the 49-kDa and PSST subunits is the matrix surface of ND1[526], the results of Earley's, Brandt's, Casida's and Dupuis' above-mentioned experiments are consistent and combining them indicates that the rotenone binding

site in mitochondrial complex I is probably located at the junction between the 49-kDa, PSST and ND1 subunits.

5.1.5 SAR analyses of rotenoids in the literature

Several SAR studies have shed light on some of the relationships between structural features of rotenone and deguelin and their effect on complex I. The SAR studies on rotenoids by Ueno and Miyoshi focussed on two isomers of *epi*-rotenone[521] and 17 rotenoids[517], respectively (see Figure 5.4, left). The former study found that *epi*-rotenone was tenfold less active than rotenone (see section 5.3.1 for *epi*-rotenone results in this work); the latter study included the striking finding that the rotenoid obtained by replacing a benzyloxy group in lieu of the E-ring (in order to allow for nine subsequent convenient modifications of the A-ring) was equipotent with rotenone. Bovine heart SMPs was used in both studies but since the electron acceptor was pentylubiquinone the physiological relevance was limited. Another study by Fang and Casida[527] examined 29 rotenoids (19 of which were variants of deguelin) extracted from cubé resin, and ranked them by their potency against bovine complex I and by their anticancer activity as reflected by inhibition of ornithine decarboxylase (see section 5.1.3) and cytotoxicity in mouse and human cancer cells: the four major constituents of cubé resin (see Figure 5.1) were found to account for most of the biological activity reported in the study. A later work by Nicolaou and Casida[528] featured a combinatorial library of over 100 benzopyran-based compounds (equivalent to the E- and D-ring core of deguelin) tested in bovine heart SMPs and 6 different cancer cell lines: the 3D lowest energy conformation of the two leads (obtained via molecular modelling) resembled the configuration of deguelin and thus explained their potency (see Figure 5.4, right). They also found that introduction of polar groups in the corresponding E-ring of deguelin was not well tolerated.

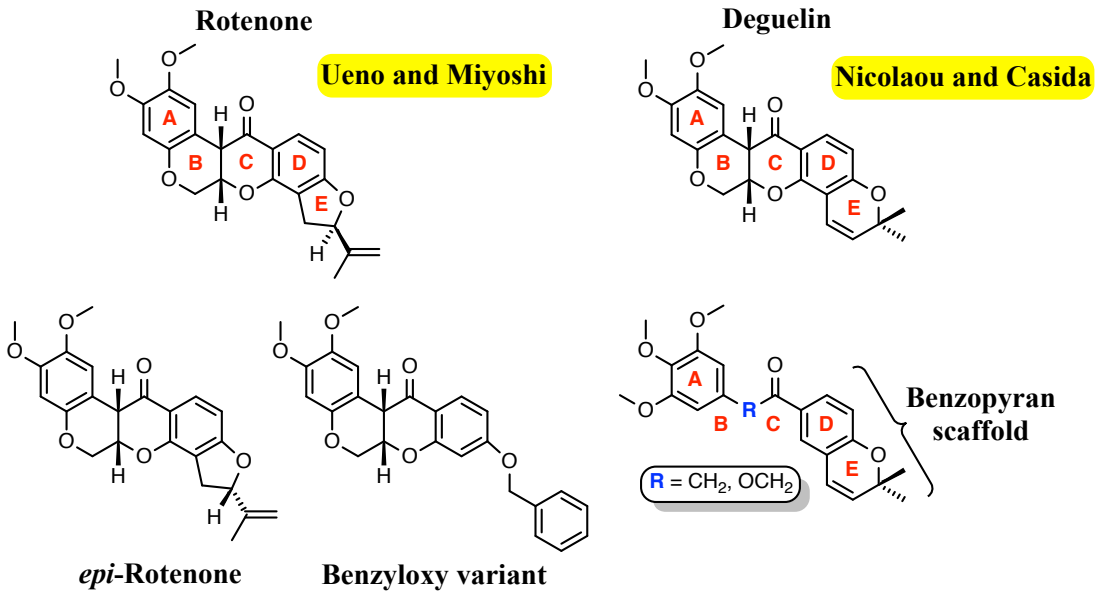

Figure 5.4. The structures of key rotenoids in SAR studies. For Ueno and Miyoshi structural changes (left) involved the E-ring of rotenone. For Nicolaou and Casida (right) extension of a benzopyran core was similar to deguelin.

5.2 The rotenoids SAR analysis

5.2.1 Description of the library

The therapeutic relevance behind the synthesis of the rotenone analogues described here was to obtain hydroxylated species that, whilst keeping their potency towards complex I, were less neurotoxic (*i.e.* less capable of crossing the blood brain barrier). The rotenoids that constitute the library used here thus possess hydroxyl groups installed at different locations across the rotenone skeleton, alterations of the E-ring (*e.g.* different stereochemistry at the junction carbon and ring opening), deoxygenations and stereochemical flattening. Lastly, a few halogenated rotenoids were included in the analysis for their potential use in structural studies. Figure 5.5 shows the areas of rotenone that were modified to construct the library.

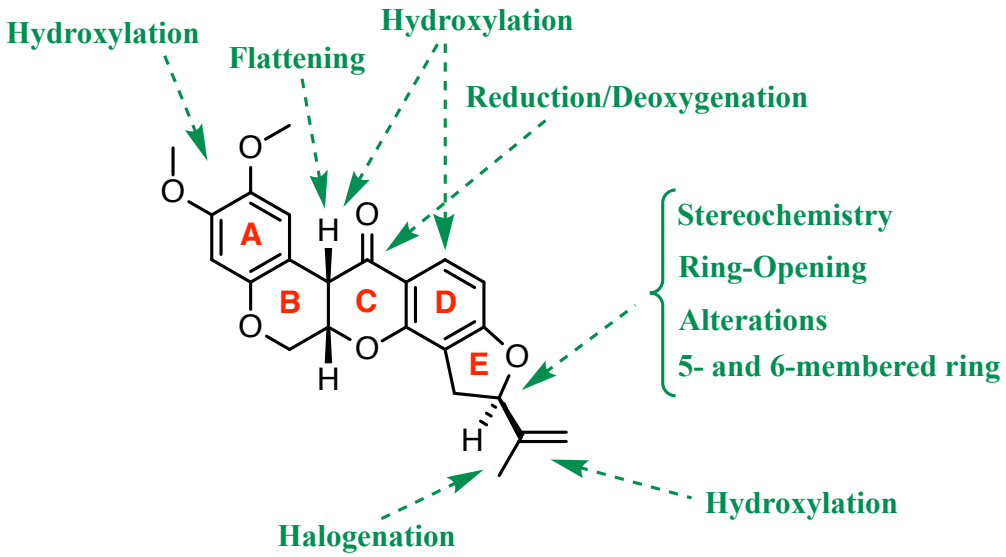

Figure 5.5. Overview of the rotenoids library. The types of modifications and their locations across the rotenone molecule are shown to summarise the library.

Some of the rotenone derivatives were tested as a mixture of diastereomers because it was not possible to separate them (every structure that includes a wavy bond in Table 5.2, Figure 5.11 and Figure 5.20, see later).

5.2.2 Measurement of complex I IC_{50} values for the rotenoid library

Membranes were used for testing the potency of rotenoids. Since the IC_{50} of rotenone is about 8 nM, it was decided to only provide an IC_{50} estimation of rotenoids whose IC_{50} values were over 2 µM: at that point their potency is so low compared to the original rotenone core that any SAR conclusions are of minor importance. For the same reason, any rotenoid whose IC_{50} is higher than 20 µM is considered inactive. Figure 5.6 shows examples of data from weak-binding rotenoids (µM-range and hundreds of µM-range IC_{50} values, second and third rows, respectively) and strong-binding rotenoids (first and last rows, nM-range IC_{50} values), for both specific activity and IC_{50} determination plots.

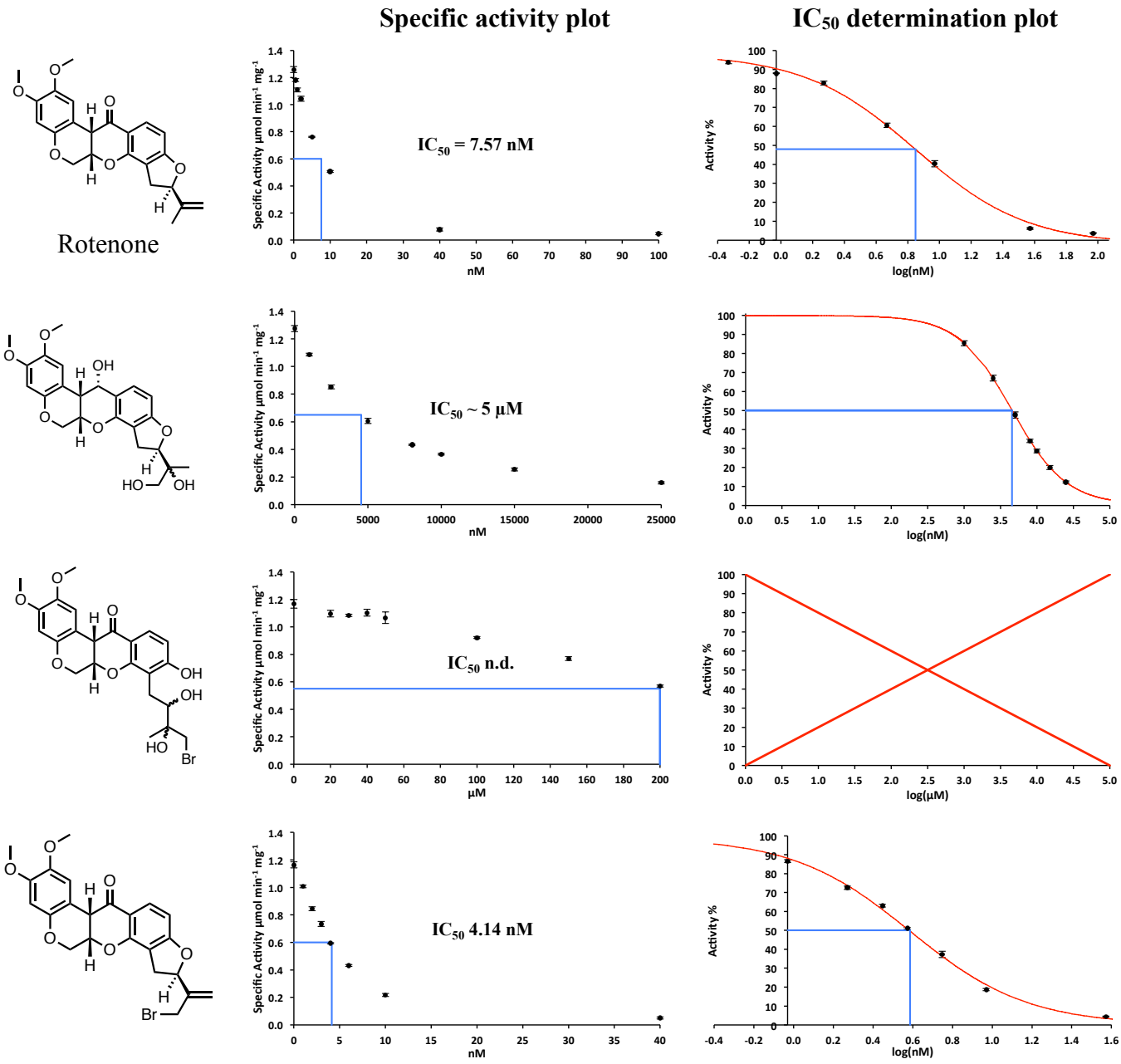

Figure 5.6. Typical procedure for IC_{50} determination. The NADH:O_2 specific activity plot (central panel) and the corresponding logarithmic dose-response curve (right) are shown for selected rotenoids. Error bars are SEM of triplicates.

5.2.3 Summary of IC_{50} results

IC_{50} values (with 95% confidence intervals), Hill coefficients and clogP values (calculated using MarvinSketch Version 16.5.2.0 Consensus Model by ChemAxon, MA[529]) are presented in Table 5.1 for all the rotenoids studied. Rotenoids that share common structural features will be described in the sections indicated in Table 5.1 in the "Paragraph" column (grouped in alternating shading).

Structure	IC_{50} nM 95% C.I.	HILL	clogP	Structure	IC_{50} nM 95% C.I.	HILL	clogP	Paragraph
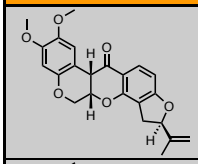	**7.57** 6.8-8.43	1.24	3.32	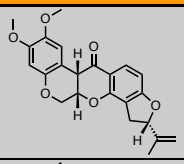	**20.5** 17.8-23.7	1.12	3.32	**5.3.1**
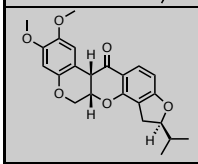	**8.78** 7.57-10.2	1.11	3.59	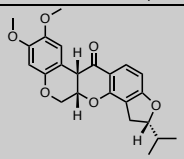	**16.4** 14.1-19	1.16	3.59	**5.3.1**
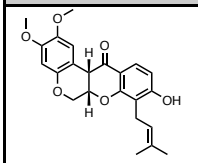	**1024** 956-1097	1.26	3.83	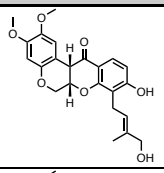	Inactive	/	2.55	**5.3.2**
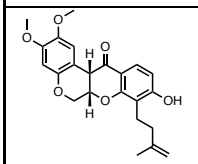	**678** 551-835	1.06	3.89	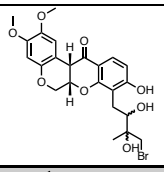	Inactive	/	2.18	**5.3.2**
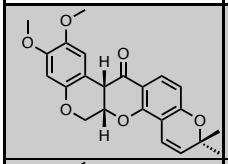	**11.5** 10.3-12.9	1.18	3.3	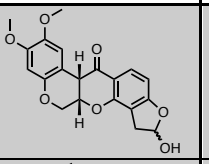	~4 µM	/	1.69	**5.3.3**
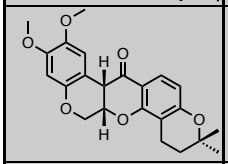	**22.3** 17.8-28	1.04	3.43	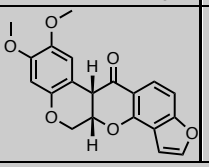	**68.4** 60.2-77.8	1.18	2.56	**5.3.3**
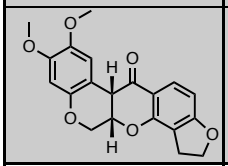	**91.7** 83.8-100	1.36	2.29					**5.3.3**
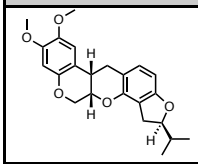	**5.79** 5.23-6.43	1.33	4.4	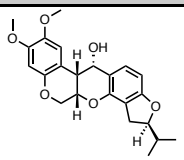	**12.7** 11.5-14	1.07	3.21	**5.3.4**
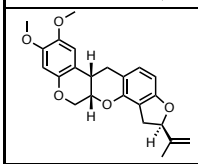	**5.04** 4.44-5.72	1.62	4.13	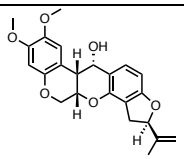	**10.6** 8.57-13	1.03	2.94	**5.3.4**
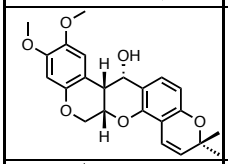	**12.2** 11.4-13.2	1.24	2.93	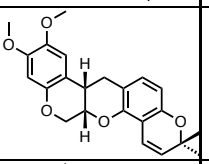	**7.71** 7.03-8.47	1.14	4.11	**5.3.4**
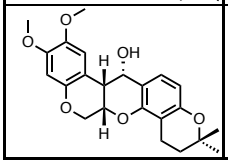	**66.2** 58.9-74.2	0.94	3.05	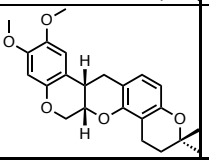	**30.0** 27.4-32.9	1.03	4.24	**5.3.4**

Structure	IC_{50} nM 95% C.I.	HILL	clogP	Structure	IC_{50} nM 95% C.I.	HILL	clogP	Paragraph
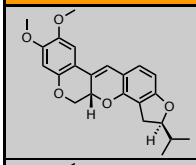	~19 µM	/	4.29	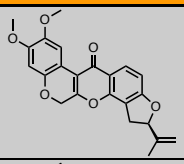	Inactive	/	3.45	**5.3.5**
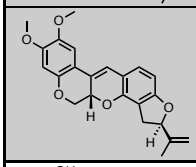	~4 µM	/	4.02	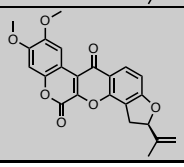	Inactive	/	3.21	**5.3.5**
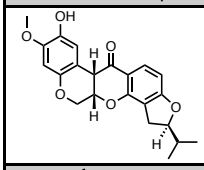	**30.5** 28.1-33.2	0.93	3.44	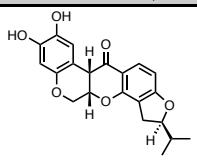	**202** 175-232	1.14	3.3	**5.3.6**
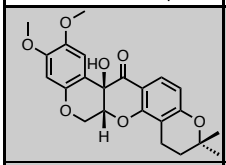	**156** 138-177	1.24	2.84	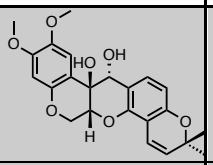	**125** 109-143	1.05	2.27	**5.3.7**
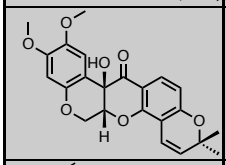	**83.5** 71.7-97.4	1.00	2.71	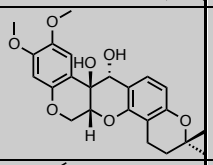	**446** 286-695	0.78	2.39	**5.3.7**
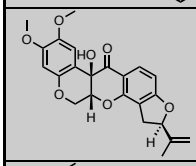	**132** 116-150	1.44	2.73	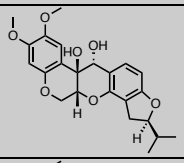	**84.9** 81.5-88.5	1.20	2.56	**5.3.7**
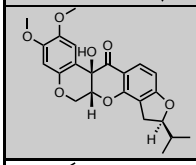	**152** 136-171	1.40	3	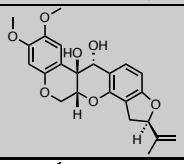	**135** 111-163	1.18	2.29	**5.3.7**
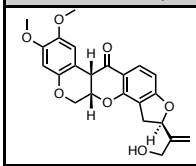	**131** 119-144	1.37	2.04	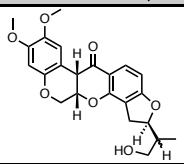	**237** 206-273	1.35	2.19	**5.3.8**
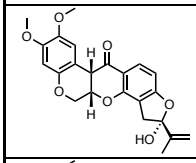	~2 µM	1.25	2.9	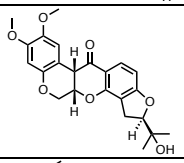	**626** 476-822	1.35	2.35	**5.3.8**
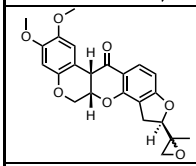	**58.1** 53-63.7	1.11	2.47	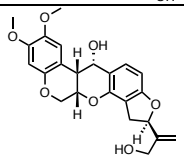	**486** 422-559	1.19	1.66	**5.3.8**
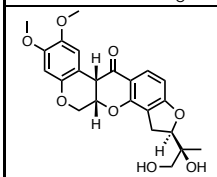	~4 µM	/	1.31	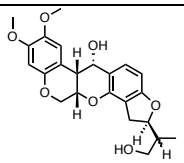	**503** 391-648	1.04	1.82	**5.3.8**
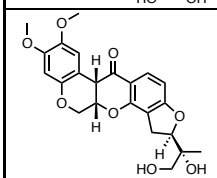	~2 µM	/	1.31	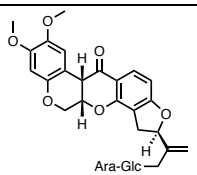	Inactive	/	-0.87	**5.3.8**

Structure	IC_{50} nM 95% C.I.	HILL	clogP	Structure	IC_{50} nM 95% C.I.	HILL	clogP	Paragraph
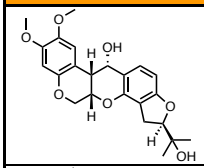	**853** 647-1130	0.94	1.97	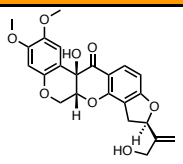	~6 µM	/	1.45	**5.3.8**
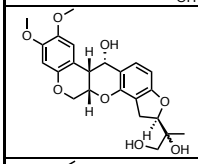	~5 µM	/	0.93	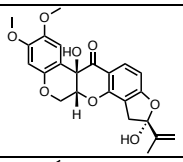	Inactive	/	2.31	**5.3.8**
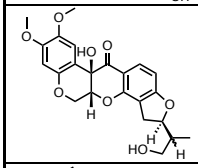	~3 µM	/	1.6	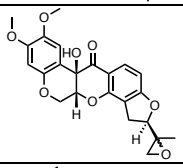	~6 µM	/	1.88	**5.3.8**
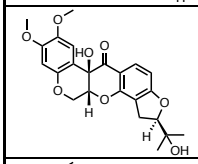	~16 µM	/	1.76	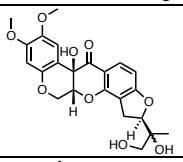	Inactive	/	0.71	**5.3.8**
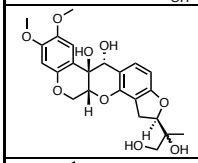	Inactive	/	0.27	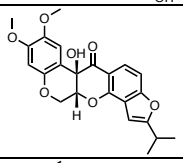	**209** 185-237	1.03	3.06	**5.3.8**
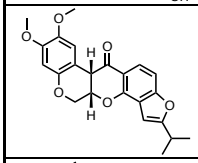	**8.94** 8.34-9.57	1.41	3.65	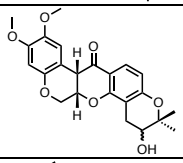	**783** 660-928	1.09	2.35	**5.3.8**
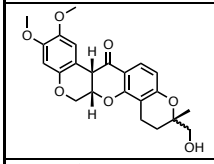	**172** 148-200	1.21	2.38	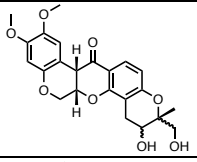	~8 µM	/	1.31	**5.3.8**
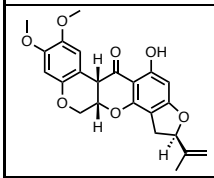	**739** 691-791	1.15	3.67	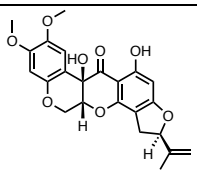	**406** 346-476	1.49	3.08	**5.3.8**
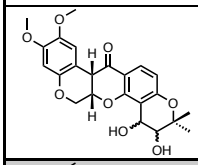	~6 µM	/	1.43					**5.3.8**
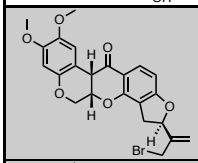	**4.14** 3.86-4.45	1.47	3.58	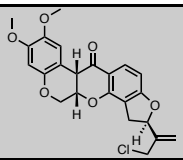	**6.00** 4.86-7.41	1.07	3.39	**5.3.9**
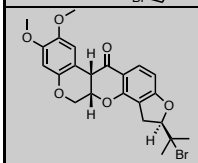	**48.5** 39.9-59.1	1.54	3.89	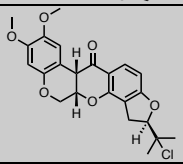	**18.9** 15.1-23.8	1.05	3.71	**5.3.9**

Table 5.1. Results of the SAR study on the rotenoid library. IC_{50} values (in nM unless otherwise specified) with 95% confidence intervals, Hill coefficients and clogP values are presented, as well as the paragraphs (alternating grey and white colours) where the compounds will be discussed in detail. Ara, arabinose; Glu, glucose.

The class of rotenoids that exhibits the tightest binding is the halogenated class, with the lowest IC_{50} in the series of 4.1 nM (see penultimate row in Table 5.1 and section 5.3.9). Even though the IC_{50} value is very low (and associated with an apparent Hill coefficient of 1.47) it is not near the stoichiometric inhibition threshold that would be detected by a very high Hill coefficient. In mitochondrial membranes approximately 10% of the protein present is complex I[159], so its concentration in the NADH:O_2 assay was about 1.5 nM. As a comparison, two species with a lower IC_{50} detected with the same assay are fenazaquin (1.69 nM, apparent Hill coefficient of 1.41) and pyridaben (1.73 nM, apparent Hill coefficient of 1.58).

The IC_{50} values reported in Table 5.1 were calculated with no constraints on the Hill coefficient: when this parameter deviates from (an ideal value of) unity, it can be diagnostic of some specific physical properties. High values (above 1.5, indicating a steep dose-response curve), may represent multisite binding or cooperativity, phase transitions (*e.g.* colloid formation or inhibitor precipitation) or (as noted above) very tight, stoichiometric inhibition[207]. The magnitude of the Hill coefficient is not an issue in this work, for the following reasons:

- It is assumed that any inhibition observed comes exclusively from complex I and not from complex III and IV, since the rotenoid core is maintained throughout the compound series and rotenone is a specific complex I inhibitor.
- The Hill coefficients (shown in Table 5.1) ranged from 0.78 to 1.62 so they do not consistently indicate a substantial cooperative behaviour.
- Solubility issues were not encountered at any rotenoid concentration used in the assays (no turbidity was observed nor were the well pathlength readings abnormally low).

Finally, to make sure that the different Hill slopes did not affect the reliability of the IC_{50} values, the latter were also calculated by constraining the Hill slope to -1 and the correlation coefficient between the two sets of IC_{50} values (unconstrained vs constrained Hill slope) was 0.99: the correlation between the same sets of data in logarithmic form is 1, as shown in Figure 5.7.

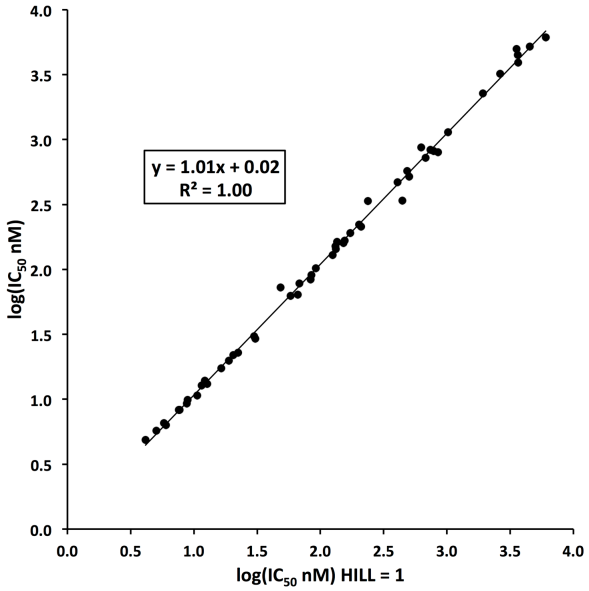

Figure 5.7. Effect of constraining the Hill coefficient to 1 on determined IC_{50} values. The plot shows that when IC_{50} values from the rotenoid library are calculated by constraining the Hill coefficient to -1 the change is negligible. A linear fit of the data with related equation and R^2 values are shown.

5.2.4 Correlation between IC_{50} and hydrophobicity

The rotenoids in the library exhibit a wide hydrophobicity range (quantified by their clogP values) and can be classified according to the number and location of additional hydroxyl groups compared to rotenone. Figure 5.8 shows how these hydroxylations correlate with inhibitory potency. The most lipophilic species are the C-ring deoxygenated rotenoids (see section 5.3.4 and 5.3.5): their clogP values are all above 4 and greater than their corresponding oxygenated species by at least one unit.

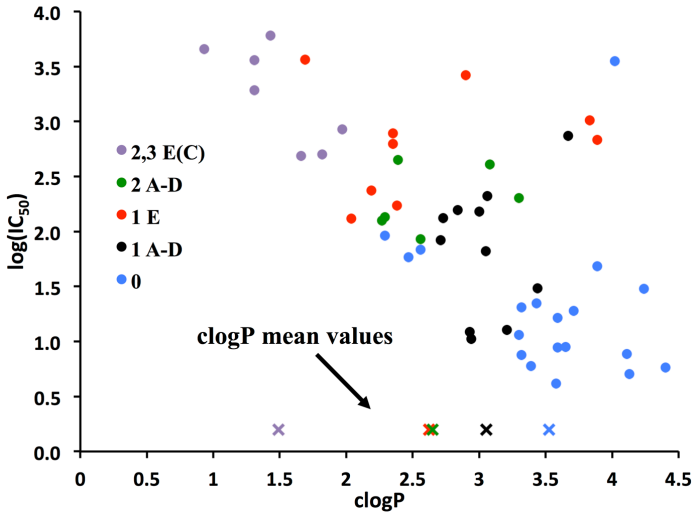

Figure 5.8. Relationship between hydrophobicity and inhibitory potency for rotenoids. The number indicates how many hydroxyl groups are included in each rotenoids of that class, the letter indicates which ring(s) the hydroxyl is attached to (the category of two or three hydroxylations at the E-ring includes 4 rotenoids hydroxylated at the C ring too). The plot shows how the hydrophobicity of rotenoids (expressed by their clogP values) correlates with the number and location (rotenoid ring attached to it) of additional OH groups and with their inhibitory potency (expressed by their IC_{50} in nM in logarithmic scale). Crosses indicate the mean clogP value for each category.

The correlation coefficient between clogP and IC_{50} values is -0.49 (-0.62 when considering logarithmic IC_{50}). The negative sign implies that the most lipophilic rotenoids (higher clogP) are most potent against complex I (lower IC_{50}), and this suggests that the rotenone binding site is located inside a hydrophobic region of the protein, such as the Q site.

The next section evaluates the structure activity relationships for different aspects of the rotenoid structure: modifications of the E-ring (change of stereochemistry, ring-opening and other alterations, sections 5.3.1-5.3.3), reduction and deoxygenation of the C-ring (section 5.3.4), flattening of the rotenone core (section 5.3.5), hydroxylation of the A-ring (section 5.3.6), hydroxylation at the B-C ring junction (section 5.3.7), D- and E-ring hydroxylations (section 5.3.8) and, lastly, chlorination and bromination of the E-ring (section 5.3.9).

5.3 Structural determinants of inhibitory potency

5.3.1 Stereochemistry at the E-ring

The importance of the alkene and the stereochemistry at the junction carbon in the E-ring were investigated by comparing rotenone with *epi*-rotenone and their corresponding hydrogenated products (Figure 5.9, IC_{50} in nM). Reversing the stereochemistry (from the R to the S configuration at the chiral outermost carbon) leads to a two to threefold increase in IC_{50}, perhaps indicating that the cavity is spatially restricted. Hydrogenation of the double bond in *epi*-rotenone generates a mild increase in potency, different from rotenone where such a transformation elicits little effect. Ueno and Miyoshi concluded in their above-mentioned rotenoids SAR study that the π-electron system of the isopropenyl group attached to the E-ring does not confer inhibitory potency[517] and these results support the same conclusion. The E-ring overall appears to be important for binding, though, and this will also be seen in later sections 5.3.2 and 5.3.8.

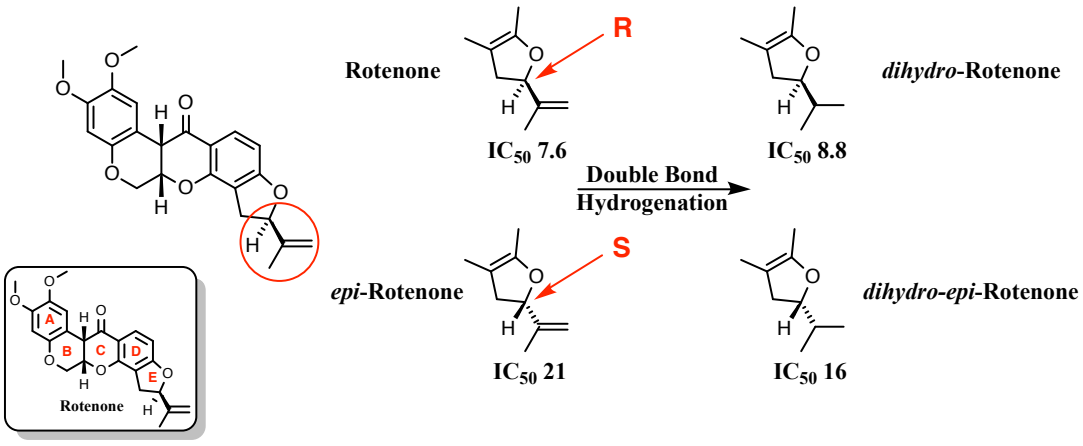

Figure 5.9. Rotenone and *epi*-rotenone. The relevance of the stereochemistry at the E-ring was investigated with rotenone and *epi*-rotenone (R and S configuration, respectively), in addition to their corresponding hydrogenated E-ring tail counterparts. IC_{50} values in nM.

5.3.2 Loss of the E-ring: formation of the prenyl unit

The general importance of the E-ring was evaluated by opening the ether junction, with subsequent formation of a prenyl unit (Figure 5.10). This causes the molecule to elongate, and a major loss of activity follows (the IC_{50} increases into the hundreds of nM range). The different potencies of the isomers, 1024 and 679 nM, may be caused by the latter being more conformationally flexible than the former (two methylene

units as opposed to one where bond rotation can occur) and therefore mimicking more closely the binding arrangement of the original rotenone. This suggests the existence of steric restriction around the E-ring in the binding pocket (as was already suggested in section 5.3.1). Consistent with this idea, hydroxylation of the prenyl moiety and loss of the double bond to a brominated 1,2-diol render the molecule inactive. However, the last two transformations also make the molecule more hydrophilic (by at least one clogP unit, see Table 5.1) and this could mean that the E-ring binding region is particularly hydrophobic.

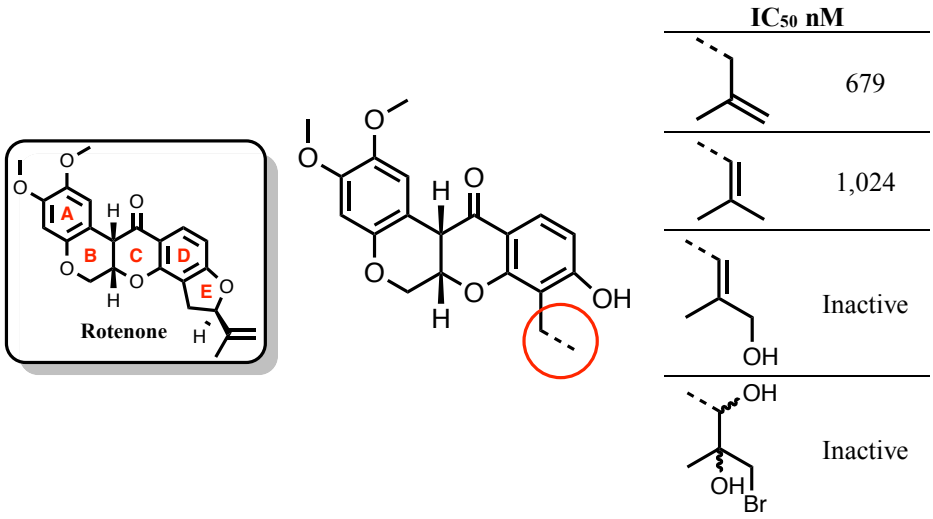

Figure 5.10. E-ring opening and modifications of the prenyl unit. The four rotenoids obtained by opening the E-ring are either poor inhibitors of (or completely inert towards) complex I. IC_{50} values in nM.

5.3.3 Alterations of the E-ring: Deguelin and Elliptone

Further insights into the importance of the E-ring in complex I inhibition came from its expansion to a 6-membered ring (Deguelin) and removal of its isopropenyl tail (Elliptone), plus their hydrogenated counterparts (Figure 5.11). Deguelin is almost as effective as rotenone but it does not tolerate hydrogenation of its E-ring as well since its IC_{50} doubles from 11 to 22 nM (see Figure 5.9). On the other hand, Elliptone possesses a flat E-ring with no alkyl groups protruding from the E-ring plane (differently to rotenone and deguelin). Hydrogenation of the double bond also leads to lower potency, and a further hydroxylation brings the IC_{50} into the μM range. The E-ring can therefore tolerate a minor isomerisation that keeps the same number of carbons as in rotenone (the IC_{50} of deguelin is similar to rotenone), but removing

carbon atoms entirely causes the IC_{50} to become almost 10x higher than rotenone (Elliptone).

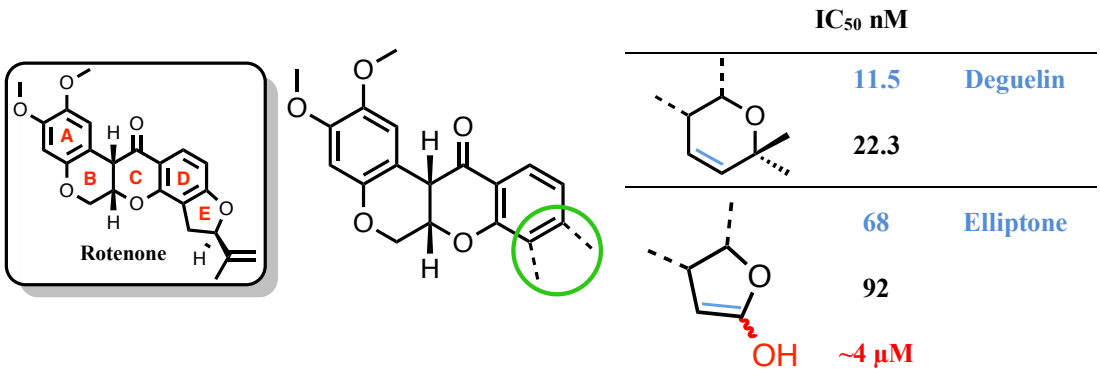

Figure 5.11. Alterations to the E-ring. The E-ring in rotenone was expanded (deguelin) or removed (Elliptone) to further investigate its importance in complex I binding. IC_{50} values in nM.

5.3.4 The C-ring carbonyl

A major structural handle within the library is the carbonyl oxygen in the C-ring: the effects of its reduction and removal were investigated as shown in Figure 5.12.

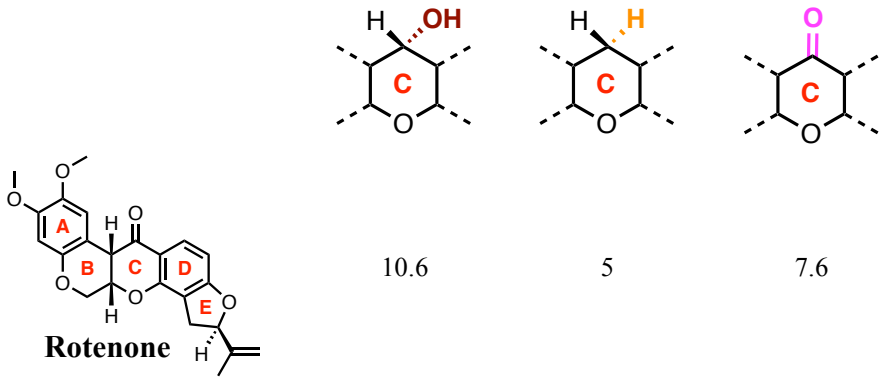

Figure 5.12. Modifications at the carbonyl (C-ring). Reduction of the C-ring carbonyl (brown), dexoygenation (orange) and related IC_{50} values. Values for rotenone and deguelin are shown for comparison (magenta). IC_{50} values in nM.

While the reduction of the C-ring carbonyl (*hydroxy*- variant) leaves the activity of rotenone and deguelin almost intact, deoxygenation (*deoxo*- variant) surprisingly improves the potency. This suggests that rotenone binding interactions with complex I do not strongly depend on the carbonyl group. Saturation of the E-ring double bond causes the IC_{50} to drop more in *hydroxy*- and *deoxo*-deguelin than in the corresponding rotenoids, in line with previous findings (see sections 5.3.1 and 5.3.3). Importantly, the cis-decalin ring system (B-C) ring inversion is probably more energetically challenging in rotenone due to steric hindrance between the junction decalin hydrogens and the carbonyl group in the C-ring, so removing the carbonyl moiety via deoxygenation may improve the flexibility of the rotenoid and make the inverted *cis*-decalin conformation energetically accessible. Such improved flexibility could allow the deoxygenated rotenoids to accommodate better within the binding site, hence their slightly lower IC_{50}.

5.3.5 Flattening of the rotenone core

Ueno and Miyoshi[521] proposed that a rigid bend at the junction of the B/C rings is paramount for inhibition: inversion of the stereochemistry at the junction (*i.e.* with the decalin hydrogens of rotenone pointing down instead of up in Figure 5.9) led to a drastic decrease in inhibitory potency compared to rotenone. On the other hand, it was recently found by Echeverri and co-workers[530] that rotenone flattened in the C-ring opposite the ether oxygen is 10 times more potent than rotenone itself against the human protozoan parasite *Leishmania panamensis* (Leishmania mitochondria contain complex I[531,532]), suggesting that in some species the requirement for a bent geometry in rotenoids is not absolute.

The rotenoid library used here includes four species with a C-C double bond that renders them flatter than rotenone, either at the B/C ring junction (resulting from the dehydrogenation of the *cis*-decalin hydrogens) or in the C-ring opposite the ether oxygen (resulting from dehydration of the carbonyl C-ring). Figure 5.13 shows how the decalin core (on the left) becomes flatter upon dehydration (top) or dehydrogenation (bottom).

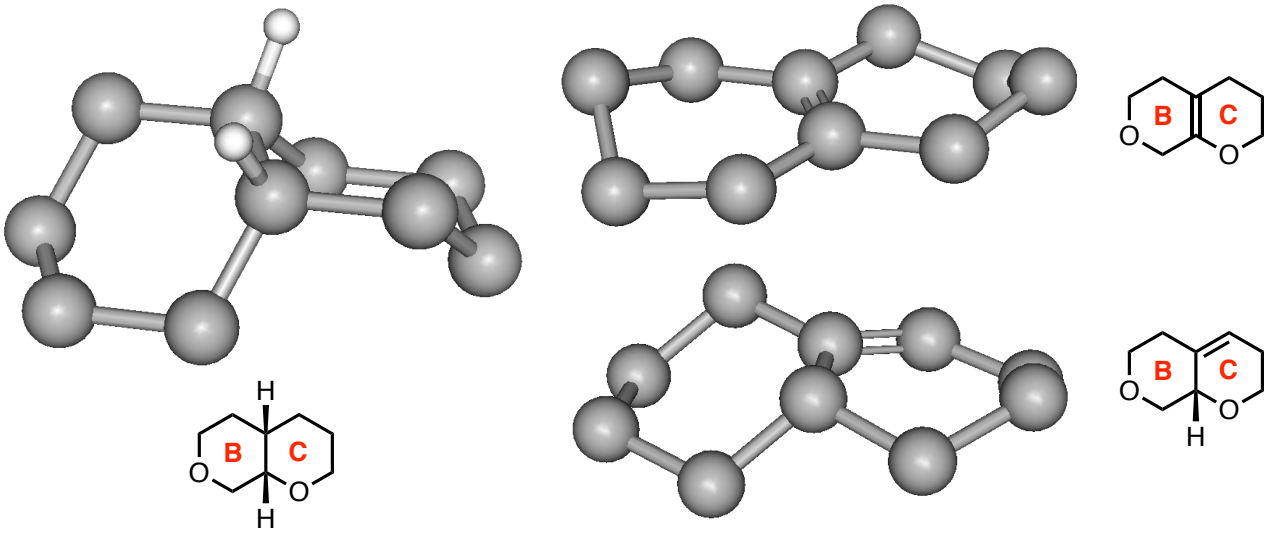

Figure 5.13. The flattening effect of C-C double bond formation. The *cis*-decalin core of rotenone (left) becomes flatter upon dehydrogenation at the B/C ring junction (upper-right corner) or upon dehydration at the C-ring opposite the ether oxygen (lower-right corner). 3D rendering of the molecules was obtained with MarvinSpace, ChemAxon, 16.5.2.0.

Figure 5.14 (teal) shows that the wedge-like geometry of rotenone is indispensable for retaining inhibitory activity: evidently the binding site is not capable of accommodating the more planar, open and extended structure that results from generation of a double bond, indicating that it recognises the shape of the molecule. The dehydrated products also include the effect on saturation of the isoproprenyl tail (upper portion of Figure 5.14, yellow) and the dehydrogenated products also include carbonyl group addition in the B-ring (lower portion of Figure 5.14, yellow).

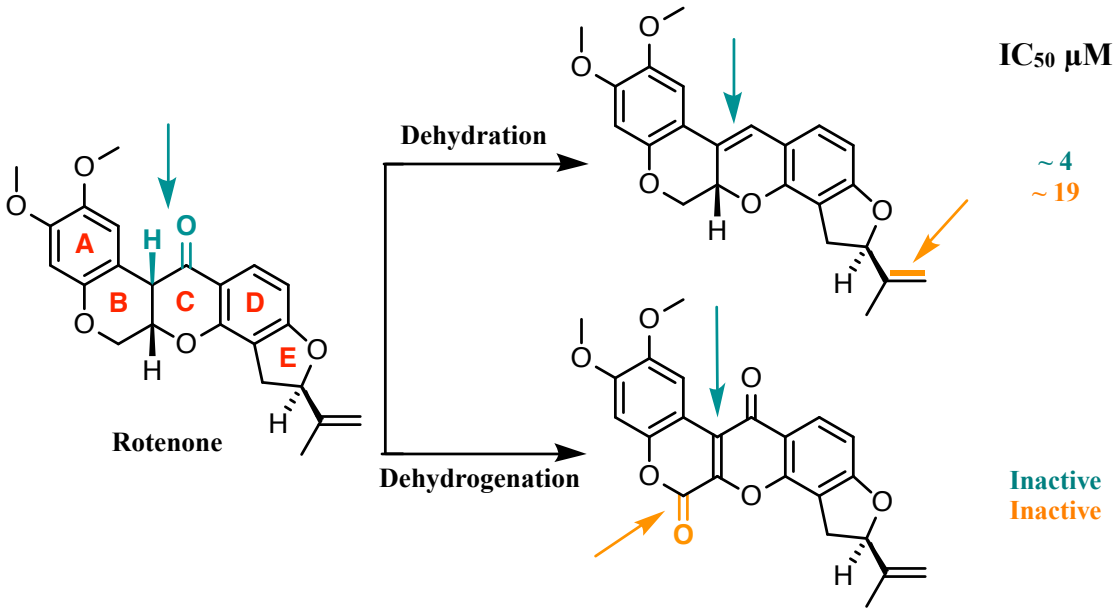

Figure 5.14. The effect of flattening of the rotenoid core. Formation of double bonds in the C-ring (teal) causes loss of flexibility and three-dimensional character. Further transformations (orange) erode the inhibitory potency even more. Estimated IC_{50} values in nM.

5.3.6 Modifications of the A-ring

The role of the *ortho*-dimethyl ether portion of the A-ring was tested by successive demethylations according to Figure 5.15 (IC_{50} in nM); the double bond in the E-ring tail was not retained because it interfered with the chemical synthesis: the progressive drop in potency from single to double hydroxylation (4x and 23x compared to the starting rotenoid) suggests the presence of hydrophobic pockets in complex I that respond favourably to alkyl groups (at least methyl). In this regard, Miyoshi concluded that while the two methoxy hydrogen-bond acceptor moieties in the A-ring are required for tight fitting into the binding site, replacing one of them with a longer ethoxy group retains the activity, suggesting the existence of a relatively spacious (or flexible) binding environment around the A-ring[505].

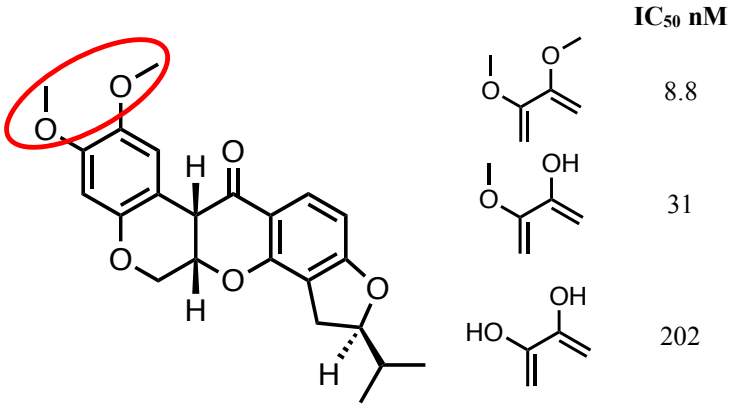

Figure 5.15. The 3,4-dimethoxy moiety in the A-ring. Progressive demethylation in the A-ring causes a drop in potency. IC_{50} values in nM.

5.3.7 Hydroxylation at the B-C junction

Figure 5.16 shows a comparison of X-ray crystal structures of rotenone and *dihydroxy*-rotenolone (courtesy of Dr. David Russell), two more highly hydroxylated rotenone analogues than the ones encountered so far and, as such, more hydrophilic (the same applies to the deguelin related tephrosin). The dihedral angle between rings A- and D- of the former is 91˚ and the same angle of the latter is 76˚ (for comparison, the same angle for *deoxo*-rotenone is 98˚, see section 5.3.4). Addition of an hydroxyl group to the carbon junction in the B-C ring does not effect any conformational change but reduction of the nearby carbonyl contributes towards a more pronounced wedge-like conformation, possibly by intramolecular hydrogen bonding between two contiguous OH in the *trans*-1,2-diol motif[515].

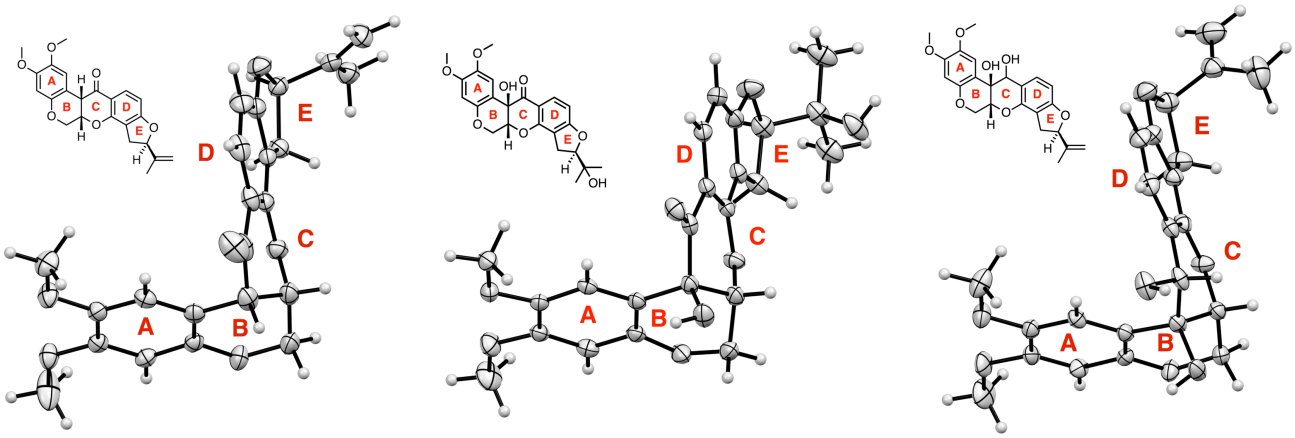

Figure 5.16 The wedge-like geometry of rotenone is more pronounced when the C-ring carbonyl is reduced. The X-ray crystal structures of rotenone (left) and *dihydroxy*-rotenolone (right) show that two hydroxy groups at the B-C junction generate a smaller dihedral angle between the A- and D-rings. The angle is similar to rotenone with only one hydroxyl group (centre) (courtesy of Dr. David Russell).

The effects of such transformation are summarised in Figure 5.17.

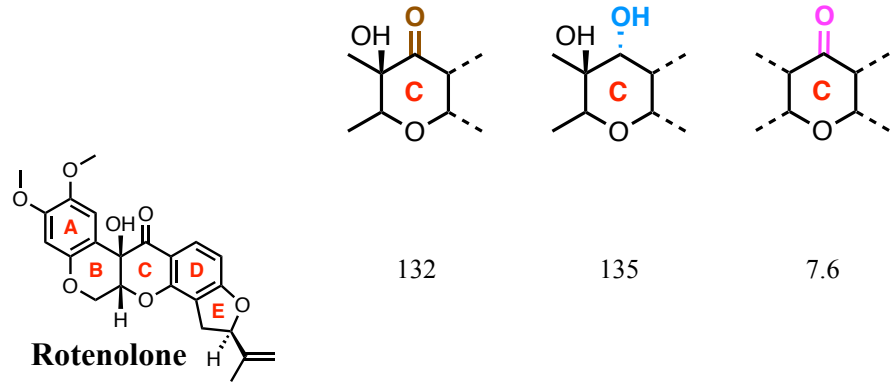

	132	135	7.6
E-Ring hydrogenation	152	85	8.8
	84	157	11.5
E-Ring hydrogenation	125	447	22.3

Figure 5.17. Rotenolone, Tephrosin and *dihydroxy*-rotenoids. Hydroxylation at the B-C ring junction generates rotenolone and tephrosin from rotenone and deguelin, respectively (brown), and further reduction of the C-ring carbonyl generates their dihydroxy counterparts (cyan). Values for rotenone and deguelin are shown for comparison (magenta). IC_{50} values in nM.

Addition of the hydroxyl group at the B-C ring junction (Rotenolone and Tephrosin, brown in Figure 5.17) renders, for the first time, the rotenone derivative less potent than the deguelin one (IC_{50} 132 and 84 nM, respectively), and E-ring saturation is detrimental to both. On the other hand, in the related dihydroxylated derivatives (cyan in Figure 5.17) the rotenone variant is more potent than the deguelin one (IC_{50} 135 and 157 nM, respectively) and, intriguingly, E-ring saturation leads to a dramatic improvement in potency (from 135 to 85 nM): it appears that the addition of OH group prevents optimal binding but a further OH group (hence a more pronounced wedge-like conformation) is tolerated.

A tentative explanation for this behaviour is that the different conformation must push the E-ring tail towards a more hydrophobic region, where more favourable binding interactions are obtained, since loss of a double bond in the tail region leads to an almost twofold rise in residual activity (Figure 5.18, IC_{50} in nM).

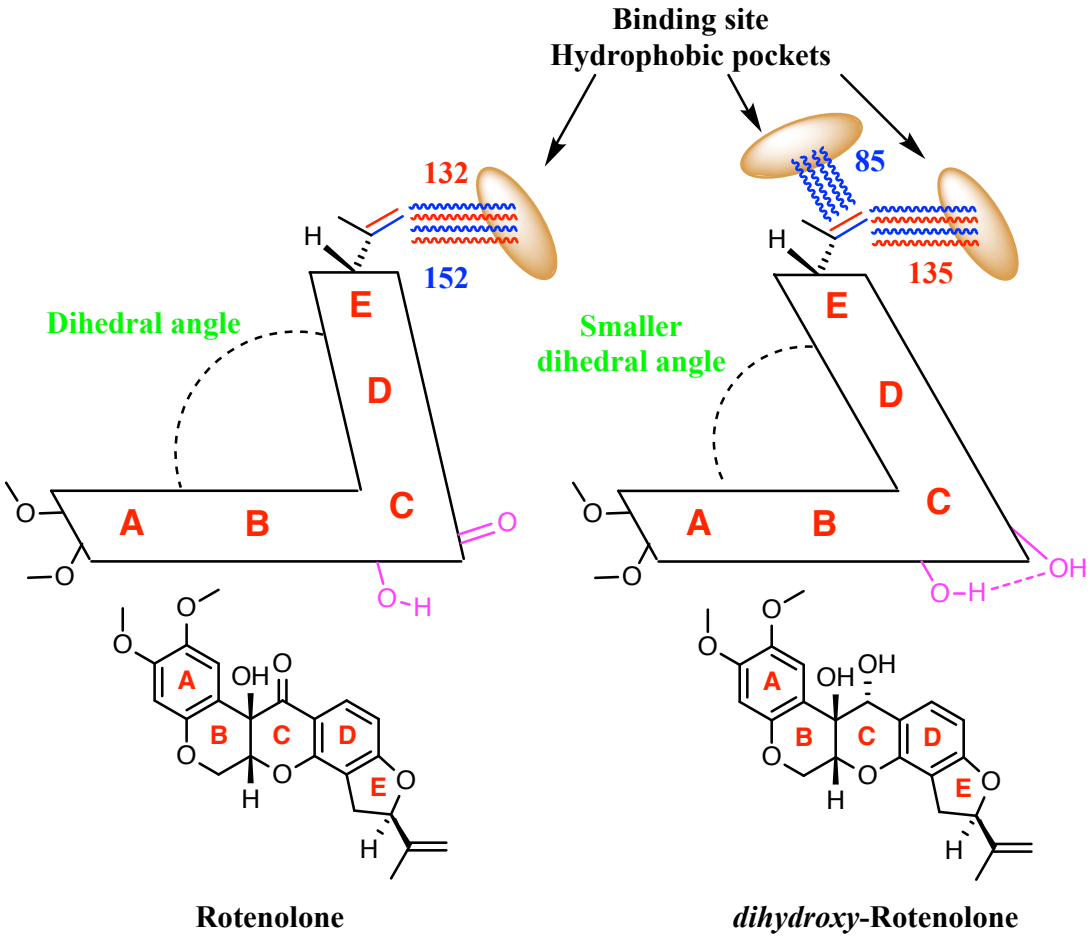

Figure 5.18. A tentative explanation of the effects of E-ring saturation upon B/C ring hydroxylation(s). E-ring saturation in rotenolone is mildly detrimental to the activity, perhaps because some hydrophobic interactions are lost in the hydrophobic pocket dedicated to the E-ring; conversely, E-ring saturation in the *dihydroxy*- derivative leads to a marked improvement in potency, possibly because the tail can reach out to a more favourable binding site thanks to newly formed H-bond interactions (magenta). IC_{50} values in nM.

When the same set of structural modifications is applied to deguelin (Figure 5.17, tephrosin), the effects are reversed compared to rotenone: hydroxylation of the B-C junction still lowers the potency (from 11.5 to 84 nM), but now the *dihydroxy*-arrangement drops it even more (from 84 to 157 nM), particularly if the double bond in the 6-membered E-ring is hydrogenated (125 and 447 nM). This could be explained by the bigger E-ring of deguelin causing different overall binding interactions than rotenone, where a more compact structure is no longer tolerated.

Fang and Casida[527] found inhibitory potencies (in bovine heart electron transport particles) for rotenolone and tephrosin similar to the ones found in this work but, surprisingly, when the hydroxyl group at the B/C ring junction points to the opposite

side (*i.e. trans*-decalin as opposed to *cis*-decalin) the result is much more detrimental (see Figure 5.19).

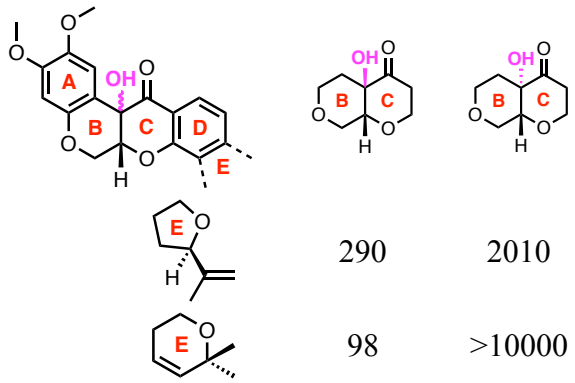

Figure 5.19. Inhibitory potencies in the Fang and Casida SAR study. Fang and Casida showed inhibitory potencies for rotenone and tephrosin similar to the ones in this work and showed the detrimental effect of reversing the stereochemistry at the B-C junction hydroxyl group. IC_{50} values in nM.

5.3.8 E- and D-ring hydroxylations

A wide array of oxidative alterations at the E-ring (combined with different oxygen patterns at the B-C rings) are presented in Table 5.2 (IC_{50} values in nM).

Hydroxylation of the E-ring destabilises the binding overall, and this is always substantially worsened by additional hydroxylations and oxygen addition at the B-C rings (going across the table from left to right), just as if the OH groups pushed the molecule further away from the binding site (this could be diagnostic of a hydrophobic binding site): with such a high loss of binding affinity, the binding mode could also be very different than for the original rotenone. Substantial potency losses derived from E-ring based oxidations are encountered with endocyclic hydroxylations (when the OH is directly attached to the E-ring, third row in Table 5.2) and with multiple oxidative modifications (seventh row in Table 5.2). Amorphigenin (Table 5.2, third row from the bottom, first column) exhibits an IC_{50} over 16x higher than rotenone, but it was recently found that it is more potent than rotenone against complex I isolated from the chinese mosquito *Culex pipiens pallens*[533]. The only glycosylated rotenoid tested (the disaccharide D-glucose-L-arabinose was attached to the E-ring) confirmed the importance of the E-ring for binding, since such a bulky substituent generated the biggest potency loss in the whole rotenoid library. The only two D-ring hydroxylated rotenoids (second row in Table 5.2) were the most

challenging ones to synthesise (the D-ring is the most unreactive portion of the rotenoid skeleton[515]) and are not very potent inhibitors at all.

A smaller set of similar structural modifications were incorporated in the E-ring of deguelin with similar results: while exocyclic alcohols (at least one carbon away from the E-ring) are still relatively well tolerated, endocyclic and multiple hydroxylations thoroughly disrupt binding (Figure 5.20). This finding is in agreement with the work of Nicolaou and Casida[528]: polar groups in the E-ring of a similar variant to deguelin were not well tolerated. Interestingly, it was found that a doubly hydroxylated deguelin (red and green handles in Figure 5.20) loses completely its potency (compared to deguelin) against Hsp90, one of the major targets that make deguelin an anticancer agent[534] (see section 5.1.3).

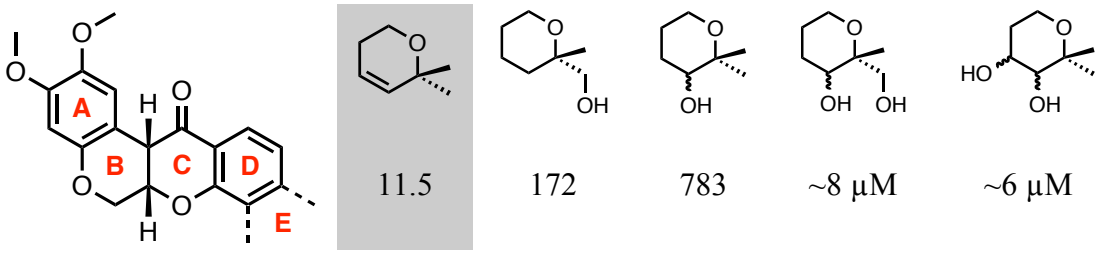

Figure 5.20. Hydroxylations at the E-ring of deguelin. The same conclusions drawn for rotenone apply to deguelin: endocyclic and double addition of OH lowers the potency more than exocyclic. Deguelin shown for comparison in grey. IC_{50} values in nM.

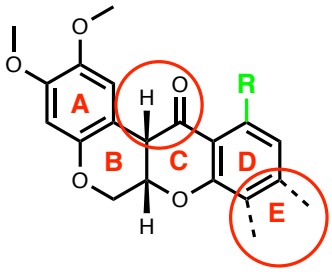

B-C / E-	H, O	H, OH	HO, O	HO, OH	R
	7.6	10.6	132	135	H
	739		406		OH
	~3 µM		Inactive		H
	626	853	~16 µM		H
	58		~6 µM		H
	237	503	~3 µM		H
	~4 µM ~2 µM	~5 µM	Inactive	Inactive	H
	Data refer to mixture of enatiomers				
	131	486	~6 µM		H
	8.9		209		H
Ara-Glc	Inactive				H

Table 5.2. Two-dimensional oxidative SAR on rotenoids: the B-C ring against the E-ring. Addition of oxygen atoms in various forms (both in the E-ring and, more importantly, at the B-C rings) causes a dramatic fall in potency (going left to right across the table). Red and blue, IC_{50} values for different diastereomers. The grey row shows values encountered in previous sections for comparison. IC_{50} values in nM unless otherwise stated.

5.3.9 Halogenated rotenoids

Figure 5.21 illustrates the set of halogenated rotenoids investigated, with the IC_{50} values for the corresponding hydroxylated rotenoids also presented for comparison (all values in nM).

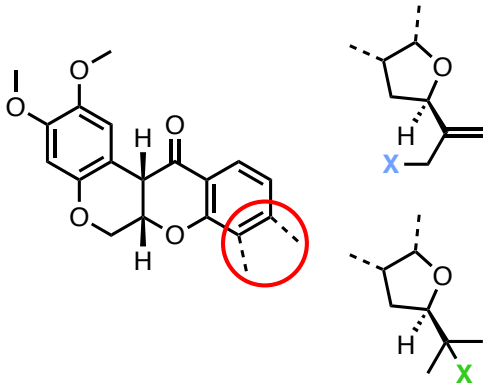

X=H	7.6	8.8
X=OH	131	626
X=Cl	6	19
X=Br	4.1	49

Figure 5.21. Halogenation of the E-ring. Chlorine and bromine were added to the E-ring in two different locations (blue and green colours). The IC_{50} values for species encountered in previous sections are shown for comparison in grey. IC_{50} values in nM.

Chlorine and bromine were added to the E-ring tail and the additions that keep the double bond intact (blue colour) render the rotenoids even more powerful than rotenone itself (blue in grey background, X=H). When the halogen addition is across the double bond (green colour), the potency loss is noticeable but much less pronounced than the effect of hydroxylation. Since the corresponding oxygenations are more detrimental, and the spatial requirements of OH, Cl and Br groups are similar to each other (and bigger than rotenone with X=H)[535], the main factor involved in adverse binding interactions (at least around the E-ring) may not be steric hindrance but hydrogen bonding. An alternative explanation for such tight binding could involve halogen bonding with nucleophilic residues within the binding chamber[536,537]. The fact that some halogenated rotenoids are potent inhibitors of complex I is advantageous for structural studies: the large electron density on halogen atoms may make structural determination easier in the future.

5.4 Discussion

The determinants of rotenoid potency towards complex I inhibition were analysed with IC_{50} measurements in bovine mitochondrial membranes as described in section 5.2.2. Most alterations of the E-ring are not well tolerated: very rarely does an E-ring

modification retain the same potency as rotenone or increase it (*e.g. dihydro*- and halogenated rotenoids in sections 5.3.1 and 5.3.9 respectively). This suggests that the rotenone binding site strictly recognises the E-ring and the room for improving potency through this handle is narrow. On the other hand, structural requirements in the C- and A-ring regions are less strict and some alterations even improve the potency compared to rotenone.

When the rotenone structure is flattened along the B/C rings, the inhibitory potency drops substantially, therefore the three-dimensional wedge-like conformation is paramount for optimal binding. The *cis*-decalin core in rotenoids is probably motionally challenged but not energetically prohibited, and some degree of conformational flexibility may contribute towards the binding affinity (*e.g. deoxo*-rotenone, section 5.3.4). In this regard, the possibility of intramolecular hydrogen bonding brought about by adding hydroxyl groups could explain, along with steric hindrance, the potency loss of some rotenoids: such intramolecular interaction would lock the rotenoid species to a specific conformation incompatible with tight binding. The putative ubiquinone-binding channel in mammalian complex I is characterised by a very distinctive bottleneck: while the channel (shown in Figure 5.22, left) is mainly uncharged and hydrophobic, the bottleneck is formed by polar and charged residues, especially arginine[86].

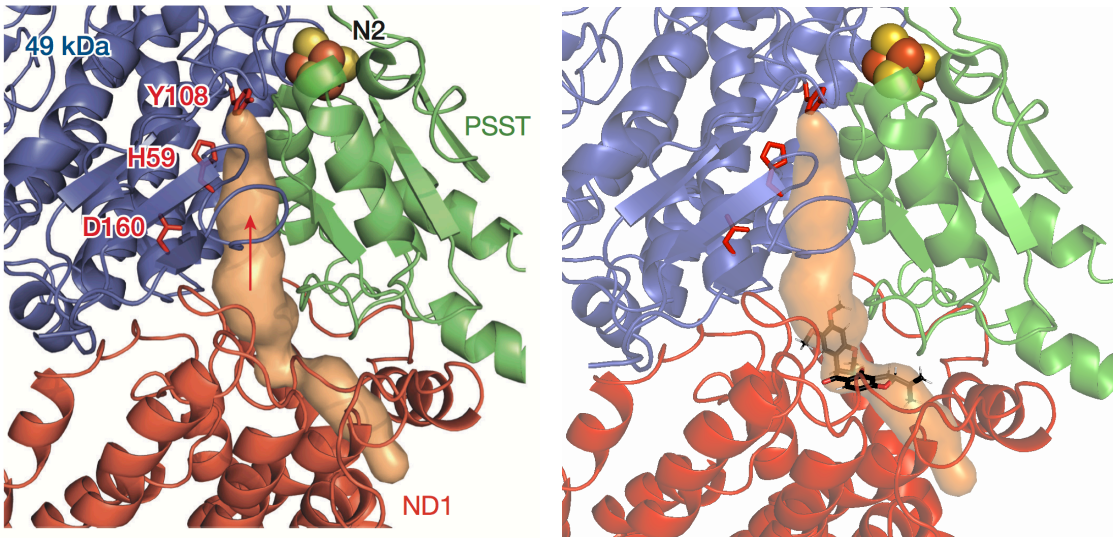

Figure 5.22. The ubiquinone-binding site in mammalian complex I. The picture on the left (from Hirst[86]) shows the main residues forming the ubiquinone-channel in bovine complex I plus the bottleneck region highlighted by the arrows. The picture on the right illustrates how rotenone would fit inside the bottleneck region in the same structure.

Given the approximate location of the rotenone biding site, it is tempting to speculate that rotenoids may access their binding site through the ubiquinone-channel (more hydrophobic rotenoids tend to be stronger inhibitors, see Figure 5.8). The bottleneck region of the ubiquinone-site actually resembles the wedge-like geometry of the rotenone core, and binding in this region could be favourable in terms of both stabilising interactions (*e.g.* hydrogen bonding with the above-mentioned polar residues) and forcing a stable wedge conformation (shown in Figure 5.22, right).

The rotenoids in the library span both a wide hydrophobicity and potency range (see Figure 5.8), hence there are opportunities to find a compound suitable for therapeutic use with limited neurotoxicity. The most promising anticancer therapeutics within the library are Rotenolone, Tephrosin and their dihydroxy-counterparts (see section 5.3.7): their low hydrophobicity and high potency makes them the best candidates for further biological evaluation.

There are numerous examples of rotenoids less hydrophilic than rotenone that possess anticancer activity: some of them shown in Figure 5.23 along with their clogP value.

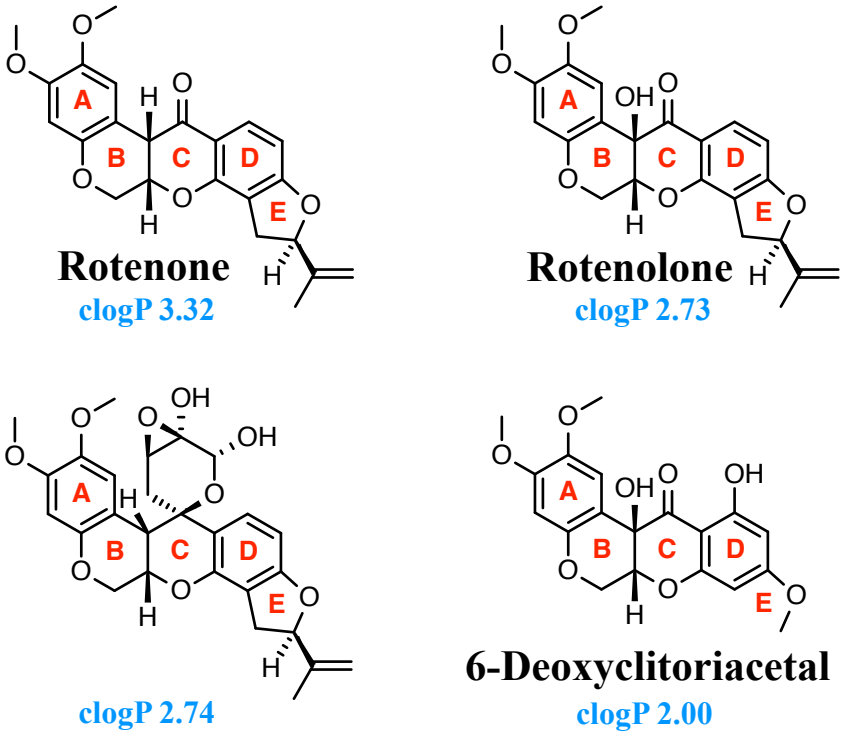

Figure 5.23. Hydrophilic rotenoids that exert anticancer activity. These hydrophilic rotenoids (their clogP values are lower than rotenone, shown for comparison) have shown promising anticancer activity in several cancer cell lines through various mechanisms. clogP values calculated using MarvinSketch Version 16.5.2.0 Consensus Model by ChemAxon.

In two recent studies by the Kinghorn group[538,539], Rotenolone was found to inhibit growth and K-Ras activity (a protein expressed by the KRAS gene required for tumor maintenance[540]) in HT-29 human colon cancer, 697 human acute lymphoblastic leukemia and Raji human Burkitt's lymphoma cells; it was also found to inhibit NF-kB signalling (crucial in KRAS mutant tumors for cell survival[541]) in HeLa cells. Rotenolone was also not cytotoxic towards CCD-112CoN human normal colon cells. An hydroxylated rotenoid (bottom-left corner in Figure 5.23) was shown to possess inhibitory activity of adipocyte differentiation in 3T3-L1 cells[542] and this could signify a potential anticancer treatment, given the several mechanisms of metabolic symbiosis between adipocytes and cancer cells, especially in breast cancer cells[543,544]. Finally, 6-Deoxyclitoriacetal (bottom-right corner in Figure 5.23) was found to exert growth inhibition activity against human oral carcinoma KB, breast cancer MCF-7 and human small lung cancer NCI-H187 cell lines, along with inhibition of topoisomerase II activity[545], a class of enzymes ubiquitous within most nucleic acid processes and targets for treating many human malignancies[546].

5.5 Summary

The rotenoids analysed thus far provide many insights into the binding interactions of rotenone towards complex I: a conformationally rigid E-ring is required for optimal binding, the reduction/deoxygenation of the C-ring carbonyl does not cause high loss of inhibitory activity (hence an hydroxyl group does not provide hydrogen bonds to the C-ring binding target) while reaching an extended and flatter conformation completely disrupts binding; finally, the methyl ethers in the A-ring point towards the presence of a hydrophobic pocket. Hydroxylation of the B-C ring junction leads to slight loss of activity, and conversion of the nearby carbonyl to hydroxyl is well tolerated: particularly rotenoids possessing the anti-diol motif are the most promising for follow-up experiments in more sophisticated systems (cell-based assays and mouse models of cancer), on account of their high hydrophilicity combined with relatively high potency. Oxidative modifications at the E-ring lead to far more varied results, depending on the hydroxylation site, so it appears that the rotenone binding site is more temperamental towards changes in the E-ring milieu. The results on the halogenated series suggest that disruption of inhibitory potency is due to hydrogen bonding interactions rather than mere steric hindrance.

6 SAR studies of complex I on-target and off-target drugs: IACS-10759 and Mubritinib

6.1 Introduction and aims

During the safety assessment process of lead compounds, toxicology studies are indispensable to predict risks for human use. Adverse toxicologic effects can be chemical-based, on-target and off-target: the former relates to the side effects linked to the physicochemical characteristics of a compound (*e.g.* cationic amphiphilic drugs incorporated into phospholipid bilayers of plasma membrane[547]), the latter two are connected with unwanted pharmacological effects at the target of interest (on-target or exaggerated pharmacology, *e.g.* bleeding events with antithrombotics[548]) or at other targets[549]. Collaborations were established with the Texas MD Anderson Cancer Center and the Leicester MRC Toxicology Unit to test two libraries of candidate drugs (and their variants) that interact with complex I in an on-target (IACS-10759) and off-target (Mubritinib) fashion: these drugs are structurally similar to each other, since they share two phenyl rings on either side and a central oxa(di)azole ring (Figure 6.1 shows representative examples of both libraries).

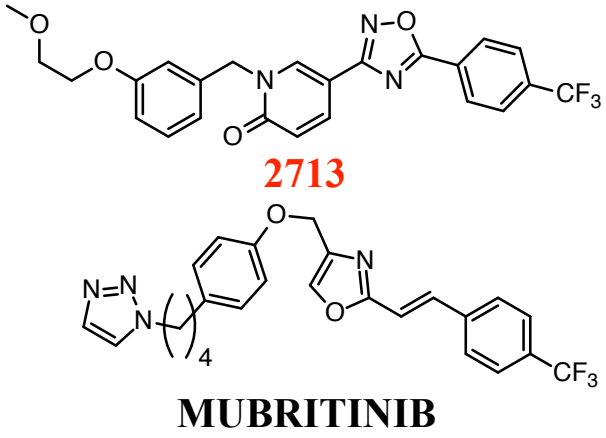

Figure 6.1. Comparison between Anderson Centre drugs and Mubritinib. There are some structural similarities between the Anderson Centre drugs (2713 is shown) and Mubritinib: two phenyl rings on either side and a central oxa(di)azole ring.

The aims of this work are to

- improve understanding of inhibition and drug binding to complex I
- assess target specificity of drugs to complex I

6.2 The Anderson Cancer Centre drugs

The collaboration with the Texas MD Anderson Cancer Center was developed in two stages. Firstly, a set of drugs (8 compounds, Library A), which had already been extensively characterised in cell based assays and xenograft models for cancer and identified as a complex I inhibitor, was tested with different assays to determine their potency and selectivity against complex I. Secondly, a bigger set of 30 related compounds (Library B), hitherto uncharacterised in terms of their biological antitumorigenic effect, was analysed to complete a SAR study on complex I. This family of molecules is considered to exert its anticancer properties via complex I inhibition. The compounds share a common structural motif that was originally explored by Bayer AG in 2013 for one of their lead candidate anticancer drugs.

6.2.1 The pyrazolyl oxadiazole scaffold: HIF suppression, energy depletion and reduced aspartate production

The pharmaceutical company Bayer AG was the first to report that pyrazolyl oxadiazoles derivatives can suppress the expression of HIF target genes under hypoxic conditions and their work culminated in the anticancer drug **87-2243** (see Figure 6.2). The most important drug in the libraries tested in this work (**10759**, see section 6.3.4) shares an almost identical scaffold with **87-2243** (1,3,4 triazolyl oxadiazole) but, interestingly, the Anderson Centre proposed a different mechanism of action for its antiproliferative activity than Bayer AG. While **87-2243** was mainly tested in HIF target gene expression, **10759** was primarily assessed in cancer metabolism. Both rationales for antitumour activity will now be summarized.

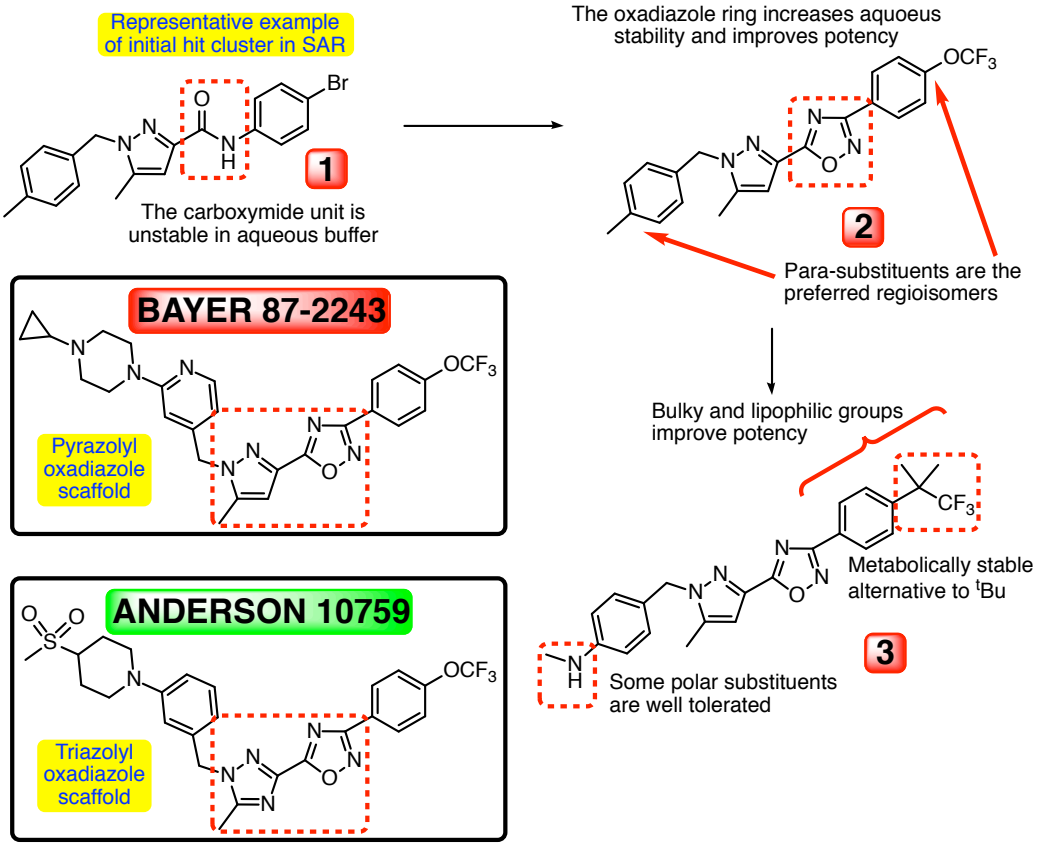

Figure 6.2. Representative structures of confirmed hit cluster from initial screening by Bayer AG. The figure illustrates the steps that Bayer took to improve potency, aqueous and metabolic stability from the original cluster **1** to lead compounds **2** and **3**. It was **87-2243** that was ultimately chosen for extensive follow-up experiments. **10759** is shown for comparison.

6.2.1.1 87-2243 by Bayer AG and the role of ROS in tumorigenesis

The stepwise development of **87-2243** is shown in Figure 6.2[550]. The key point was the introduction of the oxadiazole ring to address the lack of stability in aqueous solution. Further refinements on either side of the core led to compounds **2** and **3** that showed remarkable specificity for suppression of hypoxia-induced expression of HIF-targeted genes, as well as very favourable pharmacokinetic properties. Bayer AG discovered the pharmacologic potential of the pyrazolyl oxadiazole class in this work and this subsequently led to the development of **87-2243**.

In a further paper by the same group, **87-2243** was extensively characterized with respect to its activity towards HIF-1, mitochondria and complex I[551]. It was found that **87-2243** decreased both expression of hypoxia-targeted genes and HIF protein accumulation in H460 (human lung cancer) cells. More specifically to mitochondria, **87-2243** did not cause cell death when 13 different human cancer cell lines were

cultured in glucose but it did when the cells were cultured in galactose (when cells are more dependent on OXPHOS); additionally it decreased mitochondrial oxygen consumption (measured with the LUX-MitoXpress dye) with an IC_{50} of 10 nM. Specificity to complex I was addressed by succinate- or NDI1-rescue experiments involving H1299 lung cancer cells expressing firefly luciferase with rotenone and antimycin A (a specific complex III inhibitor), the same techniques used by the Anderson Centre, see section 6.2.1.2.

The authors of the paper erroneously concluded that the antitumorigenic effect of **87-2243** was to be ascribed to the HIF-activating role of mitochondrial ROS during hypoxia (no ROS assays were carried out in the study on **87-2243** although they did test a class of alkyliminophenylacetate inhibitors of hypoxia-induced HIF-1 activation for ROS generation mentioned in section 1.6.3). They referred to ROS generated from complex III which can form and direct superoxide ion in the intermembrane space for cytosolic signaling as well as in the matrix (as opposed to complex I and II which can only direct superoxide ion in the matrix, see chapter 1 for a review of mitochondrial ROS and the hypoxia response)[552]. The Schumacker group indeed found that hypoxia in wild type mouse and rat pulmonary arterial smooth muscle cells elevated cytosolic but not mitochondrial H_2O_2 levels[553]. In theory, however, reduced electron flow caused by inhibition upstream of complex III (for example at complex I) should disrupt electron transport, generating lower cytosolic ROS emission from this enzyme[554] and, as a result, should partially restore PHD2 activity in cancer cells (recall from chapter 1 that ROS inactivates PHD2 via disulphide bond-mediated dimerization). Within this logic, the Bayer group linked inhibition of mitochondrial complex I to lower cytosolic ROS levels that would otherwise inhibit PHD2, thus preventing accumulation of HIF-1α. It must be pointed out, however, that while a decrease in mitochondrial ROS emission in the cytosol from complex III generated by complex I inhibition may initially happen, at some point increased matrix ROS will cross the IMM and reach the cytosol in the form of H_2O_2. Forkink *et al.*[555] recently reported that a 24 hour inhibition by rotenone in HEK293 (human embryonic kidney) cells elevated cytosolic H_2O_2 levels, but not enough to cause oxidative stress or cell death. The authors did not account for the role of drug metabolising enzymes that could have mitigated the effects of rotenone inhibition (see chapter 3 for experiments with CYP450 and rotenone). The lack of ROS assays to back up the conclusions by

the Bayer group was remedied by another group within Bayer AG[556] where ROS production was addressed in melanoma cell lines. They found that **87-2243** inhibited tumorigenesis by generating high levels of both mitochondrial and cytosolic ROS that resulted in oxidative damage and, eventually, cell death. ROS scavengers were successfully used to establish the causative role of ROS in **87-2243**-induced cell death. They also found that **87-2243** was more effective in conditions of limited glucose availability. Ultimately, Bayer concluded that the antitumorigenic activity of **87-2243** occurs through complex-I generated ROS oxidative stress and ATP depletion in conditions where glucose is limited (*e.g.* in the centre of a tumour).

Further characterization by Bayer AG included xenograft models indicating that **87-2243** improves the outcome of tumour control concomitant with fractionated irradiation[557], as well as the use of compatible PET tracers to better monitor its therapeutic efficacy[558].

A recent study by the Ihnat group[559] showed that the carbazole-based compound AG311 induced necrosis in two breast cancer mouse models via mitochondrial depolarization, oxidative stress and loss of membrane integrity. A later study by the same group[560] identified complex I as the molecular target responsible for the drug mode of action and, interestingly, it was also found that AG311, by lowering oxygen consumption through complex I inhibition, mediated a localized increase in oxygen tension (hence higher PHD2 activity) within the tumour milieu (detected with pimonidazole, an hypoxia marker), thus preventing HIF-1α stabilization.

6.2.1.2 10759 by the Anderson Cancer Centre

10759 (shown in Figure 6.2) was identified with a SAR study that included compounds similar to **87-2243**. **10759** was very active (IC_{50} in units of nM) in lowering OCR in several human, mouse, rat and monkey cancer cell lines grown in galactose. The biological target was proposed to be complex I on account of succinate- or NDI1-driven electron-flow rescue experiments in permeabilised H460 cells and NADH:dQ assay on isolated mouse complex I (this last aspect will be described in the results section)[561]. A concentration-dependent degradation of HIF-1α was also observed. By generating clones of H292 (human lung cancer) cells resistant to **10759**, a common L55F mutation was found in the ND1 subunit of complex I, close to the entrance of the Q-channel, suggestive of the binding site of the drug.

10759 was then tested in two different tumour contexts: glycolytic-deficient human brain cancer cell lines and acute myeloid leukemia (AML) cells heavily reliant on OXPHOS. In both cases, inhibition of proliferation and apoptosis induction were accomplished at well tolerated doses in mice. The first tumour type was present in about 9% of a sample of tumours from the Anderson Centre patients and the consistent anti-leukemia response generated by **10759** in the second tumour context granted the beginning of a phase 1 trial for AML patients.

The mechanism of action of **10759** was further elucidated with isotope tracing experiments in AML cell lines for carbon and amino acid metabolism, and as noted below, energy depletion and reduced aspartate synthesis were concluded to account for the antiproliferative effects of the drug towards cancer cells. It was found that NADH and nucleotide monophosphate (NMP) levels were higher and nucleotide triphosphate (NTP) levels lower than in control cells, consistent with complex I inhibition and low energy charge (NTPs are generated with two equivalents of ATP via nucleoside kinases). Further metabolic changes occurring upon treatment with **10759** included higher levels of lactate and alanine and lower levels of several TCA cycle intermediates: this is consistent with the diversion of glucose to lactate (following glycolysis) and energetic distress that causes branched-chain amino acid to be used as a source of fuel[562]. Of note, the only amino acid whose biosynthesis was inhibited by **10759** was aspartate: it has been shown that this species is paramount in proliferating cells (for amino acid in proteins and de novo purine and pyrimidine synthesis) where respiration feeds electron acceptors towards its synthesis[563].

6.3 Anderson Cancer Center drugs: specific and powerful complex I inhibitors

6.3.1 Compounds features and libraries description

All of the compounds tested in the same family as **10759** belong to two different libraries, labelled A and B, and can be considered in 6 sections, according to their different functional groups. Figure 6.3 shows a representative compound of the whole series and the most common handles in each group: groups B and E are constant throughout the series, A and F are the most variable. 35 drugs possess a 2-pyridone moiety in C, the remaining 3 drugs a triazolyl moiety (*e.g.* **10759**). Notably, these

molecules are endowed with substantial conformational flexibility and can become very flat overall (see top of Figure 6.3 for a three-dimensional rendering). It was decided to illustrate the compounds in terms of relative orientation (from left to right, A to F based on the bottom panel of Figure 6.3), rather than standard chemical nomenclature, for easier reference[p].

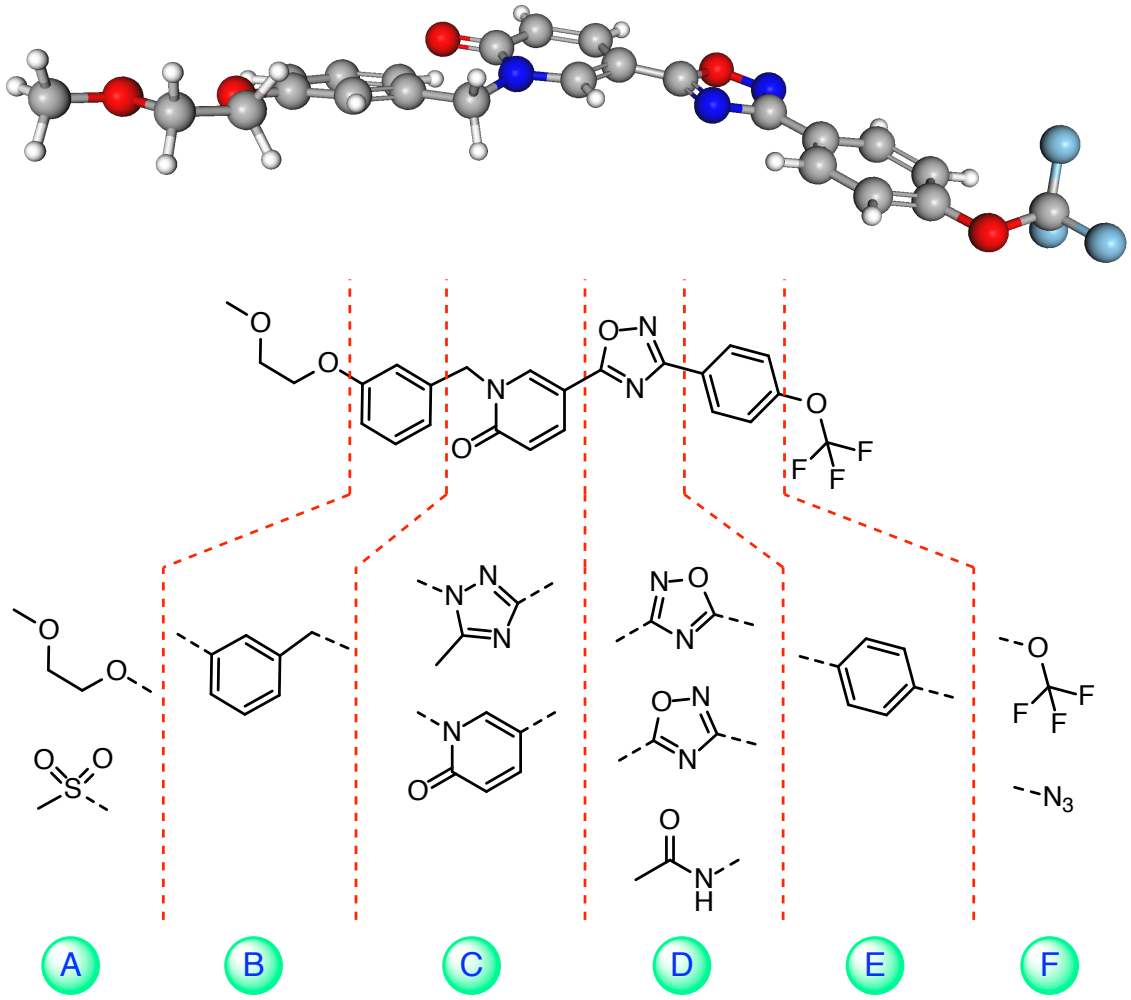

Figure 6.3. Representative scaffold for the Anderson drugs. The 38 compounds that form the two libraries can be split into 6 portions, according to the molecular handles that were modified for SAR purposes. A three-dimensional view of the the representative compound is also shown on top (3D rendering was obtained with MarvinSpace, ChemAxon, 16.5.2.0).

As for Library B, a set of 30 compounds was designed according to the left- and right-hand side groups relative to two specific orientations of the central oxadiazole core: while the former group possesses a OCF_3 handle at the right far end with the oxadiazole ring oxygen pointing towards (and different side attachments on) the left,

[p] Standard chemical nomenclature would include the segments "3-(4-(trifluoromethoxy)phenyl)-5-(2-pyridone)" and "5-(4-cyclopropylphenyl)-3-(2-pyridone)" for top and bottom species presented in Figure 6.4, respectively.

the latter group possesses a methoxyethoxy handle on the left, with the oxadiazole ring oxygen pointing towards (and different side attachments on) the right. Figure 6.4 shows the main features that distinguish the two categories from one another. Despite the orientation of the oxadiazole ring towards the left, **2430** was included in the right-hand side library for better comparison purposes (see Table 6.3 and Figure 6.8, panel C).

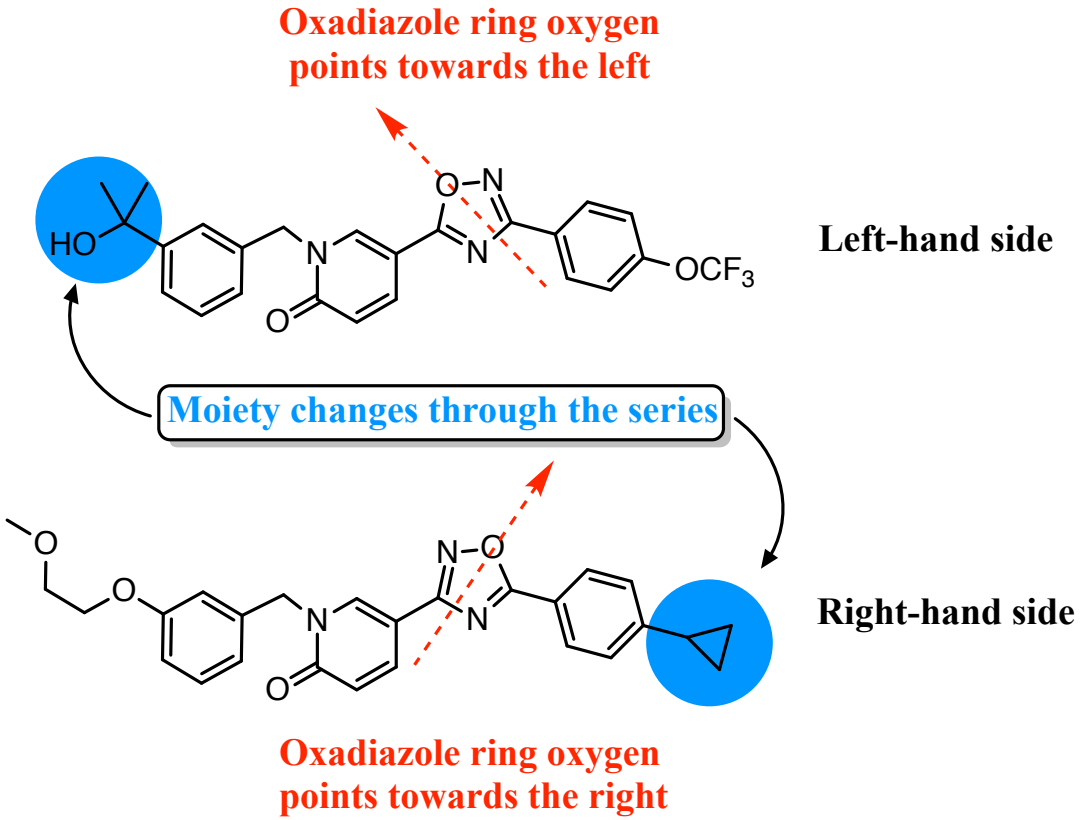

Figure 6.4. Structural elements that specifies the two categories of Library B. Orientation of the oxadiazole oxygen atom and different side attachments define the two categories of drugs in Library B.

The compounds included in Library A possess less functional groups in common with each other (and they were also delivered one year earlier) than Library B but they were tested with further experiments and systems than just the NADH:O_2 assay in order to fully elucidate their role and specificity towards complex I inhibition (Dr. Febin Varghese kindly provided the *Yarrowia* and *Paracoccus* membranes, Ahmed-Noor Adam Agip kindly provided the rat and mouse membranes).

6.3.2 Main experimental details and NADH:O_2 results

Mitochondrial membranes from bovine (and other species for Library A, see section 6.3.5 for details) enriched with exogenous cytochrome *c* were used for testing the potency of the drugs in this SAR study. All of the drugs were tested with the NADH:O_2 oxidoreduction assay and, rarely, erratic 340-380 nm absorbance traces (the R^2 was close to 0.9) were encountered at the highest drug concentrations within the titration series (drugs **2708**, **2720** and **10573**, see section 6.3.6.2). No turbidity was observed nor were the pathlengths readings abnormally low compared to the expected value. clogP values were also determined for all the drugs (calculated using MarvinSketch Version 16.5.2.0, Consensus Model, ChemAxon, MA[529]). The NADH:O_2 (and also NADH:dQ for Library A) IC_{50} determination process was exactly the same as the one used in the other chapters (4-parameters Hill equation). It was also decided to provide an IC_{50} estimation for compounds whose IC_{50} values were over 2 μM and to consider inactive the compounds whose IC_{50} was higher than 20 μM. The best-fit Hill coefficients ranged from 0.64 to 1.77 and do not consistently indicate a substantial cooperative behaviour.

IC_{50} values for the NADH:O_2 and NADH:dQ assays (with 95% confidence intervals), Hill coefficients and clogP values are presented in Table 6.1 (Library A), Table 6.2 (Library B left-hand side handle) and Table 6.3 (Library B right-hand side handle) where the compounds that make up the libraries are shown. Three representative NADH:O_2 dose-response curves (compounds **1225**, **10576** and **10573**) are shown in Figure 6.5.

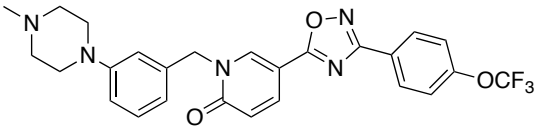

1225
IC_{50} 13.1 nM

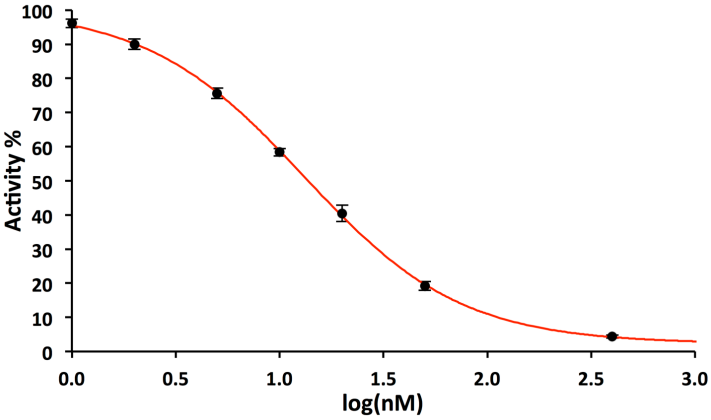

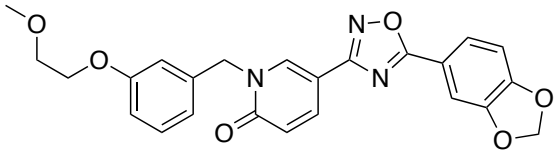

10576
IC_{50} 701 nM

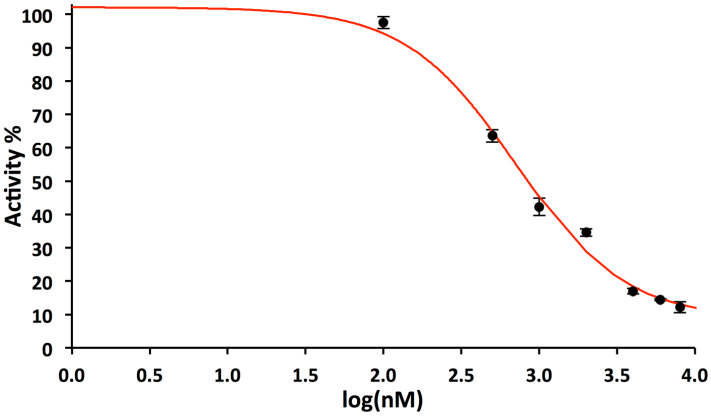

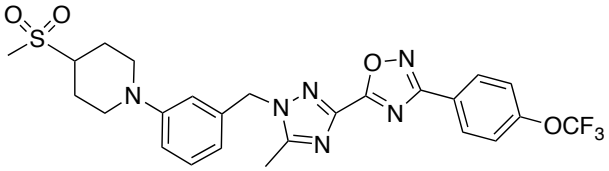

10579
IC_{50} 139 nM

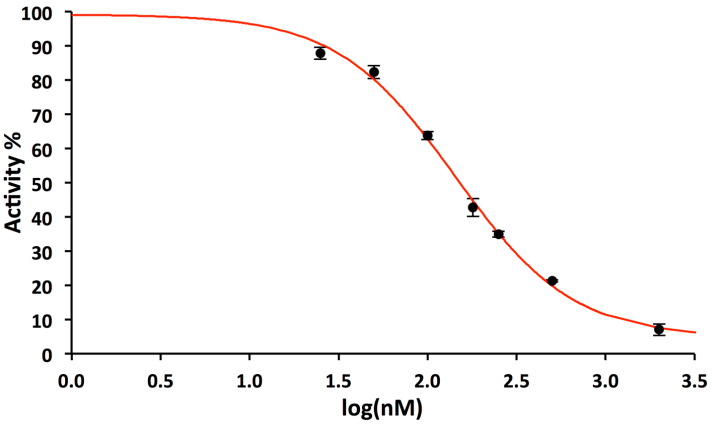

Figure 6.5. Representative dose-response curves for Anderson centre compounds. The plots show NADH:O_2 assay plots for tight (1225), moderate (10759) and poor (10576) binding compounds. Error bars are SEM of triplicates.

		NADH:O_2		NADH:dQ		
STRUCTURE	**DRUG**	**IC_{50} nM (95% C.I.)**	**HILL**	**IC_{50} nM (95% C.I.)**	**HILL**	**clogP**
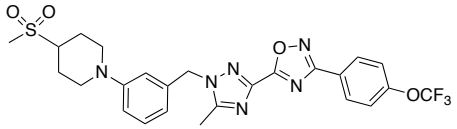	**10759**	**139 (124-155)**	**1.28**	**478 (382-599)**	**0.91**	**5.24**
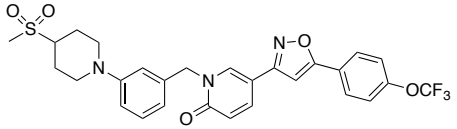	**4101**	**3.79 (3.28-4.39)**	**1.30**	**23.1 (20.2-26.3)**	**1.10**	**4.18**
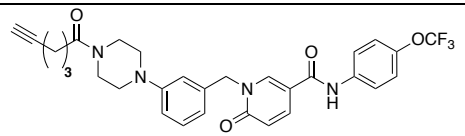	**4872**	**41.7 (33.2-52.4)**	**1.08**	**170 (128-226)**	**0.83**	**4.67**
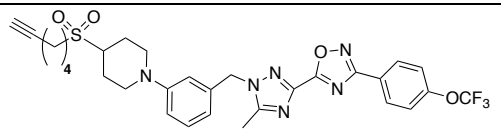	**5416**	**35.5 (30.5-41.3)**	**0.81**	**244 (201-297)**	**0.97**	**6.71**
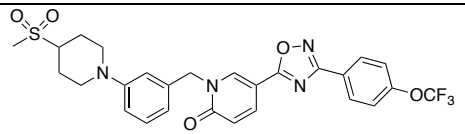	**2858**	**4.64 (4.39-4.90)**	**1.77**	**10.0 (8.69-11.5)**	**1.13**	**5.12**
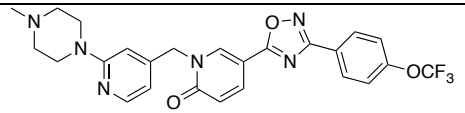	**1131**	**46.7 (43.1-50.6)**	**1.46**	**405 (332-492)**	**0.99**	**5.42**
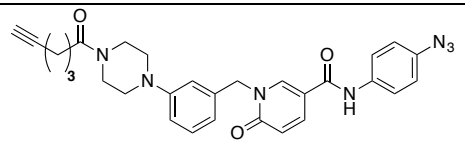	**4871**	**252 (232-273)**	**1.12**	**532 (450-627)**	**1.04**	**3.66**
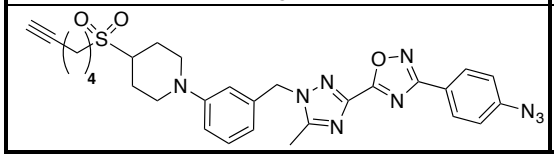	**5417**	**187 (96.6-363)**	**0.64**	**685 (527-891)**	**0.94**	**5.52**

Table 6.1. Results of SAR study on the Library A. NADH:O_2 and NADH:dQ IC_{50} values (in nM unless otherwise specified) with 95% confidence intervals, Hill coefficients and cLogP values are presented.

STRUCTURE	DRUG	IC_{50} nM (95% C.I.)	HILL	clogP
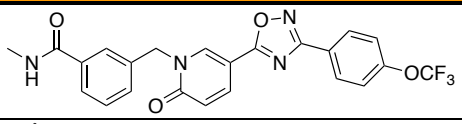	1919	1277 (569-2870)	1.00	5.01
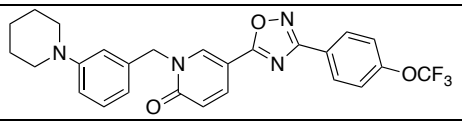	2490	20.5 (16.3-25.7)	1.05	7
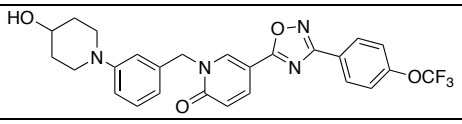	10747	16.8 (13.5-21.0)	1.01	5.54
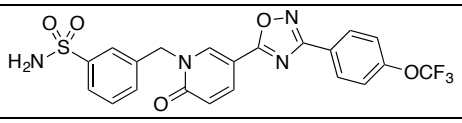	1240	840 (597-1180)	0.90	4.67
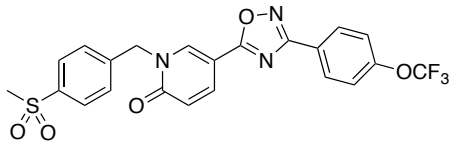	2438	Inactive	/	4.86
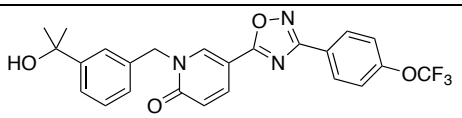	2834	82.3 (66.9-101)	1.30	5.80
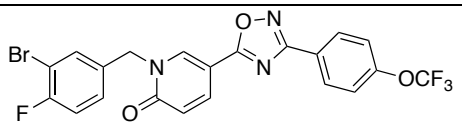	1921	806 (592-1100)	1.20	6.92
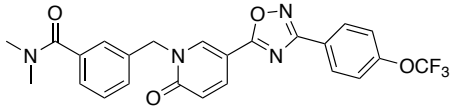	1920	404 (330-496)	1.20	5.25
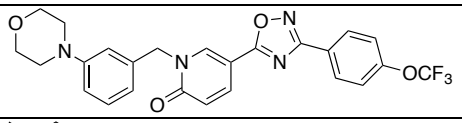	2414	83.4 (71.2-97.6)	1.01	5.91
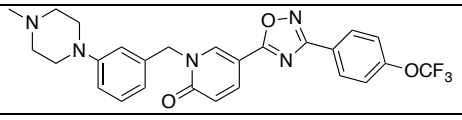	1225	13.1 (11.9-14.4)	1.15	6.03
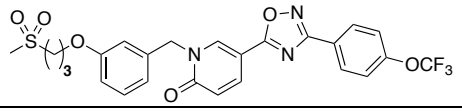	2997	14.8 (13.3-16.6)	1.09	4.65
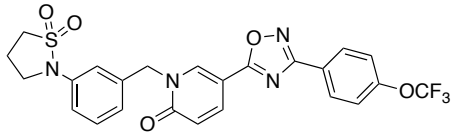	2716	13.7 (10.9-17.1)	0.95	4.81
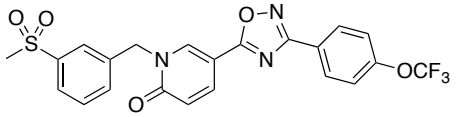	1239	666 (542-818)	1.19	4.86
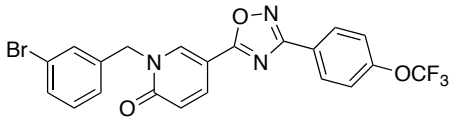	2398	821 (664-1020)	1.26	6.77

Table 6.2. Results of SAR study on the Library B – Left-hand side handles. NADH:O_2 IC_{50} values (in nM unless otherwise specified) with 95% confidence intervals, Hill coefficients and cLogP values are presented.

STRUCTURE	DRUG	IC_{50} nM (95% C.I.)	HILL	clogP
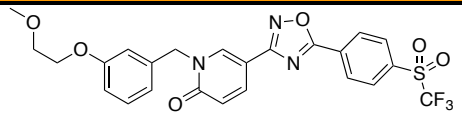	2544	1023 (372-2810)	1.07	5.13
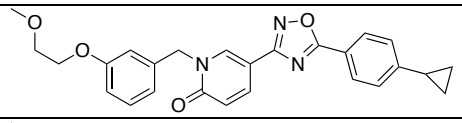	2708	395 (257-606)	1.44	4.86
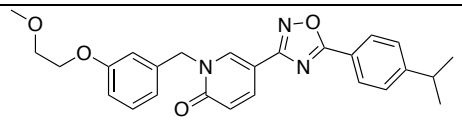	2720	262 (207-331)	1.12	5.33
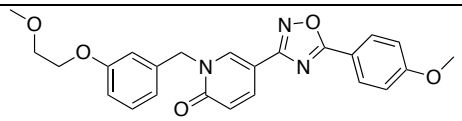	2711	674 (517-877)	1.42	3.91
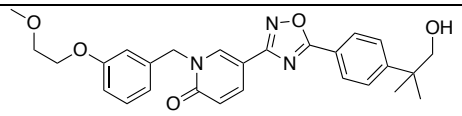	3145	~3 µM	/	4.44
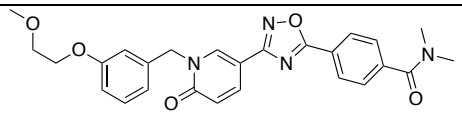	10507	~15 µM	/	3.36
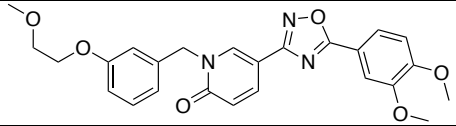	10575	~4 µM	/	3.71
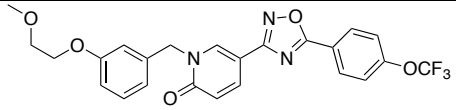	2718	299 (179-499)	0.87	5.68
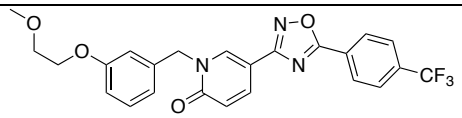	2713	639 (528-774)	1.50	4.98
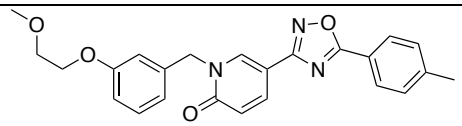	2712	1145 (935-1400)	1.48	4.61
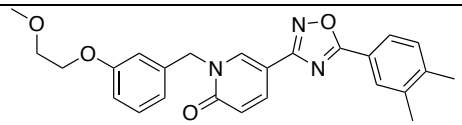	10573	1.68 (1.24-2.28) µM	0.98	5.11
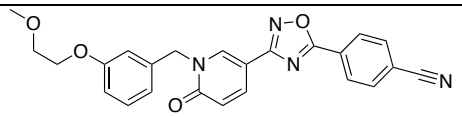	2719	~2 µM	/	3.96
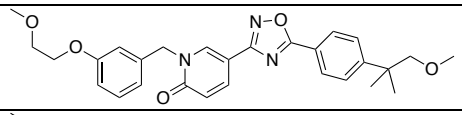	3152	912 (542-1530)	1.11	5.01
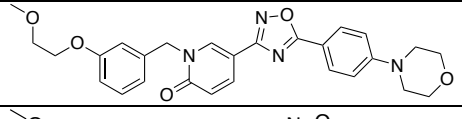	3004	660 (456-956)	1.3	4.02
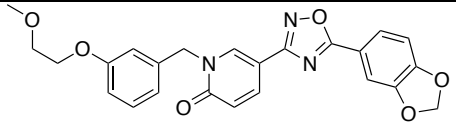	10576	701 (597-822)	1.23	3.79
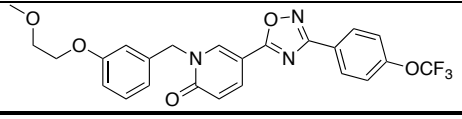	2430	72.1 (60.4-86.0)	1.46	5.68

Table 6.3. Results of SAR study on the Library B – Right-hand side handles. NADH:O_2 IC_{50} values (in nM unless otherwise specified) with 95% confidence intervals, Hill coefficients and cLogP values are presented.

6.3.3 Complex I specificity of drugs, binding site and hydrophobicity

Drugs from library A were tested to determine their specificity, binding site on complex I and level of ROS production (all assays were performed at 3x their IC_{50} in NADH:O_2 in membranes). Specificity to complex I was checked with the succinate:O_2 assay: no compounds affected the rates, indicating specificity towards complex I. The reactivity at the flavin site was tested with the NADH:FeCN and NADH:HAR assays, and no compound was found to affect these reactions. The mild stimulation of NADH:FeCN for some drugs is likely chemical in nature (this assay was found to be very prone to artefacts, see chapters 3 and 4). Lastly, ROS production (Amplex Red assay) was unaffected by all species. The overall results are summarised in Figure 6.6.

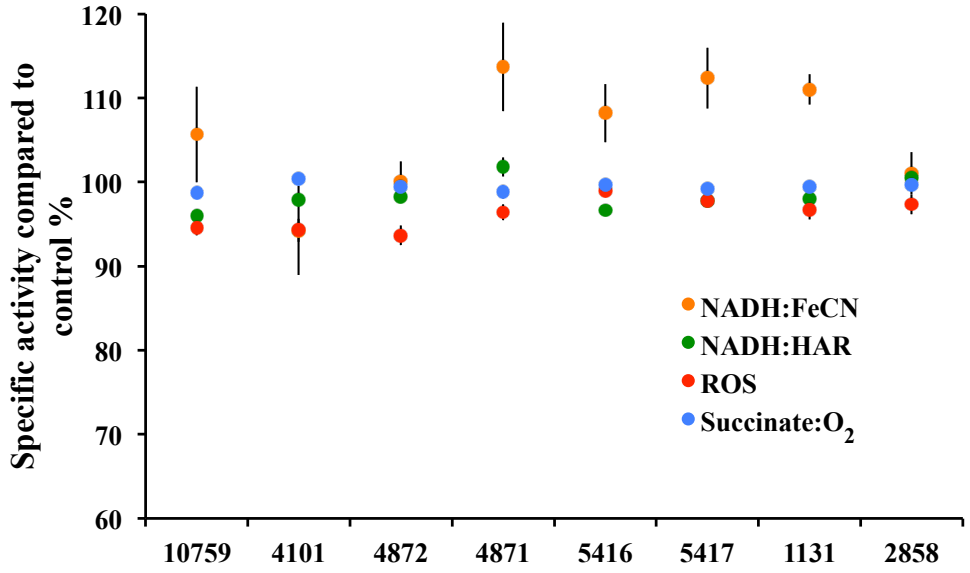

Figure 6.6. Flavin-site and succinate:O_2 reactivity of Library A. The drugs in Library A were tested at 3x their IC_{50} in the NADH:O_2 assay (see Table 6.1) to check their reactivity towards the flavin site of complex I and towards the succinate:O_2 pathway. Error bars are SEM of triplicates.

Figure 6.7 shows how lipophilicity (expressed by clogP values) correlates with inhibitory potency. The drugs are fairly hydrophobic: the average (± SEM) of clogP is 5.63 ± 0.23, 4.60 ± 0.18 and 5.07 ± 0.31 for the left-hand and the right-hand sides of Library B and Library A respectively. Similarly to the rotenoids library, a negative correlation between hydrophobicity and potency implies that the more lipophilic a drug is (higher clogP), the more potent against complex I it is (lower IC_{50}).

Surprisingly, the clogP and NADH:O_2 IC_{50} values (presented in Table 6.1, Table 6.2 and Table 6.3) correlate with each other much more in the right-hand side group than the left-hand side group (correlation coefficients of -0.563 and -0.057 respectively), and expressing the IC_{50} in logarithmic scale does not change the overall trends (-0.717 and 0.004 respectively). This suggests that hydrophobic interactions are more relevant for binding in the right-hand side of the compounds. Drugs from Library A exhibit a small correlation coefficient of -0.32 that becomes 0.01 upon logarithmic IC_{50} transformation, indicating a lack of substantial correlation.

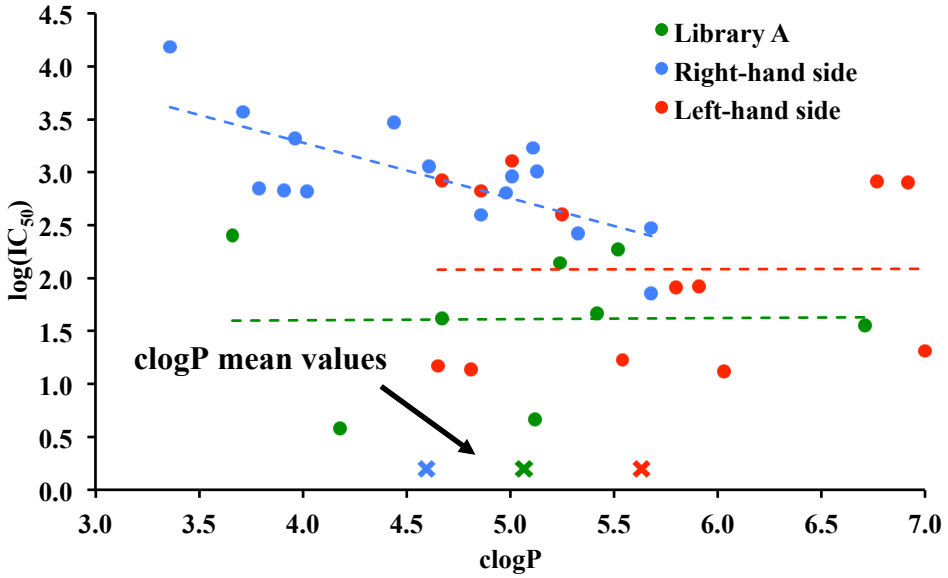

Figure 6.7. Relationship between hydrophobicity and inhibitory potency for the Anderson centre compounds. The drugs that belong to the right-hand side library are the only ones that exhibit a substantial correlation between potency and hydrophobicity. Lines are linear fits for the two variables.

6.3.4 SAR on Library A

Library A includes the only three drugs that do not possess a central oxadiazole ring and **1131** is the only species where the benzyl moiety is replaced with pyridine (see Table 6.4). Incorporation of basic nitrogen-containing aromatics to replace phenyl rings is usually performed to improve metabolic stability[564] and enhance water solubility (especially by increasing the chances of salt formation)[565] but in this case the nearby piperazine N-atom attached in *ortho* position can also play a role in both stability and solubility, given its electron withdrawing inductive effect that influences the lone pair at the pyridine nitrogen (similarly, the ammonium ion of pyridine becomes more acidic when an electron-withdrawing methoxy group is added adjacent

to the N atom in *o*-position[566]). **4101** and **2858** possess a sulfonyl group (but see also panel B in Figure 6.8): this moiety (compared to its bioisostere amide) is much more electron-withdrawing, provides a different substituent directionality (due to the sp^3 hybridisation compared to sp^2) and gives more opportunities for hydrogen bonding interactions[567].

The IC_{50} values in bovine mitochondrial membranes are summarised in Table 6.4: even though it is still possible to draw some SAR conclusions, those are more limited than the ones related to the bigger group of drugs because of the limited extent of the structural modifications that Library A encompasses. The IC_{50} for the isolated enzyme NADH:dQ are listed too: the values are well correlated with the corresponding ones for membranes, with a correlation coefficient of 0.89.

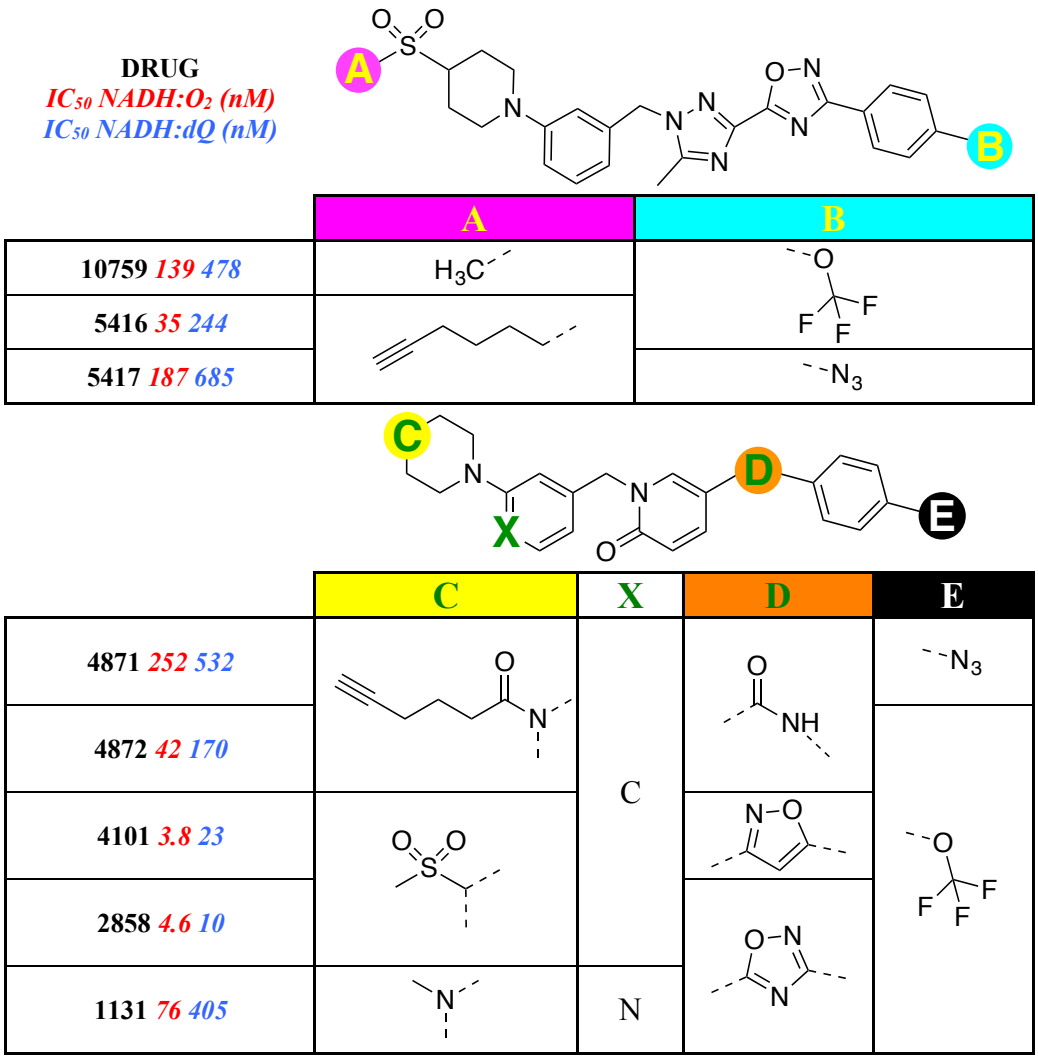

Table 6.4. Summary of SAR analysis on Library A. The 8 species can be divided into two categories depending on the different structural variables. The upper group maintains the central core throughout the series, the second group includes more variable parts. Values in nM.

4101 and **2858** are the most potent drugs and they only differ by the orientation and type of core 5-membered heterocycle (similarly to **2430** and **2718** in Figure 6.8, panel C) that does not affect their inhibitory power: the IC_{50} of **1131** is 15x higher and this is more likely due to the sulfonyl group than to the pyridine nitrogen. This is further confirmed by replacing the sulfonyl with a long-chain alkyl amide in **4872** which leads to a tenfold loss in potency (IC_{50} from 4.6 to 42 nM). Further loss in potency occurs when replacing the right-hand side OCF_3 with an azide in **4871** (IC_{50} 252 nM), which can act as a hydrogen bond acceptor[568] but in this case it only appears to provide an unfavourable binding option, just as it happens for **5416** in comparison to **5417** (from 35 to 187 nM IC_{50}): the longer left-hand side alkyl chain could reach out to a hydrophobic pocket, whereas the shorter methyl group in **10759** cannot, hence its lower potency compared to **5416**.

6.3.5 Mitochondrial membranes from different species and lead compound 10759

The Anderson Centre has turned the spotlight on drug **10759** for over 2 years now, after a medicinal chemistry campaign that included their collaboration with our group[569]. In addition to all of the above-mentioned assays (aimed at addressing specificity and potency towards complex I), a screening of how the drug interacts with mitochondrial membranes obtained from different species was performed. Drugs **4101** and **1131** were included in such screening for comparison. Table 6.5 summarises the results, with IC_{50} in nM. There are two major conclusions: firstly, these drugs have a very weak effect on bacterial and yeast complex I (the IC_{50} was only estimated given the very high drug concentration required to cause any inhibition), whereas they are very potent in mammalian tissues. Secondly, in mouse and rat systems, all the drugs display similar inhibition to each other, whereas in bovine membranes **4101** is the most potent and **10759** the weakest, with a range encompassing single to triple nanomolar digits. It appears, therefore, that bovine mitochondrial complex I possesses additional features (compared to its mouse and rat counterpart) that prevent optimal binding of **10759**. This interesting capacity of **10759** to elicit significantly different responses in complex I from different mammalian species makes it a candidate probe for identifying structural differences in different mammalian enzymes. Such a different inhibition across mammalian species has not been observed yet.

Bacterial and yeast complex I are less sensitive towards rotenone and piericidin than their corresponding bovine counterparts. The IC_{50} for *Paracoccus denitrificans* was reported to be 170 nM for rotenone and 100 nM for piericidin in the isolated enzyme for NADH:dQ[570] and between 500 and 600 nM for rotenone in mitochondrial membranes from *Yarrowia lipolytica*[571,572]. In bovine membranes IC_{50} values for rotenone and piericidin are about 8 and 5 nM respectively. Furthermore, affinities measured for rotenone in *Paracoccus denitrificans* and *Rhodobacter capsulatus* vesicles were 500 and 150 times lower (higher K_i) than bovine heart SMPs[573].

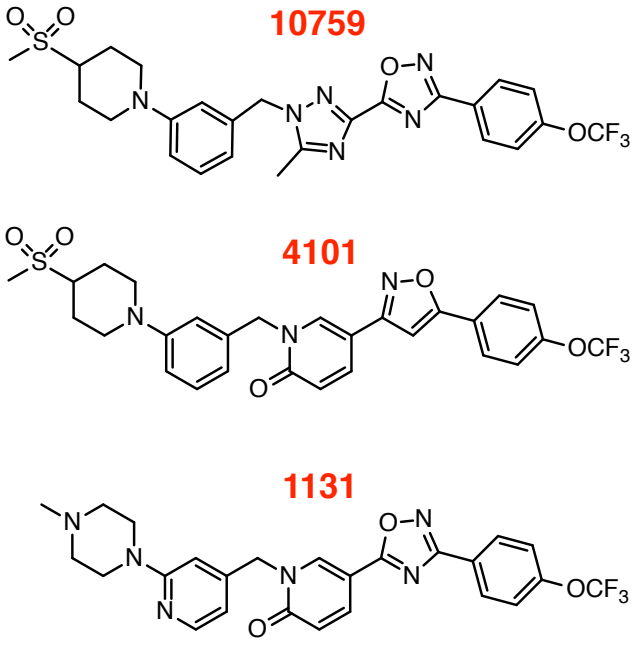

IC_{50} nM		
10759	**4101**	**1131**
NADH:dQ isolated enzyme		
Heart Bovine		
478	23	405
NADH:O_2 membranes		
Heart Bovine		
139	3.8	46.7
Mouse		
Kidney		
10.8	3.9	6.3
Heart		
9.3	2.8	4.7
	Brain	
	2.9	
	Liver	
	3.4	
Rat Heart		
6.5	4.3	
Yarrowia		
> 10 µM	> 1 µM	
Paracoccus		
> 10 µM	> 10 µM	

Table 6.5. Mitochondrial membranes interspecies screening. Three drugs were tested on mitochondrial membranes from different bacterial and mammalian species. While bacterial membranes are not affected by the drugs, rat and mouse membranes from different tissues are equally sensitive to them. In bovine membranes the compounds cause a different response. IC_{50} in nM unless otherwise stated.

There are several examples of enzymes that respond differently to inhibitors depending on the species expressing them. Winkler *et al.*[574] recently found that Kynurenine 3-monooxygenase (KMO) isolated from liver tolerates the inhibitor Ro-61-8048 over a 25-fold range among species, from rat to human all the way to cynomolgus monkey (6, 35 and 150 nM IC_{50} respectively). Remarkably, the K_m for

the substrate L-kynurenine was similar among the six mammalian species tested (13.7 ± 0.9 μM). Chang *et al.*[575] recently showed that the monoacylglycerol lipase (MAGL) inhibitor O-aryl carbamate JZL184 possesses single digit IC_{50} potency towards mouse brain and human kidney enzymes whereas O-hexafluoroisopropyl carbamate JW618, while still maintaining its potency towards the human enzyme, is over ten times weaker towards the mouse enzyme (both inhibitors exhibit three digit IC_{50} towards the corresponding rat enzymes).

6.3.6 SAR on Library B: 30 compounds and left- vs right-hand side handles

23 drugs possess an OCF_3 moiety which is generally adopted as a methyl replacement: the fluorine atoms achieve better metabolic stability and higher electronegativity[576]. Also, deshielded fluorine atoms (*i.e.* those with decreased electron density) are known to engage as lone pair donors in unconventional F · · · C=O intermolecular interactions[577]. The central oxadiazole ring is common to 35 out of 38 drugs and, as a functional group in medicinal chemistry, it is of considerable importance: interestingly, a 1,2,4-ring system was chosen for most of the drugs in both libraries, even though a 1,3,4-isomer usually imparts superior pharmacological properties, such as less lipophilicity, improved aqueous stability, reduced inhibition of hERG potassium ion channel (a typical unwanted side effect of lipophilic species) and improved metabolic (especially CYP-mediated) stability, on account of the more favourable nitrogen-based hydrogen bond acceptors and stronger dipole moment[578]. Indeed, doubly-substituted (3,5) 1,2,4-oxadiazoles sytems are known for their anti-proliferative effect against several cancer cell lines[579,580]. The floppy methoxyethoxy extension (the constant moiety in the right-hand side), included in 15 drugs, is commonly employed as a water solubilising agent, notably in the case of the anticancer agent Erlotinib[581] but it can also provide strategic hydrogen bond acceptor capabilities[582].

6.3.6.1 The left-hand side drugs

The left-hand side compounds are depicted in Figure 6.8, split into 4 different panels according to structural similarities (**2718** will also be included in Figure 6.9, panel G, for comparison purposes). Directionality of the core oxadiazole ring has an effect on

complex I inhibition: in panel C, changing the orientation of the oxygen from left (**2430**) to right (**2718**) is detrimental to the potency, from 72.1 to 299 nM.

6-membered saturated heterocycles, depicted in panel A, exhibited excellent inhibitory activity. The most marked difference occurs when oxygen belongs to the ring in **2414** (83 nM) as opposed to when it sticks out in *para* position as an hydroxyl group in **10747** (16.8 nM): there appears to be unfavourable binding interactions with the ring oxygen, given that the hydroxyl species has a very similar IC_{50} to the other two nitrogen-containing heterocycles **2490** and **1225**.

In panel B, different flavours of sulfonyl groups are presented, and the most notable finding is the major difference in potency between sulfonyl-containing substituents **1239** and **1240** compared to **2716**, a cyclic sulphonamide or sultam: sultams are usually installed in order to reduce the number of rotatable bonds and, therefore, to increase their oral bioavailability[583]. The shift of the methyl sulfonyl group further away with a 3-carbon long linker in **2997** (the same length as **2716**) makes little difference in activity (about 14 nM for both): these results suggest that the sulfonyl group is involved in a key binding interaction which is favoured by another hydrophobic interaction linked to the alkyl chain in **2716** (**2997** could obtain the same conformation as **2716** on account of its flexible chain).

Compounds in panel D display a wide range of moderate activity: addition of a methyl group to the amide (from **1919** to **1920**) improves the IC_{50} threefold, suggesting a favourable hydrophobic interaction, whereas the ^{i}PrOH handle **2834** allows to improve the inhibitory activity a further fivefold compared to **1920**. Lastly, the halogenated aryl **2398** seems to be a poor substituent and even though fluorobenzyl moieties could engage in C-H π interactions[584], the potency improvement following the addition of fluorine in *para*- position obtaining **1921** (to the bromine already present in *meta*- position in **2398**) is so minor that could well be within experimental error.

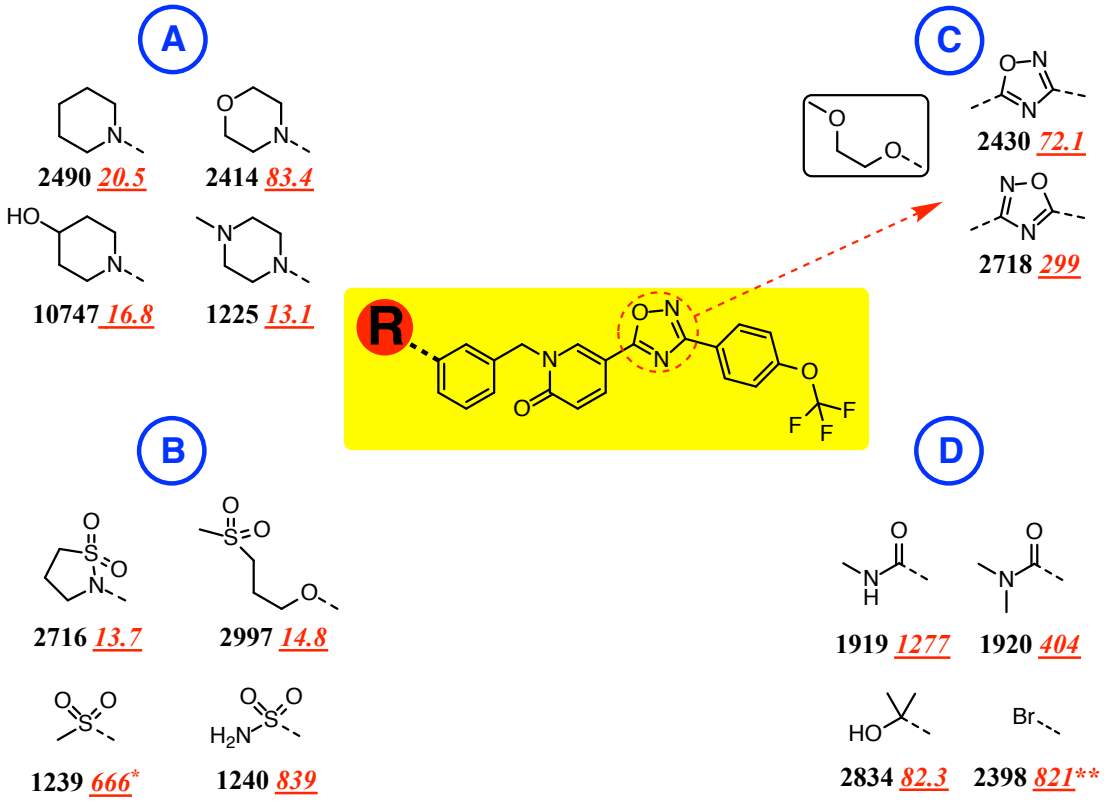

* when in para- position (2438), IC_{50} becomes inactive
** 806 when fluorine is added in *para* position together with bromine in *meta* position (1921)

Figure 6.8. The left-hand side group of Library B. 16 compounds are divided into 4 groups according to similarities between the moieties attached to the far left side of the scaffold. Panel A includes the most powerful species, 6-membered saturated heterocycles; Panel B includes sulfonyl containing groups; Panel C shows the effect of a different alignment of the central oxadiazole core; Panel D includes amides, a halogen and a hydroxy groups. IC_{50} in nM (unless otherwise stated) in underlined red.

6.3.6.2 The right-hand side drugs

All of the species in this group (depicted in Figure 6.9 and split into 4 different panels) exhibit only hundreds of nanomolar potency at best: it appears, therefore, that the methoxyethoxy handle is a poor choice for a substituent overall and the OCF_3 handle is better. In addition, some solubility issues were encountered in the NADH:O_2 assay, particularly with compounds containing aliphatic side chain substituents **2708**, **2720** and **10573**: when the drug concentration was higher than midrange in the titration series the 340-380 nm absorbance descending traces were very erratic (the R^2 was close to 0.9). This may be because of precipitation, however the data obtained are reliable since the rates refer to the initial linear region of the traces.

In panel G, three different ways of arranging the CF_3 group are presented: the oxygen atom introduced in **2713** to yield **2718** leads to a two fold improvement (from 639 to 299 nM), perhaps due to the more extended range of circular motion of the fluorines which could be partially prevented by the oxygens of the sulfonyl in **2544** (hence explaining the higher IC_{50} of 1023 nM). The electron withdrawing capability of **2544** might not be relevant to explain its low activity, unless the disturbance of the nearby phenyl π-cloud by the sulfonyl disrupt a key π-π interaction with aryl-containing residues in the pocket.

Panel H includes relatively heterogeneous handles, the most effective of which are **3004** and **2711**, both slightly higher than 650 nM: since they do not bear structural similarity with each other it could be concluded that the other 4 species disrupt binding interactions that morpholine and methyl ether do not otherwise affect. The amide in **10507** is absolutely detrimental to the potency (about 15 μM IC_{50}), possibly due to a steric clash of the two methyl groups. The slightly longer chain in **3152** than **3145** could reach an enzyme cavity which could provide some sort of binding relief (2947 and 912 nM respectively).

In panel E the methylenedioxy substituent renders **10576** over 5x more active than the corresponding 3,4-dimethoxy **10575**, possibily because the suitable configuration for proper binding is held in place[585]: interestingly, this moiety is common to a number of recreational drugs, *e.g.* MDMA, Ethylone and MDPV[586]. In some cases, it does not matter whether the ring possesses a methylenedioxy (closed) or dimethoxy (open) configuration, because the relevant hydrophobic interactions occur exclusively at the benzene moiety[587].

Panel F includes species with different aliphatic side chains attached to a benzene scaffold, and the ones where such tail extends two carbons away (**2720** and **2708**) are more potent than the ones where it extends less further in space (**2712** and **10573**): such intriguing spatial feature shifts the range from triple to quadruple digit nanomolar potency.

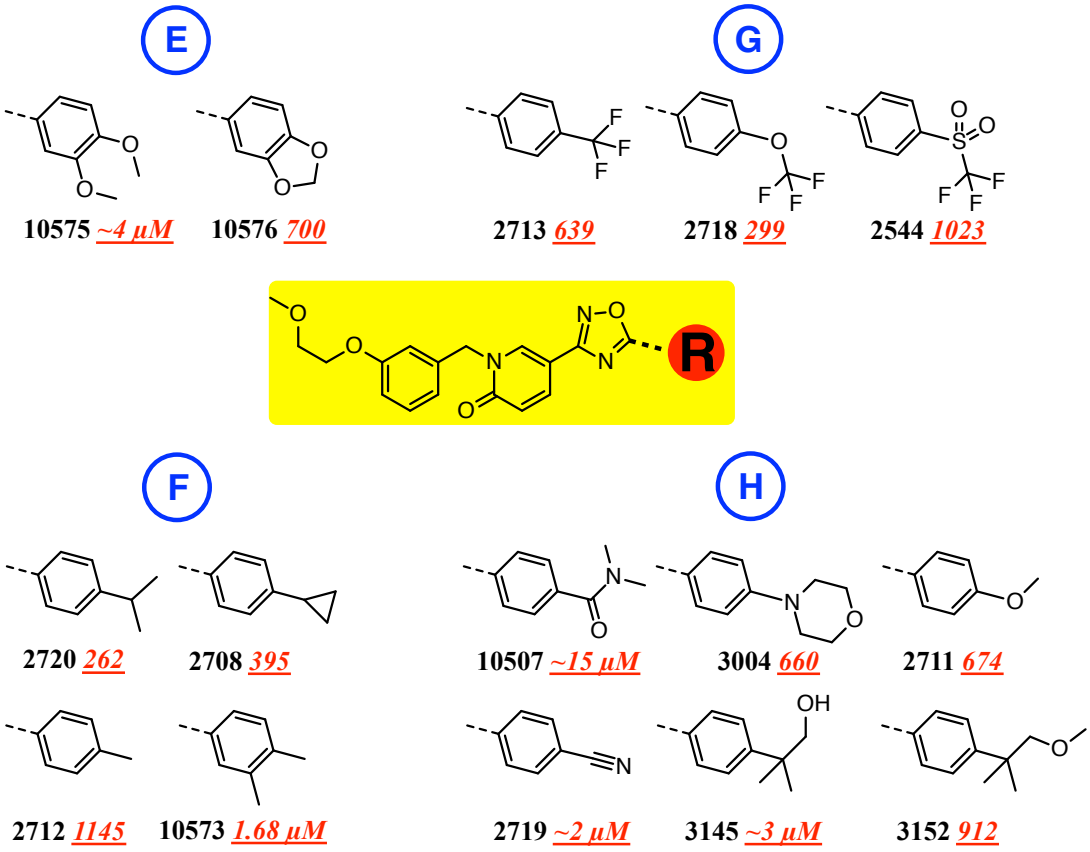

Figure 6.9. The right-hand side group of the Library B. 15 compounds are divided into 4 groups according to similarities between the moieties attached to the far right side of the scaffold. Panel E includes two different types of methoxy attachement to a benzene ring; Panel F aliphatic side chains; Panel G different CF_3 extensions; Panel H diverse O- and N-containing groups. IC_{50} in nM in underlined red.

Figure 6.10 summarises the main findings for library B.

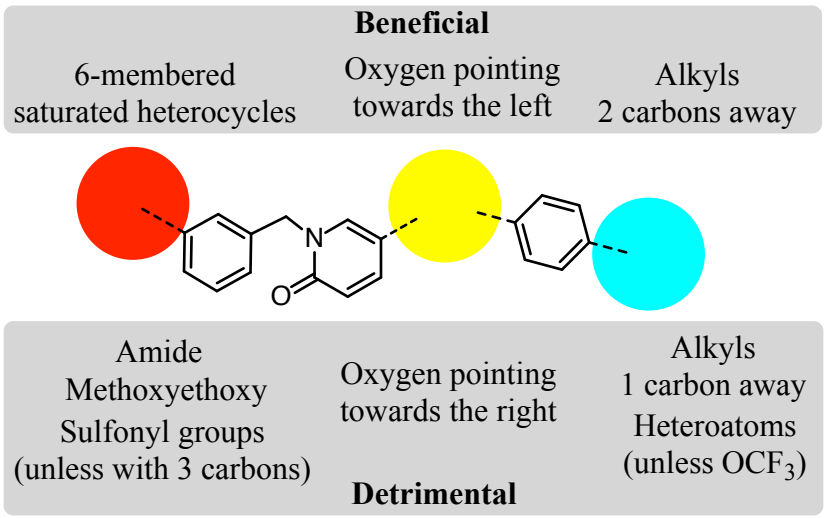

Figure 6.10. Effects of different substituents in the main structural variants in library B. Different substituents on either side plus directionality of the oxygen in the central oxadiazole ring are the handles changing throughout library B.

6.4 A collaboration with the Leicester MRC Toxicology Unit: Mubritinib

The collaboration with the Leicester MRC Toxicology Unit involved testing Mubritinib, an anti-cancer agent under development by the Japanese pharmaceutical company Takeda. At the moment the major drawback to Mubritinib transitioning to a Phase II clinical trial is its toxicity encountered in Phase I and this work aimed to confirm complex I inhibition as its off-target effect resulting in toxicity, as suggested by Seahorse assays in permeabilised cells performed by the Toxicology Unit. In addition, 12 structural variants were tested in bovine mitochondrial membranes for complex I inhibition to gain insight into the SAR of Mubritinib binding to complex I. This information could allow the development of a compound with reduced toxicity.

6.4.1 Mubritinib and its biological target HER2

The HER (human epidermal growth factor receptor or ErbB) family of proteins consists of four receptor tyrosine kinases (HER 1-4) that possess an extracellular domain, a small transmembrane region and an intracellular domain. Binding of growth factors in the extracellular region (apart from HER 2 which does not bind ligands) initiates downstream signalling pathways and also homo- and hetero-dimeric interactions between family members[588]. Activation of HER signalling leads to a wide range of cellular effects, including cell proliferation and survival, angiogenesis, cell adhesion, cell motility, development and organogenesis[589]. HER2 in particular has a strong oncogenic potential, since it is overexpressed across a remarkably large subset of cancers (especially gastric, breast, bladder and ovarian); its pro-tumorigenic signalling cascade makes HER2 an attractive therapeutic target[590].

Mubritinib (or TAK-165) is being developed by the pharmaceutical company Takeda and a phase I clinical trial study was completed in 2004[591]. It is structurally similar to the Anderson Centre drugs: two phenyl ring on either side of a relatively long scaffold and a central 5-membered heterocyclic ring (see Figure 6.1). Pre-clinical studies found it inhibits HER 2 specifically (greater than 4000-fold selectivity compared to other 6 tyrosine kinases) and also possesses antiproliferative effects on four different cancer cell lines (IC_{50} referred to growth of cell numbers in tens of nM) and in xenograft tumor models using two different cell lines in mice[592]. Furthermore, in a

recent paper, Mubritinib was successfully used in combination with all-trans retinoic acid in differentiation therapy against acute myeloid leukemia[593].

6.4.2 Main experimental details and overall results

Inhibition of the NADH:O_2 oxidoreduction reaction in membranes was performed with the library of variants and IC_{50} values (with 95% confidence interval), Hill coefficients and clogP values were obtained (reported in Table 6.6). clogP values were determined with MarvinSketch Version 16.5.2.0 (Consensus Model, ChemAxon, MA[529]). The IC_{50} determination process was exactly the same as the one used in the rotenoids SAR chapter. Also, species whose IC_{50} was higher than 20 μM were considered inactive. It was not possible to obtain IC_{50} values for all variants because some had high (minimum reachable) levels of residual activity even at the highest concentrations tested and such minimum levels were reached very early along the titration series (differently than the inactive species where a minimum level of residual activity could not be reached because the compound concentration needed would have been too high). Table 6.6 therefore includes the background NADH oxidation activity at the highest concentration tested for all the variants and highlights in red the variants whose lowest attainable residual activity was so high as to preclude an IC_{50} determination. NADH:O_2 inhibition traces for Mubritinib and variant **C** are shown in Figure 6.11 and the substantial background rate can be seen for the latter (this is similar to variants **D** and **K**): such rate can be abolished by rotenone or piericidin.

A residual percentage rate in the succinate:O_2 assay of 97.3 ± 1.0 % and in the NADH:dQ assay of 7.3 ± 0.2 % were observed upon addition of 500 nM of Mubritinib, indicating specificity towards complex I (data refers to SEM of triplicates). The same concentration of Mubritinib left a residual activity of 96.2 ± 0.6 % and 101.0 ± 4.5 % in the NADH:APAD and NADH:FeCN assays, respectively, confirming that the location of binding is outside the flavin site (data refers to SEM of triplicates).

The inhibitory potency of the drugs does not correlate with hydrophobicity, as it can be seen in the (log) IC_{50} against clogP plot (Figure 6.11, lower panel). The correlation coefficient between IC_{50} and clogP is -0.11, which becomes -0.33 upon IC_{50} logarithmic transformation.

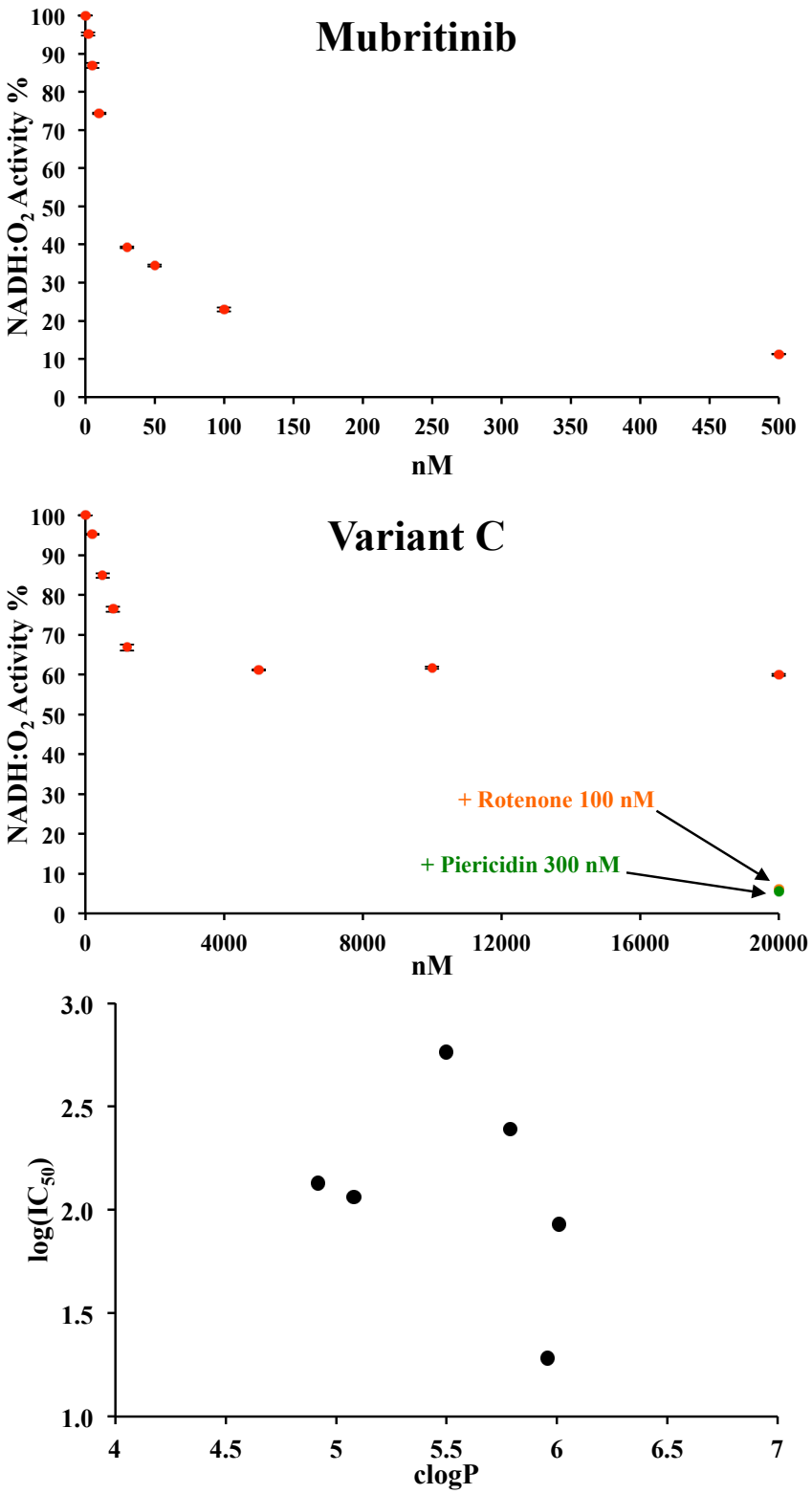

Figure 6.11. Representative NADH:O_2 inhibition traces for Mubritinib variants and relationship between hydrophobicity and inhibitory potency. While Mubritinib (upper panel) exhibits a typical descending trace to a low residual activity at high drug concentration, variant C (middle panel) maintains a very high NADH oxidation background rate regardless of the concentration used: such background rate is rotenone and piericidin sensitive. Error bars are SEM of triplicates. Lastly (lower panel) the inhibitory potency is not correlated with hydrophobicity.

STRUCTURE	IC_{50} nM 95% C.I.	HILL	Lowest Res. Act. (%, nM)	clogP	STRUCTURE	IC_{50} nM 95% C.I.	HILL	Lowest Res. Act. (%, nM)	clogP
 MUBRITINIB	19.1 17.1-21.3	-1.26	11.2 ± 0.1% 500 nM	5.96	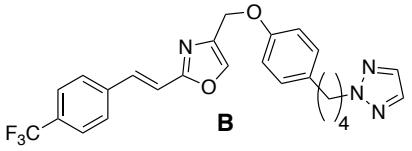 B	Inactive	/	75.4 ± 0.2% 50 µM	5.66
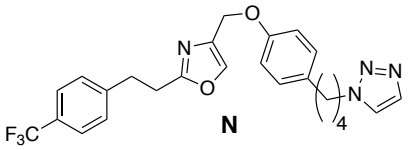 N	247 187-325	-1.2	8.3 ± 0.2% 5 µM	5.79	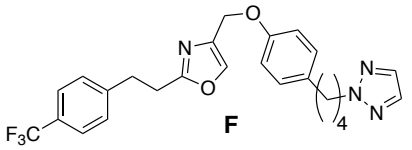 F	582 555-611	-1.1	10.7 ± 0.2% 5 µM	5.50
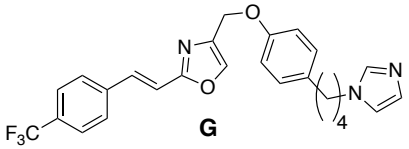 G	85 79.6-90.2	-1.50	9.2 ± 0.3% 400 nM	6.01	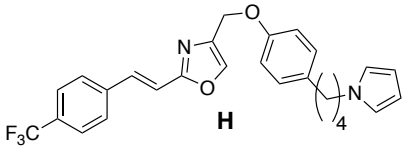 H	Inactive	/	91.1 ± 0.1% 8 µM	7.21
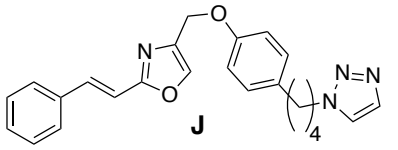 J	116 102-132	-1.14	13.9 ± 0.1% 500 nM	5.08	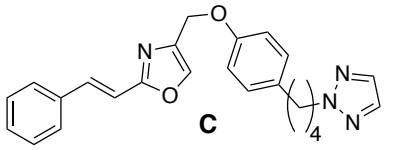 C	/	/	60.0 ± 0.2% 20 µM	4.78
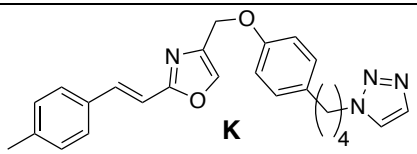 K	/	/	25.7 ± 0.3% 1 µM	5.59	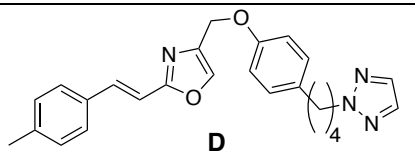 D	/	/	82.2 ± 0.5% 5 µM	5.30
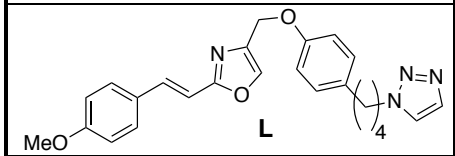 L	135 117-156	-1.19	17.2 ± 0.3% 3 µM	4.92	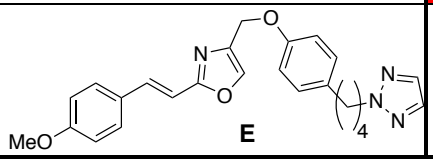 E	Inactive	/	71.8 ± 0.7% 50 µM	4.63
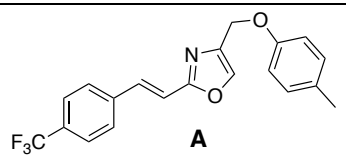 A	Inactive	/	97.0 ± 0.2% 15 µM	5.52					

Table 6.6. Results of SAR study for Mubritinib variants. IC_{50} values (in nM unless otherwise specified) with 95% confidence intervals, Hill coefficients, lowest residual activity attainable with associated concentration and clogP values are presented for the NADH:O_2 assay. Compounds highlighted in red possess the lowest residual activity attainable (and reached very early along the titration series). Similar compounds that only differ by their right-hand side ring are presented in the same rows.

6.4.3 SAR on Mubritinib library

The three different handles that vary across the Mubritinib series are displayed in Table 6.7. Most of this series is based on modification or substitution of the triazole group: this moiety has been employed towards a plethora of different biological targets (*e.g.* ß-lactamase, fatty acid synthase, cyclooxygenase) and properties (*e.g.* antibacterial, antifungal, antiviral, anticonvulsants, anticaspase-3)[594]. In addition, they are commonly employed as bioisosteres of amide groups (they join similar hydrogen bond patterns) and possess good resistance to metabolic degradation, high aromatic stabilisation and a high dipole moment[595]. Figure 6.12 shows the different types of H-bond interactions that 1H-1,2,3-triazole (attached at the peripheral nitrogen, Mubritinib) and 2H-1,2,3-triazole (attached at the central nitrogen, **B**) can undergo plus the similarities with an amide group (however, technically a H-bond donor group should have the hydrogen atoms bonded to an electronegative atom).

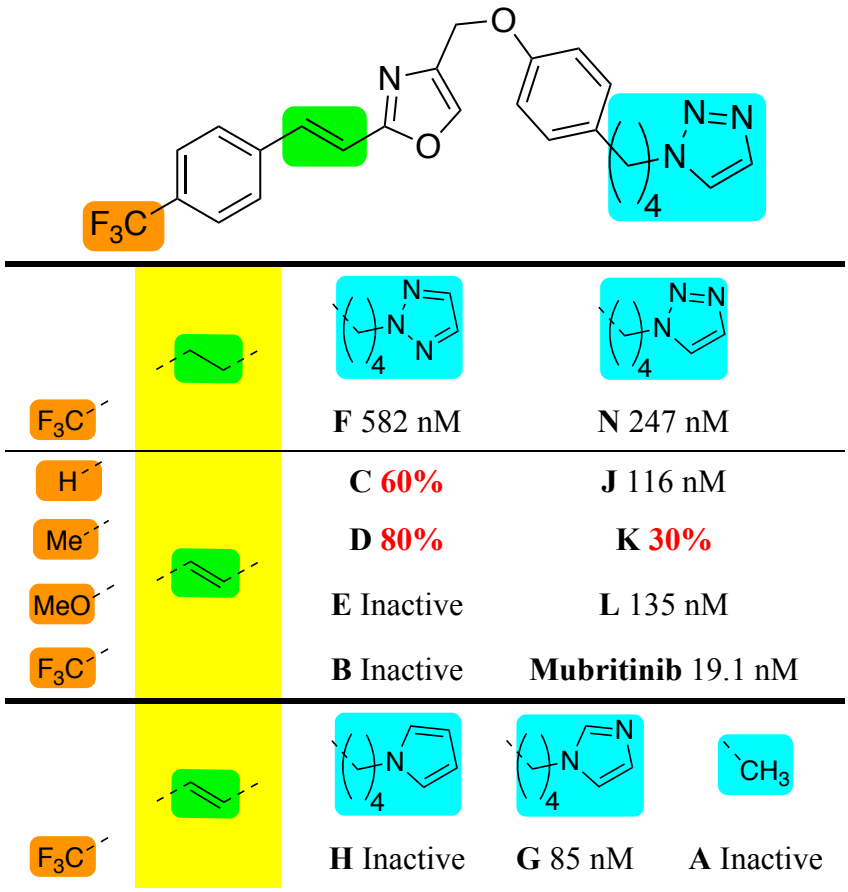

Table 6.7. Summary of SAR study on Mubritinib variants. The three structural handles that vary across the series are highlighted with different colours in the table. IC_{50} in nM unless otherwise stated. Lowest residual NADH:O_2 activity is highlighted in red.

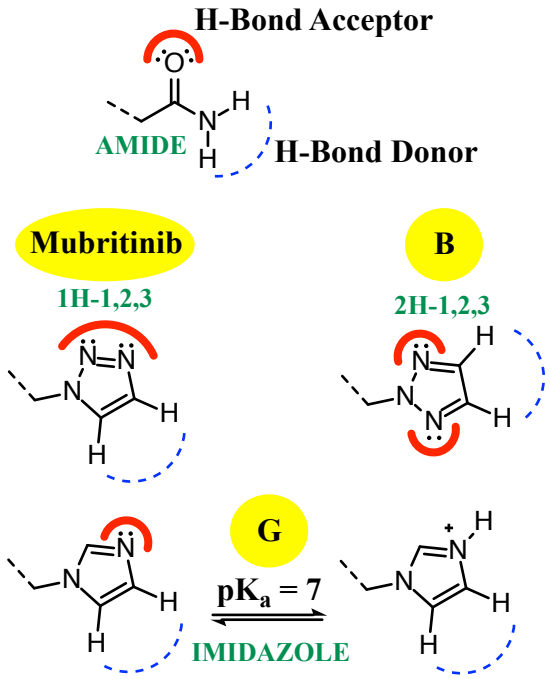

Figure 6.12. Hydrogen bond interactions of the main rings within the Mubritinib series. The hydrogen bond pattern of the heterocycles used as right-hand side handles within the Mubritinib series is similar to the one in an amide. These interactions seem to be responsible for the vast majority of Mubritinib binding to complex I.

The main finding is that a different point of attachment of the triazole moiety significantly alters the binding affinity of the variant: triazole is attached to Mubritinib as 1H-, and the shift from 1H- to 2H- in **B** generates an impressive loss of potency (IC_{50} from 19 nM to inactive) which also occurs throughout the series (upper part of Table 6.7), most of the variants on the left column possess a much poorer binding affinity compared to the variants on the right). Mubritinib binding appears to be based on the hydrogen bond interaction generated by the side nitrogen atom in the ring: the modest loss of potency upon rendering the triazole into an imidazole in **G** (from 19 nM to 85 nM) and the dramatic loss in potency upon eliminating the side nitrogen in **H** confirm this interpretation. It must be highlighted, however, that while the pK_a of 1,2,3-triazoles is about 1.17 (hence the molecule is present in non-ionised form in aqueous solution), the pK_a of imidazole is 7.00, so in physiological conditions the latter is present in ionised form in significant amount[596]: a still favourable electrostatic interaction with the ionised form of imidazole (that could be directed at a different part of the binding site than the non-ionised H-bond interaction, given their opposite charge) can explain the mild (as opposed to strong) drop in potency from

Mubritinib to **G** (or, more simply, the pH dependent equilibrium favours the non-ionised side).

The loss of the central double bond is also important for binding and, more remarkably, the decreased potency from 1H- to 2H-triazole is not as substantial as with the double bond (**N** and **F**, 247 and 582 nM IC_{50} respectively): the hydrogenation of the C=C double bond, present in Mubritinib, allows rotational motion around it and, consequently, extended binding opportunities. Mubritinib is less sensitive towards modifications in the CF_3 group, causing only a 10-fold loss of potency when such group is exchanged for methoxy or just hydrogen (**L** and **J**). Finally, it is noteworthy how complex I activity is retained with some variants (**C**, **D** and **K**) regardless of the concentration used: it is possible that a concentration-independent enzymatic conformational rearrangement upon binding of **C**, **D** and **K** to complex I partially impedes ubiquinone access to the ubiquinone binding site.

6.5 Discussion

6.5.1 Molecular flexibility as rationale for binding?

It is difficult to accurately predict the precise binding interactions for drugs in complex enzymes: this is particularly true for compounds in Libraries A and B which can be thought of as a string of individual units that possess the ability to rotate about each other and, as such, are very flexible overall (see Figure 6.3). For other complex I specific inhibitors, addressing binding interactions within the binding site may turn out to be easier. For instance, amino quinazolines are powerful complex I specific inhibitors[520,597] and their binding site was located between the 49 kDa and ND1 subunits[598]. There are several examples of amino quinazolines whose major enzymatic binding interaction is hydrogen bonding with the amino acid backbone of methionine residues: inhibitors of tyrosine kinases EGFR[599, 600] and Trk[601]. Remarkably, a quinazoline inhibitor was resolved close to Met60 of PSST and the 49 kDa subunit of complex I from *Yarrowia lipolytica*[86]. Since the kind of molecular flexibility of the Anderson drugs is not dissimilar from coenzyme Q_{10} (which also can be thought of as a string of individual units), this common structural feature between substrate and drugs could extend to their mode of binding inside or in the proximity of the Q chamber (recall that evidence suggested ND1 as the **10759** binding site, see

section 6.2.1.2). These species could, in fact, be capable of interacting with adjacent residues through the consecutive units that constitute them.

6.5.2 Putative binding location of 10759

The difference in potency across different mammalian species that the three compounds shown in Table 6.5 exert can be explained by the 2-pyridone core moiety: **10759** does not possess this functional group but a triazole instead (see Figure 6.13), and its potency is significantly lower than the other two drugs in bovine (but not mouse and rat) complex I. 2-pyridones are known to be very versatile, as they can assume several binding poses within binding sites: van der Waals interactions with the ring core[602], hydrogen bonding with C=O on its own[603] and in association with the adjacent nitrogen[604]. An inhibitor of factor Xa, a trypsin-like serine protease, was found to engage in binding with a peculiar arrangement where its 2-pyridone moiety was enveloped within an aromatic pocket of the enzyme (sandwiched between tyrosine and phenylalanine and forming an edge-to-face interaction with tryptophan)[605]. Since the 2-pyridone core of compounds **4101** and **1131** (Table 6.5) is flanked by aromatic rings (and replaced by another aromatic ring in **10759**) it was thought that an aromatic nest (akin to the one mentioned above) could be the key to understanding the binding differences found for complex I across different mammalian species. One tentative location could be I49 in bovine ND1, F49 in rat, mouse and human complex I (see Figure 6.13, sequence identities for ND1 are 78.3% in bovine-mouse, 92.7% in rat-mouse and 75.5% in bovine-rat-mouse, sequence and identity calculations obtained from UniProt database[606]). So, the 2-pyridone moiety (and its nearby benzene ring) in mouse and rat complex I could preferentially bind in this area of ND1 on account of the aromatic nest provided by F49 and F19 (the latter conserved in bovine, mouse and rat) via noncovalent aromatic interactions, which can be decisive in biochemical systems[607]. Replacing 2-pyridone with triazole (**4101** vs **10759**) and benzene with pyridine (**4101** vs **1131**) does not elicit major losses in potency in mouse and rat tissues (see Table 6.5 and Figure 6.13). On the other hand, in bovine complex I such aromatic nest is disrupted (I49 instead of F49) and the same drug transformations (replacing 2-pyridone with triazole and benzene with pyridine) lead to significant potency losses: a replacement of a carbon with nitrogen in benzene leads to reduced polarizability and spatial extent of the π-electron cloud that have major consequences in terms of binding strengths and modes[608]. There are other

aromatic residues in the vicinity of F19 and F(I)49 (all conserved in bovine, mouse, rat and human complex I) that could be a part of the above-mentioned aromatic nest: Y43, F224 and Y228. The close proximity of this area to the membrane portion of the ubiquinone binding channel (see Figure 6.13) raises the possibility that the drug could compete for the Q-site and makes it a good candidate for cryo-EM studies.

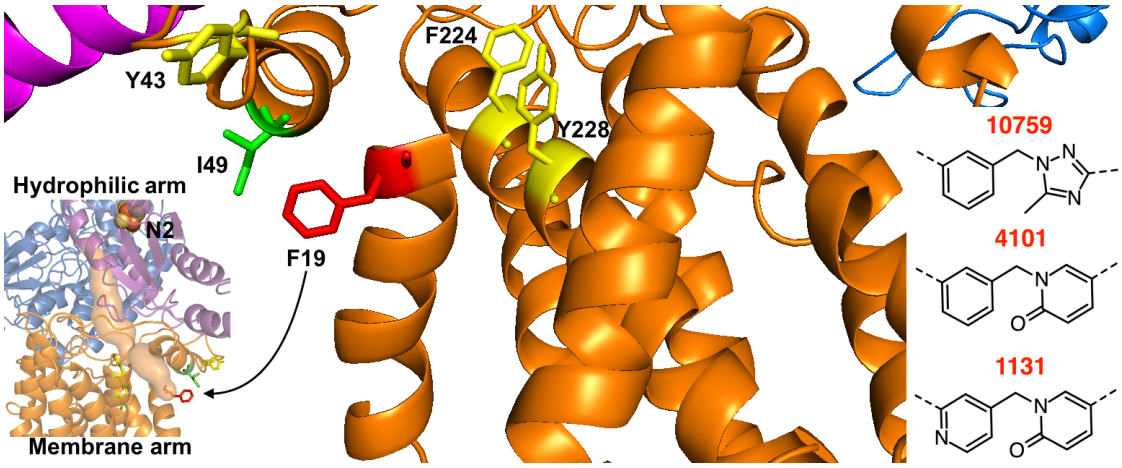

Figure 6.13. Tentative location of 10759 binding site in complex I. Complex I from Bos taurus, colour code 49 kDa (blue), PSST (magenta) and ND1 (orange). F19 residue in red, Y43, F224 and Y228 in yellow (all of these residues are present in human, bovine, mouse and rat complex I). I49 residue (bovine, F49 in human, mouse and rat) highlighted in green. Some of the helix F19 belongs to was hidden for clarity. Relevant aromatic centres of drugs 10759, 4101 and 1131 (bottom right corner) and ubiquinone binding channel (bottom left corner) are highlighted. Original structure from Hirst[86].

6.5.3 Cancer pharmacology of 10759 and Mubritinib families of drugs

A recent SAR study by Sheng *et al.* on the *in vitro* and *in vivo* inhibition of HIF-1-mediated transcription in human colon carcinoma cell line HCT-116 and of tumor cell invasion in ovarian cancer cells SKOV3 reached similar conclusions to Library B in this work and Bayer's library[609]: long handles in the left-hand and replacement of CF_3 with OCF_3 moiety in the right-hand side generated the highest potencies (similarly to **2713** and **2718**). The compounds in the study were 3-aryl-5-indazole-1,2,4-oxadiazole derivatives, with indazole replacing 2-pyridone within the oxadiazole core: Figure 6.14 shows the main features of the strongest inhibitors found in the study.

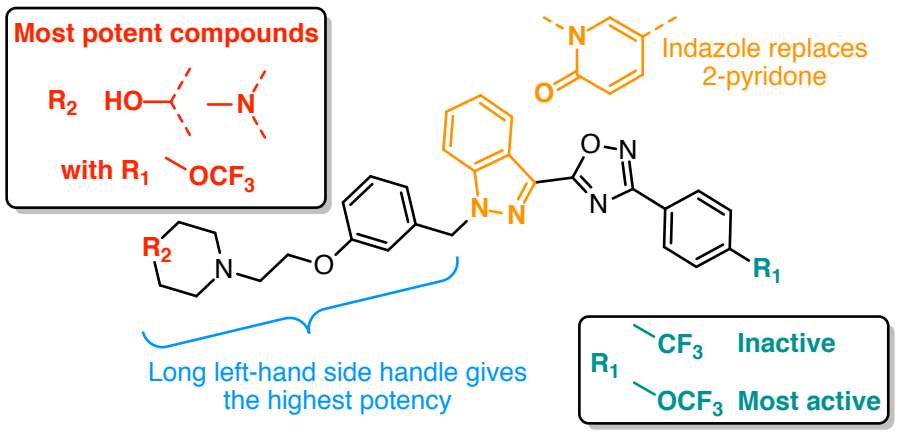

Figure 6.14. Main structural features of Sheng's HIF-1 inhibitors. Long left-hand side handles and a OCF_3 right-hand side handle were found to confer the highest potency within the oxadiazole-indazole core compounds.

A recent study by Baccelli *et al.* identified Mubritinib as a potential treatment for AML[610]. Since this disease is characterized by a high genetic complexity, the group tested a library of about 5000 compounds across 20 different AML specimens (representative of the vast array of genetic mutations involved with AML): compounds that gave a characteristic response pattern in the specimens were clustered together as to reveal promising therapeutic pathways in the form of synergistic pairs of drugs. Interestingly, one such combination was found to be Mubritinib and Deguelin: the two species were found to possess highly correlated EC_{50} values as well as similar synergistic patterns with other drugs in the library with AML cells. It is of note that **10759** gave promising results against AML cells and it is now under Phase I trial for AML patients (see section 6.2.1.2): the structural similarities between **10759** and Mubritinib corroborate the pharmacological potential to treat this particular type of cancer. Remarkably, one of the agents of proven clinical activity against AML (especially in association with intensive chemotherapy) is Sorafenib, a multi-kinase inhibitor that is structurally similar to both Mubritinib and **10759** (see Figure 6.15)[611]. In this regard, when comparing **10759** with Sorafenib, a sulfonyl group is a bioisostere for an amide (see section 6.3.4) and oxadiazole is a bioisostere for urea[612]; when comparing Mubritinib with Sorafenib, a triazole is a bioisostere for an amide (see section 6.4.3). Sorafenib was classified in this thesis as an unspecific OXPHOS inhibitor (see chapter 4).

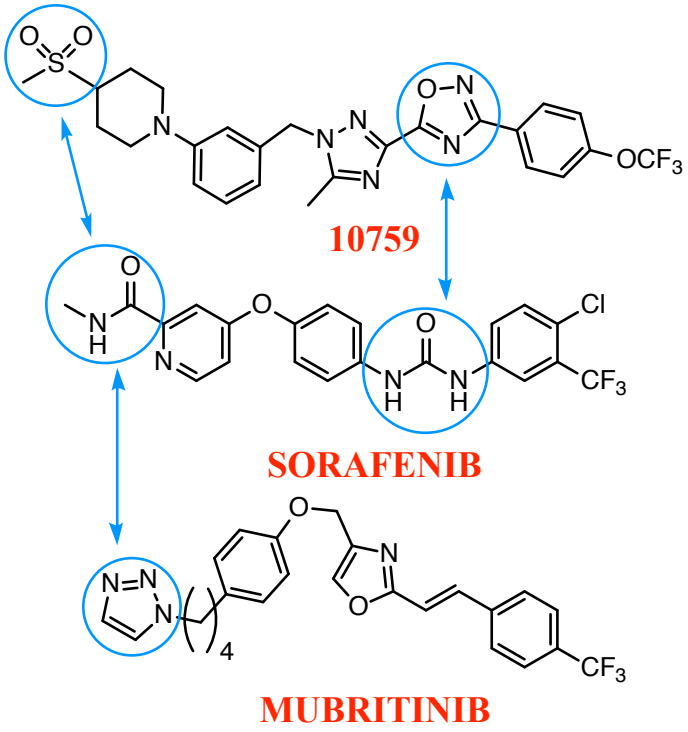

Figure 6.15. Structural similarities between 10759, Sorafenib and Mubritinib. Sorafenib possesses common features to 10759 and Mubritinib, particularly in light of bioisosterism between urea and oxadiazole on one hand and sulfonyl, amide and triazole on the other (highlighted in blue).

6.6 Summary

Mitochondrial complex I has recently emerged as a target for anticancer drugs and compounds with a pyra(tria)zolyl oxadiazole scaffold developed by the Anderson Cancer Centre and Bayer AG act through three of the several recognised modes of action (namely reduction of aspartate synthesis, HIF1α pathway and ROS damage). Other modes involve AMPK activation and angiogenesis inhibition via disruption of cellular hypoxic signalling[613]. The work presented in this chapter has shed light on some important aspects of complex I linked to its mechanism towards anticancer activity.

The collaboration with the Anderson Cancer Center was fruitful, inasmuch as it allowed us to successfully test the hypothesis, originally put forward by Bayer AG, that pyrazolyl oxadiazoles (see Figure 6.2) have a strong inhibitory power towards complex I. Almost all drugs in the libraries, though, possess a 2-pyridone oxadiazole core, with a wide range of biological activity expressed throughout the series. SAR analysis (left- and right-hand side on Library B in particular) identified the most

potent (right-hand side saturated heterocycles) and least potent (left-hand side methoxyethoxy moiety) side extensions of the series. A wider variety of assays was performed on the Library A which include **10759**, the compound put forward by the Anderson Center for Phase I clinical trials: these species exhibit a total specificity towards complex I and two of them (**4101** and **2858**) are even more powerful than rotenone.

The SAR analysis of Mubritinib was instrumental in discovering a remarkable structural feature to which complex I appears to be very sensitive, the point of attachment of 1,2,3-triazole: shifting from 1H- (peripheral nitrogen) to 2H- (central nitrogen) causes a large potency drop. Also important is the rotational flexibility around the central C-C bond of Mubritinib that makes the 1H- to 2H- potency decrease much less significant. It is noteworthy that Mubritinib and **10759** have shown promising results against AML and they are structurally similar to Sorafenib, a kinase inhibitor with clinical efficacy against this disease and classified in this thesis as an unspecific OXPHOS inhibitor.

7 Conclusions

Mitochondrial complex I (NADH:ubiquinone oxidoreductase) has essential roles in metabolism: it keeps the [NADH]/[NAD^+] ratio low in both the matrix and intermembrane space and contributes towards the protonmotive force by pumping protons across the IMM. The consequences of its inhibition are, therefore, major, and while this could be desirable for pharmaceuticals whose target is complex I, adverse toxic effects can lead to severe physiological damage. The pharmacologic characterisation of this multisubunit enzyme is, thus, the primary aim of this thesis, to pinpoint its role in drug-induced mitochondrial dysfunction. In parallel, SAR studies were performed to gain knowledge of binding mechanisms of important classes of compounds: variants of rotenoids, species with a pyrazolyl oxadiazole core and Mubritinib were thoroughly tested in order to improve potency, limit toxicity and extend their therapeutic potentials.

Chapter 3 was dedicated to generating a library of complex I specific inhibitors selected among a set of compounds that cause side effects linked to drug-induced mitochondrial dysfunction. This was carried out with an extensive literature search and the use of FDALabel, a freely accessible database. After filtering out compounds for various reasons (*e.g.* weak potency, cost, similarity to other drugs), eventually 21 drugs were selected. Several routine assays were performed on the isolated enzyme, on the whole respiratory chain and on cells to classify the compounds in terms of potency and specificity towards complex I or other OXPHOS enzymes. It emerged that the majority of the drugs specifically target complex I while the others inhibited OXPHOS with various degrees of specificity. Of note, Tamoxifen was found to be a complex III-specific inhibitor and, together with the data presented in chapter 4, its established role in drug-induced liver injury was validated. On the other hand, the flavin site of complex I was found to be relatively inert to drugs, and no significant results were obtained, not even with follow-up experiments carried out on a separate library of dibenzoheterocyclics. Microsomes were employed to mimic drug metabolism and to obtain more physiologically relevant data: the results indicated that drug-metabolising enzymes detoxified the effects of some drugs (including rotenone) towards the complex I-IV pathway. The positive outcome of this experiment has determined a future direction to take, especially by implementing mass spectrometry

to better identify the major metabolites. Cellular assays with the Seahorse XF analyser further extended the physiological relevance of the chapter, and five classes of cellular effects were identified within the library.

The methodology introduced in chapter 3 constituted a proof of principle that was subsequently applied to a much bigger commercial drug library in chapter 4. Drugs were initially screened to filter out compounds not potent enough and then complex I specificity was initially assessed by combining two assays affecting the I-IV pathway and the II-IV pathway, respectively. This method was validated with canonical OXPHOS inhibitors and implemented with data from a novel isolated enzyme assay in proteoliposomes that allowed the identification of non-specific, complex III- and I-specific inhibitors. Compounds that belong to the latter category were tested with a Seahorse assay on isolated mitochondria, and it was found that most compounds did not elicit a major effect on mitochondrial respiration, indicating an important role for transport and/or accumulation processes. Experiments with SMPs failed to characterise uncouplers selected from the initial screening and flavin-site assays confirmed the general lack of reactivity of the flavin site towards drugs found in chapter 3. Lastly, mitochondrial membranes were shown to be a convenient system to test compounds for OXPHOS-related mitochondrial dysfunction.

Chapter 5 was dedicated to a SAR study on rotenoids and crucial determinants to binding to complex I were found to be molecular flattening and hydroxylation of the E-ring. Hydroxylations at the B-C ring junction led to minor losses of potency and since those species are more hydrophilic than rotenone they are promising as anticancer agents (they would be less able to cross the blood brain barrier than their more lipophilic counterparts). Halogenation of the E-ring brought about the tightest binding in the rotenoids series, enlarging the scope of this work for future structural studies on account of the large electron density of halogens.

Further SAR studies on complex I were described in Chapter 6, where the role of complex I as a target for anticancer therapy was further developed. The libraries provided by the Anderson Cancer Centre gave many insights into binding interactions with complex I, including a hitherto undescribed inhibition across different mammalian species that spanned three orders of magnitude in potency. The Mubritinib variants provided by the Leicester Toxicology Unit revealed that complex

I responded significantly to the point of attachment of the 1,2,3-triazole moiety. The fact that the most promising anticancer drug from the Anderson Centre and Mubritinib have both been reported to be effective against AML and that they are structurally similar to Sorafenib, another agent with proven clinical activity against the disease, reveals a pharmacologic potential of the two species.

In conclusion, mitochondrial complex I appears to be a pharmacological target (away from its flavin site) for a myriad of structurally unrelated compounds: given its pivotal role in human metabolism, the results illustrated in this thesis should elevate its importance during toxicity screenings during drug development. At the same time, given the number of very potent complex I inhibitors analysed in this work, a parallel role of this enzyme as an effective target for insecticides potentially emerges.

8 References

[1] Alberts, B., Johnson, A., Lewis, J., Morgan, D., Raff, M., Roberts, K., and Walter, P. (2015). *Molecular Biology of the Cell*, 6th ed., Garland Science, 753-812

[2] Fritz, G., and Steuber, J., (2016). Sodium as Coupling Cation in Respiratory Energy Conversion, in Sigel, A., Sigel, H., and Sigel, R.K. *The Alkali Metal Ions: Their Role for Life*, Springer, 349-390

[3] Poburko, D., and Demaurex, N., (2012). Regulation of the mitochondrial proton gradient by cytosolic Ca^{2+} signals, *Pflugers Arch - Eur. J. Physiol.*, 464, 19-26

[4] Mammucari, C., Raffaello, A., Vecellio Reane, D., and Rizzuto, R. (2016). Molecular structure and pathophysiological roles of the Mitochondrial Calcium Uniporter, *Biochim. Biophys. Acta*, 1863(10), 2457-2464

[5] Cheng, J., Nanayakkara, G., Shao, Y., Cueto, R., Wang, L., Yang, W. Y., Tian, Y., Wang, H., and Yang, X., (2017). Mitochondrial Proton Leak Plays a Critical Role in Pathogenesis of Cardiovascular Diseases, in Santulli, E. (ed.) *Mitochondrial Dynamics in Cardiovascular Medicine* - *Adv. Exp. Med. Biol.*, Springer, 982, 359-370

[6] Campbell, M.K, Farrell, S.O. (2015). *Biochemistry*, Cengage, 8th ed., 577-600

[7] Nelson, D.L., Cox, M.M. (2013). *Lehninger Principles of Biochemistry*, W. H. Freeman, 6th ed., 1-44

[8] Ettema, T.J. (2016). Evolution: Mitochondria in the second act, 531(7592), 39-40

[9] Rostovtseva, T. K., Hoogerheide, D. P., Rovini, A., and Bezrukov, S. M., (2017). Lipids in Regulation of the Mitochondrial Outer Membrane Permeability, Bioenergetics, and Metabolism, in Rostovtseva, T. K. (ed.) *Molecular Basis for Mitochondrial Signaling*, Springer, 185-215

[10] van der Laan, M., Horvath, S.E., and Pfanner, N. (2016). Mitochondrial contact site and cristae organizing system, *Curr. Opin. Cell Biol.*, 41, 33-42

[11] Wai, T., and Langer, T. (2016). Mitochondrial Dynamics and Metabolic Regulation, *Trends Endocrinol. Metab.*, 27(2), 105-117

[12] Ni, H.M., Williams, J.A., and Ding, W.X. (2015). Mitochondrial dynamics and mitochondrial quality control, Redox Biol., 4, 6-13

[13] Krols, M., van Isterdael, G., Asselbergh, B., Kremer, A., Lippens, S., Timmerman, V., and Janssens, S. (2016). Mitochondria-associated membranes as hubs for neurodegeneration, *Acta Neuropathol.*, 131(4), 505-523

[14] Kühlbrandt, W., (2015). Structure and function of mitochondrial membrane protein complexes, *BMC Biology*, 13, 89

[15] Bender, D.A. (2012). *Amino Acid Metabolism*, Wiley, 3rd ed., 1-65

[16] Orrenius, S., Gogvadze, V., and Zhivotovsky, B. (2015). Calcium and mitochondria in the regulation of cell death, *Biochem. Biophys. Res. Commun.*, 460(1), 72-81

[17] Cherry, C., Thompson, B., Saptarshi, N., Wu, J., and Hoh, J. (2016). 2016: A 'Mitochondria' Odyssey, *Trends Mol. Med.*, 22(5), 391-403

[18] Houten, S.M., Violante, S., Ventura, F.V., and Wanders, R.J. (2016). The Biochemistry and Physiology of Mitochondrial Fatty Acid β-Oxidation and Its Genetic Disorders, *Ann. Rev. Physiol.*, 78, 23-44

[19] Mailloux, R. J. (2015). Still at the Center of it all - Novel Functions of the Oxidative Krebs Cycle, *Bioenergetics*, 4:1

[20] Fukao, T., Mitchell, G., Sass, J.O., Hori, T., Orii, K., and Aoyama, Y. (2014). Ketone body metabolism and its defects, *J. Inherit. Metab. Dis.*, 37(4), 541-551

[21] Barupala, D.P., Dzul, S.P., Riggs-Gelasco, P.J., and Stemmler, T.L. (2016). Synthesis, delivery and regulation of eukaryotic heme and Fe-S cluster cofactors, *Arch. Biochem. Biophys.*, 592, 60-75

[22] Raffaello, A., Mammucari, C., Gherardi, G., and Rizzuto, R. (2016). Calcium at the Center of Cell Signaling: Interplay between Endoplasmic Reticulum, Mitochondria, and Lysosomes, *Trends Biochem. Sci.*, 41(12), 1035-1049

[23] Schertl, P., and Braun, H.P. (2014). Respiratory electron transfer pathways in plant mitochondria, *Front. Plant Sci.*, 5, 163

[24] DeBalsi, K.L., Hoff, K.E., and Copeland, W.C. (2017). Role of the mitochondrial DNA replication machinery in mitochondrial DNA mutagenesis, aging and age-related diseases, *Ageing Res. Rev.*, 33, 89-104

[25] Milenkovic, D., Blaza, J.N., Larsson, N.G., and Hirst, J. (2017). The Enigma of the Respiratory Chain Supercomplex, *Cell Metab.*, 25(4), 765-776

[26] Jones, A.J., Blaza, J.N., Varghese, F., and Hirst, J. (2017). Respiratory Complex I in *Bos taurus* and *Paracoccus denitrificans* Pumps Four Protons across the Membrane for Every NADH Oxidized, *J. Biol. Chem.*, 292(12), 4987-4995

[27] Vinothkumar, K.R., Zhu, J., and Hirst, J. (2014). Architecture of mammalian respiratory complex I, *Nature* 515(7525), 80-84

[28] Brandt, U. (2013). Inside view of a giant proton pump, *Angew. Chem. Int. Ed. Engl.*, 52(29), 7358-7360

[29] Wirth, C., Brandt, U., Hunte, C., and Zickermann, V. (2016). Structure and function of mitochondrial complex I, *Biochim. Biophys. Acta*, 1857(7), 902-914

[30] Sazanov, L.A. (2015). A giant molecular proton pump: structure and mechanism of respiratory complex I, *Nat. Rev. Mol. Cell. Biol.*, 16(6), 375-388

[31] Hirst, J., (2013). Mitochondrial Complex I. *Annu. Rev. Biochem.* 82, 551-575

[32] Houtkooper, R.H., Cantó, C., Wanders, R.J., and Auwerx. J., (2010). The secret life of NAD^+: an old metabolite controlling new metabolic signaling pathways, *Endocr. Rev.*, 31(2), 194-223

[33] Cantó, C., Menzies, K., and Auwerx, J. (2015). NAD^+ metabolism and the control of energy homeostasis - a balancing act between mitochondria and the nucleus, *Cell Metab.*, 22(1), 31-53

[34] Da Poian, A.T., Castanho, M.A.R.B. (2015). Integrative human biochemistry: A textbook for medical biochemistry, Springer, 185-222

[35] Stein, L.R. and Imai, S. (2012). The dynamic regulation of NAD metabolism in mitochondria, *Trends Endocrinol. Metab.* 23(9), 420-428

[36] Zhang, D.X., Zhang, J.P., Hu, J.Y., and Huang, Y.S. (2016). The potential regulatory roles of $NAD(^+)$ and its metabolism in autophagy, *Metabolism*, 65(4), 454-62

[37] Kane, D.A. (2014). Lactate oxidation at the mitochondria: a lactate-malate-aspartate shuttle at work, *Front. Neurosci.*, 8:366

[38] Menzies, K.J., Zhang, H., Katsyuba, E., Auwerx, J., (2016). Protein acetylation in metabolism - metabolites and cofactors. *Nat. Rev. Endocrinol.* 12(1), 43-60

[39] Gameiro, P.A., Laviolette. L.A., Kelleher, J.K., Iliopoulos, O., and Stephanopoulos, G. (2013). Cofactor balance by nicotinamide nucleotide transhydrogenase (NNT) coordinates reductive carboxylation and glucose catabolism in the tricarboxylic acid (TCA) cycle, *J. Biol. Chem.*, 3 288(18) 12967-12977

[40] Santidrian, A.F., Matsuno-Yagi, A., Ritland, M., Seo, B.B., LeBoeuf, S.E., Gay, L.J., Yagi, T., and Felding-Habermann, B. (2013). Mitochondrial complex I activity and NAD^+/NADH balance regulate breast cancer progression, *J. Clin. Invest.*, 123(3), 1068-1081

[41] McMurry, J. (2016). *Organic Chemistry*, 9th ed., Cengage Learning, 964-1012

[42] Nakamura, M.T., and Nara, T.Y. (2004) Structure, function, and dietary regulation of Δ6, Δ5, and Δ9 desaturases, *Ann. Rev. Nutr.*, 24, 345-376

[43] Gnoni, G.V., Priore, P., Geelen, M.J., and Siculella. L. (2009). The mitochondrial citrate carrier: metabolic role and regulation of its activity and expression, *IUBMB Life*, 61(10), 987-994

[44] Newman, J.C., and Verdin, E. (2014). Ketone bodies as signaling metabolites, *Trends Endocrinol. Metab.*, 25(1), 42-52

[45] Louvet, A., and Mathurin, P. (2015). Alcoholic liver disease: mechanisms of injury and targeted treatment, *Nat. Rev. Gastroenterol. Hepatol.*, 12(4), 231-242

[46] Grant, G.A. (2012). Contrasting catalytic and allosteric mechanisms for phosphoglycerate dehydrogenases, *Arch. Biochem. Biophys.*, 519(2), 175-185

[47] Kikuchi G1, Motokawa Y, Yoshida T, and Hiraga K., (2008). Glycine cleavage system: reaction mechanism, physiological significance, and hyperglycinemia, *Proc. Jpn. Acad. Ser. B Phys. Biol. Sci.*, 84(7), 246-263

[48] Pemberton, T.A., and Tanner, J.J. (2013). Structural basis of substrate selectivity of Δ(1)-pyrroline-5-carboxylate dehydrogenase (ALDH4A1): semialdehyde chain length, *Arch. Biochem. Biophys.*, 538(1), 34-40

[49] Hedstrom, L. (2009). IMP dehydrogenase: structure, mechanism, and inhibition, *Chem. Rev.*, 109(7), 2903-2928

[50] Kussmaul, L., and Hirst, J. (2006). The mechanism of superoxide production by NADH:ubiquinone oxidoreductase (complex I) from bovine heart mitochondria, *Proc. Natl. Acad. Sci. USA*, 103(20), 7607-7612

[51] Walsh, C.T., and Wencewicz, T.A. (2013). Flavoenzymes: versatile catalysts in biosynthetic pathways, *Nat. Prod. Rep.*, 30(1), 175-200

[52] Pedrolli D.B., Jankowitsch, F., Schwarz, J., Langer, S., Nakanishi, S., and Mack, M. (2014). Natural riboflavin analogs, in Weber, S., and Schleicher, E. (ed.) Flavins and flavoproteins: Methods and protocols, Humana Press, 1146, 41-63

[53] Giancaspero, T.A., Colella, M., Brizio, C., Difonzo, G., Fiorino, G.M., Leone, P., Brandsch, R., Bonomi, F., Iametti, S., and Barile, M. (2015). Remaining challenges in cellular flavin cofactor homeostasis and flavoprotein biogenesis, *Front. Chem.*, 3:30

[54] Barile, M., Giancaspero, T.A., Leone, P., Galluccio, M., and Indiveri, C. (2016). Riboflavin transport and metabolism in humans, *J. Inherit. Metab. Dis.*, 39, 545-557

[55] Viscomi, C., Bottani, E., and Zeviani, M. (2015). Emerging concepts in the therapy of mitochondrial disease, *Biochim. Biophys. Acta*, 1847(6-7), 544-557

[56] Rouault TA, (2015). Mammalian iron-sulphur proteins: novel insights into biogenesis and function, *Nat. Rev. Mol. Cell Biol.*, 16(1), 45-55

[57] Pain, D., Dancis, A. (2016). Roles of Fe-S proteins: from cofactor synthesis to iron homeostasis to protein synthesis, *Curr. Opin. Genet. Dev.*, 38, 45-51

[58] Maio, N., and Rouault, T.A. (2015). Iron-sulfur cluster biogenesis in mammalian cells: New insights into the molecular mechanisms of cluster delivery, *Biochim. Biophys. Acta*, 1853(6), 1493-1512

[59] Sharpe, A.G., and Housecroft, C.E. (2012). *Inorganic Chemistry*, 4th ed., Pearson, 1065-1107

[60] Crack, J. C., Green, J., Thomson, A. J., and Le Brun, N. E. (2014). Iron−Sulfur Clusters as Biological Sensors: The Chemistry of Reactions with Molecular Oxygen and Nitric Oxide, *Acc. Chem. Res.*, 47, 3196−3205

[61] Fuss, J.O., Tsai, C.L., Ishida, J.P., and Tainer, J.A. (2015). Emerging critical roles of Fe-S clusters in DNA replication and repair, *Biochim. Biophys. Acta*, 1853(6), 1253-1271

[62] Crichton, R. (2016). *Iron Metabolism - From Molecular Mechanisms to Clinical Consequences*, Wiley, 4th ed., 22-70

[63] Bak, D.W., Elliott, S.J. (2014). Alternative FeS cluster ligands: tuning redox potentials and chemistry, *Curr. Opin. Chem. Biol.*, 19, 50-58

[64] Hayashi, T., and Stuchebrukhov, A. A. (2011). Quantum Electron Tunneling in Respiratory Complex I, *J. Phys. Chem. B*, 115(18), 5354-5364

[65] Trixler, F. (2013). Quantum Tunnelling to the Origin and Evolution of Life, *Curr. Org. Chem.*, 17(16), 1758-1770

[66] Ichiye, T. (2014). Chemistry of iron-sulfur clusters, in Rouault, T. *Iron-Sulfur Clusters in Chemistry and Biology*, de Gruyter, 11-20

[67] Shriver, D., Weller, M., Overton, T., Rourke, J., and Armstrong F. (2014). *Inorganic Chemistry*, 6th ed., W.H. Freeman, 763-819

[68] Sarewicz, M., and Osyczka, A. (2015). Electronic connection between the quinone and cytochrome *c* redox pools and its role in regulation of mitochondrial electron transport and redox signalling, *Physiol. Rev.*, 95(1), 219-243

[69] Hirst, J., and Roessler, M.M. (2016). Energy conversion, redox catalysis and generation of reactive oxygen species by respiratory complex I, *Biochim. Biophys. Acta*, 1857(7), 872-883

[70] Becker, T., and Ullmann, G. M. (2008). Kinetic Simulations of the C-Subunit of the Bacterial Reaction Center, in Allen, J.F., Osmond, B., Goldbeck, J.H., and Gantt, E. (ed.) *Photosynthesis. Energy from the Sun*, Springer, 553-557

[71] Moser, C.C., Anderson, J.L., and Dutton, P.L. (2010). Guidelines for tunneling in enzymes, *Biochim. Biophys. Acta*, 1797(9), 1573-1586

[72] Alric, J., Lavergne, J., Rappaport, F., Verméglio, A., Matsuura, K., Shimada, K., and Nagashima, K.V. (2006). Kinetic performance and energy profile in a roller coaster electron transfer chain: a study of modified tetraheme-reaction center constructs, *J. Am. Chem. Soc.*, 128(12), 4136-4145

[73] Nowicka. B., and Kruk, J. (2010). Occurrence, biosynthesis and function of isoprenoid quinones, *Biochim. Biophys Acta*, 1797(9), 1587-1605

[74] Wang, Y. and Hekimi, S. (2016). Understanding Ubiquinone, *Trends Cell Biol.*, 26(5), 367-378

[75] Vinogradov, A.D., Grivennikova, V.G. (2016). Oxidation of NADH and ROS production by respiratory complex I, *Biochim. Biophys. Acta*, 1857(7), 863-871

[76] Onur, S., Niklowitz, P., Fischer, A., Metges, C.C., Grune, T., Menke, T., Rimbach, G. and Döring, F. (2014). A comparative study into alterations of coenzyme Q redox status in ageing pigs, mice, and worms, *Biofactors*, 40(3), 346-354

[77] Wang, Y., and Hekimi, S., (2013). Molecular genetics of ubiquinone biosynthesis in animals, *Crit. Rev. Biochem. Mol. Biol.*, 48(1), 69-88

[78] Hargreaves, I.P. (2014). Coenzyme Q_{10} as a therapy for mitochondrial disease, *Int. J. Biochem. Cell. Biol.*, 49, 105-111

[79] Suksomboon, N., Poolsup, N., and Juanak, N. (2015). Effects of coenzyme Q_{10} supplementation on metabolic profile in diabetes: a systematic review and meta-analysis, *J. Clin. Pharm. Ther.*, 40(4), 413-418

[80] Flowers, N., Hartley, L., Todkill, D., Stranges, S., and Rees, K. (2014). Co-enzyme Q10 supplementation for the primary prevention of cardiovascular disease, *Cochrane Database Syst. Rev.*, (12), CD010405

[81] Skulachev, V.P., Bogachev, A.V., and Kasparinsky, F.O. (2013). *Principles of Bioenergetics*, Springer-Verlag, 87-118

[82] Zwicker, K., Galkin, A., Dröse, S., Grgic, L., Kerscher, S., and Brandt, U. (2006). The Redox-Bohr group associated with iron-sulfur cluster N2 of complex I, *J. Biol. Chem.*, 281(32), 23013-23017

[83] Nicholls, D.G., and Ferguson, S.J. (2013). *Bioenergetics*, 4th ed., Associated Press, 91-157

[84] Sazanov, L.A. (2014). The mechanism of coupling between electron transfer and proton translocation in respiratory complex I, *J. Bioenerg. Biomembr.*, 46(4), 247-253

[85] Babot, M., Birch, A., Labarbuta, P., and Galkin, A. (2014). Characterisation of the active/de-active transition of mitochondrial complex I, *Biochim. Biophys. Acta*, 1837(7), 1083-1092

[86] Zhu, J., Vinothkumar, K.R., and Hirst, J. (2016). Structure of mammalian respiratory complex I, *Nature*, 536(7616), 354-358

[87] Babot, M., Labarbuta, P., Birch, A., Kee, S., Fuszard, M., Botting, C.H., Wittig, I., Heide, H., and Galkin, A. (2014). ND3, ND1 and 39kDa subunits are more exposed in the de-active form of bovine mitochondrial complex I, *Biochim. Biophys. Acta*, 1837(6), 929-939

[88] Babot, M., and Galkin, A. (2013). Molecular mechanism and physiological role of active-deactive transition of mitochondrial complex I, *Biochem. Soc. Trans.*, 41(5), 1325-1330

[89] Chouchani, E.T., Methner, C., Nadtochiy, S.M., Logan, A., Pell, V.R., Ding, S., James, A.M., Cochemé, H.M., Reinhold, J., Lilley, K.S., et al. (2013). Cardioprotection by S-nitrosation of a cysteine switch on mitochondrial complex I, *Nat. Med.*, 19(6), 753-759

[90] Roberts, P.G., and Hirst, J., (2012). The deactive form of respiratory complex I from mammalian mitochondria is a Na^+/H^+ antiporter, *J. Biol. Chem.* 287(41), 34743-34751

[91] Dröse, S. (2013). Differential effects of complex II on mitochondrial ROS production and their relation to cardioprotective pre- and postconditioning, *Biochim. Biophys. Acta*, 1827(5), 578-587

[92] Kluckova, K., Bezawork-Geleta, A., Rohlena, J., Dong, L., and Neuzil, J. (2013). Mitochondrial complex II, a novel target for anti-cancer agents, *Biochim. Biophys. Acta*, 1827(5), 552-564

[93] Sun, F., Zhou, Q., Pang, X., Xu, Y., and Rao, Z. (2013). Revealing various coupling of electron transfer and proton pumping in mitochondrial respiratory chain, *Curr. Opin. Struct. Biol.*, 23(4), 526-538

[94] Iverson, T.M. (2013). Catalytic mechanisms of complex II enzymes: a structural perspective, *Biochim. Biophys. Acta*, 1827(5), 648-657

[95] Van Vranken, J.G., Na, U., Winge, D.R., and Rutter, J. (2015). Protein-mediated assembly of succinate dehydrogenase and its cofactors, *Crit. Rev. Biochem. Mol. Biol.*, 50(2), 168-180

[96] Millett, F., Havens, J., Rajagukguk, S. and Durham, B. (2013). Design and use of photoactive ruthenium complexes to study electron transfer within cytochrome bc1 and from cytochrome *bc*1 to cytochrome *c*, *Biochim. Biophys. Acta*, 1827(11-12), 1309-1319

[97] Cooley, J.W. (2013). Protein conformational changes involved in the cytochrome bc1 complex catalytic cycle, *Biochim. Biophys. Acta*, 1827(11-12), 1340-1345

[98] Xia, D., Esser, L., Tang, W.K., Zhou, F., Zhou, Y., Yu, L., and Yu, C.A. (2013). Structural analysis of cytochrome bc1 complexes: implications to the mechanism of function, *Biochim. Biophys. Acta.*, 1827(11-12), 1278-1294

[99] Berry, E.A., De Bari, H., and Huang, L.S. (2013). Unanswered questions about the structure of cytochrome bc1 complexes, *Biochim. Biophys. Acta*, 1827(11-12), 1258-1277

[100] Konstantinov, A.A. (2012). Cytochrome c oxidase: Intermediates of the catalytic cycle and their energy-coupled interconversion, *FEBS Lett.*, 586(5), 630-639

[101] Kadenbach, B., Hüttemann, M. (2015). The subunit composition and function of mammalian cytochrome c oxidase, *Mitochondrion*, 24, 64-76

[102] Yoshikawa, S., and Shimada, A. (2015). Reaction Mechanism of Cytochrome *c* Oxidase, *Chem. Rev.*, 115 (4), 1936-1989

[103] Nyquist, R.M., Heitbrink, D., Bolwien, C., Gennis, R.B., and Heberle, J. (2003). Direct observation of protonation reactions during the catalytic cycle of cytochrome *c* oxidase, *PNAS*, 100(15), 8715-8720

[104] Mannella, C.A., Lederer, W.J., and Jafri, M.S. (2013). The connection between inner membrane topology and mitochondrial function, *J. Mol. Cell. Cardiol.*, 62, 51-57

[105] Lu, P., Lill, H., Bald, D., (2014). ATP synthase in mycobacteria: special features and implications for a function as drug target, *Biochim. Biophys. Acta*, 1837(7), 1208-1218

[106] Nakanishi-Matsui, M., Sekiya, M., Futai, M. (2016). ATP synthase from Escherichia coli: Mechanism of rotational catalysis, and inhibition with the ε subunit and phytopolyphenols, *Biochim. Biophys. Acta*, 1857(2), 129-140

[107] Iwasa, J. and Marhsall, W. (2016). *Karp's Cell and Molecular Biology: Concepts and Experiments*, Wiley, 8th ed., 168-198

[108] Igamberdiev, A.U., Kleczkowski, L.A. (2015). Optimization of ATP synthase function in mitochondria and chloroplasts via the adenylate kinase equilibrium, *Front. Plant. Sci.*, 6:10

[109] Walker, J.E. (2013). The ATP synthase: the understood, the uncertain and the unknown, *Biochem. Soc Trans.*, 41(1), 1-16

[110] Nesci, S., Trombetti, F., Ventrella, V., Pagliarani, A. (2016). The *c*-Ring of the F_1F_O-ATP Synthase: Facts and Perspectives, *J. Membr. Biol.*, 249(1-2), 11-21

[111] Biasutto, L., Azzolini, M., Szabò, I., and Zoratti, M., (2016). The mitochondrial permeability transition pore in AD 2016: An update, *Biochim. Biophys. Acta*, 1863(10), 2515-2530

[112] Bernardi, P., and Di Lisa, F. (2015). The mitochondrial permeability transition pore: molecular nature and role as a target in cardioprotection, *J. Mol. Cell Cardiol.*, 78, 100-106

[113] Bernardi, P., Rasola, A., Forte, M., and Lippe, G. (2015). The Mitochondrial Permeability Transition Pore: Channel Formation by F-ATP Synthase, Integration in Signal Transduction, and Role in Pathophysiology, *Physiol. Rev.*, 95(4), 1111-1155

[114] Amodeo, G.F., Torregrosa, M.E.S., and Pavlov, E.V. (2017). From ATP synthase dimers to C-ring conformational changes: unified model of the mitochondrial permeability transition pore, *Cell Death Dis.*, 20178:1

[115] Warne, J., Pryce, G., Hill, J.M., Shi, X., Lennerås, F., Puentes, F., Kip, M., Hilditch, L., Walker, P., Simone M.I., *et al.*, (2016). Selective Inhibition of the Mitochondrial Permeability Transition Pore Protects against Neurodegeneration in Experimental Multiple Sclerosis, *J. Biol. Chem.*, 291(9), 4356-4373

[116] Mercer, A.E., Regan, S.L., Hirst, C.M., Graham, E.E., Antoine, D.J., Benson, C.A., Williams, D.P., Foster, J., Kenna, J.G., and Park, B.K. (2009). Functional and toxicological consequences of metabolic bioactivation of methapyrilene via thiophene S-oxidation: Induction of cell defence, apoptosis and hepatic necrosis, *Toxicol. Appl. Pharmacol.*, 239(3), 297-305

[117] Kupsch, K., Hertel, S., Kreutzmann, P., Wolf, G., Wallesch, C.W., Siemen, D., and Schönfeld, P. (2009). Impairment of mitochondrial function by minocycline, *FEBS J.*, 276(6), 1729-1738

[118] Mullauer, F.B., Kessler, J.H., and Medema, J.P. (2009). Betulin is a potent anti-tumor agent that is enhanced by cholesterol, *PLoS One*, 4(4), e1

[119] Yan, C., Xin-Ming, Q., Li-Kun, G., Lin-Lin, L., Fang-Ping, C., Ying, X., Xiong-Fei, W., Xiang-Hong, L., and Jin, R. (2006). Tetrandrine-induced apoptosis in rat primary hepatocytes is initiated from mitochondria: caspases and endonuclease G (Endo G) pathway, *Toxicology*, 218(1), 1-12

[120] Bachi, A., Dalle-Donne, I., Scaloni, A. (2013). Redox proteomics: chemical principles, methodological approaches and biological/biomedical promises, *Chem. Rev.*, 113(1), 596-698

[121] Grivennikova, V.G., and Vinogradov, A.D. (2013). Mitochondrial production of reactive oxygen species, *Biochemistry (Mosc).*, 78(13), 1490-1511

[122] Murphy, M.P. (2009). How mitochondria produce reactive oxygen species, *Biochem. J.*, 417(1), 1-13

[123] Sheng, Y., Abreu, I.A., Cabelli, D.E., Maroney, M.J., Miller, A.F., Teixeira, M., and Valentine, J.S. (2014). Superoxide dismutases and superoxide reductases, *Chem. Rev.*, 114(7), 3854-3918

[124] Weidinger, A., and Kozlov, A.V. (2015). Biological Activities of Reactive Oxygen and Nitrogen Species: Oxidative Stress versus Signal Transduction, *Biomolecules*, 15, 5(2), 472-484

[125] Brown, G.C., and Borutaite, V. (2012). There is no evidence that mitochondria are the main source of reactive oxygen species in mammalian cells, *Mitochondrion*, 12(1), 1-4

[126] Dan Dunn, J., Alvarez, L.A., Zhang, X., and Soldati, T. (2015). Reactive oxygen species and mitochondria: A nexus of cellular homeostasis, *Redox Biol.*, 6, 472-485

[127] Kim, H.J., Ha, S., Lee, H.Y., and Lee, K.J. (2015). ROSics: chemistry and proteomics of cysteine modifications in redox biology, *Mass Spectrom. Rev.*, 34(2), 184-208

[128] Yang, J., Carroll, K.S., and Liebler, D.C. (2016). The Expanding Landscape of the Thiol Redox Proteome, *Mol. Cell Proteomics*, 15(1), 1-11

[129] Paulsen, C.E., and Carroll, K.S. (2013). Cysteine-mediated redox signaling: chemistry, biology, and tools for discovery, *Chem. Rev.*, 113(7), 4633-4679

[130] Mailloux, R.J., McBride, S.L., and Harper, M.E. (2013). Unearthing the secrets of mitochondrial ROS and glutathione in bioenergetics, *Trends Biochem. Sci.*, 38(12), 592-602

[131] Rindler, P.M., Plafker, S.M., Szweda, L.I., and Kinter, M. (2013). High dietary fat selectively increases catalase expression within cardiac mitochondria, *J. Biol. Chem.*, 288(3), 1979-1990

[132] Sanz, A. (2016). Mitochondrial reactive oxygen species: Do they extend or shorten animal lifespan?, *Biochim. Biophys. Acta*, 1857(8), 1116-1126

[133] Chouchani, E.T., Pell, V.R., Gaude, E., Aksentijević, D., Sundier, S.Y., Robb, E.L., Logan, A., Nadtochiy, S.M., Ord, E.N., Smith, A.C. *et al.* (2014). Ischaemic accumulation of succinate controls reperfusion injury through mitochondrial ROS, *Nature*, 515, 431-443

[134] McElroy, G.S., and Chandel, N.S. (2017). Mitochondria control acute and chronic responses to hypoxia, *Exp. Cell Res.*, 356(2), 217-222

[135] Waypa, G. B., Smith, K. A., and Schumacker, P. T., (2016). O_2 sensing, mitochondria and ROS signaling: The fog is lifting, *Molecular Aspects of Medicine*, (47-48), 76-89

[136] Jung, H.J., Shim, J.S., Lee, J., Song, Y.M., Park, K.C., Choi, S.H., Kim, N.D., Yoon, J.H., Mungai, P.T., Schumacker, P.T., *et al.* (2010). Terpestacin inhibits tumor angiogenesis by targeting UQCRB of mitochondrial complex III and suppressing hypoxia-induced reactive oxygen species production and cellular oxygen sensing, *J. Biol. Chem.* 285, 11584-11595

[137] Chang, J., Jung, H.J., Jeong, S.H., Kim, H.K., Han, J., and Kwon, H.J. (2014). A mutation in the mitochondrial protein UQCRB promotes angiogenesis through the generation of mitochondrial reactive oxygen species, *Biochem. Biophys. Res. Commun.* 455, 290-297

[138] Orr, A.L., Vargas, L., Turk, C.N., Baaten, J.E., Matzen, J.T., and Dardov, V.J., (2015). Suppressors of superoxide production from mitochondrial complex III. *Nat. Chem. Biol.* 11 (11), 834-836

[139] Vriend, J., and Reiter, R. J. (2016). Melatonin and the von Hippel-Lindau HIF-1 oxygen sensing mechanism: A review, *Biochimica et Biophysica Acta* 1865, 176-183

[140] Gunther, U.L., Chong, M.G., Volpari, T., Koczula, K.M., Atkins, K., Bunce, C.M., and Khanim, F.L. (2015). Metabolic fluxes in cancer metabolism. in *Tumor Cell Metabolism: Pathways, Regulation and Biology*, Mazurek, S., Shoshan, M., (Ed.), Springer, 315-348

[141] Ravenna, L., Salvatori, L., and Russo, M. A., HIF3α: the little we know, (2016). *FEBS J.*, 283(6), 993-1003

[142] Semenza, G.L. (2014). Oxygen sensing, hypoxia-inducible factors, and disease pathophysiology, *Annu. Rev. Pathol.* 9, 47-71

[143] Yang, M., Su, H., Soga, T., Kranc, K.R., and Pollard, P.J. (2014). Prolyl hydroxylase domain enzymes: important regulators of cancer metabolism. *Hypoxia*, 2, 127-142

[144] Balamurugan, K. (2015). HIF-1 at the crossroads of hypoxia, inflammation, and cancer, *Int. J. Cancer*, 138(5), 1058-1066

[145] Lu, J., Tan, M., and Cai, Q. (2015). The Warburg effect in tumor progression: mitochondrial oxidative metabolism as an anti-metastasis mechanism, *Cancer Lett.* 356, 156-164

[146] Weinberg, F., Hamanaka, R., Wheaton, W.W., Weinberg, S., Joseph, J., Lopez, M., Kalyanaraman, B., Mutlu, G.M., Budinger, G.R., and Chandel, N.S. (2010). Mitochondrial metabolism and ROS generation are essential for Kras-mediated tumorigenicity, *Proc. Natl. Acad. Sci.* USA, 107, 8788-8793

[147] Berridge, M. V., and Herst, P. M., (2015). *Tumor Cell Complexity and Metabolic Flexibility in Tumorigenesis and Metastasis*, in Mazurek, S., Shoshan M. (Ed.) *Tumor Cell Metabolism: Pathways, Regulation and Biology* (Springer), 23-43

[148] Sabharwal, S. S., and Schumacker, P. T. (2014). Mitochondrial ROS in cancer: initiators, amplifiers or an Achilles' heel? *Nat. Rev. Cancer*, 14, 709-721

[149] Bienert, G.P., and Chaumont, F. (2014). Aquaporin-facilitated transmembrane diffusion of hydrogen peroxide, *Biochim. Biophys Acta*, 1840(5), 1596-1604

[150] Lee, G., Won, H.S., Lee, Y.M., Choi, J.W., Oh, T.I., Jang, J.H., Choi, D.K., Lim, B.O., Kim, Y.J., Park, J.W., et al. (2016). Oxidative Dimerization of PHD2 is Responsible for its Inactivation and Contributes to Metabolic Reprogramming via HIF-1α Activation, *Sci Rep.* 6, 18928

[151] Weinberg, S.E., and Chandel, N.S. (2015). Targeting mitochondria metabolism for cancer therapy, *Nat. Chem. Biol.*, 11, 9-15

[152] Movafagh, S., Crook, S., and Vo, K. (2015). Regulation of hypoxia-inducible factor-1a by reactive oxygen species: new developments in an old debate. *J. Cell. Biochem.*, 116, 696-703

[153] Hu, Y., Liu, J., and Huang, H. (2013). Recent agents targeting HIF-1a for cancer therapy, *J. Cell. Biochem.*, 114, 498-450

[154] Neuzil, J., Dong, L.F., Rohlena, J., Truksa, J., and Ralph, S.J., (2013). Classification of mitocans, anti-cancer drugs acting on mitochondria, *Mitochondrion*, 13, 199-208

[155] Sullivan, L.B., and Chandel, N.S., (2014). Mitochondrial reactive oxygen species and cancer, *Cancer Metab.* 2 (17)

[156] Lin, X., David, C.A., Donnelly, J.B., Michaelides, M., Chandel, N.S., Huang, X., Warrior, U., Weinberg, F., Tormos, K.V., Fesik, S.W., and Shen, Y., (2008). A chemical genomics screen highlights the essential role of mitochondria in HIF-1 regulation, *Proc. Natl. Acad. Sci. USA*, 105, 174-179

[157] Walker, J.E., Skehel, J.M., and Buchanan, S.K. (1995). Structural analysis of NADH: ubiquinone oxidoreductase from bovine heart mitochondria, *Methods Enzymol.*, 260, 14-34

[158] Sharpley, M.S., Shannon, R.J., Draghi, F., and Hirst, J. (2006). Interactions between phospholipids and NADH:ubiquinone oxidoreductase (complex I) from bovine mitochondria, *Biochemistry*, 45(1), 241-248

[159] Pryde, K.R., and Hirst, J. (2011). Superoxide is produced by the reduced flavin in mitochondrial complex I: a single, unified mechanism that applies during both forward and reverse electron transfer, *J. Biol. Chem.*, 286(20), 18056-18065

[160] Jones, A.J., and Hirst, J. (2013). A spectrophotometric coupled enzyme assay to measure the activity of succinate dehydrogenase, *Anal. Biochem.*, 442(1), 19-23

[161] Jones, A.J., Blaza, J.N., Bridges, H.R., May, B., Moore, A.L., and Hirst, J. (2016). A Self-Assembled Respiratory Chain that Catalyzes NADH Oxidation by Ubiquinone-10 Cycling between Complex I and the Alternative Oxidase, *Angew. Chem. Int. Ed. Engl.*, 55(2), 728-731

[162] Yakovlev, G., and Hirst, J. (2007). Transhydrogenation reactions catalyzed by mitochondrial NADH-ubiquinone oxidoreductase (Complex I), *Biochem.*, 46(49), 14250-14258

[163] Kirby, D.M., Thorburn, D.R., Turnbull, D.M., and Taylor, R.W. (2007). Biochemical assays of respiratory chain complex activity, *Methods in Cell Biol.*, 80, 93-119

[164] Covian, R., Gutierrez-Cirlos, E.B., and Trumpower, B.L. (2004). Anti-cooperative oxidation of ubiquinol by the yeast cytochrome bc1 complex, *J. Biol. Chem.*, 279(15), 15040-15049

[165] Spinazzi, M., Casarin, A., Pertegato, V., Salviati, L., and Angelini, C. (2012). Assessment of mitochondrial respiratory chain enzymatic activities on tissues and cultured cells, *Nat. Protoc.*, 7(6), 1235-1246

[166] Ames, B.N. (1966). Assay of inorganic phosphate, total phosphate and phosphatases, *Methods Enzymol.*, 8, 115-118

[167] Hansen, G., Christensen, P., Tüchsen E, and Lund T. (2004). Sensitive and selective analysis of coenzyme Q_{10} in human serum by negative APCI LC-MS, *Analyst*, 129(1), 45-50

[168] Roberts, P.G., and Hirst, J. (2012) The deactive form of respiratory complex I from mammalian mitochondria is a Na+/H+ antiporter, *J. Biol. Chem.*, 287(41), 34743-34751

[169] Bridges, H.R., Jones, A.J., Pollak, M.N., and Hirst, J. (2014). Effects of metformin and other biguanides on oxidative phosphorylation in mitochondria, *Biochem. J.*, 462(3), 475-487

[170] Birrell, J.A., Yakovlev, G., and Hirst, J. (2009). Reactions of the flavin mononucleotide in complex I: a combined mechanism describes NADH oxidation coupled to the reduction of $APAD^+$, ferricyanide, or molecular oxygen, *Biochemistry*, 48(50), 12005-12013

[171] King, M.S., Sharpley, M.S., and Hirst, J. (2009). Reduction of hydrophilic ubiquinones by the flavin in mitochondrial NADH:ubiquinone oxidoreductase (Complex I) and production of reactive oxygen species, *Biochemistry*, 48(9), 2053-2062

[172] Fato, R., Estornell, E., Di Bernardo, S., Pallotti, F., Parenti Castelli, G., and Lenaz, G. (1996). Steady-state kinetics of the reduction of coenzyme Q analogs by complex I (NADH:ubiquinone oxidoreductase) in bovine heart mitochondria and submitochondrial particles, *Biochemistry*, 35(8), 2705-2716

[173] Bridges, H.R., Sirviö, V.A., Agip, A.N., and Hirst, J. (2016). Molecular features of biguanides required for targeting of mitochondrial respiratory complex I and activation of AMP-kinase, *BMC Biol.*, 14, 65

[174] Walker, L., Yip, V., and Pirmohamed, M. (2014). *Adverse Drug Reactions*, in Padmanabhan, S. (ed.) *Handbook of Pharmacogenomics and Stratified Medicine*, Associated Press, 404-435

[175] Urban, T.J., and Tillmann, H. (2014). *Drug-Induced Liver Injury*, in Padmanabhan, S. (ed.) *Handbook of Pharmacogenomics and Stratified Medicine*, Associated Press, 467-477

[176] Grant, L.M., and Rockey, D.C. (2012). Drug-induced liver injury, *Curr. Opin. Gastroenterol.*, 28(3), 198-202

[177] Hoofnagle, J. H., Serrano, J., Knoben, J. E., and Navarro, V. J. (2013). LiverTox: A website on drug-induced liver injury, *Hepatology*, 57(3), 873-874

[178] Williams, C. D., and Jaeschke, H. (2012). Role of innate and adaptive immunity during drug-induced liver injury, *Toxicol. Res.*, 1, 161-170

[179] Kaplowitz, N. (2013). *Drug-Induced Liver Injury*, in Kaplowitz, N., DeLeve, L. (ed.) *Drug-Induced Liver Disease*, Academic Press, 3rd ed., 3-14

[180] Pandit, A., Sachdeva, T., and Bafna, P. (2012). Drug-Induced Hepatotoxicity: A Review. *J. App. Pharm. Sc.*, 02 (05), 233-243

[181] Antoine, D. J., Harrill, A. H., Watkins, P. B., and Park, B. K. (2014). Safety biomarkers for drug-induced liver injury - current status and future perspectives, *Toxicol. Res.*, 3, 75-85

[182] Hodgman, M.J., and Garrard, A.R. (2012). A review of acetaminophen poisoning. *Crit. Care Clin.*, 28, 499-516

[183] Pessayre, D., Berson, A., and Fromenty, B. (2008). *Features And Mechanisms Of Drug-induced Liver Injury*, in Dyckens, J.A., Will, Y. (ed.) *Drug-induced Mitochondrial Dysfunction*, Wiley, 143-203

[184] Au, J.S., Navarro, V.J., and Rossi, S. (2011). Review article: Drug-induced liver injury: its pathophysiology and evolving diagnostic tools, *Aliment. Pharmacol. Ther.,* 34, 11-20

[185] Pessayre, D., Fromenty, B., Berson, A., Robin, M., A., Lettéron, P., Moreau, R., and Mansouri, A. (2012). Central role of mitochondria in drug-induced liver injury, *Metab. Rev.*, 44(1), 34-87

[186] Labbe, G., Pessayre, D., and Fromenty, B. (2008). Drug-induced liver injury through mitochondrial dysfunction: mechanisms and detection during preclinical safety studies, *Fundam. Clin. Pharmacol.*, 22, 335-353

[187] Leung, L., Kalgutkar, A.S., and Obach, R.S. (2012). Metabolic activation in drug-induced liver injury, *Drug Metab. Rev.*, 44(1), 18-33

[188] Gómez-Lechón, M.J., Tolosa, L., and Donato, M.T. (2016). Metabolic activation and drug-induced liver injury: in vitro approaches for the safety risk assessment of new drugs, *J. Appl. Toxicol.*, 36(6), 752-768

[189] Cimic, A., and Sirintrapun, J. (2013). Amiodarone Hepatotoxicity with Absent Phospholipidosis and Steatosis: A Case Report and Review of Amiodarone Toxicity in Various Organs, *C. Rep. in Path.*, Article ID 201095

[190] Holt, D. H. (2009) *Adverse Effects of Drugs on the Liver*, in Koda-Kimble, M. A., Young, L. Y., Alldredge, B. K., Corelli, R. L., Guglielmo, B. J., Kradjan, W. A., Williams, B. R. (ed.) *Applied Therapeutics: The Clinical Use of Drugs*, Lippincott Williams & Wilkins, 9th ed., 29(1-21)

[191] Devarbhavi, H. (2012). An update on drug-induced liver injury, *J. Clin. Exp. Hepatol.*, 2, 247-259

[192] Scatena, R., Bottoni, P., Botta, G., Martorana, G.E., and Giardina, B., (2007). The role of mitochondria in pharmacotoxicology: a reevaluation of an old, newly emerging topic, *Am. J. Physiol. Cell Physiol.*, 293(1), C12-21

[193] Carvalho, F.S., Burgeiro, A., Garcia, R., Moreno, A.J., Carvalho, R.A., and Oliveira, P.J. (2014). Doxorubicin-induced cardiotoxicity: from bioenergetic failure and cell death to cardiomyopathy, *Med. Res. Rev.*, 34(1), 106-135

[194] Diezi, M., Buclin, T., and Kuntzer, T. (2013). Toxic and drug-induced peripheral neuropathies: updates on causes, mechanisms and management, *Curr. Opin. Neur.*, 26(5), 481-488

[195] Hernández, E. P., and Dawood, H. (2010). Stavudine-Induced Hyperlactatemia/Lactic Acidosis at a Tertiary Communicable Diseases Clinic in South Africa, *JIAPAC*, 9, 109-112

[196] Hohenegger, M. (2012). Drug induced rhabdomyolysis, *Current Opinion in Pharmacology*, 12(3), 335-339

[197] Stringer, H. A. J., Sohi, G.K., Maguire, J. A., and Côté, H.C.F. (2013). Decreased skeletal muscle mitochondrial DNA in patients with statin-induced myopathy, *J. Neur. Sc.*, 325, 142-147

[198] McComsey, G. A., Kitch, D., Sax, P. E., Tebas, P., Tierney, C., Jahed, N. C., Myers, L., Melbourne, K., Ha, B., and Daar, E. S. (2011). Peripheral and Central Fat Changes in Subjects Randomized to Abacavir-Lamivudine or Tenofovir-Emtricitabine With Atazanavir-Ritonavir or Efavirenz: ACTG Study A5224s, *Clin. Inf. Dis.*, 53(2), 185-196

[199] Degli Esposti, M. (1998). Inhibitors of NADH-ubiquinone reductase: an overview, *Biochim. Biophys. Acta.*, 1364, 222-235

[200] Hroudova, J., and Fisar, Z. (2010). Activities of respiratory chain complexes and citrate synthase influenced by pharmacologically different antidepressants and mood stabilizers, *NeuroEndocrinol. Lett.*, 31(3), 336-342

[201] Sirvent, P., Bordenave, S., Vermaelen, M., Roels, B., Vassort, G., Mercier, J., Raynaud, E., and Lacampagne, A. (2005). Simvastatin induces impairment in skeletal muscle while heart is protected, *Biochem. Biophys. Res. Commun.*, 23, 338(3), 1426-1434

[202] Blaza, J.N., Serreli, R., Jones, A.J., Mohammed, K., and Hirst, J. (2014). Kinetic evidence against partitioning of the ubiquinone pool and the catalytic relevance of respiratory-chain supercomplexes, *Proc. Natl. Acad. Sci. USA*, 111(44), 15735-15740

[203] Degli Esposti, M, and Lenaz, G. (1982). Kinetics of ubiquinol-1-cytochrome *c* reductase in bovine heart mitochondria and submitochondrial particles, *Biochim. Biophys. Acta*, 682, 189-200

[204] Ryu, C.S., Klein, K., and Zanger, U.M. (2017). Membrane Associated Progesterone Receptors: Promiscuous Proteins with Pleiotropic Functions - Focus on Interactions with Cytochromes P450, *Front. Pharmacol.*, 8:159

[205] Wermuth, C.G. (2008). *The Practice of Medicinal Chemistry*, Associated Press, 3rd ed., 637-654

[206] Nadanaciva, S., Bernal, A., Aggeler, R., Capaldi, R., and Will, Y. (2007). Target identification of drug induced mitochondrial toxicity using immunocapture based OXPHOS activity assays, *Toxicol. In Vitro*, 21(5), 902-911

[207] Shoichet, B.K. (2006)**.** Interpreting steep dose-response curves in early inhibitor discovery, *J. Med. Chem.*, 49(25), 7274-7277

[208] Tuquet, C., Dupont, J., Mesneau, A., and Roussaux, J. (2000). Effects of tamoxifen on the electron transport chain of isolated rat liver mitochondria, *Cell Biol. Toxicol.*, 16(4), 207-219

[209] Cheah, K.S., and Waring, J.C. (1983). Effect of trifluoperazine on skeletal muscle mitochondrial respiration, *Biochim. Biophys. Acta*, 723(1), 45-51

[210] Wallace, K.B. (2003). Doxorubicin-induced cardiac mitochondrionopathy, *Pharmacol. Toxicol.*, 93(3), 105-115

[211] Wright, M.V., and Kuhn, T.B. (2002). CNS neurons express two distinct plasma membrane electron transport systems implicated in neuronal viability, *J. Neurochem.*, 83(3), 655-664

[212] Yilmaz, G., Aydogan, B., Temel, G., Arsu, N., Moszner, N., and Yagci, Y., (2010). Thioxanthone-Fluorenes as Visible Light Photoinitiators for Free Radical Polymerization, *Macromolecules*, 43, 4520-4526

[213] Wutzel, H., Jarvid, M., Bjuggren, J.M., Johansson, A., Englund, V., Gubanskib, S., and Andersson, M. R. (2015). Thioxanthone derivatives as stabilizers against electrical breakdown in cross-linked polyethylene for high voltage cable applications, *Polymer Degradation and Stability*, (112), 63-69

[214] Arsu, N., Aydin, M., Yagci, Y., Jickusch, S., and Turro, N.J. (2006). One component thioxanthone based type II photoinitiators in Fouassier, J.P. (ed.) *Photochemistry and UV curing: new trends*, Kerala: Research Signpost, 1-13

[215] Thull, U., and Testa, B. (1994) Screening of unsubstituted cyclic compounds as inhibitors of monoamine oxidases, *Biochem. Pharmacol.* 47(12), 2307-2310

[216] Nadanaciva, S., Rana, P., Beeson, G.C., Chen, D., Ferrick, D.A., Beeson, C.C., and Will, Y. (2012). Assessment of drug-induced mitochondrial dysfunction via altered cellular respiration and acidification measured in a 96-well platform, *J. Bioenerg. Biomembr.*, 44(4), 421-437

[217] Derrick, D.A., Neilson, A., and Beeson, C. (2008). Advances in measuring cellular bioenergetics using extracellular flux, *Drug Discov. Today*, 13(5-6), 268-274

[218] Liu, S., Miriyala, S., Keaton, M.A., Jordan, C.T., Wiedl, C., Clair, D.K., and Moscow, J.A. (2014). Metabolic effects of acute thiamine depletion are reversed by rapamycin in breast and leukemia cells, *PLoS One*, 9(1), e85702

[219] Lagadinou, E.D., Sach, A., Callahan, K., Rossi, R.M., Neering, S.J., Minhajuddin, M., Ashton, J.M., Pei, S., Grose, V., O'Dwyer, K.M. *et al.* (2013). BCL-2 inhibition targets oxidative phosphorylation and selectively eradicates quiescent human leukemia stem cells, *Cell Stem Cell*, 12(3), 329-341

[220] Pike, L.S., Smift, A.L., Croteau, N.J., Ferrick, D.A., and Wu, M. (2011) Inhibition of fatty acid oxidation by etomoxir impairs NADPH production and increases reactive oxygen species resulting in ATP depletion and cell death in human glioblastoma cells, *Biochim. Biophys. Acta.*, 1807(6), 726-734

[221] Pike Winer, L.S., and Wu, M. (2014). Rapid analysis of glycolytic and oxidative substrate flux of cancer cells in a microplate, *PLoS One*, 9(10), e109916

[222] Wu, M., Neilson, A., Swift, A.L., Moran, R., Tamagnine, J., Parslow, D., Armistead, S., Lemire, K., Orrell, J., Teich, J. *et al.* (2007). Multiparameter metabolic analysis reveals a close link between attenuated mitochondrial bioenergetic function and enhanced glycolysis dependency in human tumor cells, *Am. J. Physiol. Cell Physiol.*, 292(1), C125-136

[223] Dykens, J.A., Jamieson, J.D., Marroquin, L.D., Nadanaciva, S., Xu, J.J., Dunn, M.C., Smith, A.R., and Will, Y. (2008) In vitro assessment of mitochondrial dysfunction and cytotoxicity of nefazodone, trazodone, and buspirone, *Toxicol Sci.*, 103(2), 335-345

[224] Funes, H.A., Blas-Garcia, A., Esplugues, J.V., and Apostolova, N., (2015). Efavirenz alters mitochondrial respiratory function in cultured neuron and glial cell lines, *J. Antimicrob. Chemother.*, 70(8), 2249-2254

[225] Kamalian, L., Chadwick, A.E., Bayliss, M., French, N.S., Monshouwer, M., Snoeys, J., and Park, B.K. (2015). The utility of HepG2 cells to identify direct mitochondrial dysfunction in the absence of cell death, *Toxicol. In Vitro*, 29(4), 732-740

[226] Ahlin, G., Hilgendorf, C., Karlsson, J., Szigyarto, C.A., Uhlén, M., and Artursson, P. (2009). Endogenous gene and protein expression of drug-transporting proteins in cell lines routinely used in drug discovery programs, *Drug Metab. Dispos.*, 37(12), 2275-2283

[227] Gallicano K. (2000). Antiretroviral-drug concentrations in semen, *Antimicrob. Agents Chemother.*, 44, 1117-1118

[228] Regenthal, R., Krueger, M., Koeppel, C., and Preiss, R. (1999). Drug levels: therapeutic and toxic serum/plasma concentrations of common drugs, *J. Clin. Monit. Comput.*, 15(7-8), 529-544

[229] Domańska, U., Pelczarska, A., and Pobudkowska, A. (2011). Solubility and pKa determination of six structurally related phenothiazines, *Int. J. Pharm.*, 421(1), 135-144

[230] Bennouna, M., Ferreira-Marques, J., Banerjee, S., Caspers, J. and Ruysschaert, J. M., (1997). Interaction of Chlorpromazine with Phospholipid Membranes: A Monolayer and a Microelectrophoresis Approach, *Langmuir*, 13, 6533-6539

[231] Lenkey, N., Karoly, R., Kiss, J.P., Szasz, B.K., Vizi, E.S., and Mike, A. (2006). The mechanism of activity-dependent sodium channel inhibition by the antidepressants fluoxetine and desipramine. *Mol. Pharmacol.*, 70(6), 2052-2063

[232] Flanagan, R. J., Taylor, A., Watson, I. D., and Whelpton, R. (2007). *Fundamentals of Analytical Toxicology*, Wiley, 49-94

[233] Schulz, M., Schmoldt, A., Donn, F., and Becker, H. (1988). The pharmacokinetics of flutamide and its major metabolites after a single oral dose and during chronic treatment, *Eur. J. Clin. Pharmacol.*, 34(6), 633-636

[234] Álvarez-Lueje, A., Peña, C., Núñez-Vergara, L. J., and Squella, J. A. (1998). Electrochemical Study of Flutamide, an Anticancer Drug, and Its Polarographic, UV Spectrophotometric and HPLC Determination in Tablets, *Electroanalysis*, 10(15), 1043-1051

[235] Cheng, S.M., Chu, K.M., and Lai, J.H. (2010). The modulatory mechanisms of fenofibrate on human primary T cells, *Eur. J. Pharm. Sci.*, 11, 40(4), 316-324

[236] Waaseth, M., Bakken, K., Dumeaux, V., Olsen, K.S., Rylander, C., Figenschau, Y., and Lund, E. (2008). Hormone replacement therapy use and plasma levels of sex hormones in the Norwegian Women and Cancer Postgenome Cohort - a cross-sectional analysis, *BMC Womens Health*, 8:1, 1-11

[237] Brittain, H.G., Profiles of Drug Substances (2007). *Excipients and Related Methodology*, Vol. 33, Associated Press, 35-424

[238] Choe, H., Lee, Y.K., Lee, Y.T., Choe, H., Ko, S.H., Joo, C.U., Kim, M.H., Kim, G.S., Eun, J.S., Kim, J.H., et al. (2003). Papaverine blocks hKv1.5 channel current and human atrial ultrarapid delayed rectifier K^+ currents, *J. Pharmacol. Exp. Ther.*, 304(2), 706-712

[239] Thakare, A., Bhate, K., and Kathariya, R. (2014). Comparison of 4% articaine and 0.5% bupivacaine anesthetic efficacy in orthodontic extractions: Prospective, randomized crossover study, *Acta Anaest. Taiw*., 59-63

[240] Becker, D.E., and Reed, K.L. (2006). Essentials of local anesthetic pharmacology, *Anesth. Prog.*, 53(3), 98-108

[241] Montes, R., Rodríguez, I., Casado, J., López-Sabater, M.C., and Cela, R. (2015). Determination of the cardiac drug amiodarone and its N-desethyl metabolite in sludge samples, *J. Chromatogr. A*, 1394, 62-70

[242] Abe, A., and Shayman, J.A. (2009). The role of negatively charged lipids in lysosomal phospholipase A2 function, *J. Lipid Res.*, 50(10), 2027-2035

[243] Jeong, I., Choi, B.H., and (2011). Hahn, S.J. Rosiglitazone inhibits Kv4.3 potassium channels by open-channel block and acceleration of closed-state inactivation, *Br. J. Pharmacol.*, 163(3), 510-520

[244] Lombardo, F., Obach, R.S., Shalaeva, M.Y., and Gao, F. (2004). Prediction of human volume of distribution values for neutral and basic drugs. 2. Extended data set and leave-class-out statistics, *J. Med. Chem.*, 47(5), 1242-1250

[245] Loftsson, T., Vogensen, S.B., Desbos, C., and Jansook, P. (2008). Carvedilol: solubilization and cyclodextrin complexation: a technical note, *AAPS PharmSciTech.*, 9(2), 425-430

[246] Hamed, R., Awadallah, A., Sunoqrot, S., Tarawneh, O., Nazzal, S., Al Baraghthi, T., Al Sayyad, J., Abbas, A. (2016). pH-Dependent Solubility and Dissolution Behavior of Carvedilol - Case Example of a Weakly Basic BCS Class II Drug, *AAPS PharmSciTech.*, 17(2), 418-426

[247] Antunes, M.V., Rosa, D.D., Viana, T.S., Andreolla, H., Fontanive, T.O., and Linden, R. (2013). Sensitive HPLC-PDA determination of tamoxifen and its metabolites N-desmethyltamoxifen, 4-hydroxytamoxifen and endoxifen in human plasma, *J .Pharm. Biomed. Anal.*, 25, 13-20

[248] Dayan, G., Lupien, M., Auger, A., Anghel, S.I., Rocha, W., Croisetière, S., Katzenellenbogen, J.A., and Mader, S. (2006). Tamoxifen and raloxifene differ in their functional interactions with aspartate 351 of estrogen receptor alpha, *Mol. Pharmacol.*, 70(2), 579-588

[249] Al Lawati, H. A. J., Kadavilpparampu, A. M., and Suliman, F. O. (2014). Combination of capillary micellar liquid chromatography with on-chip microfluidic chemiluminescence detection for direct analysis of buspirone in human plasma, *Talanta*, 127(1), 230-238

[250] Chilmonczyk, Z., Cybulski, J., Bronowska, A., and Les, A. (2000). Molecular modelling of buspirone-serotonin receptor interaction, *Acta Pol. Pharm. - Drug Res.*, 57(4), 281-288

[251] Völgyi, G., Ruiz, R., Box, K., Comer, J., Bosch, E., and Takács-Novák, K. (2007). Potentiometric and spectrophotometric pKa determination of water-insoluble compounds: validation study in a new cosolvent system, *Anal. Chim. Acta*, 583(2), 418-428

[252] Zanatta, G., Nunes, G., Bezerra, E.M., da Costa, R.F., Martins, A., Caetano, E.W., Freire, V.N., and Gottfried, C. (2014). Antipsychotic haloperidol binding to the human dopamine D3 receptor: beyond docking through QM/MM refinement toward the design of improved schizophrenia medicines, *ACS Chem. Neurosci.*, 5(10), 1041-1054

[253] Goodman, V.L., Rock, E.P., Dagher, R., Ramchandani, R.P., Abraham, S., Gobburu, J.V., Booth, B.P., Verbois, S.L., Morse, D.E., Liang, C.Y., Chidambaram, N., Jiang, J.X., Tang, S., Mahjoob, K., Justice, R., and Pazdur, R. (2007). Approval summary: sunitinib for the treatment of imatinib refractory or intolerant gastrointestinal stromal tumors and advanced renal cell carcinoma, *Clin. Cancer. Res.*, 1, 13(5), 1367-1373

[254] Gotink, K.J., Broxterman, H.J., Labots, M., de Haas, R.R., Dekker, H., Honeywell, R.J., Rudek, M.A., Beerepoot, L.V., Musters, R.J., Jansen, G., *et al.* (2011). Lysosomal sequestration of sunitinib: a novel mechanism of drug resistance, *Clin. Cancer Res*., 17(23), 7337-7346

[255] Schulz, M., Iwersen-Bergmann, S., Andresen, H., and Schmoldt, A. (2012). Therapeutic and toxic blood concentrations of nearly 1,000 drugs and other xenobiotics, *Crit. Care*, 16(4), R136

[256] Malheiros, S.V., de Paula, E., Meirelles, NC. (1998). Contribution of trifluoperazine/lipid ratio and drug ionization to hemolysis, *Biochim. Biophys. Acta*, 1373(2), 332-340

[257] Chaiyasit, K., Khovidhunkit, W., and Wittayalertpanya, S., (2009). Pharmacokinetic and The Effect of Capsaicin in Capsicum frutescens on Decreasing Plasma Glucose Level, *J. Med. Assoc. Thai.*, 92(1), 108-113

[258] McLatchie, L. M, and Bevan, S. (2001). The effects of pH on the interaction between capsaicin and the vanilloid receptor in rat dorsal root ganglia neurons, *Br. J. Pharmacol.*, 132(4), 899-908

[259] Minati, L., Antonini, V., Torrengo, S., Serra, M.D., Boustta, M., Leclercq, X., Migliaresi, C., Vert, M., and Speranza, G. (2012). Sustained in vitro release and cell uptake of doxorubicin adsorbed onto gold nanoparticles and covered by a polyelectrolyte complex layer, *Int. J. Pharm.*, 438(1-2), 45-52

[260] Bienvenu, E., Swart, M., Dandara, C., and Ashton, M. (2014). The role of genetic polymorphisms in cytochrome P450 and effects of tuberculosis co-treatment on the predictive value of CYP2B6 SNPs and on efavirenz plasma levels in adult HIV patients, *Antiviral Res.*, 102, 44-53

[261] Fox, D., O'Connor, R., Mallon, P., and McMahon, G. (2011). Simultaneous determination of efavirenz, rifampicin and its metabolite desacetyl rifampicin levels in human plasma, *J. Pharm. Biomed. Anal.*, 56(4), 785-791

[262] Rabel, S.R., Patel, M., Sun, S., and Maurin, M.B. (2001). Electronic and resonance effects on the ionization of structural analogues of efavirenz, *AAPS PharmSci.*, 3(4), E28

[263] Wolf, K.K., Gufford, B.T., Brantley, S.J., Watkins, P.B., and Paine, M.F. (2015) *Drug Metabolism, Transport, and Pharmacogenomics*, in Podolsky, D. K., Camilleri, M., Fitz, J. G., Kallo, A. N., Shanahan, F., Wang, T. C. (ed.) *Yamada' s Textbook of Gastroenterology*, 6th ed., 626-638

[264] Coleman, M.D. (2010). *Human drug metabolism: An introduction* (Wiley-Blackwell), 2nd ed., 1-12

[265] Tafazoli, S., and O'Brien, P.J. (2005). Peroxidases: a role in the metabolism and side effects of drugs, *Drug Discov Today*, 10(9), 617-625

[266] Cruciani, G., Valeri, A, Goracci, L., Pellegrino, R.M., Buonerba, F., and Baroni, M. (2014). Flavin monooxygenase metabolism: why medicinal chemists should matter, *J. Med. Chem.*, 57(14), 6183-6196

[267] Strolin Benedetti, M. (2011). FAD-dependent enzymes involved in the metabolic oxidation of xenobiotics, *Ann. Pharm. Fr.*, 69(1), 45-52

[268] Penning, T.M., (2015) The aldo-keto reductases (AKRs): Overview, *Chem. Biol. Interact.*, 234, 236-246

[269] Bhatia, C., Oerum, S., Bray, J., Kavanagh, K.L., Shafqat, N., Yue, W., and Oppermann, U. (2015) Towards a systematic analysis of human short-chain dehydrogenases/reductases (SDR): Ligand identification and structure-activity relationships, *Chem. Bio.l Interact.*, 234, 114-125

[270] Bock, K.W. (2016). The UDP-glycosyltransferase (UGT) superfamily expressed in humans, insects and plants: Animal-plant arms-race and co-evolution, *Biochem. Pharmacol.*, 99, 11-17

[271] Tibbs, Z.E., Rohn-Glowacki, K.J., Crittenden, F., Guidry, A.L., and Falany, C.N. (2015) Structural plasticity in the human cytosolic sulfotransferase dimer and its role in substrate selectivity and catalysis, *Drug Metab. Pharmacokinet.*, 30(1), 3-20

[272] Sim, E., Lack, N., Wang, C.J., Long, H., Westwood, I., Fullam, E., and Kawamura, A. (2008). Arylamine N-acetyltransferases: structural and functional implications of polymorphisms, *Toxicology*, 254(3), 170-183

[273] Mazzetti, A.P., Fiorile, M.C., Primavera, A., and Lo Bello, M., (2015) Glutathione transferases and neurodegenerative diseases, *Neurochem. Int.*, 82, 10-18

[274] Rendic, S., and Guengerich, F.P., (2015). Survey of Human Oxidoreductases and Cytochrome P450 Enzymes Involved in the Metabolism of Xenobiotic and Natural Chemicals, *Chem. Res. Toxicol.*, 28(1), 38-42

[275] Guengerich, F. P. (2015). *Human cytochrome P450 enzymes*, in De Montellano, O. (ed.) *Cytochrome P450: Structure, Mechanism, and Biochemistry*, 4th ed., Springer, 523-785

[276] Zanger, U.M., and Schwab, M. (2013). Cytochrome P450 enzymes in drug metabolism: regulation of gene expression, enzyme activities, and impact of genetic variation, *Pharmacol. Ther.*, 138(1), 103-141

[277] Olsen, L., Oostenbrink, C., and Jørgensen, F.S. (2015). Prediction of cytochrome P450 mediated metabolism., *Adv. Drug. Deliv. Rev.*, 86, 61-71

[278] Pandey, A.V., and Flück, C.E. (2013) NADPH P450 oxidoreductase: structure, function, and pathology of diseases, *Pharmacol Ther.*, 138(2), 229-254

[279] Guengerich, F.P., *Fifty Years of Progress in Drug Metabolism and Toxicology: What Do We Still Need to Know About Cytochrome P450 Enzymes?* (2014) in Yamazaki, H. (Ed.), *Fifty Years of Cytochrome P450 Research*, Springer, 17-41

[280] Cederbaum, A.I. (2015) Molecular mechanisms of the microsomal mixed function oxidases and biological and pathological implications, *Redox Biology*, 4, 60-73

[281] Avadhani, N.G., Sangar, M.C., Bansal, S., and Bajpai, P. (2011). Bimodal targeting of cytochrome P450s to endoplasmic reticulum and mitochondria: the concept of chimeric signals, *FEBS J.*, 278(22), 4218-4229

[282] Jia, L., and Liu, X. (2007). The Conduct of Drug Metabolism Studies Considered Good Practice (II): In Vitro Experiments, *Curr. Drug Metab.*, 8(8), 822-829

[283] Ma, B., Zhang, G., Qin, J., and Lin, B. (2009). Characterization of drug metabolites and cytotoxicity assay simultaneously using an integrated microfluidic device, *Lab Chip*, 9(2), 232-238

[284] Yang, H., Zheng, Y., Zhao, B., Shao, T., Shi, Q., Zhou, N., and Cai, W. (2013). Encapsulation of liver microsomes into a thermosensitive hydrogel for characterization of drug metabolism and toxicity, *Biomaterials*, 34(38), 9770-9778

[285] Lee, M.Y., Park, C.B., Dordick, J.S., and Clark, D.S. (2005). Metabolizing enzyme toxicology assay chip (MetaChip) for high-throughput microscale toxicity analyses, *Proc. Natl. Acad. Sci. USA*, 102(4), 983-987

[286] Shirakawa, M., Sekine, S., Tanaka, A., Horie, T., and Ito, K. (2015). Metabolic activation of hepatotoxic drug (benzbromarone) induced mitochondrial membrane permeability transition, *Toxicol. Appl. Pharmacol.*, 288(1), 12-18

[287] Obach, R.S. (2008) *Inhibition of drug metabolizing enzymes and drug-drug interactions in drug discovery and development*, in Li, A.P. (ed.), *Drug-Drug Interactions in Pharmaceutical Development*, Wiley-Interscience, 75-95

[288] Mazur, C.S., Kenneke, J.F., Goldsmith, M.R., and Brown, C. (2009) Contrasting influence of NADPH and a NADPH-regenerating system on the metabolism of carbonyl-containing compounds in hepatic microsomes, *Drug Metab. Dispos.*, 37(9), 1801-1805

[289] Milczarek, R., Sokołowska, E., Hallmann, A., Kaletha, K., and Klimek, J. (2008). NADPH- and iron-dependent lipid peroxidation inhibit aromatase activity in human placental microsomes, *J. Steroid Biochem. Mol. Biol.*, 110(3-5), 230-235

[290] McLure, J.A., Miners, J.O., and Birkett, D.J. (2000). Nonspecific binding of drugs to human liver microsomes, *Br. J. Clin. Pharmacol.*, 49(5), 453-461

[291] Chauret, N., Gauthier, A., and Nicoll-Griffith, D.A. (1998). Effect of common organic solvents on in vitro cytochrome P450-mediated metabolic activities in human liver microsomes, *Drug Metab. Dispos.* 26(1), 1-4

[292] Joo, H., Choi, K., and Hodgson, E., (2010). Human metabolism of atrazine, *Pesticide Biochemistry and Physiology*, 98, 73-79

[293] Rashba-Step, J., and Cederbaum, A.I. (1994). Generation of reactive oxygen intermediates by human liver microsomes in the presence of NADPH or NADH, *Mol. Pharmacol.*, (1), 150-157

[294] Rastogi, S., Das, M., and Khanna, S.K. (2002). A novel approach to study the activity and stoichiometry simultaneously for microsomal pentoxyresorufin-O-dealkylase reaction, *FEBS Lett.*, 512(1-3), 121-124

[295] Dinger, J., Woods, C., Brandt, S.D., Meyer, M.R., and Maurer, H.H. (2016). Cytochrome P450 inhibition potential of new psychoactive substances of the tryptamine class, *Toxicol. Lett.*, 241, 82-94

[296] Maurer, H.H., personal communication

[297] Ogilvie, B. W., Usuki, E., Yerino, P. and Parkinson, A. (2008). In vitro approaches for studying the inhibition of drug-metabolizing enzymes and identifying the drug-metabolizing enzymes responsible for the metabolism of drugs (reaction phenotyping) with emphasis on cytochrome P450, in Rodrigues, A. D. (ed.) *Drug-Drug Interactions*, 2nd ed., Informa Healthcare, 231-358

[298] Sohl, C.D., Cheng, Q., and Guengerich, F.P. (2009). Chromatographic assays of drug oxidation by human cytochrome P450 3A4, *Nat. Protoc.*, 4(9), 1252-1257

[299] Coe, K.J., and Koudriakova, T., (2014). Metabolic stability assessed by liver microsomes and hepatocytes, in Caldwell, G.W., Yan, Z. (ed.), *Optimization in Drug Discovery*, Humana Press, 2nd ed., 87-99

[300] Balijepalli, S., Boyd, M.R., and Ravindranath, V. (1999). Inhibition of mitochondrial complex I by haloperidol: the role of thiol oxidation, *Neuropharmacology*, 38(4), 567-577

[301] Ribeiro, M.P., Santos, A.E., and Custódio, J.B. (2014). Mitochondria: the gateway for tamoxifen-induced liver injury, *Toxicology*, 323, 10-18

[302] Larosche, I., Lettéron, P., Fromenty, B., Vadrot, N., Abbey-Toby, A., Feldmann, G., Pessayre, D., and Mansouri, A. (2007). Tamoxifen inhibits topoisomerases, depletes mitochondrial DNA, and triggers steatosis in mouse liver, *J. Pharmacol. Exp. Ther.*, 321(2), 526-535

[303] Theodossiou, T.A., Yannakopoulou, K., Aggelidou, C., and Hothersall, J.S. (2012). Tamoxifen subcellular localization; observation of cell-specific cytotoxicity enhancement by inhibition of mitochondrial ETC complexes I and III, Photochem. Photobiol., 88(4), 1016-1022

[304] Theodossiou, T.A., Wälchli, S., Olsen, C.E., Skarpen, E., and Berg, K. (2016). Deciphering the Nongenomic, Mitochondrial Toxicity of Tamoxifens As Determined by Cell Metabolism and Redox Activity, *ACS Chem. Biol.*, 11(1), 251-262

[305] Lowe III, J.A. (2013). *CNS Drugs*, in Li, J.J., Corey, E. J. (ed.), *Drug Discovery: Practices, Processes, and Perspectives*, Wiley, 245-286

[306] Miyoshi, H. (1998). Structure-activity relationships of some complex I inhibitors. *Biochim. Biophys. Acta*, 1364(2), 236-244

[307] Hamid, N., and Krise, J. P. (2016). The Mechanisms and Therapeutic Consequences of Amine-Containing Drug Sequestration in Lysosomes, in Maxfield, F. R., Willard, J. M., Lu, S. (ed.), *Lysosomes: Biology, Diseases, and Therapeutics*, Wiley

[308] Milane, L., Trivedi, M., Singh, A., Talekar, M., and Amiji, M. (2015). Mitochondrial biology, targets, and drug delivery, *J. Control Release*, 207, 40-58

[309] Horobin, R.W., Trapp, S., and Weissig, V. (2007). Mitochondriotropics: a review of their mode of action, and their applications for drug and DNA delivery to mammalian mitochondria, *J. Control Release*, 121(3), 125-136

[310] Zheng, N., Tsai, H.N., Zhang, X., Shedden, K., and Rosania, G,R. (2011). The subcellular distribution of small molecules: a meta-analysis, *Mol. Pharm.*, 8(5), 1611-1618

[311] Modica-Napolitano, J.S., and Weissig, V. (2015). Treatment Strategies that Enhance the Efficacy and Selectivity of Mitochondria-Targeted Anticancer Agents, *Int. J. Mol. Sci.*, 16(8), 17394-17421

[312] Caboni, P., Sherer, T.B., Zhang, N., Taylor, G., Na, H.M., Greenamyre, J.T., and Casida, J.E. (2004). Rotenone, deguelin, their metabolites, and the rat model of Parkinson's disease, *Chem. Res. Toxicol.*, 17(11), 1540-1548

[313] Chanda, S., Bashir, M., Babbar, S., Koganti, A., and Bley, K. (2008). In vitro hepatic and skin metabolism of capsaicin, *Drug Metab. Dispos.*, 36(4), 670-675

[314] Wilén, G., and Ylitalo, P. (1982). Metabolism of [^{14}C] papaverine in man, *J. Pharm. Pharmacol.*, 34(4), 264-266

[315] Davila, J.C., Reddy, C.G., Davis, P.J., and Acosta, D. (1990). Toxicity assessment of papaverine hydrochloride and papaverine-derived metabolites in primary cultures of rat hepatocytes, *In Vitro Cell Dev. Biol.*, 26(5), 515-524

[316] Mayol, R.F., Cole, C.A., Luke, G.M., Colson, K.L., and Kerns, E.H. (1994). Characterization of the metabolites of the antidepressant drug nefazodone in human urine and plasma*, Drug Metab. Dispos.*, 22(2), 304-311

[317] Dai, C., Li, J., and Li, J., (2013). New insight in colistin induced neurotoxicity with the mitochondrial dysfunction in mice central nervous tissues, *Exp. Toxicol. Pathol.,* 65(6), 941-948

[318] Dalakas, M.C., (2001). Peripheral neuropathy and antiretroviral drugs, *J. Peripher. Nerv. Syst.*, 6(1), 14-20

[319] Tanji, N., Tanji, K, Kambham, N., Markowitz, G.S., Bell, A., and D'agati, V.D. (2001). Adefovir nephrotoxicity: possible role of mitochondrial DNA depletion, *Hum. Pathol.*, 32(7), 734-740

[320] Nissim, I., Horyn, O., Daikhin, Y., Nissim, I., Luhovyy, B., Phillips, P.C., and Yudkoff, M., (2006). Ifosfamide-induced nephrotoxicity: mechanism and prevention, *Cancer Res.*, 66(15), 7824-7831

[321] Pereira, G.C., Silva, A.M., Diogo, C.V., Carvalho, F.S., Monteiro, P., and Oliveira, P.J., (2011). Drug-induced cardiac mitochondrial toxicity and protection: from doxorubicin to carvedilol, *Curr. Pharm. Des.*, 17(20), 2113-2129

[322] Gleeson, J. P., Ryan, S. M., and Brayden, D. J. (2016). Oral delivery strategies for nutraceuticals: Delivery vehicles and absorption enhancers, *Trends in Food Science & Technology*, 53, 90-101

[323] Alvarez-Lueje, A., Sturm, J., Squella, J.A., and Núñez-Vergara, L.J. (2002). Hydrolytic degradation of nitrendipine and nisoldipine, *J. Pharm. Biomed. Anal.*, 28(5), 887-895

[324] Marinkovic, V.D., Agbaba, D., Karljikovic-Rajic, K., Vladimirov, S., and Nedeljkovic, J.M. (2003). Photochemical degradation of solid-state nisoldipine monitored by HPLC, *J. Pharm. Biomed. Anal.*, 32(4-5), 929-935

[325] Spruill, W.J., Wade, E.W., DiPiro, J.T., Blouin, R.A., and Pruemer, J.M. (2014). *Concepts in Clinical Pharmacokinetics*, 6th ed., ASHP, 1-19

[326] Jones, C.M., Mack, K.A., Paulozzi, L.J. (2013). Pharmaceutical overdose deaths, United States, 2010, *JAMA*. 309(7), 657-659

[327] Chen, M., Suzuki, A., Borlak, J., Andrade, R.J., and Lucena, M.I. (2015). Drug-induced liver injury: Interactions between drug properties and host factors, *J. Hepatol.*, 63(2), 503-514

[328] Irwin, J.J., Duan, D., Torosyan, H., Doak, A.K., Ziebart, K.T., Sterling, T., Tumanian, G., and Shoichet, B.K. (2015). An aggregation advisor for ligand Discovery, *J. Med. Chem.*, 58(17), 7076-7087

[329] Shoichet, B.K. (2006). Screening in a spirit haunted world, *Drug Discov. Today*, (13-14), 607-615

[330] Seidler, J., McGovern, S. L., Doman, T. N., and Shoichet, B. K. (2003). Identification and prediction of promiscuous aggregating inhibitors among known drugs, *J. Med. Chem*., 46, 4477-4486

[331] Rieske, J.S., and Das Gupta, U. (1972). On the sigmoidal relationship between inhibition of respiration and antimycin titer, *FEBS Lett.*, 20(3), 316-320

[332] Moreno-Sánchez, R., Bravo, C., and Westerhoff, H.V. (1999). Determining and understanding the control of flux. An illustration in submitochondrial particles of how to validate schemes of metabolic control, *Eur. J. Biochem.*, 264(2), 427-433

[333] Kunz, W.S., Kudin, A., Vielhaber, S., Elger, C.E., Attardi, G., and Villani, G. (2000). Flux control of cytochrome c oxidase in human skeletal muscle, *J. Biol. Chem.*, 275(36), 27741-27745.

[334] Capaldi, R.A. (1982). Arrangements of proteins in the mitochondrial inner membrane, *Biochim. Biophys. Acta*, 694, 291-306

[335] Alikhan, A., Taylor, C. R., and Armstrong, A. W. (2012). *Pharmacology of fungal infections.* 618-628 in Golan, D.E., Tashjian, A.H. Jr., Armstrong, E.J., Armstrong, A.W. (ed.), *Principles of Pharmacology: The Pathophysiologic Basis of Drug Therapy*, 3rd ed., LWW

[336] Ciesielski, F., Griffin, D. C., Loraine, J., Rittig, M., Delves-Broughton, J., and Bonev, B. B. (2016). Recognition of membrane sterols by polyene antifungals Amphotericin B and Natamycin, A ^{13}C MAS NMR study, *Front. Cell Dev. Biol.*, 4, 57

[337] Subissi, A., Monti, D., Togni, G., and Mailland, F. (2010). Ciclopirox: recent nonclinical and clinical data relevant to its use as a topical antimycotic agent, *Drugs*, 70(16), 2133-2152

[338] Corena-McLeod, M. (2015). Comparative Pharmacology of Risperidone and Paliperidone, *Drugs R D*, 15(2), 163-174

[339] Zhai, B., Wu, C., Wang, L., Sachs, M.S., and Lin, X. (2012). The antidepressant sertraline provides a promising therapeutic option for neurotropic cryptococcal infections, *Antimicrob. Agents Chemother.*, 56(7), 3758-3766

[340] Lass-Flörl, C., Dierich, M.P., Fuchs, D., Semenitz, E., and Ledochowski, M., (2001). Antifungal activity against Candida species of the selective serotonin-reuptake inhibitor, sertraline, *Clin. Infect. Dis.*, **33**(12), E135-136

[341] Jones, A.J., Blaza, J.N., Bridges, H.R., May, B., Moore, A.L., and Hirst, J. (2016). A Self-Assembled Respiratory Chain that Catalyzes NADH Oxidation by Ubiquinone-10 Cycling between Complex I and the Alternative Oxidase, *Angew. Chem. Int. Ed. Engl.*, 55(2), 728-731

[342] Moore, A.L., Shiba, T., Young, L., Harada, S., Kita, K., and Ito, K. (2013). Unraveling the heater: new insights into the structure of the alternative oxidase, *Ann. Rev. Plant Biol.*, 64, 637-663

[343] Fontanesi, F. (2015). Mitochondria: Structure and Role in Respiration, *Encyclopedia of Life Sciences (eLS)*, Wiley, a0001380.pub2

[344] Gassner, B., Wüthrich, A., Scholtysik, G., and Solioz, M. (1997). The pyrethroids permethrin and cyhalothrin are potent inhibitors of the mitochondrial complex I, *J. Pharmacol. Exp Ther.*, 281(2), 855-860

[345] Ashton, T.M., Fokas E., Kunz-Schughart, L.A., Folkes, L.K., Anbalagan, S., Huether, M., Kelly, C.J., Pirovano, G., Buffa, F.M., Hammond, E.M., et al. (2016). The anti-malarial atovaquone increases radiosensitivity by alleviating tumour hypoxia, *Nat. Commun.*, 7, 12308

[346] Fiorillo, M., Lamb, R., Tanowitz, H.B., Mutti, L., Krstic-Demonacos, M., Cappello, A.R., Martinez-Outschoorn, U.E., Sotgia, F., and Lisanti, M.P. (2016). Repurposing atovaquone: targeting mitochondrial complex III and OXPHOS to eradicate cancer stem cells, *Oncotarget*, 7(23), 34084-34099

[347] Gohil, V.M., Sheth, S.A., Nilsson, R., Wojtovich, A.P., Lee, J.H., Perocchi, F., Chen, W., Clish, C.B., Ayata, C., Brookes, P.S., et al. (2010). Nutrient-sensitized screening for drugs that shift energy metabolism from mitochondrial respiration to glycolysis, *Nat. Biotechnol.*, 28(3), 249-255

[348] Gohil, V.M., Zhu, L., Baker, C.D., Cracan, V., Yaseen, A., Jain, M., Clish, C.B., Brookes, P.S., Bakovic, M., and Mootha, V.K. (2013). Meclizine inhibits mitochondrial respiration through direct targeting of cytosolic phosphoethanolamine metabolism, *J. Biol. Chem.*, 288(49), 35387-35395

[349] Ayzenberg, I., Hoepner, R., and Kleiter, I. (2016). Fingolimod for multiple sclerosis and emerging indications: appropriate patient selection, safety precautions, and special considerations, *Ther. Clin. Risk Manag.*, 12, 261-272

[350] Pavletic, A.J., and Pao, M. (2015). Exercise-induced elevation of liver enzymes in a healthy female research volunteer, *Psychosomatics*, 56(5), 604-606

[351] Contreras-Zentella, M.L., and Hernández-Muñoz, R. (2016). Is Liver Enzyme Release Really Associated with Cell Necrosis Induced by Oxidant Stress?, *Oxid. Med. Cell Longev.*, 3529149

[352] Woreta, T.A., and Alqahtani, S.A. (2014). Evaluation of abnormal liver tests, *Med. Clin. North Am.*, 98(1), 1-16

[353] Kappos, L., Cohen, J., Collins, W., de Vera, A., Zhang-Auberson, L., Ritter, S., von Rosenstiel, P., and Francis, G. (2014). Fingolimod in relapsing multiple sclerosis: An integrated analysis of safety findings, *Mult. Scler. Relat. Disord.*, 3(4), 494-504

[354] David, O.J., Kovarik, J.M., and Schmouder, R.L. (2012). Clinical pharmacokinetics of fingolimod, *Clin. Pharmacokinet.*, 51(1), 15-28

[355] Huang, C., Chen, D., Xie, Q., Yang, Y., and Shen, W. (2013). Nebivolol stimulates mitochondrial biogenesis in 3T3-L1 adipocytes, *Biochem. Biophys. Res. Commun.*, 438(1), 211-217

[356] Sgobbo, P., Pacelli, C., Grattagliano, I., Villani, G., and Cocco, T. (2007). Carvedilol inhibits mitochondrial complex I and induces resistance to H_2O_2 -mediated oxidative insult in H9C2 myocardial cells, *Biochim. Biophys. Acta*, 1767(3), 222-232

[357] Bartl, R., and von Tresckow, E. (2015). Pharmacological Aspects of Antiresorptive Drugs: Bisphosphonates and Denosumab, in Otto, S., *Medication-related osteonecrosis of the jaws: bisphosphonates, denosumab, and new agents*, Springer

[358] Reid, I.R. (2011). Bisphosphonates in the treatment of osteoporosis: a review of their contribution and controversies, *Skeletal Radiol.*, 40(9), 1191-1196

[359] Meloun, M., Ferenčíková, Z., Málková, H., and Pekárek, T. (2012). Thermodynamic dissociation constants of risedronate using spectrophotometric and potentiometric pH-titration, *Cent. Eur. J. Chem.*, 10(2), 338-353

[360] Ezra, A., and Golomb, G., (2000). Administration routes and delivery systems of bisphosphonates for the treatment of bone resorption, *Adv. Drug Deliv. Rev.*, 42(3), 175-195

[361] Meloun, M., Ferencíkovà, Z., Netolickà, L., and Pekàrek, T. (2011). Thermodynamic Dissociation Constants of Alendronate and Ibandronate by Regression Analysis of Potentiometric Data, *J. Chem. Eng. Data*, 56, 3848-3854

[362] Boichenko, A. P., Markov, V. V., Le Kong, H., Matveeva, A. G., and Loginova, L. P., (2009). Re-evaluated data of dissociation constants of alendronic, pamidronic and olpadronic acids, *Cent. Eur. J. Chem.*, 7(1), 8-13

[363] Mu, L., Xie, F., Li, S., and Yu, P. (2014). Determination of Strong Acidic Drugs in Biological Matrices: A Review of Separation Methods, *Chromatography Research International Volume*, Article ID 469562

[364] Nancollas, G.H., Tang, R., Phipps, R.J., Henneman, Z., Gulde, S., Wu, W., Mangood, A., Russell, R.G., and Ebetino, F.H. (2006). Novel insights into actions of bisphosphonates on bone: differences in interactions with hydroxyapatite, *Bone*, 38(5), 617-627

[365] David, P., Nguyen, H., Barbier, A., and Baron, R. (1996). The bisphosphonate tiludronate is a potent inhibitor of the osteoclast vacuolar H(+)-ATPase, *J. Bone Miner. Res.*, 11(10), 1498-1507

[366] Mast, N., Zheng, W., Stout, C.D., and Pikuleva, I.A. (2013). Antifungal Azoles: Structural Insights into Undesired Tight Binding to Cholesterol-Metabolizing CYP46A1, *Mol. Pharmacol.* 84(1), 86-94

[367] Sagatova, A.A., Keniya, M.V., Wilson, R.K., Monk, B.C., and Tyndall, J.D. (2015). Structural Insights into Binding of the Antifungal Drug Fluconazole to Saccharomyces cerevisiae Lanosterol 14α-Demethylase, *Antimicrob. Agents Chemother.*, 59(8), 4982-4989

[368] Nowosielski, M., Hoffmann, M., Wyrwicz, L.S., Stepniak, P., Plewczynski, D.M., Lazniewski, M., Ginalski, K., and Rychlewski, L. (2011). Detailed mechanism of squalene epoxidase inhibition by terbinafine, *J. Chem. Inf. Model.*, 51(2), 455-462

[369] Liu, R., Liu, Y., Cheng, C., and Yang, Y. (2017). Magnetic Solid-Phase Extraction and Ionic Liquid Dispersive Liquid-Liquid Microextraction Coupled with High-Performance Liquid Chromatography for the Determination of Hexachlorophene in Cosmetics, *Chromatographia*, 80, 783-791

[370] Narayan, M., Peralta, D.A., Gibson, C., Zitnyar, A., and Jinwal, U.K. (2015). An optimized InCell Western screening technique identifies hexachlorophene as a novel potent TDP43 targeting drug, *J. Biotechnol.*, 207, 34-38

[371] Boyle, A., and Ondo, W. (2015). Role of apomorphine in the treatment of Parkinson's disease, *CNS Drugs*, 29(2), 83-89

[372] Gardenhire, D.S. (2016). Adrenergic (Sympathomimetic) Bronchodilators, in Gardenhire, D.S. (ed.) *Rau's Respiratory Care Pharmacology*, Elsevier, 9th ed., 97-122

[373] Santus, P., Radovanovic, D., Paggiaro, P., Papi, A., Sanduzzi, A., Scichilone, N., and Braido, F. Why use long acting bronchodilators in chronic obstructive lung diseases? An extensive review on formoterol and salmeterol, *Eur. J. Intern. Med.*, 26(6), 379-384

[374] Jitrapakdee, S., St Maurice, M., Rayment, I., Cleland, W. W., Wallace, J. C., and Attwood, P. V. (2008). Structure, mechanism and regulation of pyruvate carboxylase. *Biochem. J.*, 413, 369-387

[375] Vuda, M., and Kamath, A. (2016). Drug induced mitochondrial dysfunction: Mechanisms and adverse clinical consequences, *Mitochondrion*, 31, 63-74

[376] Weber, C., and Dumont, E., (1997). Pharmacokinetics and pharmacodynamics of 9-cis-retinoic acid in healthy men, *J. Clin. Pharmacol.*, 37(7), 566-574

[377] Koch, K. M., Palmer, J. L., Noordin, N., Tomlinson, J. J., and Baidoo, C., (2002). Sex and age differences in the pharmacokinetics of alosetron, *Br. J. Clin. Pharmacol.*, 53(3), 238-242

[378] http://www.ema.europa.eu/docs/en_GB/document_library/EPAR - Product_Information/human/000527/WC500026537.pdf, accessed on 13th April 2016

[379] Simpson, D., and Plosker, G.L. (2004). Atomoxetine: a review of its use in adults with attention deficit hyperactivity disorder, *Drugs*, 64(2), 205-222

[380] Roder, C., and Thomson, M. J., (2015). Auranofin: Repurposing an Old Drug for a Golden New Age, *Drugs R D,* 15, 13-20

[381] http://www.accessdata.fda.gov/drugsatfda_docs/nda/2000/21-056_Targretin_biopharmr_P1.pdf, accessed on 14th April 2016

[382] https://www.accessdata.fda.gov/drugsatfda_docs/label/2002/21408lbl.pdf, accessed on 16th April 2016

[383] https://www.gynazole.com/pdf/PI.pdf, accessed on 16th April 2016

[384] http://www.enstilar.com/pdf/enstilar-pi.pdf, accessed on 13th April 2016

[385] Trump, D.L., Hershberger, P.A., Bernardi, R.J., Ahmed, S., Muindi, J., Fakih, M., Yu, W.D., and Johnson, C.S. (2004). Anti-tumor activity of calcitriol: pre-clinical and clinical studies, *J. Steroid Biochem. Mol. Biol.,* 89-90(1-5), 519-526

[386] http://solutions.3mcanada.ca/3MContentRetrievalAPI/BlobServlet?lmd=1326817103000&locale=en_CA&assetType=MMM_Image&assetId=1319218897052&blobAttribute=ImageFile, accessed on 14th April 2016

[387] Deeks, E. D., and Perry, C. M., (2008). Ciclesonide A Review of its Use in the Management of Asthma, *Drugs*, 68(12), 1741-1770

[388] Kim, Y.H., Ghim, J.L., Jung, J.A., Cho, S.H., Choe, S., Choi, H.Y., Bae, K.S., and Lim, H.S. (2015). Pharmacokinetic comparison of sustained- and immediate-release formulations of cilostazol after multiple oral doses in fed healthy male Korean volunteers, *Drug Des. Devel. Ther.*, 9, 3571-3577

[389] Padhi, D., and Harris, R., (2009). Clinical Pharmacokinetic and Pharmacodynamic Profile of Cinacalcet Hydrochloride, *Clin. Pharmacokinet.*, 48(5), 303-311

[390] Mazur, D., Schug, B.S., Evers, G., Larsimont, V., Fieger-Büschges, H., Gimbel, W., Keilbach-Bermann, A., and Blume, H.H. (1999). Bioavailability and selected pharmacokinetic parameters of clindamycin hydrochloride after administration of a new 600 mg tablet formulation, *Int. J. Clin. Pharmacol. Ther.*, 37(8), 386-392

[391] Peloquin, C. A., and Auclair, B. (2000). Pharmacology of the second-line antituberculosis drugs, 163-174 in Bastian, I., Portaels, F. (ed.) *Multidrug-resistant tuberculosis: Resurgent and Emerging Infectious Diseases*, Kluwer Academic Publishers

[392] Mürdter, T.E., Kerb, R., Turpeinen, M., Schroth, W., Ganchev, B., Böhmer, G.M., Igel, S., Schaeffeler, E., Zanger, U., Brauch, H., and Schwab, M. (2012). Genetic polymorphism of cytochrome P450 2D6 determines oestrogen receptor activity of the major infertility drug clomiphene via its active metabolites, *Hum. Mol. Genet.*, 21(5), 1145-1154

[393] Rifai N., Sakamoto, M., Law, T., Platt, O., Mikati, M., Armsby, C. C., and Brugnara C., (1995). HPLC Measurement, Blood Distribution, and Pharmacokinetics of Oral Clotrimazole, Potentially Useful Antisickling Agent, *Clin. Chem.*, 41(3), 387-391

[394] Mendes, G.D., Arruda, A., Chen, L.S., de Almeida Magalhães J.C., Alkharfy, K.M., and De Nucci, G. (2012). Quantification of cyproheptadine in human plasma by high-performance liquid chromatography coupled to electrospray tandem mass spectrometry in a bioequivalence study, *Biomed. Chromatogr.*, 26(1), 129-136

[395] Aguilar-Carrasco, J. C., Carrasco-Portugal, N. A., Carrasco-Portugal, M. C., Herrera, J. E., and Flores-Murrieta, F. J. (2006). Comparative Bioavailability of Two Oral Formulations of Danazol in Mexican Subjects, *Proc. West. Pharmacol. Soc.*, 49, 48-50

[396] http://www.accessdata.fda.gov/drugsatfda_docs/label/2012/021513s010lbl.pdf, accessed on 16th April 2016

[397] http://www.ema.europa.eu/docs/en_GB/document_library/EPAR_-_Scientific_Discussion/human/000709/WC500056995.pdf, accessed on 15th April 2016

[398] Gessner, T., Preisler, H.D., Azarnia, N., Bolanowska, W., Vogler, W.R., Grunwald, H., Joyce, R., and Goldberg, J. (1987). Plasma levels of daunorubicin metabolites and the outcome of ANLL therapy, *Med. Oncol. Tumor Pharmacother.*, 4(1), 23-31

[399] Goldzieher, J.W., (1993). Pharmacology of contraceptive steroids, 17-25 in *Contraception: Clinical Perspectives in Obstetrics and Gynecology*, Shoupe, D. Haseltine, F. P., (Ed.), Springer-Verlag

[400] http://www.accessdata.fda.gov/drugsatfda_docs/nda/2013/204141Orig1s000PharmR.pdf, accessed on 15th April 2016

[401] Moreno, R.A., Oliveira-Silva. D., Sverdloff, C.E., Borges, B.C., Rebelo Galvinas, P.A., Astigarraga, R.B., and Borges, N.C. (2010). Determination of chlorpheniramine in human plasma by HPLC-ESI-MS/MS: application to a dexchlorpheniramine comparative bioavailability study *Biomed. Chromatogr.*, 24(7), 774-781

[402] Venn, R.M., Karol, M.D., and Grounds, R.M. (2002). Pharmacokinetics of dexmedetomidine infusions for sedation of postoperative patients requiring intensive care, *Br. J. Anaesth.*, 88(5), 669-675

[403] Putnam, W.S., Woo, J.M., Huang, Y., and Benet, L.Z. (2005). Effect of the MDR1 C3435T variant and P-glycoprotein induction on dicloxacillin pharmacokinetics, *J. Clin. Pharmacol.*, 45(4), 411-421

[404]http://www.accessdata.fda.gov/drugsatfda_docs/anda/99/40230_Dicyclomine%20Hydrochloride_Bioeqr.pdf, accessed on 15th April 2016

[405] http://www.accessdata.fda.gov/drugsatfda_docs/label/2015/022252s004lbl.pdf, accessed on 15th April 2016

[406] Daly, A.L., Linares, O.A., Smith, M.J., Starling, M.R., and Supiano, M.A., (1997). Dobutamine pharmacokinetics during dobutamine stress echocardiography, *Am. J. Cardiol.*, 79(10), 1381-1386

[407] Le Coz, F., Funck-Brentano, C., Morell, T., Ghadanfar, M.M., and Jaillon, P. (1995). Pharmacokinetic and pharmacodynamic modeling of the effects of oral and intravenous administrations of dofetilide on ventricular repolarization, *Clin Pharmacol Ther.*, 57(5), 533-542

[408] Gupta, S.K., Southam, M., and Hwang, S. (1992). Pharmacokinetics of droperidol in healthy volunteers following intravenous infusion and rectal administration from an osmotic drug delivery module *Pharm. Res.*, 9(5), 694-696

[409] Blode, H., Wuttke, W., Loock, W., Röll, G., and Heithecker, R. (2000). A 1-year pharmacokinetic investigation of a novel oral contraceptive containing drospirenone in healthy female volunteers, *Eur. J. Contracept. Reprod. Health Care*, 5(4), 256-264

[410] Ganesan, M., Ashok, P., Ragunath, M. P., Kathiravan, S., Sudha, A., Elangovan, N., Punitha, T., and Venkatrao, K. (2013). A single-dose, randomized two sequence, open-label crossover study of two different formulations of Dutasteride capsule in healthy Indian adult, human male volunteers under fasting conditions, *Asian J. Pharm. Clin. Res.*, 6(2), 75-77

[411] http://www.fda.gov/downloads/Drugs/DevelopmentApprovalProcess/DevelopmentResources/UCM376099.pdf, accessed on 13th April 2016

[412] Adkins, J. C., and Noble, S. (1998). Efavirenz, *Drugs*, 56 (6), 1055-1064

[413] Sarashina, A., Tatami, S., Yamamura, N., Tsuda, Y., and Igarashi, T. (2005). Population pharmacokinetics of epinastine, a histamine H1 receptor antagonist, in adults and children, *Br. J. Clin. Pharmacol.*, 59(1), 43-53

[414] Doose, D.R., Wang, S.S., Padmanabhan, M., Schwabe, S., Jacobs, D., and Bialer, M. (2003). Effect of topiramate or carbamazepine on the pharmacokinetics of an oral contraceptive containing norethindrone and ethinyl estradiol in healthy obese and nonobese female subjects, *Epilepsia*, 44(4), 540-549

[415] Timmer, C. J., and Mulders, T.M.T., (2000). Pharmacokinetics of Etonogestrel and Ethinylestradiol Released from a Combined Contraceptive Vaginal Ring, *Clin. Pharmacokinet.*, 39(3), 233-242

[416] Traina, T.A., Poggesi, I., Robson, M., Asnis, A., Duncan, B.A., Heerdt, A., Dang, C., Lake, D., Moasser, M., Panageas, K., Borgen, P., Norton, L., Hudis, C., and Dickler, M.N. (2008). Pharmacokinetics and tolerability of exemestane in combination with raloxifene in postmenopausal women with a history of breast cancer, *Breast Cancer Res. Treat.*, 111(2), 377-388

[417] http://www.accessdata.fda.gov/drugsatfda_docs/label/2008/021445s019lbl.pdf, accessed on 17th April 2016

[418] Ruffmann, R., (1988). A Review of Flavoxate Hydrochloride in the Treatment of Urge Incontinence, *J. Int. Med. Res.*, 16, 317-333

[419] Möllmann, H, Derendorf, H., Barth, J., Meibohm, B., Wagner, M., Krieg, M., Weisser, H., Knöller, J., Möllmann, A., and Hochhaus, G. (1997). Pharmacokinetic/pharmacodynamic evaluation of systemic effects of flunisolide after inhalation. *J. Clin. Pharmacol.*, 37(10), 893-903

[420] Swaisland, H.C., Smith, R.P., Laight, A., Kerr, D.J., Ranson, M., Wilder-Smith, C.H., and Duvauchelle, T. (2005). Single-dose clinical pharmacokinetic studies of gefitinib, *Clin. Pharmacokinet.*, 44(11), 1165-1177

[421] http://www.accessdata.fda.gov/drugsatfda_docs/anda/98/74517_Guanabenz%20Acetate_Bioeqr.pdf, accessed on 14th April 2016

[422] Roesch, B., Corcoran, M.E., Fetterolf, J., Haffey, M., Martin, P., Preston, P., Purkayastha, J., Wang, P., and Ermer, J. (2013). Pharmacokinetics of coadministered guanfacine extended release and lisdexamfetamine dimesylate, *Drugs R D*, 13(2), 119-128

[423] Indik, J.H., Pearson, E.C., Fried, K., and Woosley, R.L. (2006). Bazett and Fridericia QT correction formulas interfere with measurement of drug-induced changes in QT interval, *Heart Rhythm*, 3(9), 1003-1007

[424] Buckley, M. M., and Lamb, H. M., (1997). Oral Idarubicin A Review of its Pharmacological Properties and Clinical Efficacy in the Treatment of Haematological Malignancies and Advanced Breast Cancer, *Drugs & Aging*, 11(1), 61-86

[425] Harrison, L.I., Skinner, S.L., Marbury, T.C., Owens, M.L., Kurup, S., McKane, S., and Greene, R.J. (2004). Pharmacokinetics and safety of imiquimod 5% cream in the treatment of actinic keratoses of the face, scalp, or hands and arms, *Arch. Dermatol. Res.*, 296(1), 6-11

[426] Baraka, O.Z., Mahmoud, B.M., Marschke, C.K., Geary, T.G., Homeida, M.M., and Williams, J.F. (1996). Ivermectin distribution in the plasma and tissues of patients infected with Onchocerca volvulus, *Eur. J. Clin. Pharmacol.*, 50(5), 407-410

[427] Freston, J.W., Pilmer, B.L., Chiu, Y.L., Wang, Q., Stolle, J.C., Griffin, J.S., and Lee, C.Q. (2004). Evaluation of the pharmacokinetics and pharmacodynamics of intravenous lansoprazole, *Aliment. Pharmacol. Ther.*, 19(10), 1111-1122

[428] Sjöquist, B., and Stjernschantz, J., (2002). Ocular and systemic pharmacokinetics of latanoprost in humans, *Surv. Ophthalmol.* 47,1, S6-12

[429] Roos, T. C., Alam, M., Roos, S., Merk, H. F., and Bickers, D. R. (2001). Pharmacotherapy of Ectoparasitic Infections, *Drugs*, 61(8), 1067-1088

[430] Leggio, G.M., Incognito, T., Privitera, G., Marano, M.R., and Drago, F. (2006). Comparative bioavailability of different formulations of levothyroxine and liothyronine in healthy volunteers, *J. Endocrinol Invest.*, 29(11), RC35-38

[431] Kamali, F., and Huang, M.L. (1996). Increased systemic availability of loperamide after oral administration of loperamide and loperamide oxide with cotrimoxazole, *Br. J. Clin. Pharmacol.*, 41(2), 125-128

[432] Davidson, M.H., Lukacsko, P., Sun, J.X., Phillips, G., Walters, E., Sterman, A., Niecestro, R., and Friedhoff, L. (2002). A multiple-dose pharmacodynamic, safety, and pharmacokinetic comparison of extended- and immediate-release formulations of lovastatin, *Clin. Ther.*, 24(1), 112-125

[433] http://www.acutetox.eu/pdf_human_short/11-Malathion%20revised.pdf, accessed on 17th April 2016

[434] Wang, Z., Lee, B., Pearce, D., Qian, S., Wang, Y., Zhang, Q., and Chow, M.S. (2012). Meclizine metabolism and pharmacokinetics: formulation on its absorption, *J. Clin. Pharmacol.*, 52(9), 1343-1349

[435] Zhou, X.F., Shao, Q.X., Han, X.J., Weng, L.J., and Sang, G.W. (1998). Pharmacokinetics of medroxyprogesterone acetate after single and multiple injection of Cyclofem in Chinese women, *Contraception*, 57(6), 405-411

[436] http://www.bmscanada.ca/static/products/en/pm_pdf/Megace_OS_EN_PM.pdf, accessed on 13th April 2016

[437] http://www.accessdata.fda.gov/drugsatfda_docs/nda/2010/022404Orig1s000ClinPharmR.pdf, accessed on 15th April 2016

[438] http://www.accessdata.fda.gov/drugsatfda_docs/nda/2012/202107Orig1s000ClinPharmR.pdf, accessed on 16th April 2016

[439] Schaff, E. A., DiCenzo, R., and Fieldinga S. L., (2005). Comparison of misoprostol plasma concentrations following buccal and sublingual administration, *Contraception,* 71, 22-25

[440] Nicoletto, M.O., Padrini, R., Galeotti, F., Ferrazzi, E., Cartei, G., Riddi, F., Palumbo, M., De Paoli, M., and Corsini, A. (2000). Pharmacokinetics of intraperitoneal hyperthermic perfusion with mitoxantrone in ovarian cancer, *Cancer Chemother Pharmacol.*, 45(6), 457-462

[441] Hedner, T., Samulesson, O., Währborg, P., Wadenvik, H., Ung, K.A., and Ekbom, A. (2004). Nabumetone: therapeutic use and safety profile in the management of osteoarthritis and rheumatoid arthritis, *Drugs*, 64(20), 2315-2343

[442] http://www.fda.gov/downloads/Drugs/DevelopmentApprovalProcess/DevelopmentResources/UCM425044.pdf, accessed on 16th April 2016

[443] http://www.ema.europa.eu/docs/en_GB/document_library/EPAR_-_Product_Information/human/000818/WC500027158.pdf, accessed on 13th April 2016

[444] Gaillard, M. (1996). Pharmacodynamics and Pharmacokinetics of Nilutamide in Animal and Man, in Denis L., Veronesi, U. (ed.) *Antiandrogens in Prostate Cancer: A Key to Tailored Endocrine Treatment*, Springer-Verlag

[445] Spence, R., Mandagere, A., Walker, G., Dufton, C., and Boinpally, R., (2010). Effect of Steady-State Ambrisentan on the Pharmacokinetics of a Single Dose of the Oral Contraceptive Norethindrone (Norethisterone) 1 mg/Ethinylestradiol 35 lg in Healthy Subjects An Open-Label, Single-Sequence, Single-Centre Study, *Clin. Drug Investig.*, 30(5), 313-324

[446] McNeely, W., and Benfield, P. (1998). Orlistat, *Drugs*, 56(2), 241-249

[447] Pfaller, M.A. (2010). Oxiconazole, 1923-1925 in Grayson, ML., *Kucers' the Use of antibiotics, A Clinical Review of Antibacterial, Antifungal, Antiparasitic and Antiviral Drugs*, 6th ed., Vol. I, Taylor & Francis

[448] Gupta, S.K., and Sathyan, G. (1999). Pharmacokinetics of an oral once-a-day controlled-release oxybutynin formulation compared with immediate-release oxybutynin, *J. Clin. Pharmacol.*, 39(3), 289-296

[449] Eisenberg, P., MacKintosh, F.R., Ritch, P., Cornett, P.A., and Macciocchi, A. (2004). Efficacy, safety and pharmacokinetics of palonosetron in patients receiving highly emetogenic cisplatin-based chemotherapy: a dose-ranging clinical study, *Ann. Oncol.*, 15(2), 330-337

[450] Hurwitz, H.I., Dowlati, A., Saini, S., Savage, S., Suttle, A.B., Gibson, D.M., Hodge, J.P., Merkle, E.M., and Pandite, L. (2009). Phase I trial of pazopanib in patients with advanced cancer, *Clin. Cancer Res.*, 15(12), 4220-4227

[451] Franz, T.J., Lehman, P.A., Franz, S.F., and Guin, J.D. (1996). Comparative percutaneous absorption of lindane and permethrin, *Arch. Dermatol.*, 132(8), 901-905

[452] http://www.mhra.gov.uk/home/groups/par/documents/websiteresources/con131987.pdf, accessed on 16th April 2016

[453] Li, Y., Theuretzbacher, U., Clancy, C.J., Nguyen, M.H., and Derendorf, H. (2010). Pharmacokinetic/pharmacodynamic profile of posaconazole, *Clin. Pharmacokinet.*, 49(6), 379-396

[454] Farid, N.A., Kurihara, A., and Wrighton, S.A. (2010). Metabolism and disposition of the thienopyridine antiplatelet drugs ticlopidine, clopidogrel, and prasugrel in humans, *J. Clin. Pharmacol.*, 50(2), 126-142

[455] Levy, T., Yairi, Y., Bar-Hava, I., Shalev, J., Orvieto, R., and Ben-Rafael, Z. (2000). Pharmacokinetics of the progesterone-containing vaginal tablet and its use in assisted reproduction. *Steroids*., 65(10-11), 645-649

[456] http://www.ema.europa.eu/docs/en_GB/document_library/EPAR_-_Public_assessment_report/human/001075/WC500091423.pdf, accessed on 13th April 2016

[457] Jerling, M., (2006). Clinical pharmacokinetics of ranolazine, *Clin. Pharmacokinet.*, 45(5), 469-491

[458] Kempsford, R., Handel, M., Mehta, R., De Silva, M., and Daley-Yates, P. (2005). Comparison of the systemic pharmacodynamic effects and pharmacokinetics of salmeterol delivered by CFC propellant and non-CFC propellant metered dose inhalers in healthy subjects, *Respir. Med.* 99, Suppl. A, S11-19

[459] Croxtall, J. D., and Plosker, G. L., (2009). Sertaconazole A Review of Its Use in the Management of Superficial Mycoses in Dermatology and Gynaecology, *Drugs*, 69(3), 339-359

[460] http://www.medsafe.govt.nz/profs/datasheet/f/flamazinecrm.pdf, accessed on 16th April 2016

[461] Furuse, J., Ishii, H., Nakachi, K., Suzuki, E., Shimizu, S., and Nakajima, K. (2008). Phase I study of sorafenib in Japanese patients with hepatocellular carcinoma, *Cancer Sci.*, 99(1), 159-165

[462] Lankheet, N.A., Knapen, L.M., Schellens, J.H., Beijnen, J.H., Steeghs, N., and Huitema, A.D. (2014). Plasma concentrations of tyrosine kinase inhibitors imatinib, erlotinib, and sunitinib in routine clinical outpatient cancer care, *Ther. Drug. Monit.*, 36(3), 326-334

[463] http://www.accessdata.fda.gov/drugsatfda_docs/label/2005/020579s016lbl.pdf, accessed on 15th April 2016

[464] Tang-Liu, D. D.-S., Matsumoto, R. M., and Usansky, J. I., (1999). Clinical Pharmacokinetics and Drug Metabolism of Tazarotene A Novel Topical Treatment for Acne and Psoriasis *Clin. Pharmacokinet.*, 37(4), 273-287

[465] McClellan, K. J., Wiseman L. R., and Markham A., (1999). Terbinafine An Update of its Use in Superficial Mycoses, *Drugs*, 58(1), 179-202

[466] http://www.fougera.com/products/documents/1289.PI.pdf, accessed on 16th April 2016

[467] Scott, L. J., (2011). Tetrabenazine For Chorea Associated with Huntington's Disease, *CNS Drugs*, 25(12), 1073-1085

[468] Brynne, N., Svanström, C., Aberg-Wistedt, A., Hallén, B., and Bertilsson, L. (1999). Fluoxetine inhibits the metabolism of tolterodine-pharmacokinetic implications and proposed clinical relevance, *Br. J. Clin. Pharmacol.*, 48(4), 553-563

[469] Taras, T.L., Wurz, G.T., Linares, G.R., and DeGregorio, M.W. (2000). Clinical pharmacokinetics of toremifene, *Clin. Pharmacokinet.*, 39(5), 327-334

[470] http://www.accessdata.fda.gov/drugsatfda_docs/label/2006/021994lbl.pdf, accessed on 15th April 2016

[471] http://www.accessdata.fda.gov/drugsatfda_docs/nda/2006/050802s000_ClinPharmR.pdf, accessed on 15th April 2016

[472] Regenthal, R., Krueger, M., Koeppel, C., and Preiss, R. (1999). Drug levels: therapeutic and toxic serum/plasma concentrations of common drugs, *J. Clin. Monit. Comput.*, 15(7-8), 529-544

[473] Lemke, T.L., Williams, D.A., Roche, V.F., and Zito, S.W. (2013). *Foye's Principles of Medicinal Chemistry*, Wolters Kluwer, 7th ed., 1469-1479

[474] Wahajuddin, Raju, K. S. R., and Taneja, I. (2013). Bioanalysis of antimalarials using liquid chromatography, *Trends in Analytical Chemistry*, (42), 186-204

[475] Barth, A.B., de Oliveira, G.B., Malesuik, M.D., Paim, C.S., and Volpato, N.M. (2011). Stability-indicating LC assay for butenafine hydrochloride in creams using an experimental design for robustness evaluation and photodegradation kinetics study, *J. Chromatogr. Sci.*, 49(7), 512-518

[476] Lu, S., Jessen, B., Will, Y. and Stevens, G. (2016). Lysosome Dysfunction: An Emerging Mechanism of Xenobiotic-Induced Toxicity, in Maxfield, F. R., Willard, J. M., and Lu, S., *Lysosomes: Biology, Diseases, and Therapeutics: Biology, Diseases, and Therapeutics*, Wiley, 445-485

[477] Groth, L., and Jørgensen, A. (1997). In vitro microdialysis of hydrophilic and lipophilic compounds, *An. Chim. Acta*, 355, 75-83

[478] McLatchie, L.M., and Bevan, S. (2001). The effects of pH on the interaction between capsaicin and the vanilloid receptor in rat dorsal root ganglia neurons, *Br. J. Pharmacol.*, 132(4), 899-908

[479] Nirogi, R., Kandikere, V., Komarneni, P., Aleti, R., Padala, N., and Kalaikadiban, I. (2011). Quantification of cinacalcet by LC-MS/MS using liquid-liquid extraction from 50 µL of plasma, *J. Pharm. Biomed. Anal.*, 56(2), 373-381

[480] Hermawan, D., Wan, Ibrahim, W.A., Sanagi, M.M., Aboul-Enein, H.Y. (2010). Chiral separation of econazole using micellar electrokinetic chromatography with hydroxypropyl-gamma-cyclodextrin, *J. Pharm. Biomed. Anal.*, 53(5), 1244-1249

[481] Avdeef, A. (2012). *Absorption and drug development: Solubility, permeability, and charge state*, Wiley Interscience, 31-173

[482] Vialpando, M., Backhuijs, F., Martens, J.A., and Van den Mooter, G. (2012). Risk assessment of premature drug release during wet granulation of ordered mesoporous silica loaded with poorly soluble compounds itraconazole, fenofibrate, naproxen, and ibuprofen, *Eur. J. Pharm. Biopharm.*, 81(1), 190-198

[483] Thoma, K., Ziegler, I., (1998). Simultaneous quantification of released succinic acid and a weakly basic drug compound in dissolution media, *Eur. J. Pharm. Biopharm.*, 46(2), 183-190

[484] Bastings, E. (2010). Clinical Pharmacology/Biopharmaceutics Review - Fingolimod, FDA Memorandum, 5-10

[485] Papas, E. S., Chaldezos, C.N., Atta-Politou, J., and Koupparis, M. A. (2010). Construction of a fluoxetine ion chemical sensor and its application for the determination of pKa value of fluoxetine conjugated acid, complexation Study with β-Cyclodextrin and formulations assay, *Anal. Lett.*, 43, 2171-2183

[486] Australian Public Assessment Report for Iloperidone (2012). Department of Health and Ageing (Australian Government), 5-7

[487] Pauwels, P.J., Leysen, J.E., Janssen, P.A. (1989). Beta-adrenoceptor-mediated cAMP accumulation in cardiac cells: effects of nebivolol, *Eur. J. Pharmacol.*, 172(6), 471-479

[488] Tuğcu-Demiröz, F., Acartürk, F., and Erdoğan, D. (2013). Development of long-acting bioadhesive vaginal gels of oxybutynin: formulation, in vitro and in vivo evaluations, *Int. J. Pharm.*, 457(1), 25-39

[489] Wan, H., Holmén, A., Någård, M., and Lindberg, W. (2002). Rapid screening of pKa values of pharmaceuticals by pressure-assisted capillary electrophoresis combined with short-end injection, *J. Chromatogr. A*, 979(1-2), 369-377

[490] Hatami, M., Karimnia, E., Farhadi, K. (2013). Determination of salmeterol in dried blood spot using an ionic liquid based dispersive liquid-liquid microextraction coupled with HPLC, *J. Pharm. Biomed. Anal.*, 85, 283-287

[491] Heidarinasab, A., Ahmad Panahi, H., Faramarzi, M., and Farjadian, F. (2016). Synthesis of thermosensitive magnetic nanocarrier for controlled sorafenib delivery, *Mater. Sci. Eng. C Mater. Biol. Appl.*, 67, 42-50

[492] Chen, J., Du, Y., Zhu, F., Chen, B., Zhang, Q., Du, S., and Li, P. (2015). Study of the enantioseparation capability of chiral dual system based on chondroitin sulfate C in CE, *Electrophoresis*, 36(4), 607-614

[493] Zsila, F., and Fitos, I. (2010). Combination of chiroptical, absorption and fluorescence spectroscopic methods reveals multiple, hydrophobicity-driven human serum albumin binding of the antimalarial atovaquone and related hydroxynaphthoquinone compounds, *Org. Biomol. Chem.*, 8(21), 4905-4914

[494] Forest Laboratories Canada Inc. (2016). *BYSTOLIC Product Monograph*, 1-36

[495] Pavela, R. (2014). Limitation of Plant Biopesticides, in Singh, D. (ed.) *Advances in Plant Biopesticides*, Springer, 347-359

[496] Han, G., Casson, R.J., Chidlow, G., and Wood, J.P. (2014). The mitochondrial complex I inhibitor rotenone induces endoplasmic reticulum stress and activation of GSK-3β in cultured rat retinal cells, *Invest. Ophthalmol. Vis. Sci.*, 55(9), 5616-5628

[497] Kamari, A., Aljafree, N. F. A., and Yusoff, S. N. M. (2016). Oleoyl-carboxymethyl chitosan as a new carrier agent for the rotenone pesticide, *Environ. Chem. Lett.*, 14, 417-422

[498] Lazo, C.R., Guillot, T.S., and Miller, G.F. (2014). Rotenone, in Aminoff, M.J., Daroff, R.B. (ed.) *Encyclopedia of the Neurological Sciences*, Vol. 1, Academic Press, 74-76

[499] Rhee, J., Yum, H., Moon, S., In, S., Lee, S., and Seo, J. (2016). Rotenone Analysis by Liquid Chromatography-Tandem Mass Spectrometry with Information-Dependent Acquisition in a Fatal Case of Rotenone Poisoning with a Commercial Organic Insecticide Being Sold in Korea, *J. Anal. Toxicol.*, 40(6), 460-465

[500] Cabezas, R., El-Bachá, R.S., González, J., and Barreto, G.E. (2012). Mitochondrial functions in astrocytes: neuroprotective implications from oxidative damage by rotenone, *Neurosci. Res.* 74(2), 80-90

[501] Karlsson, M., Ehinger, J.K., Piel, S., Sjövall, F., Henriksnäs, J., Höglund, U., Hansson, M.J., and Elmér, E. (2016). Changes in energy metabolism due to acute rotenone-induced mitochondrial complex I dysfunction - An in vivo large animal model, *Mitochondrion*, 31, 56-62

[502] Boyd, J., and Han, A. (2016). Deguelin and its role in chronic diseases, in Gupta, S.C., Prasad, S., and Aggarwal, B.B. (ed.), *Drug discovery from mother nature*, Springer, 363-376

[503] Vats, S., and Kamal, R. (2014). Cassia occidentalis L. (a new source of rotenoids): its in vitro regulation by feeding precursors and larvicidal efficacy, *Plant Cell Tissue Organ Cult.*, 116, 403-409

[504] Bueno Pérez, L., Pan, L., Muñoz Acuña, U., Li, J., Chai, H.B., Gallucci, J.C., Ninh, T.N., Carcache de Blanco, E.J., Soejarto, D.D., and Kinghorn, A.D. (2014). Caeruleanone A, a rotenoid with a new arrangement of the D-ring from the fruits of Millettia caerulea, *Org. Lett.* 16(5), 1462-1465

[505] Miyoshi, H. (1998). Structure-activity relationships of some complex I inhibitors *Biochim. Biophys. Acta*, 1364, 236-244

[506] Clayden, J., Greeves, N., and Warren, S. (2012). Organic Chemistry, (Oxford University Press), 2nd ed., 360-381

[507] Fang, N., and Casida, J.E. (1998). Anticancer action of cubé insecticide: correlation for rotenoid constituents between inhibition of NADH:ubiquinone oxidoreductase and induced ornithine decarboxylase activities, PNAS, 95(7), 3380-3384

[508] Rowlands, J.C., and Casida, J.E. (1998). NADH: ubiquinone oxidoreductase inhibitors block induction of ornithine decarboxylase activity in MCF-7 human breast cancer cells, *Pharmacol. Toxicol.*, 83(5), 214-219

[509] Linsalata, M., Orlando, A., and Russo, F. (2014). Pharmacological and dietary agents for colorectal cancer chemoprevention: effects on polyamine metabolism (review), *Int. J. Oncol.*, 45(5), 1802-1812

[510] Palorini, R., Simonetto, T., Cirulli, C., and Chiaradonna, F. (2013). Mitochondrial complex I inhibitors and forced oxidative phosphorylation synergize in inducing cancer cell death, *Int. J. Cell Biol.*, 243876

[511] Bhat, T.A., Kumar, S., Chaudhary, A.K., Yadav, N., and Chandra, D. (2015). Restoration of mitochondria function as a target for cancer therapy, *Drug Discov. Today*, 20(5), 635-643

[512] Lee, S.C., Min, H.Y., Choi, H., Bae, S.Y., Park, K.H., Hyun, S.Y., Lee, H.J., Moon, J., Park, S.H., Kim, J.Y. *et al.* (2016). Deguelin Analogue SH-1242 Inhibits Hsp90 Activity and Exerts Potent Anticancer Efficacy with Limited Neurotoxicity, *Cancer research*, 76, 686-699

[513] Lee, S.C., Min, H.Y., Choi, H., Kim, H.S., Kim, K.C., Park, S.J., Seong, M.A., Seo, J.H., Park, H.J., Suh, Y.G. *et al.* (2015). Synthesis and evaluation of a novel deguelin derivative, L80, which disrupts ATP binding to the C-terminal domain of heat shock protein 90, *Mol. Pharmacol.*, 88, 245-255.

[514] Thamilselvan, V., Menon, M., and Thamilselvan, S. (2011). Anticancer efficacy of deguelin in human prostate cancer cells targeting glycogen synthase kinase-3 β/β-catenin pathway, *Int. J. Cancer*, 129(12), 2916-2927

[515] Russell, D., personal communication

[516] Fang, J., Wang, Y., and Beattie, D.S. (2001). Isolation and characterization of complex I, rotenone-sensitive NADH: ubiquinone oxidoreductase, from the procyclic forms of Trypanosoma brucei, *Eur. J. Biochem.*, 268(10), 3075-3082

[517] Ueno, H., Miyoshi, H., Inoue, M., Niidome, Y., and Iwamura, H. (1996). Structural factors of rotenone required for inhibition of various NADH-ubiquinone oxidoreductases, *Biochim. Biophys. Acta*, 1276(3), 195-202

[518] Earley, F.G., and Ragan, C.I. (1984). Photoaffinity labelling of mitochondrial NADH dehydrogenase with arylazidoamorphigenin, an analogue of rotenone, *Biochem. J.*, 224(2), 525-534

[519] Earley, F.G., Patel, S.D., Ragan, I., and Attardi, G. (1987). Photolabelling of a mitochondrially encoded subunit of NADH dehydrogenase with [^{3}H]dihydrorotenone, *FEBS Lett.*, 219(1), 108-112

[520] Okun, J.G., Lümmen, P., and Brandt, U. (1999). Three classes of inhibitors share a common binding domain in mitochondrial complex I (NADH:ubiquinone oxidoreductase), *J. Biol. Chem.*, 274(5), 2625-2630

[521] Ueno, H., Miyoshi, H., Ebisui, K., and Iwamura, H. (1994). Comparison of the inhibitory action of natural rotenone and its stereoisomers with various NADH-ubiquinone reductases, *Eur. J. Biochem.*, 225(1), 411-417

[522] Fendel, U., Tocilescu, M.A., Kerscher, S., and Brandt, U. (2008). Exploring the inhibitor binding pocket of respiratory complex I, *Biochim. Biophys. Acta*, 1777, (7-8), 660-665

[523] Angerer, H., Nasiri, H.R., Niedergesäß, V., Kerscher, S., Schwalbe, H., and Brandt, U. (2012). Tracing the tail of ubiquinone in mitochondrial complex I, *Biochim. Biophys. Acta*, 1817(10), 1776-1784

[524] Schuler, F., Yano, T., Di Bernardo, S., Yagi, T., Yankovskaya, V., Singer, T.P., and Casida, J.E. (1999). NADH-quinone oxidoreductase: PSST subunit couples electron transfer from iron-sulfur cluster N2 to quinone, *PNAS*, 96(7), 4149-4153

[525] Prieur, I., Lunardi, J. and Dupuis, A. (2001). Evidence for a quinone binding site close to the interface between NUOD and NUOB subunits of Complex I, *Biochim. Biophys. Acta*, 1504(2-3), 173-178

[526] Zickermann, V., Wirth, C., Nasiri, H., Siegmund, K, Schwalbe, H., Hunte, C., and Brandt, U. (2015). Structural biology. Mechanistic insight from the crystal structure of mitochondrial complex I, *Science*, 347(6217), 44-49

[527] Fang, N., and Casida, J.E. (1999). Cubé resin insecticide: identification and biological activity of 29 rotenoid constituents, *J. Agric. Food. Chem.*, 47(5), 2130-2136

[528] Nicolaou, K., Pfefferkorn, J., Schuler, F., Roecker, A., Cao, G., and Casida, J. (2000). Combinatorial synthesis of novel and potent inhibitors of NADH:ubiquinone oxidoreductase, *Chem Biol.*, 7(12), 979-992

[529] Klopman, G., Li, J., Wang, S., Dimayuga, M. (1994). Computer Automated log P Calculations Based on an Extended Group Contribution Approach, *J. Chem. Inf. Comput. Sci.*, 34 (4), 752-781

[530] Upegui, Y., Gil, J.F., Quiñones, W., Torres, F., Escobar, G., Robledo, S.M., and Echeverri, F. (2014). Preparation of rotenone derivatives and in vitro analysis of their antimalarial, antileishmanial and selective cytotoxic activities, *Molecules*, 19(11), 18911-18922

[531] McConville, M.J., de Souza, D., Saunders, E.C., Pyke, J., Naderer, T., Ellis, M.A., Sernee, M.F., Ralton, J.E., and Likic, V.A. (2008). Analysis of the Leishmania metabolome, in Mayler, P.J., Fasel, N. (ed.), *Leishmania: After The Genome*, Caister Academic Press, 75-106

[532] Subramanian, A., Jhawar, J., and Sarkar, R.R. (2015). Dissecting Leishmania infantum Energy Metabolism - A Systems Perspective, *PLOS One*, 10(9), e0137976

[533] Ji, M., Liang, Y., Gu, Z., and Li, X. (2015). Inhibitory Effects of Amorphigenin on the Mitochondrial Complex I of Culex pipiens pallens Coquillett (Diptera: Culicidae), *Int. J. Mol. Sci.*, 16(8), 19713-19727

[534] Chang, D.J., An, H., Kim, K.S., Kim, H.H., Jung, J., Lee, J.M., Kim, N.J., Han, Y.T., Yun, H., Lee, et al. (2012). Design, synthesis, and biological evaluation of novel deguelin-based heat shock protein 90 (HSP90) inhibitors targeting proliferation and angiogenesis, *J. Med. Chem.*, 55(24), 10863-10884

[535] Forster, H., and Vogtle, F., (1977). Steric Interactions in Organic Chemistry: Spatial Requirements of Substituents, *Angew. Chem. Int. Ed. Engl.*, 16, 429-441

[536] Cavallo, G., Metrangolo, P., Milani, R., Pilati, T., Priimagi, A., Resnati, G., and Terraneo, G. (2016). The Halogen Bond, *Chem. Rev.*, 116, 2478−2601

[537] Jiang, S., Zhang, L., Cui, D., Yao, Z., Gao, B., Lin, J., and Wei, D. (2016). The Important Role of Halogen Bond in Substrate Selectivity of Enzymatic Catalysis, *Sci. Rep.*, 6:34750

[538] Ren, Y., Benatrehina, P.A., Muñoz Acuña. U., Yuan, C., Chai, H.B., Ninh, T.N., Carcache de Blanco, E.J., Soejarto, D.D., and Kinghorn, A.D. (2016). Isolation of Bioactive Rotenoids and Isoflavonoids from the Fruits of Millettia caerulea, *Planta Med.*, 82(11-12), 1096-1104

[539] Bueno Pérez, L., Li, J., Lantvit, D.D., Pan, L., Ninh, T.N., Chai, H.B., Soejarto, D.D., Swanson, S.M., Lucas, D.M., and Kinghorn, A.D. (2013). Bioactive constituents of *Indigofera spicata*, *J. Nat. Prod.*, 76(8), 1498-1504

[540] Baker, N.M., and Der, C.J. (2013). Cancer: Drug for an 'undruggable' protein, *Nature*, 497(7451), 577-578

[541] Pak, C., and Miyamoto, S. (2013). A new alpha in line between KRAS and NF-κB activation?, *Cancer Discov.*, 3(6), 613-615

[542] Park, C.H., Chung, B.Y., Lee, S.S., Bai, H.W., Cho, J.Y., Jo, C., and Kim, T.H. (2013). Radiolytic transformation of rotenone with potential anti-adipogenic activity, *Bioorg. Med. Chem. Lett.*, 23(4), 1099-1103

[543] Nieman, K.M., Romero, I.L., Van Houten, B., and Lengyel, E. (2013). Adipose tissue and adipocytes support tumorigenesis and metastasis, *Biochim. Biophys. Acta*, 1831(10), 1533-1541

[544] Hoy, A.J., Balaban, S., and Saunders, D.N. (2017). Adipocyte-Tumor Cell Metabolic Crosstalk in Breast Cancer, *Trends Mol. Med.*, 23(5), 381-392

[545] Sangthong, S., Krusong, K., Ngamrojanavanich, N., Vilaivan, T., Puthong, S., Chandchawan, S., and Muangsin, N. (2011). Synthesis of rotenoid derivatives with cytotoxic and topoisomerase II inhibitory activities, *Bioorg. Med. Chem. Lett.*, 21(16), 4813-4818

[546] Pendleton, M., Lindsey, R.H., Felix, C.A., Grimwade, D., and Osheroff, N. (2014). Topoisomerase II and leukemia, *Ann. N. Y. Acad. Sci.*, 1310, 98-110

[547] Willard, J. M., and De Felice, A. (2016). Lysosomes and Phospholipidosis in Drug Development and Regulation, in Maxfield, F. R., Willard, J. M., Lu, S. (ed.) *Lysosomes: Biology, Diseases, and Therapeutics*, Wiley

[548] Kramer, J.A., Sagartz, J.E., and Morris, D.L. (2007). The application of discovery toxicology and pathology towards the design of safer pharmaceutical lead candidates, *Nat. Rev. Drug Discov.*, 6(8), 636-649

[549] Rudmann, D.G. (2013). On-target and off-target-based toxicologic effects, *Toxicol. Pathol.*, 41(2), 310-314

[550] Härter, M., Thierauch, K.H., Boyer, S., Bhargava, A., Ellinghaus, P., Beck, H., Greschat-Schade, S., Hess-Stumpp, H., and Unterschemmann, K., (2014). Inhibition of hypoxia-induced gene transcription by substituted pyrazolyl oxadiazoles: initial lead generation and structure-activity relationships, *ChemMedChem.* 9(1), 61-66

[551] Ellinghaus, P., Heisler, I., Unterschemmann, K., Haerter, M., Beck, H., Greschat, S., Ehrman, A., Summer, H., Flamme, I., Oehme, F., et al. (2013). BAY 87-2243, a highly potent and selective inhibitor of hypoxia-induced gene activation has antitumor activities by inhibition of mitochondrial complex I. *Cancer Med.* 2, 611-624

[552] Diebold, L., and Chandel, N.S. (2016). Mitochondrial ROS regulation of proliferating cells, *Free Radic. Biol. Med.*, 100, 86-93

[553] Waypa, G.B., Marks, J.D., Guzy, R.D., Mungai, P.T., Schriewer, J.M., Dokic, D., Ball, M.K., and Schumacker, P.T. (2013). Superoxide generated at mitochondrial complex III triggers acute responses to hypoxia in the pulmonary circulation, *Am. J. Respir. Crit. Care Med.*, 187(4), 424-432

[554] Wedgwood, S., Lakshminrusimha, S., Schumacker, P.T., and Steinhorn, R.H. (2015). Cyclic stretch stimulates mitochondrial reactive oxygen species and Nox4 signaling in pulmonary artery smooth muscle cells, *Am. J. Physiol. Lung Cell Mol. Physiol.*, 309(2), L196-203

[555] Forkink, M., Basit, F., Teixeira, J., Swarts, H.G., Koopman, W.J., and Willems, P.H. (2015). Complex I and complex III inhibition specifically increase cytosolic hydrogen peroxide levels without inducing oxidative stress in HEK293 cells, *Redox Biol.*, 6, 607-616

[556] Schöckel, L., Glasauer, A., Basit, F., Bitschar, K., Truong, H., Erdmann, G., Algire, C., Hägebarth, A., Willems, P.H., Kopitz, C., *et al.* (2015). Targeting mitochondrial complex I using BAY 87-2243 reduces melanoma tumor growth, *Cancer Metab.*, 3:11

[557] Helbig, L., Koi, L., Brüchner, K., Gurtner, K., Hess-Stumpp, H., Unterschemmann, K., Baumann, M., Zips, D., and Yaromina, A. (2014). BAY 87-2243, a novel inhibitor of hypoxia-induced gene activation, improves local tumor control after fractionated irradiation in a schedule-dependent manner in head and neck human xenografts, *Radiat. Oncol.*, 9:207

[558] Chang, E., Liu, H., Unterschemmann, K., Ellinghaus., P., Liu, S., Gekeler, V., Cheng, Z., Berndorff, D., and Gambhir, S.S. (2015). 18F-FAZA PET Imaging Response Tracks the Reoxygenation of Tumors in Mice upon Treatment with the Mitochondrial Complex I Inhibitor BAY 87-2243, *Clin. Cancer Res.*, 21(2), 335-346

[559] Bastian, A., Thorpe, J.E., Disch, B.C., Bailey-Downs, L.C., Gangjee, A., Devambatla, R.K., Henthorn, J., Humphries, K.M., Vadvalkar, S.S. and Ihnat, M.A. (2015). A small molecule with anticancer and antimetastatic activities induces rapid mitochondrial-associated necrosis in breast cancer, *J. Pharmacol. Exp. Ther.*, 353(2), 392-404

[560] Bastian, A., Matsuzaki, S., Humphries, K.M., Pharaoh, G.A., Doshi, A., Zaware, N., Gangjee, A., and Ihnat, M.A. (2017). AG311, a small molecule inhibitor of complex I and hypoxia-induced HIF-1α stabilization, *Cancer Lett.*, 388, 149-157

[561] Molina, J. R., Sun, Y., Protopopova, M., Gera, S., Bandi, M., McAfoos, T., Morlacchi, P., Bardenhagen, J., Bristow, C. Gao, G. *et al.*, unpublished results submitted for publication

[562] O'Connell, T.M (2013). The complex role of branched chain amino acids in diabetes and cancer, *Metabolites*, 3(4), 931-945

[563] Sullivan, L.B., Gui, D.Y., Hosios, A.M., Bush, L.N., Freinkman, E., and Vander Heiden, M.G., (2015). Supporting Aspartate Biosynthesis Is an Essential Function of Respiration in Proliferating Cells, *Cell*, 162(3), 552-563

[564] Pearson, J., Dahal, U.P., Rock, D., Peng, C.C., Schenk, J.O., Joswig-Jones, C., and Jones, J.P. (2011). The kinetic mechanism for cytochrome P450 metabolism of type II binding compounds: evidence supporting direct reduction, *Arch. Biochem. Biophys.*, 511(1-2), 69-79

[565] Cao, X., Sun, Z., Cao, Y., Wang, R., Cai, T., Chu, W., Hu, W., and Yang, Y. (2014). Design, synthesis, and structure-activity relationship studies of novel fused heterocycles-linked triazoles with good activity and water solubility, *J. Med. Chem*. 57(9), 3687-3706

[566] Wang, T., Yin, Z., Zhang, Z., Bender, J.A., Yang, Z., Johnson, G., Yang, Z., Zadjura, L.M., D'Arienzo, C.J., DiGiugno Parker, et al. (2009). Inhibitors of human immunodeficiency virus type 1 (HIV-1) attachment. 5. An evolution from indole to azaindoles leading to the discovery of 1-(4-benzoylpiperazin-1-yl)-2-(4,7-dimethoxy-1H-pyrrolo[2,3-c]pyridin-3-yl)ethane-1,2-dione (BMS-488043), a drug candidate that demonstrates antiviral activity in HIV-1-infected subjects, *J. Med. Chem.*, 52(23), 7778-7787

[567] Prime, M.E., Andersen, O.A., Barker, J. J., Brooks, M.A., Cheng, R.K.Y., Toogood-Johnson, I., Courtney, S.M., Brookfield, F.A., Yarnold, C.J., Marston, R.W., (2012). Discovery and Structure−Activity Relationship of Potent and Selective Covalent Inhibitors of Transglutaminase 2 for Huntington's Disease, *J. Med. Chem.*, 55, 1021-1046

[568] Lockhart, C.L., Conger, M.A., Pittman, D.S., and Liptak, M.D. (2015). Hydrogen bond donation to the heme distal ligand of Staphylococcus aureus IsdG tunes the electronic structure, *J. Biol. Inorg. Chem*., 20(5), 757-770

[569] The University of Texas MD Anderson Cancer Centre, Annual Report 2014, https://www.mdanderson.org/documents/publications/annual-report/AnnualReport2014.pdf

[570] Yip, C.Y., Harbour, M.E., Jayawardena, K., Fearnley, I.M., and Sazanov, L.A. (2011). Evolution of respiratory complex I: "supernumerary" subunits are present in the alpha-proteobacterial enzyme, *J. Biol Chem.*, 18, 286(7), 5023-5033

[571] Kashani-Poor, N., Zwicker, K., Kerscher, S., and Brandt, U. (2001). A central functional role for the 49-kDa subunit within the catalytic core of mitochondrial complex I, *J. Biol. Chem.*, 276(26), 24082-24087

[572] Ahlers, P.M., Garofano, A., Kerscher, S.J., and Brandt, U. (2000). Application of the obligate aerobic yeast Yarrowia lipolytica as a eucaryotic model to analyse Leigh syndrome mutations in the complex I core subunits PSST and TYKY, *Biochim. Biophys. Acta*, 1459(2-3), 258-265

[573] Grivennikova, V.G., Roth, R., Zakharova, N.V., Hägerhäll, C., Vinogradov, A.D. (2003). The mitochondrial and prokaryotic proton-translocating NADH:ubiquinone oxidoreductases: similarities and dissimilarities of the quinone-junction sites, *Biochim. Biophys. Acta*, 1607(2-3), 79-90

[574] Winkler, D., Beconi, M., Toledo-Sherman, L.M., Prime, M., Ebneth, A., Dominguez, C., and Muñoz-Sanjuan, I. (2013). Development of LC/MS/MS, high-throughput enzymatic and cellular assays for the characterization of compounds that inhibit kynurenine monooxygenase (KMO), *J. Biomol. Screen.*, 18(8), 879-889

[575] Chang, J.W., Niphakis, M.J., Lum, K.M., Cognetta, A.B., Wang, C., Matthews, M.L., Niessen, S., Buczynski, M.W., Parsons, L.H., and Cravatt, B.F. (2012). Highly selective inhibitors of monoacylglycerol lipase bearing a reactive group that is bioisosteric with endocannabinoid substrates, *Chem. Biol.*, 19(5), 579-588

[576] Panini, P., and Chopra, D. (2015). Understanding of Noncovalent Interactions Involving Organic Fluorine, in Li, Z., Wu, L. (ed.) *Hydrogen Bonded Supramolecular Structures*, Lecture Notes in Chemistry Vol. 87, Springer, 37-67

[577] Dalvit, C., and Vulpetti, A., (2012). Intermolecular and Intramolecular Hydrogen Bonds Involving Fluorine Atoms: Implications for Recognition, Selectivity, and Chemical Properties, *ChemMedChem*, 7, 262-272

[578] Boström, J., Hogner, A., Llinàs, A., Wellner, E., and Plowright, A.T. (2012). Oxadiazoles in medicinal chemistry *J. Med. Chem.*, 8, 55(5), 1817-1830

[579] Kemnitzer, W., Kuemmerle, J., Zhang, H.Z., Kasibhatla, S., Tseng, B., Drewe, J., and Cai, S.X. (2009). Discovery of 3-aryl-5-aryl-1,2,4-oxadiazoles as a new series of apoptosis inducers. 2. Identification of more aqueous soluble analogs as potential anticancer agents, *Bioorg. Med. Chem. Lett.*, 19(15), 4410-4415

[580] Kumar, D., Patel, G., Johnson, E.O., and Shah, K. (2009). Synthesis and anticancer activities of novel 3,5-disubstituted-1,2,4-oxadiazoles, *Bioorg. Med. Chem. Lett.*, 19(10), 2739-2741

[581] Boschelli, D.H., Powell, D., Golas, J.M., and Boschelli, F. (2003). Inhibition of Src kinase activity by 4-anilino-5,10-dihydro-pyrimido[4,5-b]quinolines, *Bioorg. Med. Chem. Lett.*, 13(18), 2977-2980

[582] Hohlfeld, K., Wegner, J.K., Kesteleyn, B., Linclau, B., and Unge, J. (2015). Disubstituted Bis-THF Moieties as New P2 Ligands in Nonpeptidal HIV-1 Protease Inhibitors (II), *J. Med. Chem.* 58(9), 4029-4038

[583] Qian, Y., Bolin, D. R., Conde-Knape, K., Gillespie, P., Hayden, S., Huang, K., Liu, M., Olivier, A.R., Ren, Y., Sergi, J., et al. (2013). N-substituted sultam carboxylic acids as novel glycogen synthase activators, *Med. Chem. Commun.*, 4, 833-838

[584] Hohlfeld, K., Tomassi, C., Wegner, J.K., Kesteleyn, B., and Linclau B. (2011). Disubstituted Bis-THF Moieties as New P2 Ligands in Nonpeptidal HIV-1 Protease Inhibitors, *ACS Med. Chem. Lett.*, 2, 461-465

[585] Moreno, L., Berenguer, I., Diaz, A., Marín, P., Párraga, J., Caignard, D.H., Figadère, B., Cabedo, N., and Cortes, D. (2014). Synthesis of new melatoninergic hexahydroindenopyridines, *Bioorg. Med. Chem. Lett.*, 24(15), 3534-3536

[586] Simmler, L.D., Buser, T.A., Donzelli, M., Schramm, Y., Dieu, L.H., Huwyler, J., Chaboz, S., Hoener, M.C., and Liechti, M.E. (2013). Pharmacological characterization of designer cathinones in vitro, *Br. J. Pharmacol.*, 168(2), 458-470

[587] Hammuda, A., Shalaby, R., Rovida, S., Edmondson, D.E., Binda, C., and Khalil, A. (2016). Design and synthesis of novel chalcones as potent selective monoamine oxidase-B inhibitors, *Eur. J. Med. Chem.*, 114, 162-169

[588] Tebbutt, N., Pedersen, M.W., and Johns, T.G. (2013). Targeting the ERBB family in cancer: couples therapy, *Nat. Rev. Cancer*, 13(9), 663-673

[589] Roskoski, R. (2014). The ErbB/HER family of protein-tyrosine kinases and cancer, *Pharmacol. Res.*, 79, 34-74

[590] Yan, M., Schwaederle, M., Arguello, D., Millis, S.Z., Gatalica, Z., and Kurzrock, R. (2015). HER2 expression status in diverse cancers: review of results from 37,992 patients, *Cancer Met. Rev.*, 34(1), 157-164

[591] https://clinicaltrials.gov/ct2/show/NCT00034281, accessed on 12th February 2017

[592] Nagasawa, J., Mizokami, A., Koshida, K., Yoshida, S., Naito, K., and Namiki, M. (2006). Novel HER2 selective tyrosine kinase inhibitor, TAK-165, inhibits bladder, kidney and androgen-independent prostate cancer in vitro and in vivo, *Int. J. Urol.*, 13(5), 587-592

[593] Shao, X., Liu, Y., Li, Y., Xian, M., Zhou, Q., Yang, B., Ying, M., and He, Q. (2016). The HER2 inhibitor TAK165 Sensitizes Human Acute Myeloid Leukemia Cells to Retinoic Acid-Induced Myeloid Differentiation by activating MEK/ERK mediated RARα/STAT1 axis, *Sci. Rep.*, 6:24589

[594] da Silva, F. C., Cardoso, M. F., Ferreira, P. G., and Ferreira, V. F. (2015). Biological Properties of 1H-1,2,3- and 2H-1,2,3-Triazoles, in Dehaen, W., Bakulev, V. A. (ed.) *Chemistry of 1,2,3-Triazoles - Top. Heterocycl. Chem.*, Springer, (40), 117-166

[595] Lauria, A., Delisi, R., Mingoia, F., Terenzi, A., Martorana, A., Barone, G., and Almerico, A. M., (2014). 1,2,3-Triazole in Heterocyclic Compounds, Endowed with Biological Activity, through 1,3-Dipolar Cycloadditions, *Eur. J. Org. Chem*, 16, 3289-3306

[596] Eicher, T., Hauptmann, S., and Speicher, A. (2012). *The Chemistry of Heterocycles*, Wiley-VCH, 3rd ed., 61-296

[597] Ino, T., Nishioka, T., and Miyoshi, H. (2003). Characterization of inhibitor binding sites of mitochondrial complex I using fuorescent inhibitor, *Biochim. Biophys. Acta*, 1605, 15-20

[598] Murai, M., Mashimo, Y., Hirst, J., and Miyoshi, H. (2011). Exploring interactions between the 49 kDa and ND1 subunits in mitochondrial NADH-ubiquinone oxidoreductase (complex I) by photoaffinity labelling, *Biochemistry*, 50(32), 6901-6908

[599] Shao, J., Chen, E., Shu, K., Chen, W., Zhang, G., and Yu, Y. (2016). 6-Oxooxazolidine-quinazolines as noncovalent inhibitors with the potential to target mutant forms of EGFR, *Bioorg. Med. Chem.*, 24(16), 3359-3370

[600] Tu, Y., OuYang, Y., Xu, S., Zhu, Y., Li, G., Sun, C., Zheng, P., and Zhu, W. (2016). Design, synthesis, and docking studies of afatinib analogs bearing cinnamamide moiety as potent EGFR inhibitors, *Bioorg. Med. Chem.*, 24(7), 1495-1503

[601] Bernard-Gauthier, V., Mahringer, A., Vesnaver, M., Fricker, G., and Schirrmacher, R. (2017). Design and synthesis of a fluorinated quinazoline-based type-II Trk inhibitor as a scaffold for PET radiotracer development, *Bioorg. Med. Chem. Lett.*, 27(12), 2771-2775

[602] Kusakabe, K., Tada, Y., Iso, Y., Sakagami, M., Morioka, Y., Chomei, N., Shinonome, S., Kawamoto, K., Takenaka, H., Yasui, K., *et al.* (2013). Design, synthesis, and binding mode prediction of 2-pyridone-based selective CB2 receptor agonists, *Bioorg. Med. Chem.*, 21(7), 2045-2055

[603] Igoe, N., Bayle, E.D., Fedorov, O., Tallant, C., Savitsky, P., Rogers, C., Owen, D.R., Deb, G., Somervaille, T.C., Andrews, D.M. et al. (2017). Design of a Biased Potent Small Molecule Inhibitor of the Bromodomain and PHD Finger-Containing (BRPF) Proteins Suitable for Cellular and in Vivo Studies, *J. Med. Chem.*, 60(2), 668-680

[604] Yang, X., Li, F., Konze, K.D., Meslamani, J., Ma, A., Brown, P.J., Zhou, M.M., Arrowsmith, C.H., Kaniskan, H.Ü., Vedadi, M., et al. (2016). Structure-Activity Relationship Studies for Enhancer of Zeste Homologue 2 (EZH2) and Enhancer of Zeste Homologue 1 (EZH1) Inhibitors, *J. Med. Chem.*, 59(16), 7617-7633

[605] Corte, J.R., Fang, T., Pinto, D.J., Han, W., Hu, Z., Jiang, X.J., Li, Y.L., Gauuan, J.F., Hadden, M., Orton, D., et al. (2008). Structure-activity relationships of anthranilamide-based factor Xa inhibitors containing piperidinone and pyridinone P4 moieties, *Bioorg. Med. Chem. Lett.*, 18(9), 2845-2849

[606] The UniProt Consortium (2017). UniProt: the universal protein knowledgebase, *Nucleic Acids Res.*, 45, D158-D169

[607] Wheeler, S.E., and Bloom, J.W. (2014). Toward a more complete understanding of noncovalent interactions involving aromatic rings, *J. Phys. Chem. A*, 118(32), 6133-6147

[608] Hohenstein, E.G., and Sherrill, C.D. (2009). Effects of heteroatoms on aromatic pi-pi interactions: benzene-pyridine and pyridine dimer, *J. Phys. Chem. A*, 113(5), 878-886

[609] Sheng, R., Li, S., Lin, G., Shangguana, S., Guc, Y., Qiua, N., Cao, J., Heb, Q., Yang, B., and Hu, Y. (2015). Novel potent HIF-1 inhibitors for the prevention of tumor metastasis: discovery and optimization of 3-aryl-5-indazole-1,2,4-oxadiazole derivatives, *RSC Adv.*, 5, 81817-81830

[610] Baccelli, I., Krosl, J., Boucher, G., Boivin, I., Lavallée, V.P., Hébert J., Lemieux, S., Marinier, A., and Sauvageau, G. (2017). A novel approach for the identification of efficient combination therapies in primary human acute myeloid leukemia specimens, *Blood Cancer J.*, 7(2), e529

[611] Saygin, C., and Carraway, H.E. (2017). Emerging therapies for acute myeloid leukemia, *J. Hematol. Oncol.*, 10(1), 93

[612] Nandeesh, K.N., Swarup, H.A., Sandhya, N.C., Mohan, C.D., Pavan Kumar, C.S., Kumara, M.N., Mantelingu, K., Ananda S. and Rangappa, K. S. (2016). Synthesis and antiproliferative efficiency of novel bis(imidazol-1-yl)vinyl-1,2,4-oxadiazoles, *New J. Chem.*, 40, 2823-2828

[613] Urra, F.A., Muñoz, F., Lovy, A., and Cárdenas, C. (2017). The Mitochondrial Complex(I)ty of Cancer, *Front. Oncol.*, 7,118